Assembly dynamics and structure-function analysis of an unusual kinetochore in the pathogenic basidiomycetous budding yeast *Cryptococcus neoformans*

A thesis submitted for the degree of

Doctor of Philosophy

By

Shreyas Sridhar

To

Molecular Biology and Genetics Unit,

Jawaharlal Nehru Centre for Advanced Scientific Research,

Jakkur, Bangalore- 560064, India

December 2019

Stay Hungry.

Stay foolish.

- Stewart Brand
Final edition “Whole Earth Catalogue”.

Dedicated to my parents and brother.

DECLARATION

I do hereby declare that this thesis entitled *"Assembly dynamics and structure-function analysis of an unusual kinetochore in the pathogenic basidiomycetous budding yeast Cryptococcus neoformans"* is an authentic record of research work carried out by me towards my Doctor of Philosophy under the guidance and supervision of **Prof. Kaustuv Sanyal** at the Molecular Biology and Genetics Unit, Jawaharlal Nehru Centre for Advanced Scientific Research, Bangalore, India and that this work has not been submitted elsewhere for the award of any other degree.

In keeping with the norm of reporting scientific observations, due acknowledgments have been made whenever the work described was based on the findings of other investigators. Any omission, which might have occurred by oversight or misjudgement, is regretted.

Shreyas Sridhar

Place: Bangalore

Date:

Jawaharlal Nehru Center for Advanced Scientific Research

Kaustuv Sanyal PhD, FAAM (USA), FNA, FASc, FNASc
Professor & Tata Innovation Fellow

Certificate

This is to certify that the work described in this thesis *"Assembly dynamics and structure-function analysis of an unusual kinetochore in the pathogenic basidiomycetous budding yeast Cryptococcus neoformans"* is the result of the investigations carried out by **Mr. Shreyas Sridhar** towards his Doctor of Philosophy degree as part of the Integrated-PhD program at the Molecular Biology and Genetics Unit, Jawaharlal Nehru Centre for Advanced Scientific Research, Bangalore, India under my guidance and that the results presented in this thesis have not previously formed the basis for the award of any other diploma, degree or fellowship.

Kaustuv Sanyal

Place: Bangalore
Date:

Molecular Mycology Laboratory, Molecular Biology & Genetics Unit, JNCASR, Jakkur Post, Bangalore 560064, India
Tel: +91 80 2208 2878; email: sanyal@jncasr.ac.in; web: http://www.jncasr.ac.in/sanyal

Acknowledgments

My journey in JNCASR as an Integrated-PhD. student has been an exciting one and I am grateful to a one and all for the part they played in it. The process of learning and experimenting was fun and captivating. It gave me an opportunity to work on topics I knew little about before joining here. It was also a voyage involving several collaborations and I am grateful to have gotten an opportunity to learn from people with different specialization and address several unique questions extending from basic biology to therapeutic applications, using model systems ranging from yeast to mice.

I am very fortunate to have had Prof. Kaustuv Sanyal as my mentor and guide through this journey. His curious spirit and excitement towards addressing unconventional questions have remained something I look up to. I appreciate the fact that he pushed me to get the best of my abilities and on other occasions, was very understanding. A lot of the mentioned collaboration was a result of my mentor's efforts towards helping his students address questions from angles that might not have been possible otherwise. It was always exciting to carry out experiments (authorized and unauthorized ones) with the freedom he provided. Sir, thank you!

At the beginning of the integrated Ph.D. program, I was introduced into the world of experimental science and could not have asked for a better laboratory teacher than Dr. GR Ramesh. His teaching us of the basics and principles behinds molecular biology techniques aided to a great extent when I actually had to carry out my own experiments and troubleshoot. I still recall to this day "plan, execute and analyze", the three mantras which go hand in hand that he introduced us to.

I am grateful to Dr. Ravi Manjithaya for all his discussions, suggestions and assistance wherever required. I am thankful to him for giving me the opportunity to work on an exciting project during my tenure in his lab. I recall and learned from his enthusiasm and advice on being productive and organized.

Biology is diverse and hard to read it all, in this aspect I would like to thank the MBGU faculty, Prof. Uday Kumar Ranga, Prof. Tapas Kumar Kundu, Prof. Maneesha Inamdar, Prof. Hemalatha Balaram, Prof. Anuranjan Anand, Prof. Namita Surolia, Prof. MRS Rao, Prof. Kaustuv Sanyal and Dr. Ravi Manjithaya, for their course work which introduced me to a world of amazingly diverse topics in biology. Further I would also like to thank them, including Dr. Kushagra Bansal, for their inputs and discussions during my presentation and interactions. A special thanks to Dr. James Chelliah for the inputs on my work and towards facilitating me to learn and perform mice work in his lab.

Towards the kinetochore work performed in this thesis, I am especially grateful to have a collaboration with Prof. Tatsuo Fukagawa through the DBT-JSPS program. This allowed me to spend a couple of months learning and performing experiments in his lab at Osaka

University, which greatly helped mature this work. During that time, I received a lot of specific inputs on the work and his experience in the kinetochore field was invaluable. Interactions with him and the lab made me be more critical of my work. The biochemical studies in addition to the *in vitro* work were made possible by the teaching and technical help of his lab members: Dr. Tetsuya Hori, Dr. Masatoshi Hara, Dr. Mariko Ariyoshi, Dr. Fumiaki Makino and Reito Watanabe. Also grateful to all the lab members for their help and generosity during my stay there.

I am very fortunate to have had several exciting collaborations during my Ph.D. tenure which help expose me to a wide range of questions and means of addressing them. A special thanks to my collaborators for their productive collaborations: Prof. Raja Paul and his student Sabysachi Sutradhar (*in silico* modeling of budding yeast systems), Dr. Lukasz Kozubowki and his students for the initial work on *C. neoformans* mitotic dynamics and later on addressing drug-induced ploidy change, and Dr. Shilpee Jain and her student Kaushik Suneet for work on hyperthermia as an adjunct anti-fungal therapy.

Attending conferences help me discuss my work with people from all over the globe, troubleshooting problems, exploring novel possibilities and in making new friends. I am grateful to Prof. Joseph Heitman, Dr. Jeyaprakash Arulanandam, Prof. Harmit Malik, Prof. Andrea Musacchio, Prof. Geert Kops and Prof. Scott Keeney for their inputs and encouraging discussions. I also want to thank Dr. Ganesh Nagaraju and Dr. Deepak Saini for being reviewers of my MS thesis and Ph.D. comprehensive exam and provided useful inputs and constructive criticism which has helped shape the work.

I grateful to JNCASR and CSIR for my fellowship. I am also appreciative of the JNCASR student fund and the EMBO travel grant for financial assistance towards conference expenses. This work would not have been possible if not for the in-house technical facilities at JNCASR. I thank Suma Ma'am and Mr. Sunil for their technical assistance at the confocal facility, Anita ma'am for the sequencing facility and Dr. Prakash for his assistance with the animal facility. The beautiful JNCASR campus makes it special studying here, and I appreciate and thank the gardening team for their efforts.

I am fortunate to have been given the opportunity to work at the Molecular Mycology Laboratory (MML). I am very grateful to all the members of the Molecular Mycology Laboratory for all their inputs and critical suggestion over the years towards improving my work. I am thankful to my seniors: Dr. Gautam, Dr. Sreyoshi, Dr. Laxmi, Dr. Jitendra, Dr. Neha, Dr. Vikas and Dr. Babhrubahan for their discussion and help during my years in the lab. I would also like to thank the current lab members Dr. Lakshmi, Sundar, Krishnendu, Rima, Priya J, Priya B, Satya, Rashi, Kuladeep, Padma, Dr. Hashim, Dr. Shweta, Dr. Aswathy, Tejas and Srijana for creating a friendly, helpful and a cheerful environment to do science in. I will treasure the time I spent in the lab. A morning in MML is not complete without seeing the ever-smiling face of our beloved lab attender

Mr. Nagaraj. I will always be very grateful to his help in providing clean lab equipment and reagents on time.

I would like to thank my batchmates Sundar, Lakshmeesha, Pooja, Stephanie, Piyush, Neha, Prabhu, Simi, and Shalini for all the good times. I would also like to thank all my friends in JNCASR that have made my stay here pleasant.

Being a local of Bangalore, I'm fortunate to have a great of bunch of folks, starting from my school friends around me all the time. To Prajval, Sneha, Rutwick (who introduced me to JNCASR), Aravind, Hitha, Shruthi, Parvathi, Prithivi, Dev and Mayank I am grateful for the amazing memories we had over the years!

I have a passion for exploring places and cultures while travelling on two wheels. This was my getaway, whenever needed. Little did I know I would meet people from all walks to life and I am grateful to good friends I made along my journeys. The biking community is incredible!

A PhD. degree is not the easiest of journeys to undertake, and my parents and brother have had a large role to play in me reaching this stage today. I am fortunate to have had a very loving and encouraging set of parents who supported me to pursue any of my interests. I'm glad to have had them close by, quite literally, throughout my journey. No acknowledgments will ever be enough. I am grateful to my batchmate-turned-fiancé, Dr. Stephanie for all the her support and love.

Shreyas Sridhar

Table of contents

Table of figures:

Introduction

Results

Discussion

Material and methods

Chapter 1 : Introduction

Chromosome segregation and its importance

Biologists have been fascinated with understanding the process of inheritance for over a century. Great leaps bolstered this quest in the late 19th and early 20th century with the discovery of DNA by Freidrich Meischer (Miescher, 1871) in 1869, followed by the naming of chromosomes in 1888 by HWG von Waldeyer-Hartz. Subsequently, Theodor Boveri (Boveri, 1904) and Walter Sutton (Sutton, 1902, 1903) proposed the "Chromosome theory of inheritance". Thomas Morgan Hunt experimentally verified the chromosome theory by using fly genetics (Morgan, 1915). From these exciting beginnings, researchers have been able to work towards decoding the elegant choreography of chromosome segregation with the identification of the centromere, kinetochore, signaling events, and associated processes.

Arising concurrently with these discoveries came the understanding that dysregulation or errors in chromosome segregation lead to aneuploidy often seen in disastrous disease states. Abnormal chromosome numbers were recognized as a near-ubiquitous feature of human cancers from as far back as the 19th century (Hansemann, 1890). With studies in colorectal cancers showing that ~85% are aneuploid with an average chromosome number ranging from 60-90 (Pellman, 2001). Consequences of aneuploidy in mitosis affect somatic cells of the individual. Aneuploidy in germ cells generated as a consequence of meiotic defects is passed on to the next generation and often manifests as genetic disorders, such as is with Down syndrome (trisomy of chromosome 21). Amongst fungi, aneuploidy is often observed in hospital isolates of pathogenic fungi such as *Cryptococcus neoformans* and *Candida albicans*. These karyotypic abnormalities have been associated with drug resistance and increased virulence in fungi (Fries and Casadevall, 1998; Selmecki et al., 2008, 2009).

Until a few years ago, our understanding of the process of chromosome segregation was restricted to model systems. With the advent of genome sequencing and the availability of improved bioinformatic tools, research in non-model systems is opening a new domain wherein systems exhibiting potential variation from standard models are being discovered. Thus, revealing the plasticity of the system while retaining the goal of accurate genetic inheritance (Akiyoshi and Gull, 2014; Hooff et al., 2017; Navarro-

Mendoza et al., 2019; Nuria Cortes-Silva et al., 2019; Oliferenko, 2018; Yadav et al., 2018a).

In this thesis, I sought to understand the composition, dynamics, and organization of the kinetochore in the human fungal pathogen *Cryptococcus neoformans.* Here I report the identified of a previously unknown kinetochore protein and its role as an unconventional linker between the microtubule-binding outer kinetochore network and centromeric chromatin.

Mitosis

New cells can emerge only through the duplication of an existing cell. This profound insight in the 19th century paved the way for understanding the processes of cell division from unicellular prokaryotic bacteria to multicellular eukaryotic systems. Here we focus on mitosis, a eukaryotic mode of cell division observed in somatic cells that give rise to two identical daughter cells with identical genetic makeup as the parent cell. Duplication of the genetic material takes place in the S phase, while two significant events of chromosome segregation and cell division take place in the M phase (Figure 1-1).

Events in the M phase can traditionally be divided into five stages: prophase, prometaphase, metaphase, anaphase, and telophase (Figure 1-1). At prophase, chromosomes condense, and assembly of the mitotic spindle begins. Chromosome attachment to the spindle and breakdown of the **n**uclear **e**nvelope (NE) takes place in prometaphase. These events are followed by the attachment of sister chromatids to spindle **m**icro**t**ubules (MTs) arising from opposite poles and alignment of chromosomes on the metaphase spindle. Subsequently, sister chromatids separate from each other by the pull of depolymerizing microtubules to the opposite poles and into daughter cells during anaphase. The M phase concludes with the reformation of the NE and the de-condensation of chromosomes (Figure 1-1). Following the M phase, cytokinesis divides the cell into two daughter cells. The gap phases G1 (prior to S phase onset) and G2 (between S phase and M phase) are often observed in humans and fission yeast (Figure 1-1 and 1-2A), although variations are noticed in budding yeast (Figure 1-2B). Even though the general time of the mitotic cell cycle varies across eukaryotes, the events of mitosis are finely controlled by molecular clocks and checks. These cell cycle regulators were

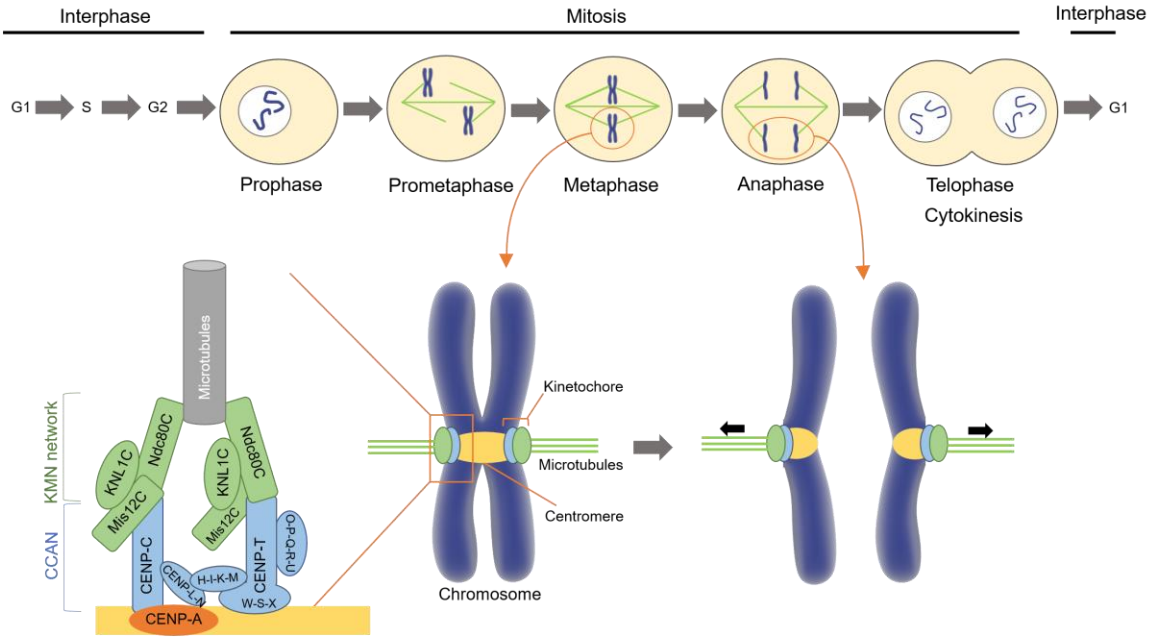

Figure 1-1: Chromosome segregation and the kinetochore architecture in vertebrate mitosis.

Mitosis involves the equal segregation of the duplicated genome to the next generation. Spindle microtubules capture condensed chromosomes, starting from prometaphase to metaphase. The microtubules attach to kinetochores, which are formed on a special chromosome locus called the centromere. The kinetochore harnesses the force from the microtubules, bringing the segregated chromosomes (sister chromatids) to the opposite spindle poles during anaphase. The kinetochore consists of chromatin proximal inner kinetochore (blue) and the microtubule proximal outer kinetochore (green).

---

revealed by elegant studies done in budding and fission yeast species by Leland Hartwell and Sir Paul Nurse, respectively, and in sea urchin by Tim Hunt (Bruce, 2001).

The outcome of mitosis is identical across systems, yet it is achieved in strikingly different ways. Most metazoans employ “open” mitosis, which entails the complete breakdown of the NE to ensure attachment of chromosomes to the mitotic spindle. However, many unicellular eukaryotes, such as yeasts, undergo “closed” mitosis wherein the NE remains intact, and events of mitosis such as chromosome capture by spindle microtubules and chromosome segregation take place inside the intact nucleus (Figure 1-2C).

Intermediate forms of open and closed mitosis are also observed, wherein the nuclear membrane is not seen to disintegrate completely, rather nuclear permeability is increased

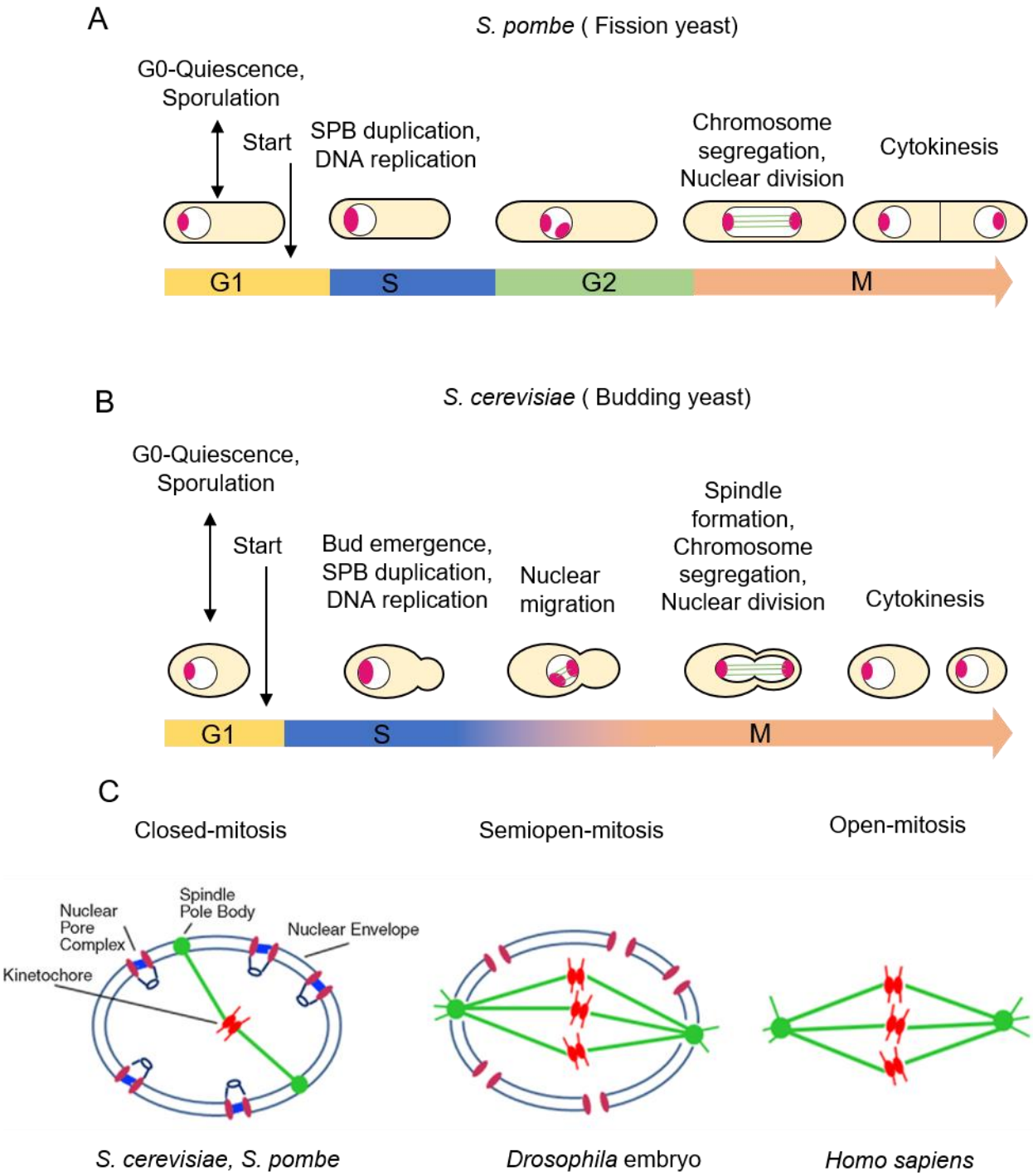

Figure 1-2: Cell cycle events in yeast and the types of mitosis in comparison with other systems.

(A) The fission yeast has a typical eukaryotic cell cycle with G1, S, G2, and M phases. **(B)** The budding yeast cell cycle comprises of a standard G1 and S phases but does not exhibit a conventional G2 phase. Instead, the microtubule-based spindle begins to form in the S phase, and cells enter mitosis soon after, proceeding to segregate chromosomes. **(C)** Various forms of mitosis observed in the eukaryotic kingdom.

on account of partial nuclear pore complex disassembly, observed in systems such as *Aspergillus nidulans, C. neoformans* and the *Drosophila* embryo (Kozubowski et al., 2013; Paddy et al., 1996; De Souza et al., 2004).

Semi-open mitotic can also be a result of a rupture or break in the NE a consequence of microtubule induced shear forces, as observed in *Schizosaccharomyces japonicus* and *C. neoformans* (Boettcher and Barral, 2013; Kozubowski et al., 2013; O'Donnell and McLaughlin, 1984; De Souza and Osmani, 2007; Straube et al., 2005). I describe the process of *C. neoformans* nuclear division in detail, later in this section.

Molecular players of chromosome segregation

Chromosome segregation in mitosis entails the division of sister chromosomes into daughter cells. To enable this process, chromosomes require to be linked to the push-pull forces of the cell. The mitotic spindle apparatus generates the forces of movement, while a macromolecular protein bridge called the kinetochore forms on centromere DNA linking the spindle to the chromosome (Figure 1-1). In the following subsections, I will discuss the role and functioning of these critical players of chromosome segregation.

Mitotic Spindle apparatus

The mitotic spindle apparatus consists of microtubules, motors, and **m**icro**t**ubule-**a**ssociated **p**roteins (MAPs) (Karsenti and Vernos, 2001). Walther Flemming first described the morphology of the mitotic spindle in 1888 (Paweletz, 2001). The underlying architecture of the spindle is built by α/β-tubulin heterodimers in a uniform head-to-tail fashion forming microtubules arranged in two anti-parallel arrays (Figure 1-3). β-tubulin subunits are exposed at the faster polymerizing "plus ends (+)" facing the equator, while α-tubulin subunits are exposed at the slower polymerizing "minus ends (-)" directed towards the two spindle poles.

The spindle apparatus is a dynamic structure that switches between phases of growth and shrinkage brought about by polymerization and depolymerization, respectively (Dumont and Mitchison, 2009). At the polymerizing ends of the microtubules, tubulin subunits

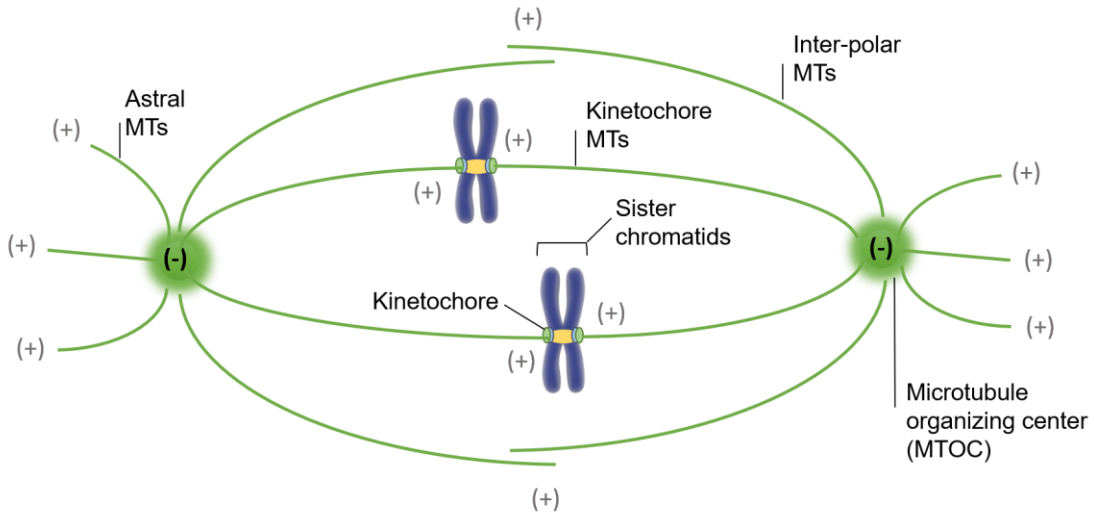

Figure 1-3: The mitotic spindle is formed by a bipolar array of microtubules.

The minus ends of microtubules are located at the spindle poles, comprising of the **m**icrotubule-**o**rganizing **c**enters (MTOCs). The antiparallel array is generated by the overlap of the radial array of microtubule plus ends directed towards the equator. The resulting spindle comprises of three different types of microtubules: kinetochore microtubules which attach the chromosome to the spindle poles, inter-polar microtubules which help in separation of the opposite poles and provide stability, and astral microtubules which radiate out from the spindle poles and contact the cell cortex, playing critical roles in spindle positioning.

bound to **g**uanosine **t**ri**p**hosphate (GTP)/ (GTP-tubulin) are incorporated. The bound GTP is subsequently hydrolyzed during or after polymerization, and Pi is released (Alushin et al., 2014; Stewart et al., 1990). This process results in the formation of a microtubule lattice that comprises of tubulin subunits bound to **g**uanosine **di**phosphate (GDP)/ (GDP-tubulin). At any given point in a population of microtubules, a subset of microtubules is rapidly growing while others are shrinking. This co-existence of polymerizing and depolymerizing microtubules generate dynamic instability (Mitchison and Kirschner, 1984). The process of transition from growth to shrinkage is called catastrophe, while the transition from shrinkage to growth is called rescue.

The formation of a bipolar spindle is critical to pull the two sets of sister chromatids into two daughter cells (Figure 1-3). The ability of mitotic chromosomes to stabilize microtubules, motor proteins to organize microtubules into a bipolar array, and two spindle poles to nucleate microtubules are critical to forming the bipolar spindle. The mitotic spindle is nucleated from **m**icro**t**ubule **o**rganizing **c**enters (MTOCs), known as centrosomes in animals or **s**pindle **p**ole **b**odies (SPBs) in yeast (Figure 1-3).

In *S. cerevisiae*, the chromosomes are attached to the spindle microtubule throughout the cell cycle (Figure 1-2B and C). While in metazoan cells the attachment of chromosomes to the spindle apparatus takes place at prometaphase (Figure 1-1). The completion of the spindle assembly in metazoans requires the breakdown of the nuclear envelope (Figure 1-2C). In systems undergoing closed mitosis, spindle assembly takes place within the nucleus and can occur before mitotic entry (Figure 1-2C) (Boettcher and Barral, 2013; De Souza and Osmani, 2007).

Centromere

The centromere was first described as the primary constriction on a mitotic chromosome. Since then, the structure of centromere DNA and its determinants have been identified across a large number of organisms (Figure 1-4) (Buscaino et al., 2010; Carroll and Straight, 2006; Yadav et al., 2018a). The first functional centromere was identified in *S. cerevisiae* by Louise Clarke and John Carbon in 1980 (Clarke and Carbon, 1980). The centromere was described as a region that can provide stability to an **a**utonomously **r**eplicating **s**equence (ARS) plasmid through mitosis and meiosis. The *S. cerevisiae* centromere is defined by an ~125 bp stretch containing three **c**entromere **D**NA **e**lements (CDEs) (Figure 1-4A). Such genetically defined short centromeres (<400 bp) is now called a point centromere. Only organisms in Hemiascomycota have point centromeres been described, and these are thought to have appeared only once during evolution (Roy and Sanyal, 2011).

The vast majority of known centromeres to date do not show strict dependence on the genetic sequence and thus thought to be epigenetically defined. Epigenetically defined centromeres can be further subdivided into short (up to 20 kb) and long (>20 kb) regional centromeres. The centromeres of *C. albicans* and *Candida dublinensis* are ~3-5 kb in length and contain unique DNA sequences across all chromosomes (Padmanabhan et al., 2008; Sanyal et al., 2004). Long regional centromeres of *S.* pombe, *C. neoformans* (described in detail later in this section) and in humans contain a mix of repetitive elements and unique DNA sequences and span from ~30 kb to several Mb (Figure 1-4B and C) (Chikashige et al., 1989; Clarke and Baum, 1990; Nechemia-arbely et al., 2019; Schueler and Sullivan, 2006; Yadav et al., 2018b).

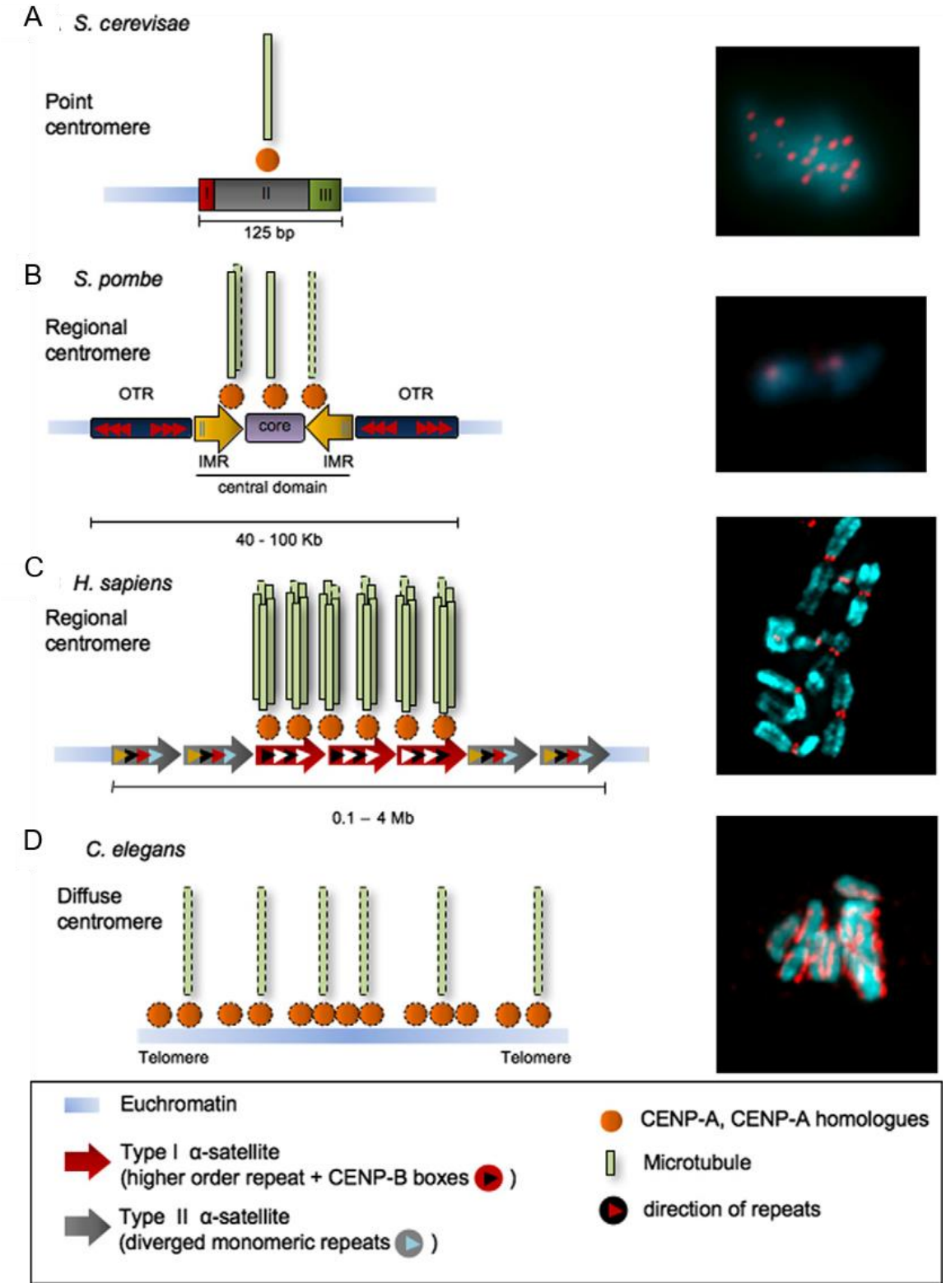

Figure 1-4: Centromere organization in eukaryotes.

CENP-A is the defining feature of most centromeres, although DNA sequence variations across species are observed. **(A)** Point centromeres of the budding yeast. Each kinetochore has been suggested to make a single microtubule attachment. *(right)* Meiotic chromosome spread of *S. cerevisiae*. Red - Ndc10 kinetochore protein; Blue - DNA. **(B)** The regional centromere of *S. pombe.* Kinetochore assembly takes place on to CENP-A,

which localizes to the non-repetitive central core (violet). This region is surrounded by innermost repeats (IMR, yellow box arrows). The outer repeats (OTR, black box) flanking the central domain are heterochromatic. 2-4 microtubule attachments are thought to be made at each kinetochore. *(right)* Chromosomes of *S. pombe*. Red – CENP-A^{Cnp1}; Blue – DNA. **(C)** A more complex regional centromere is seen in humans, which contain two families of α-satellite DNA (red and grey arrow boxes). The type-I α-satellite (red box arrow), which is associated with CENP-A, is composed of regular chromosome-specific higher-order repeating units and is characterized by the presence of CENP-B boxes (white triangles). Type-II α-satellite (grey box arrows) consists of diverged alphoid monomer units (different colored triangles). ~14-17 microtubules attach to each human kinetochore. *(right)* Partial metaphase spread of human chromosomes. Red – CENP-A; Blue – DNA. (D) Holocentric centromeres of *C. elegans.* CENP-A and kinetochore colocalize with microtubule-binding sites across the length of the chromosome. *(right)* Metaphase chromosomes of *C. elegans*. Red – Knl1; Blue – DNA. Adapted from (Vagnarelli et al., 2008).

Of interest is the recent report of the centromere architecture in the mucoromycete *Mucor circinelloides,* which suggests it may have mosaic centromeres with features of both point and regional centromeres. An ~200-bp AT-rich sequence followed by a centromere-specific motif, reminiscent of point centromere, was found to lie in a large gene-free genomic locus (~15-75 kb) containing a novel centromere-specific retroelement Grem-LINE1 (Navarro-Mendoza et al., 2019).

The above-described types of centromeres occur once per chromosome and form mono-centric chromosomes. The discovery of centromeres in nematodes suggested that the entire chromosomes can serve as sites for microtubule attachments through the kinetochore (Figure 1-4D) (Maddox et al., 2004). Such chromosomes are called holocentric chromosomes and contain holocentromeres. Insects, plants, and nematodes have been described to contain such chromosomes (Drinnenberg et al., 2014; Monen et al., 2005). Recent studies suggest that in *Caenorhabditis elegans,* the centromeres are polycentric, with point centromere like features spread across the entire chromosome (Steiner and Henikoff, 2014).

Centromere sequences are some of the fastest evolving sequences in the genome (Drinnenberg et al., 2016; Henikoff, 2001; Padmanabhan et al., 2008; Rosin and Mellone, 2017). Further, a large number of centromeres with different sequence architecture in organisms have been reported. Thus, it is a paradox that they all function to attain the same goal of mediating high fidelity chromosome segregation through the recruitment of the kinetochore (Drinnenberg et al., 2016; Henikoff, 2001).

Kinetochore

The kinetochore is a macromolecular protein bridge that forms on the centromeric loci and connects the spindle forces of the cell to chromosomes, towards ensuring accurate chromosome segregation. More than 100 proteins, including around 30 structural proteins, constitute the kinetochore ensemble in model systems, including budding yeast and human cells (Figure 1-5) (Musacchio and Desai, 2017). While the primary function of the kinetochore is to form load-bearing attachments, the kinetochore also controls the feedback mechanism for the correction of inaccurate microtubule attachments through the recruitment of components involved in the error correction mechanism and **s**pindle **a**ssembly **c**heckpoint (SAC) (Lara-Gonzalez et al., 2012; Maresca and Salmon, 2010). Additionally, kinetochore contributes to its self-preservation through the generations at the provided loci, the centromere.

Early work on the kinetochore architecture identified an inner and outer plate that was separated by a translucent layer (Brinkley and Stubblefield, 1966; Rieder, 1982). Microtubules were found to terminate on the outer plate. Today we distinguish the kinetochore sub-complexes into two layers, the inner (proximal to centromeric chromatin) and outer (proximal to spindle microtubules) layers (Figure 1-1 and Figure 1-5). In the last 20 years, great progress has been made towards the identification, analysis of sub-complex function, and their organization at the kinetochore.

More recently, the structure of whole sub-networks of proteins have been resolved, and the kinetochore particle has been reconstituted *in vitro* (Akiyoshi et al., 2010; Dimitrova et al., 2016; Hinshaw and Harrison, 2019; Jenni and Harrison, 2018; Petrovic et al., 2016; Weir et al., 2016; Yan et al., 2019). Information regarding the spatial organization of kinetochore proteins *in vivo* has been revealed in several model systems through optical and electron microscopy studies (Figure 1-5B). The budding yeast kinetochores forming on point centromeres are shown to be ~68 nm in length with a width of ~25 nm (Joglekar et al., 2009). A common feature observed across these systems in that the kinetochore length shortens in anaphase, attributed mainly to the change in conformation of the Ndc80 complex (Joglekar et al., 2009; Suzuki et al., 2011; Wan et al., 2009). The study from Tatsuo Fukagawa's group also found that the inner kinetochore is also drastically deformed in the presence of tension. CENP-T was a vital player involved in this deformation (Suzuki et al., 2011).

A

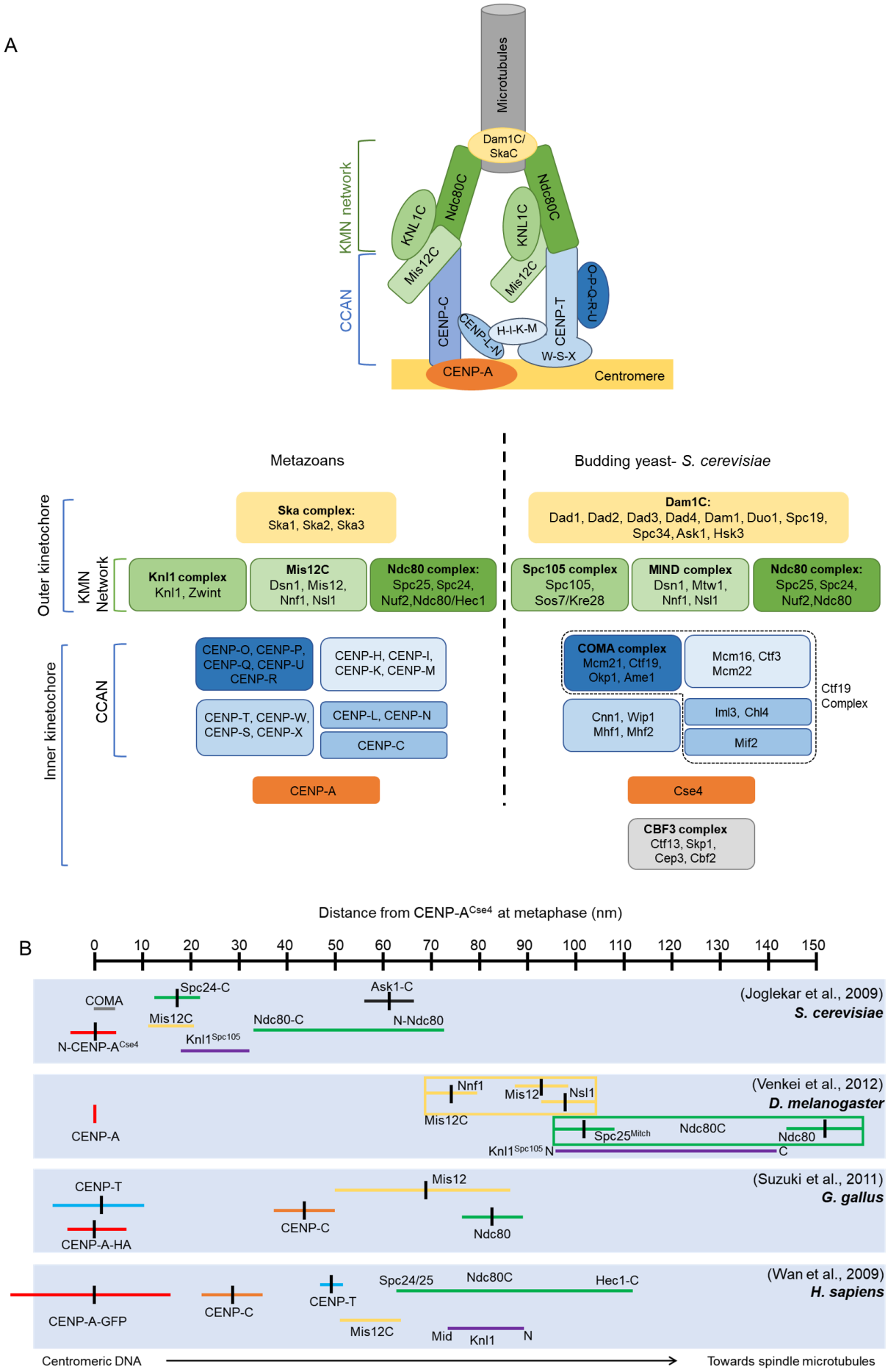
Microtubules
Dam1C/
SkaC
KMN network
CCAN
KNL1C
Ndc80C
Mis12C
CENP-C
CENP-L-N
H-I-K-M
CENP-T
W-S-X
CENP-O-P-Q-R-U
CENP-A
Centromere
Metazoans
Budding yeast- S. cerevisiae
Outer kinetochore
KMN Network
Ska complex:
Ska1, Ska2, Ska3
Knl1 complex
Knl1, Zwint
Mis12C
Dsn1, Mis12,
Nnf1, Nsl1
Ndc80 complex:
Spc25, Spc24,
Nuf2,Ndc80/Hec1
Dam1C:
Dad1, Dad2, Dad3, Dad4, Dam1, Duo1, Spc19,
Spc34, Ask1, Hsk3
Spc105 complex
Spc105,
Sos7/Kre28
MIND complex
Dsn1, Mtw1,
Nnf1, Nsl1
Ndc80 complex:
Spc25, Spc24,
Nuf2,Ndc80
Inner kinetochore
CCAN
CENP-O, CENP-P,
CENP-Q, CENP-U
CENP-R
CENP-H, CENP-I,
CENP-K, CENP-M
CENP-T, CENP-W,
CENP-S, CENP-X
CENP-L, CENP-N
CENP-C
CENP-A
COMA complex
Mcm21, Ctf19,
Okp1, Ame1
Mcm16, Ctf3
Mcm22
Ctf19
Complex
Cnn1, Wip1
Mhf1, Mhf2
Iml3, Chl4
Mif2
Cse4
CBF3 complex
Ctf13, Skp1,
Cep3, Cbf2

B

Distance from CENP-ACse4 at metaphase (nm)
0 10 20 30 40 50 60 70 80 90 100 110 120 130 140 150
COMA
Spc24-C
Ask1-C
Mis12C
Ndc80-C
N-Ndc80
N-CENP-ACse4
Knl1Spc105
(Joglekar et al., 2009)
S. cerevisiae
Nnf1
Mis12
Nsl1
Mis12C
CENP-A
Spc25Mitch
Ndc80C
Ndc80
Knl1Spc105 N
C
(Venkei et al., 2012)
D. melanogaster
CENP-T
Mis12
CENP-A-HA
CENP-C
Ndc80
(Suzuki et al., 2011)
G. gallus
Spc24/25
Ndc80C
Hec1-C
CENP-T
CENP-A-GFP
CENP-C
Mis12C
Mid
Knl1
N
(Wan et al., 2009)
H. sapiens
Centromeric DNA
Towards spindle microtubules

Figure 1-5: A model for the kinetochore and its constituents in human cells and budding yeast.

(A) Homologous kinetochore components of the inner and outer kinetochore are color-coded similarly across metazoans and budding yeast. The Ska complex in metazoans is thought to perform the homologous function of the Dam1 complex, towards assisting the maintenance of microtubule attachments as observed in fungi. The CBF3 complex in budding yeast seeds the formation of the kinetochore with its binding to the DNA sequence specified point centromeres in *S. cerevisiae.* **(B)** Spatial organization of kinetochore proteins across eukaryotes. Fluorescence microscopy was used to determine the spatial location of kinetochore subunits in the budding yeast (*S. cerevisiae*), fruit fly (*D.* melanogaster), and human cells (*H.* sapiens). Immuno-EM helped determined the ultra-structure of the kinetochore in chicken cells (*Gallus gallus*). Black vertical lines represent the mean distances of proteins from CENP-A^{Cse4}.

While our knowledge of the kinetochore is primarily through studies in model systems, analysis of the kinetochore in non-model systems is gaining importance.

The inner kinetochore

The inner kinetochore comprises of the centromeric histone H3 variant CENP (**cen**tromere **p**rotein)-A and the 16-member **c**onstitutive **c**entromere **a**ssociated **n**etwork (CCAN). The CCAN is comprised of CENP-C, CENP-H, CENP-I, CENP-K, CENP-M, CENP-O, CENP-P, CENP-Q, CENP-U, CENP-R, CENP-T, CENP-W, CENP-S, CENP-X, CENP-L, and CENP-N (Figure 1-5A). Inner kinetochore proteins were first identified by using sera from patients diagnosed with the autoimmune syndrome CREST (Calcinosis, Reynaud's syndrome, Esophageal dysmotility, Sclerodactyly, Telangiectasia) (Moroi et al., 1980). The antibodies identified three antigens CENP-A, CENP-B, and CENP-C (Earnshaw, 2015; Earnshaw and Rothfield, 1985).

CENP-A

CENP-A is in most organisms, the mark of an active centromere, although recent studies have discovered organisms that lack this essential protein (Figure 1-4 and 1-5) (Akiyoshi and Gull, 2014; Drinnenberg et al., 2014; Navarro-Mendoza et al., 2019; Nuria Cortes-Silva et al., 2019). CENP-A replaces canonical histone H3 in the nucleosome structure (Black et al., 2004). Much debate has surrounded as to what makes the CENP-A

nucleosome “special.” Structural studies suggest a more compact CENP-A nucleosome over a conventional nucleosome with subtle differences (Hasson et al., 2013; Tachiwana et al., 2011). CENP-A sequences have a highly variable **a**mino (N)-terminus (Black and Cleveland, 2011). A 22 amino acid stretch, the **C**ENP-**A t**argeting **d**omain (CATD), within the histone fold domain helps target CENP-A to the centromere (Black et al., 2004). Further debate exists as to the composition of the CENP-A nucleosome. With models existing suggesting both homotypic and heterotypic CENP-A nucleosomes in octameric or tetrameric states through the cell cycle (Black and Cleveland, 2011; Padeganeh et al., 2013; Perpelescu and Fukagawa, 2011). Given the importance of CENP-A in assembling the kinetochore, it is critical to understand its organization and inheritance.

In most organisms, CENP-A loading at the centromeres is not coupled to DNA replication, thus raising the question of how inheritance of centromeric properties is maintained in light of this dilution (Jansen et al., 2007; Pearson et al., 2004; Wisniewski et al., 2014). Several proposals, including tetrameric nucleosomes, place-holder function of histone H3.3, and the role of other factors have been suggested (Black et al., 2007; Dunleavy et al., 2011; Hayashi et al., 2004; McKinley and Cheeseman, 2014, 2015). CENP-A is loaded at the centromere through its dedicated chaperone HJURP across various systems (Erhardt et al., 2008; Mizuguchi et al., 2007; Pidoux et al., 2009; Sanchez-Pulido et al., 2009; Williams et al., 2009). With certain exceptions, CENP-A is a nearly universal feature of centromeres, yet tethering of CENP-A to an ectopic chromosomal locus is sufficient for the formation of a functional kinetochore only in a few systems (Gascoigne et al., 2011). Interestingly it has been well documented that CENP-A can be incorporated into non-centromeric loci. However, it is not well understood how cells distinguish centromeric CENP-A from non-centromeric CENP-A (Hori et al., 2014). One hypothesis is that CENP-A associated with other kinetochore proteins, those of the CCAN, are more concentrated at the centromeres (Carroll et al., 2009; Guse et al., 2011; Kato et al., 2013; Nechemia-arbely et al., 2019).

Constitutive centromere associated network (CCAN)

CCAN proteins are sub-divided into four discrete complexes: the CENP-HIKM complex, CENP-LN complex, CENP-OPQUR, complex, and the CENP-TWSX complex (Figure 1-

4). Most homologs of CCAN proteins have been identified in the budding yeast *S. cerevisiae* which is collectively named the Ctf19 complex (Figure 1-5 and 1-6B) (Akiyoshi et al., 2009; Hinshaw and Harrison, 2019; Meraldi et al., 2006; Ortiz et al., 1999; De Wulf et al., 2003). Two recent studies have revealed the structure of the CCAN/Ctf19 complex in budding yeast using cryoEM studies. These studies describe a Y-shaped opening in the CCAN/Ctf19 complex structure to accommodate CENP-A^{Cse4} (Hinshaw and Harrison, 2019; Yan et al., 2019).

CCAN proteins have several vital functions, which include the recruitment and stabilization of CENP-A, recruitment of other CCAN proteins, and in the recruitment of the microtubule-binding outer kinetochore network (Figure 1-6A) (Hara and Fukagawa, 2017, 2018, 2019; Musacchio and Desai, 2017). With these critical functions performed by the CCAN, it is surprising that CCAN components are predicted to be less conserved through evolution than their outer kinetochore counterparts. The apparent loss of most proteins of the CCAN, except CENP-C in *C. elegans* and *Drosophila melanogaster* and the importance of CCAN proteins in species that have retained them is puzzling and suggest that there is much to learn about their function and contribution at the centromere (Hara and Fukagawa, 2017; Richter et al., 2016; Westermann and Schleiffer, 2013).

CENP-C and CENP-N are two CCAN components that have been identified to interact directly with CENP-A. CENP-N interacts with the CATD on CENP-A (Carroll et al., 2009). On the other hand, CENP-C, through its central region and the CENP-C motif has been shown to interact with the divergent tail of CENP-A in addition to interactions with the acidic patch of H2A and H2B (Falk et al., 2016; Guse et al., 2011; Kato et al., 2013; Westhorpe et al., 2015). Interestingly, CENP-N and CENP-C show only a modest selectivity for CENP-A over CENP-C *in vitro* (Carroll et al., 2010; Weir et al., 2016).

The CENP-HIKM complex is implicated in stabilizing the CENP-A complex (Weir et al., 2016). Further, the CENP-HIKM complex has also been shown to be required for the recruitment of the CCAN complexes of CENP-OPQUR and CENP-TWSX (Basilico et al., 2014; Foltz et al., 2006; Okada et al., 2006; Pekgöz Altunkaya et al., 2016; Samejima et al., 2015; Thakur and Henikoff, 2016).

All members of the tetrameric CENP-TWSX complex have been shown to harbor a histone fold domain (Figure 1-8B). The CENP-TW and CENP-SX subcomplexes can

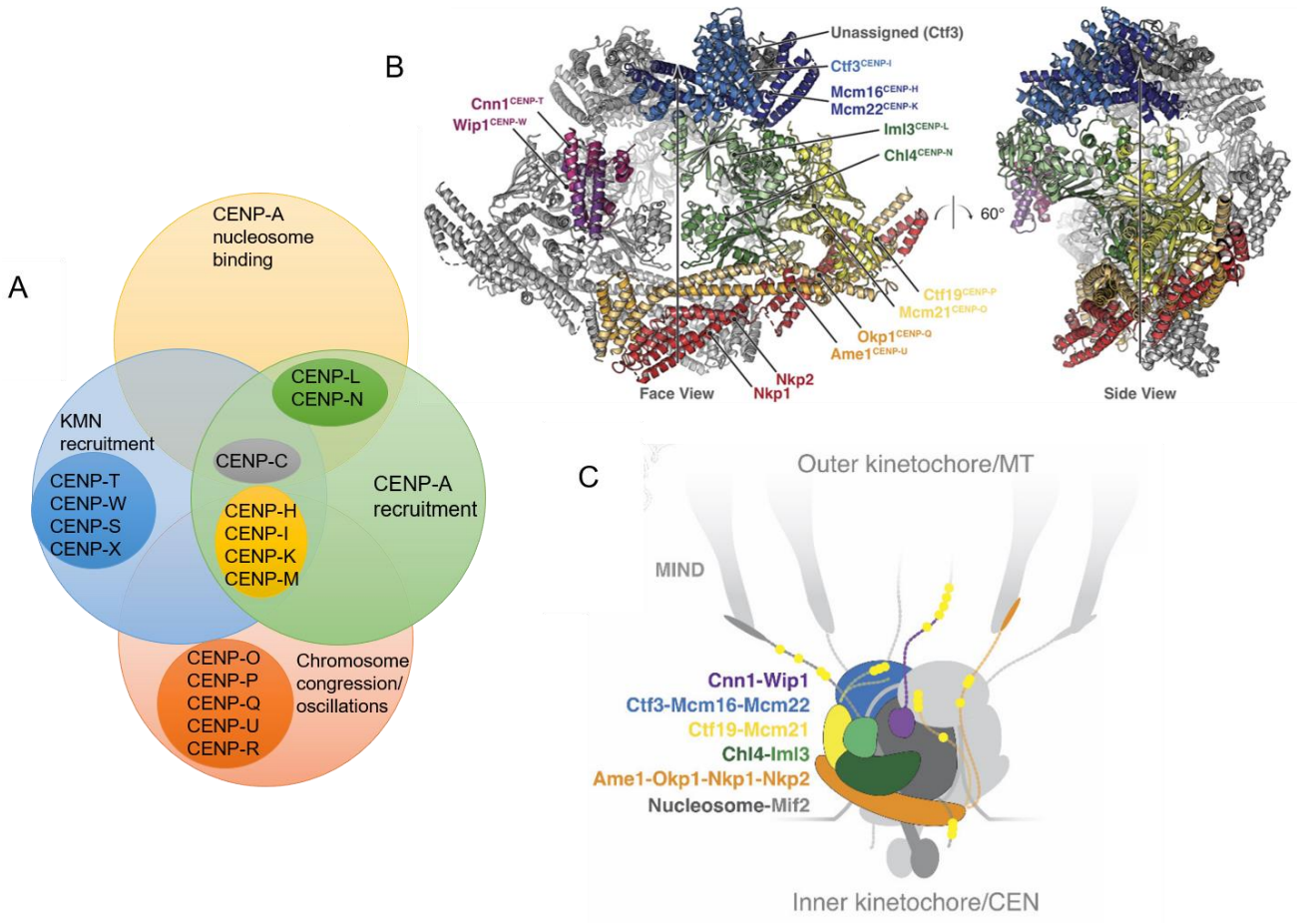

Figure 1-6: Function of the CCAN and the molecular model of the CCAN^{Ctf19}.

(A) Functions of the 16-member CCAN, grouped into sub-complexes, are mentioned based on reports for at least one of the subunits. **(B and C)** Structural model of the Ctf19 complex. **(B)**An arrow marks the twofold symmetry axis. Subunits from one monomeric assembly are colored according to their identities. Those related by twofold symmetry are colored gray. **(C)** Model of the CCAN^{Ctf19C}-CENP-C^{Mif2}-CENP-A^{Cse4} nucleosome complex. CCAN^{Ctf19C} proteins are colored as in (B). Yellow circles mark approximate positions of phosphorylation sites. Adapted from (Hinshaw and Harrison, 2019; McKinley and Cheeseman, 2015).

stably exist, while the tetrameric complex has been shown to form a nucleosome like structure (Nishino et al., 2012; Singh et al., 2010; Yan et al., 2010). The nucleosome like structure was shown to bind ~100 bp DNA *in vitro*, inducing positive supercoiling (Takeuchi et al., 2014). No chaperones have yet been shown to be required by the CENP-TWSX complex towards interaction with centromeric chromatin. Although the CENP-TWSX complex forms a nucleosome like structure with DNA, its interaction with the CENP-HIKM complex is essential for its kinetochore recruitment (Basilico et al., 2014; Pekgöz Altunkaya et al., 2016; Samejima et al., 2015; Thakur and Henikoff, 2016).

The functional role of the CENP-OPQUR complex seems to vary in different organisms. It has been shown to bind microtubules through CENP-U and CENP-Q and required for the recruitment of CENP-E in metazoans (Amaro et al., 2010; Bancroft et al., 2015; Hua et al., 2011). CENP-U is reported to be required for the recruitment of **P**olo-**l**ike **k**inase 1 (Plk1) (Kang et al., 2011). In budding yeast, the CENP-U homolog Ame1 has been shown to interact with Mis12^{Mtw1} (Hornung et al., 2014).

Localization of the CCAN is insufficient for kinetochore activity towards forming attachments to spindle microtubules. For a functional kinetochore, the recruitment of outer kinetochore proteins onto the CCAN is critical.

The outer kinetochore

The outer kinetochore functions as the primary attachment site for spindle microtubules. It also functions to recruit a feedback mechanism to correct for inaccurate attachments. The outer kinetochore is primarily composed of the KMN network (**K**NL1 complex [KNL1C], **M**is12 complex [Mis12C], and **N**dc80 complex [Ndc80C]) (Figure 1-5 and 1-7A). The protein complexes of the Dam1 complex (Dam1C) in fungi and the Ska complex (SkaC) in metazoans are considered to be part of the outer kinetochore. Their distinct roles are elaborated below.

KMN protein network

The Ndc80 complex is consisting of the four subunits Ndc80, Nuf2, Spc25, and Spc24 forms the primary contact site for microtubule attachment at the kinetochore (Cheeseman et al., 2006; Kline et al., 2006). The Ndc80 complex is largely coiled-coil, which is flanked by globular domains in the form of a dumbbell shape (Figure 1-7A). The **c**alponin-**h**omology (CH) domains mediate the microtubule-binding at the N-terminal of Ndc80 and Nuf2 (Ciferri et al., 2008; Wei et al., 2007). In addition to the CH domain an ~80 residue highly basic, a disordered region in the N-terminal tail of Ndc80 has been described to interact with microtubules (Figure 1-7A) (Ciferri et al., 2008; Guimaraes et al., 2008; Miller et al., 2008; Wei et al., 2007). Recruitment of the Ndc80 complex to the

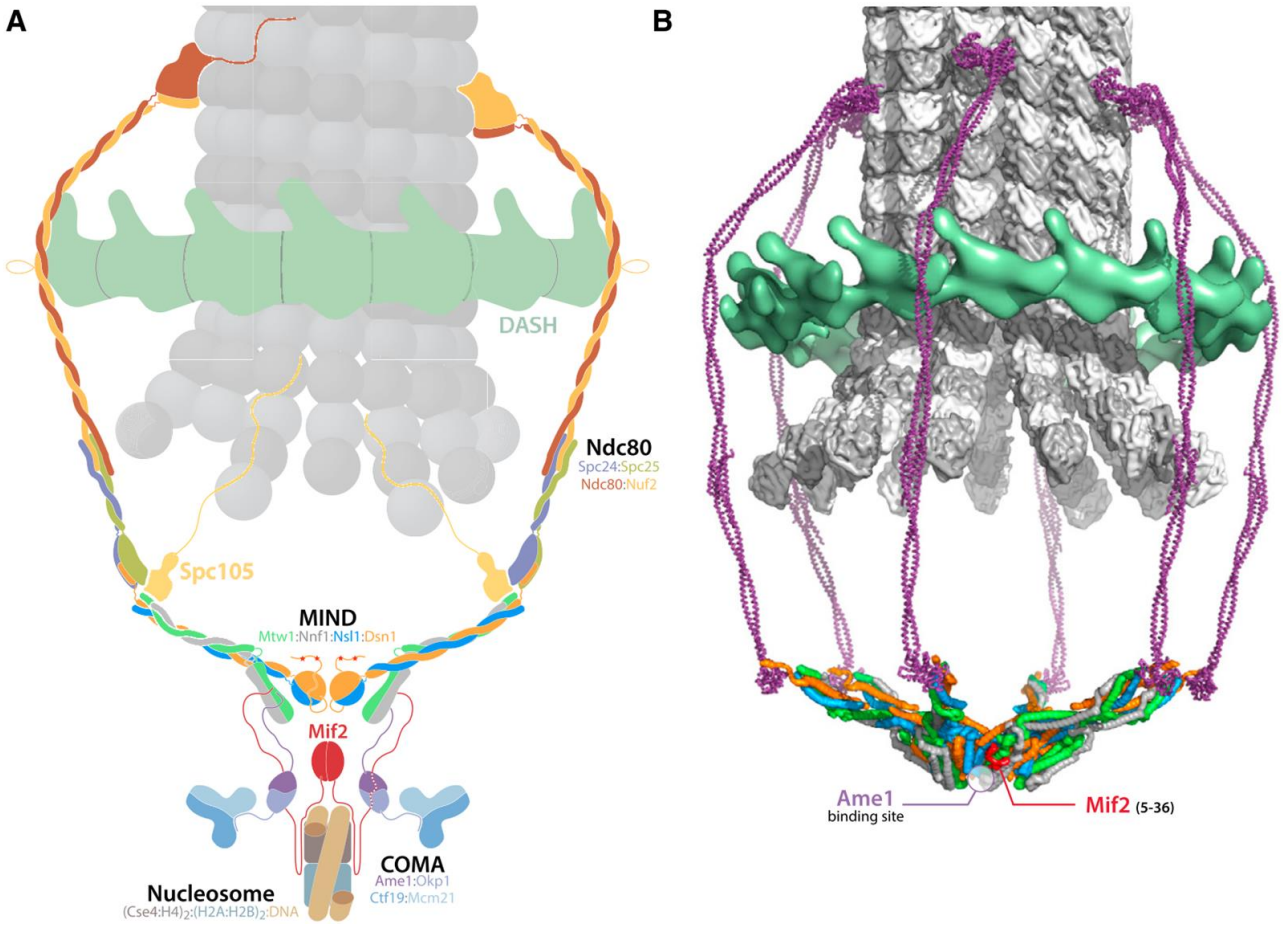

Figure 1-7: The yeast kinetochore model.

(A) Schematic of the cross-section through a point-centromere kinetochore. Various conserved molecular complexes are labeled and color-coded. The Mis12 complex occupies a central position in the hierarchy extending from the nucleosome to Ndc80/ Dam1 complex. **(B)** Surface rendering of a 3D view similar to the cross-section in (A), but omitting the nucleosome-proximal components. The choice of a 6-fold structure is arbitrary—EM images appear to show five, six, and seven (Gonen et al., 2012). Adapted from (Dimitrova et al., 2016).

---

kinetochore is mediated by the **c**arboxy (C)-terminus of Spc24 and Spc25 (Ciferri et al., 2005; Wei et al., 2005, 2006, 2007).

The Mis12 complex (known as the MIND complex in yeast) through binding sites for both the Ndc80 complex and KNL1 complex acts as a hub for the interaction of the KMN network. The Mis12 complex links other KMN subunits to the inner kinetochore through interaction with CENP-C and CENP-T (Figure 1-7A and 1-8A). Recent structural studies revealed that the subunits of the Mis12 complex (Dsn1, Nsl1, Mis12, and Nnf1) have high helical content. It was further shown that Dsn1: Nsl1and Mis12: Nnf1 pair together.

Dsn1: Nsl1motifs close to their C-terminus provided the binding sites for Spc24 and Spc25 through their C-terminal RWD domains (Figure 1-8A) (Dimitrova et al., 2016; Malvezzi et al., 2013; Petrovic et al., 2010, 2016). The C-terminus motif of Nsl1, together with the Mis12 stalk, formed the binding site for Knl1.

Knl1 is primarily intrinsically disordered and contains several docking sites for proteins. At the N-terminus, it has a conventional PP1 binding site followed by a number of Met-Glu-Leu-Thr (MELT) repeats, which are the binding sites for the SAC proteins Bub1: Bub3 (Joglekar, 2016; Musacchio, 2015). The C-terminus is more ordered and seems to contain RWD domains, as observed in Spc24 and Spc25, which is essential for its interaction with the Mis12 complex. Zwint (Sos7 in fission yeast or Kre28 in budding yeast) binds to a coiled-coil region at the C-terminus of Knl1 and forms the KNL1C (Jakopec et al., 2012; Petrovic et al., 2010, 2014, 2016).

Dam1/ Ska complex

It is speculated that a special structure is required to maintain the association of the kinetochore with the ends of the dynamic spindle microtubules. Recent studies suggest that the Dam1 and the Ska complex have the potential to perform such a function. Although for a long time, the Dam1 complex was thought to be restricted to fungi and the Ska complex to metazoans, a recent study suggested that in an exceptionally inverse manner, both complexes are widespread amongst eukaryotes (Hooff et al., 2017). Further, they go on to suggest that all subunits of the Dam1 and Ska complexes are ancient paralogs and that the Ska complex was present in the **l**ast **e**ukaryotic **c**ommon **a**ncestor (LECA) (van Hooff et al., 2017).

The Dam1 complex also called the DASH complex, is composed of 10 members (Dad1, Dad2, Dad3, Dad4, Spc34, Ask1, Dam1, Spc19, Duo1, and Hsk3) (Cheeseman, 2014). Recent cryo-EM and structural studies describe the heterodecamers to form a T-shaped like structure which subsequently comes together at conserved polar and non-polar contact sites to form a ring that can encircle a microtubule (Figure 1-6A and B) (Jenni and Harrison, 2018; Miranda et al., 2005). The complete ring has a 17-fold symmetry (Ng et al., 2019). Contacts with microtubules are predicted to occur through Dam1 and Duo1,

while Spc19 and Spc34 are suspected of interacting with Ndc80: Nuf2 of the Ndc80 complex (Kim et al., 2017; Legal et al., 2016; Zelter et al., 2015).

The Ska complex is a W-shaped heterohexamer consisting of two molecules, each of Ska1, Ska2, and Ska3 (Jeyaprakash et al., 2012). Ska1, through its winged-helix motif, interacts with the exposed microtubule surface, while the C-terminus unstructured domain on Ska3 aids in Ska1-microtubule interaction (Abad et al., 2016). Like the Dam1 complex, the Ska complex is reported to bind the Ndc80 complex and strengthen Ndc80 complex-mediated microtubule interactions (Helgeson et al., 2018; Janczyk et al., 2017).

Linker proteins and their mode of action

The kinetochore links spindle microtubules to centromere DNA. As the kinetochore itself includes distinct structures to interact with microtubules and DNA, unique proteins called linkers are needed to connect these two sets of molecular networks at the kinetochore. Although components of the CCAN are not as conserved as their outer kinetochore counterparts across a diverse set of organisms, yet to date, the only known linkers are CENP-T, CENP-C, and CENP-U^{Ame1} (Figure 1-14). These known linker proteins share a common feature in that they are recruited to the inner kinetochore following which they can interact with outer kinetochore components.

CENP-T^{Cnn1} and CENP-C^{Mif2} are the two primary mechanisms to link the outer kinetochore to centromeric chromatin, while there exists a third pathway described in budding yeast through CENP-U^{Ame1} (Musacchio and Desai, 2017). CENP-C^{Mif2}, through its N-terminus ~45 residues, interacts directly with Mis12^{Mtw1} (Figure 1-8 and 1-9A) (Dimitrova et al., 2016; Petrovic et al., 2016). In the budding yeast *S. cerevisiae*, the 4-subunit COMA complex (CENP-P^{Ctf19}, CENP-Q^{Okp1}, CENP-O^{Mcm21}, and CENP-U^{Ame1}) a part of the CCAN^{Ctf19C} has also been shown to bind to Mis12^{Mtw1}. Thus, further reinforcing the attachment of Mis12^{Mtw1} to the inner kinetochore (Figure 1-10) (Hornung et al., 2014). The CENP-U^{Ame1} pathway seems to be the dominant linker in *S. cerevisiae* since CENP-U^{Ame1} is essential for viability, whereas the Mis12^{Mtw1} binding domain of CENP-C^{Mif2} and CENP-T^{Cnn1} are dispensible (Hornung et al., 2014).

The second major linker pathway involves the CENP-TWSX complex which interacts with the Ndc80 and Mis12 complexes of the KMN network (Figure 1-8B). The RWD

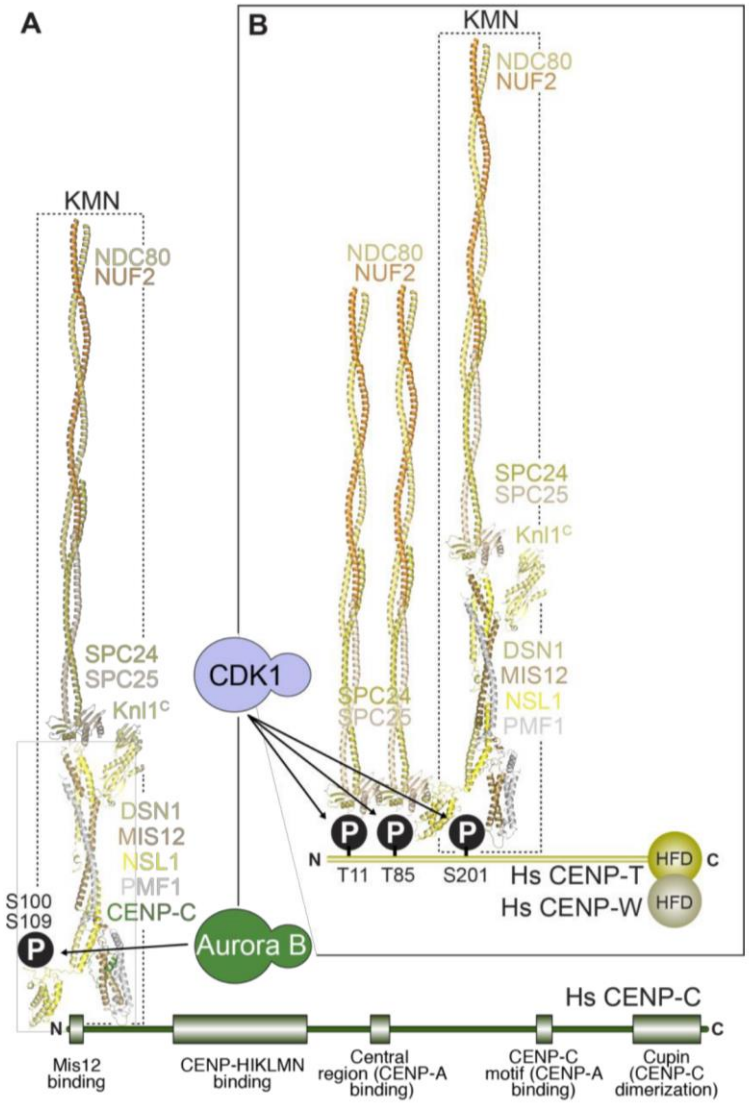

Figure 1-8: Linkages between the inner and outer kinetochore.

Structures of a portion of the Ndc80 complex, without the N-terminal globular domains of Ndc80 and Nuf2, the Mis12 complex, and the C-terminal kinetochore-targeting domain of Knl1 are used to depict a KMN particle in humans. **(A)** Interaction of the KMN network with CENP-C formes the first linkage. Phosphorylation of residues S100 and S109 on the N-terminal region of the Dsn1 subunit of the Mis12 complex enhances the interaction. (B) Up to two Ndc80 complexes interact with two CDK1-phosphorylation residues (T11 and T85) in the N-terminal of CENP-T, forming the second linkage. Additionally, a second KMN particle is recruited via a CDK1-dependent interaction of the Mis12 complex with S201 of CENP-T. The structures shown are for human complexes. Adapted from (Musacchio and Desai, 2017).

---

domains of Spc24 and Spc25 have been shown to interact with the N-terminus extension of CENP-T at two short sequence motifs within the first ~100 residues (Gascoigne et al., 2011; Hori et al., 2013; Huisin'T Veld et al., 2016; Malvezzi et al., 2013; Nishino et al.,

2013; Pekgöz Altunkaya et al., 2016; Rago et al., 2015; Schleiffer et al., 2012). In humans, this interaction requires the phosphorylation of the two CENP-T motifs by CDK1, while in the budding yeast, the interaction may be independent of phosphorylation (Gascoigne et al., 2011; Malvezzi et al., 2013; Nishino et al., 2013). Thus, through the two binding sites, it is suggested that two molecules of the Ndc80 complex can be recruited directly (Figure 1-8B).

Interestingly recent studies have suggested that the N-terminus of CENP-T, in addition to the recruitment of the Ndc80 complex, can also recruit one Mis12 complex in humans (Huisin'T Veld et al., 2016; Rago et al., 2015; Suzuki et al., 2015). While this recruitment of the Mis12 complex by CENP-T has not been described in budding yeast, in human cells, a single CENP-T can recruit up to three molecules of Ndc80 (Figure 1-8B).

Despite performing the critical function of recruiting the outer kinetochore, the architectural dependency of the linker proteins varies strikingly across evolution. In budding yeast CENP-T^{Cnn1}, CENP-C^{Mif2} and CENP-U^{Ame1} have been shown to interact with outer kinetochore proteins. In this system, CENP-T^{Cnn1} and the outer kinetochore interacting CENP-C^{Mif2} N-terminus have been described to be non-essential for viability. Thus suggesting a critical function for CENP-U^{Ame1} in budding yeast. While amongst *S. pombe*, a suppressor mutation can improve the growth of a CENP-C^{Cnp3} null mutant, while CENP-T has been described to be essential (Tanaka et al., 2009).

In metazoans, interaction with the outer kinetochore has been reported only for CENP-T and CENP-C. Recent studies in chicken have suggested that CENP-T can generate ectopic microtubule-binding sites independent of CENP-C (Nishino et al., 2013). Further, CENP-T at the native kinetochore was shown to be critical for cell viability, although the CENP-C pathway exists (Hara et al., 2018; Hori et al., 2013; Suzuki et al., 2015). In contrast, CENP-T loss in human cells results in extensive defects but is not critical (Gascoigne et al., 2011; Hori et al., 2008; Kim and Yu, 2015; Rago et al., 2015; Takeuchi et al., 2014). While disruption of the CENP-C pathway in the presence of an intact CENP-T pathway is lethal to cells. These studies suggest a dominant role of CENP-T and CENP-C in chicken and human cells, respectively.

Taken together, these results raise the question as to why systems have multiple linker pathways evolved if there is redundancy built into the architecture. More so since systems such as *D. melanogaster* and *C. elegans* exist where only CENP-C is retained with no

other linker protein present (Liu et al., 2016; Richter et al., 2016). It would be of interest to the field to understand, what are the forces driving the retention of multiple redundant linker pathways, although some pathways are non-essential for viability. A few of the possible factors are discussed in the subsequent subsection.

Kinetochore function

Rapid progress in recent years, from the reconstitution of the kinetochore to cryoEM studies resolving structures of whole kinetochore networks, has provided insights into kinetochore organization in model systems. In this section, we will discuss how kinetochore organization contributes to function, which includes the bipolar attachment, regulation, and detection of aberrant attachments and subsequent transmission of spindle forces to ensure accurate chromosome segregation.

Force propagation

While studies are focused on understanding the mechanism(s) by which a kinetochore is attached to spindle microtubules. A relative lacuna in the field exists regarding the understanding of how a kinetochore performs the critical function of propagating mitotic forces through its sub-complexes, towards the movement of chromosomes. In this aspect, linker proteins play a crucial role as they are the contact sites for the outer kinetochore and centromeric chromatin. In addition to performing the role of recruiting the outer kinetochore, linker proteins such as CENP-T and CENP-C can stretch and propagate force through them (Hara et al., 2018; del Rio et al., 2009; Ye et al., 2016). A mechanical model for force generation involving the microtubule interacting with Ndc80 and Dam1 complexes was recently described through the insertion of a FRET sensor within the Ndc80 complex (Suzuki et al., 2016).

A critical requirement for the propagation of force is to create sufficient interaction strength between the outer kinetochore complexes and the linker proteins. The interaction strength of the two prominent linker pathways is controlled by phosphorylation

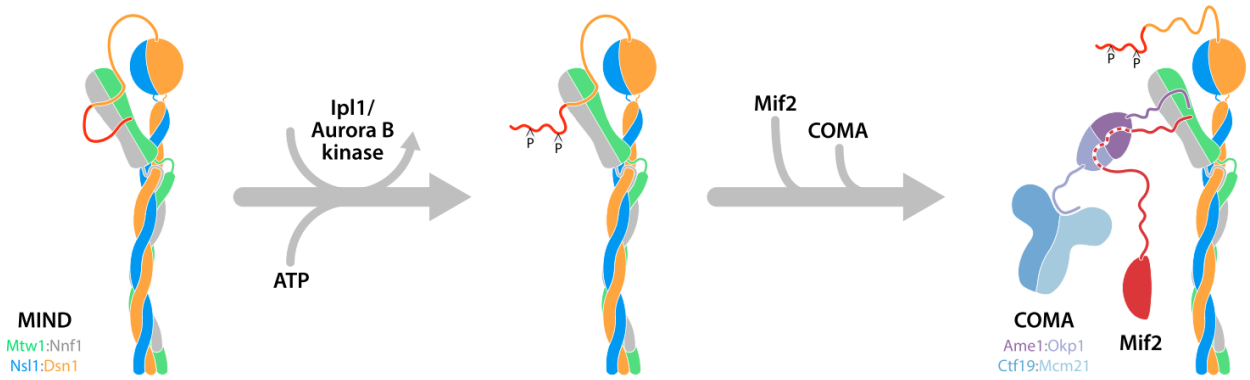

Figure 1-9: Schematic of phospho-Dsn1 binding CENP-C^{Mif2} and COMA complex.

(Left) The unphosphorylated N-terminal arm of Dsn1 205–255 in the Mis12 complex, binds two distinct sites on head I. *(Middle)* Upon phosphorylation of Dsn1 at S213 and S223 disassociates the N-terminal region of Dsn1 arm from head I. *(Right)* Mis12^{MIND} complex autoinhibition is relieved upon phosphorylation of Dsn1 S213, S223. Thus, permitting binding of CENP-C^{Mif2}1–41 and CENP-U^{Ame1}1–24 (COMA complex), which together recruit Mis12C to kinetochores. The dashed red CENP-C^{Mif2} segment indicates uncertainty concerning the interaction between COMA complex and CENP-C^{Mif2} preceding Mis12 complex recruitment. Adapted from (Dimitrova et al., 2016).

(Figure 1-8) (Dimitrova et al., 2016; Gascoigne et al., 2011; Huisin'T Veld et al., 2016; Malvezzi et al., 2013; Nishino et al., 2013; Petrovic et al., 2016). CENP-T's interaction with the Ndc80 complex is under the influence of CDK1 mediated phosphorylation in metazoans (Huisin'T Veld et al., 2016; Nishino et al., 2013; Rago et al., 2015). It is not known if this interaction is negatively influenced by PP1 post-anaphase onset.

Aurora B^{Ipl1} phosphorylation of Dsn1 has been shown to increase the binding affinity of CENP-C^{Mif2} to Mis12^{Mtw1} (Figure 1-8A and 1-9) (Dimitrova et al., 2016; Lang et al., 2018; Petrovic et al., 2016). Dsn1, in its unphosphorylated state through the competitive autoinhibitory mechanism, binds and masks the site on Mis12^{Mtw1} required for its interaction with CENP-C^{Mif2}. This autoinhibition is relieved upon Aurora B^{Ipl1} phosphorylation (Figure 1-9) (Kim and Yu, 2015; Welburn et al., 2010). Dsn1 phosphorylation is suggested to occur prior to metaphase. It is speculated to be countered by PP1 dephosphorylation upon anaphase onset, thereby effectively reducing binding affinity between CENP-C^{Mif2} and Mis12^{Mtw1} (Emanuele et al., 2008; Liu et al., 2010).

In organisms containing multiple linker pathways, the loss of one of the linkers has been shown to be compensated to a great extent by the other linker pathways (Figure 1-9)

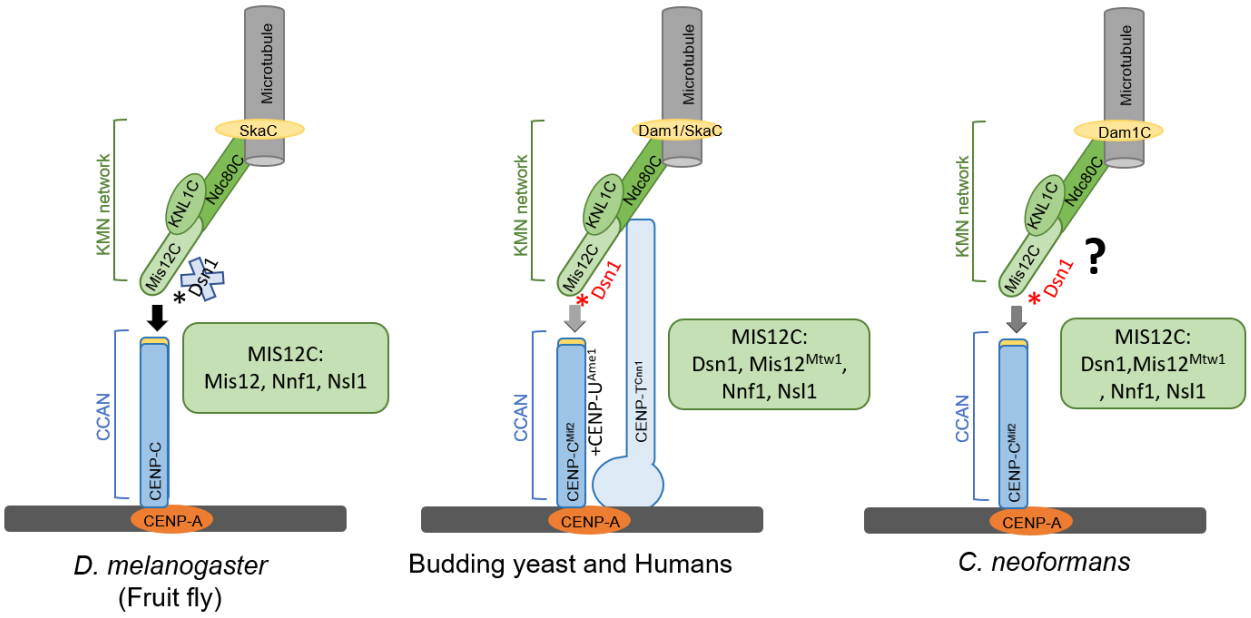

Figure 1-10: Possible outcomes of Dsn1 autoinhibition on kinetochore configuration.

(Left) Absence of CCAN and loss of Dsn1 in *D. melanogaster.* *(Middle)* In budding yeast and humans, Dsn1 is phosphorylated, as mentioned in figure 1-8A and 1-9, thereby strengthening the interaction. However, PP1's influence may drive the need for a parallel linker pathway when the interaction is compromised. *(Right)* In *C. neoformans,* Dsn1, including its basic autoinhibitory motif, is present, while linker proteins of CENP-T^{Cnn1} and CENP-U^{Ame1} are predicted to be lost. Phosphorylated Dsn1 is depicted in red. The composition of the Mis12 complex in each of the systems mentioned.

(Bock et al., 2012; Gascoigne et al., 2011; Hara et al., 2018; Malvezzi et al., 2013; Schleiffer et al., 2012; Tanaka et al., 2009). Therefore, across different organisms, it is not understood why variations over the structural dependence of one linker pathway over another exist. Taking together, a central question that has emerged is why the presence of multiple mechanisms to link the outer kinetochore to centromeric chromatin is required and if they are widely employed (Musacchio and Desai, 2017). Several studies hint at roles for multiple linker pathways towards providing sufficient force propagation to overcome Dsn1 autoinhibition (Hara et al., 2018; Hornung et al., 2014; Lang et al., 2018).

It is interesting to note that systems such as *D. melanogaster* exist wherein a single linker pathway, through CENP-C, is known. Could it be that the *D. melanogaster* kinetochore can accommodate the loss of multiple linker pathways due to the changes it has undergone at its outer kinetochore, including the loss of the Dsn1 homolog (Figure 1-10) (Liu et al., 2016; Richter et al., 2016)? Further, could the presence of numerous

kinetochore-microtubule attachment sites across the chromosome in the holocentric chromosomes of *C. elegans* overcome Dsn1 autoinhibition by a sheer number of attachment sites? It will be interesting to test if a single linker pathway is sufficient in the presence of Dsn1 autoinhibition if such a system exists. *C. neoformans* seems to offer such a system wherein bioinformatic predictions have suggested the retention of only the CENP-C^{Mif2} linker pathway while having a conserved outer kinetochore, including Dsn1 (Figure 1-10) (Hooff et al., 2017; Sridhar et al., 2017).

Forming kinetochore-microtubule attachments

Accurate chromosome segregation critically relies on the formation of attachments between microtubules arising from opposite poles to each sister chromatid (Vallardi et al., 2017). Attaining end-on attachments with the embedding of the microtubule plus-end within the kinetochore is the goal. However, kinetochores may initially associate laterally with the microtubule rather than the end. The microtubule lattice provides a larger surface than the ends, possibly providing for more effective kinetochore capture. In budding yeast, a single kinetochore attaches to a single microtubule (Winey, 1995). Hence, lateral and end-on attachments are mutually exclusive. Hence the conversion of lateral to end-on attachments results in a change in kinetochore orientation. Such conversions occur stochastically when the plus-end of the microtubule shrinks to the kinetochore attachment site (Figure 1-11A). In vertebrate cells, kinetochores bind to multiple microtubules, forming K-fibers (McEwen et al., 1997). In addition to the fibrous corona, long extensions from the outer kinetochore distribute around unattached kinetochores in a crescent-like shape, thereby forming a larger surface area for kinetochore capture (Dong et al., 2007; Wynne and Funabiki, 2015). This allows for the formation of end-on attachments while maintaining lateral attachments at the edge. In this system, end-on attachments can be formed directly or stochastically by the shrinkage of microtubules after lateral attachments, as described in budding yeast (Tanaka, 2012). In addition, several factors influence the correction of lateral to end-on attachments, as reviewed in (Monda and Cheeseman, 2018).

It is shown that the depolymerizing microtubules have sufficient force to move chromosomes through their binding by the kinetochore (Coue, 1991; Grishchuk et al.,

2005). The Ndc80 complex has been described to be the central player at the kinetochore required for forming stable kinetochore-microtubule attachment (McIntosh et al., 2008; Powers et al., 2009; Umbreit et al., 2012). Interestingly, *in vitro* studies have shown that individual Ndc80 complexes in isolation are unable to track the ends of depolymerizing microtubules unless they are oligomerized (McIntosh et al., 2008; Powers et al., 2009; Schmidt et al., 2012). *In vivo,* the bundling of Ndc80 complexes at the outer kinetochore may effectively mimic the *in vitro* oligomerized states (Dhatchinamoorthy et al., 2017; Suzuki et al., 2015). Additionally, *in vivo,* the attachment strength of the Ndc80 complex is modulated by the Aurora B^{Ipl1} phosphorylation (Cheerambathur et al., 2017; Cheeseman et al., 2006; DeLuca et al., 2018; Long et al., 2017; Posch et al., 2010).

Although being critical, the Ndc80 complex is not the sole player required to establish kinetochore-microtubule attachments. In fungi, the Dam1 complex has been shown to facilitate microtubule processivity by binding to the Ndc80 complex and microtubules. This entails the formation of a Dam1 ring that slides along microtubules as the protofilaments peel away during depolymerization (Grishchuk et al., 2008; Lampert et al., 2010; Miranda et al., 2005; Tien et al., 2010; Westermann et al., 2005). In metazoans, the previously described Ska complex is thought to be the functional homolog of the Dam1 complex (Gaitanos et al., 2009; Welburn et al., 2009). Additional factors have also been described to facilitate kinetochore-microtubules interactions (Foley and Kapoor, 2013; Maiato, 2004).

In humans, ~14-17 microtubules bind on to a single kinetochore, while in budding yeast, a single kinetochore-microtubule attachment is made (Figure 1-4) (Joglekar et al., 2008; Suzuki et al., 2015; Wendell et al., 1993). However, a characteristic shared feature for mitotic progression is the need to ensure that all kinetochores are attached to microtubules from opposite poles, referred to as amphitelic attachments. Errors in attachment can lead to one of the following states: a) unattached kinetochores b) monotelic attachments, where only one of the kinetochore of the sister chromatid pair is attached to microtubules c) merotelic attachment occurs when one of the kinetochores is attached to microtubules emanating from both poles and d) when both kinetochores are attached to microtubules from the same pole they form syntelic attachments (Figure 1-11 B-F) (Vallardi et al., 2017).

Aurora B^{Ipl1} has been implicated in the generation of unattached kinetochores upon

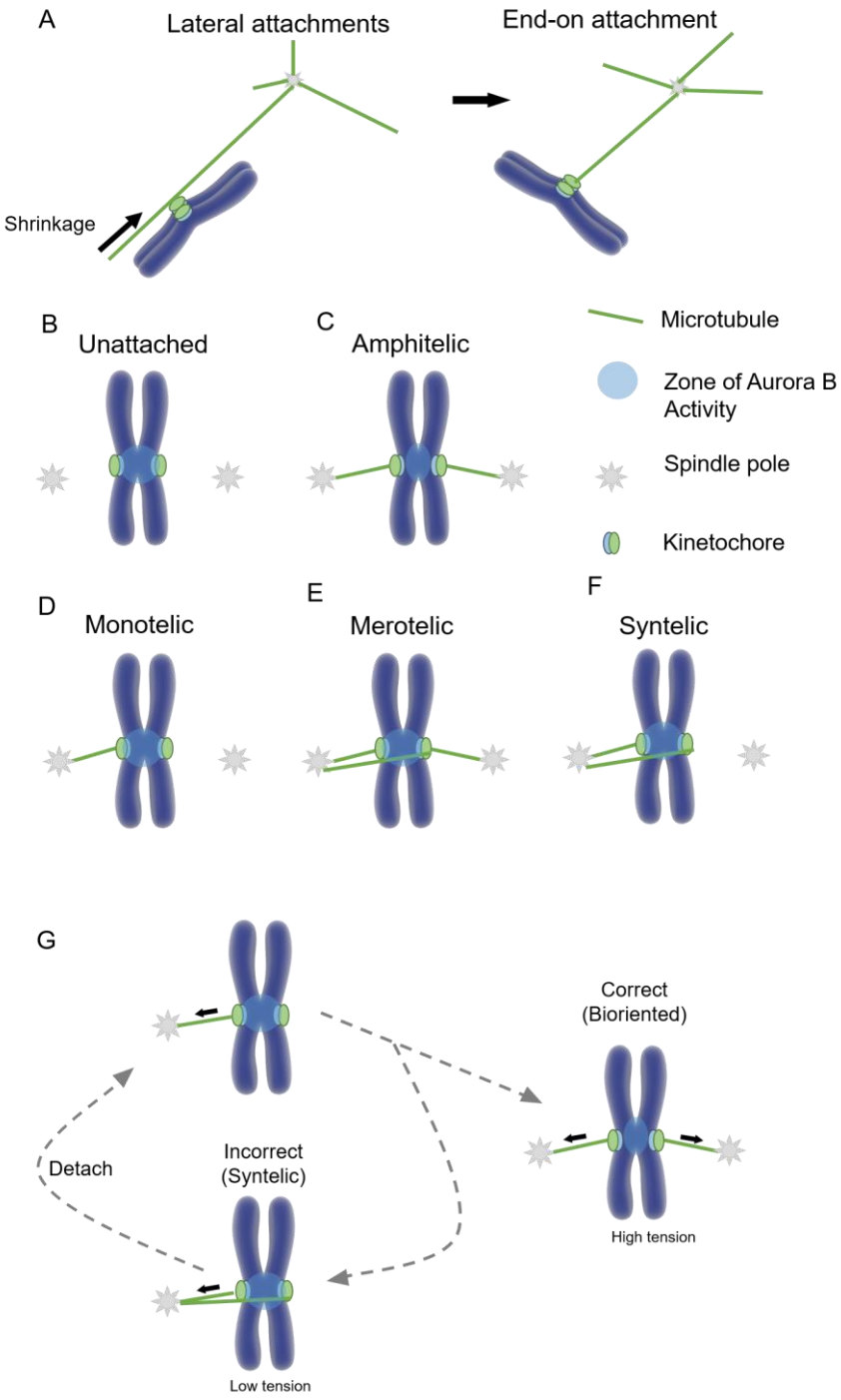

Figure 1-11: The different types of kinetochore-microtubule attachments regulated during error-correction.

(A) Lateral attachments in budding yeast are converted to end-on attachments when microtubules shrink to the kinetochore-microtubule attachment site. **(B)** A zone of Aurora B^{Ipl1} activity encompasses unattached kinetochores to destabilize any kinetochore-microtubule attachments that form. **(C)** Following bipolar attachment, tension across the kinetochore stabilizes microtubules by restricting Aurora B^{Ipl1} from phosphorylating critical kinetochore substrates. **(D-F)** The various types of microtubule attachments that do not generate sufficient tension and can, therefore, be destabilized by Aurora B^{Ipl1}. **(G)** The accuracy of mitosis depends on trial-and-error and selective stabilization of correctly

‘bioriented’ attachments. Incorrect attachments are detached by Aurora B^{Ipl1} phosphorylation of the outer kinetochore components, including Ndc80. Adapted from (Sarangapani and Asbury, 2014; Vallardi et al., 2017).

sensing unequal tension at the kinetochore, a readout for improper attachments. Such a situation arises primarily during synthetic or merotelic attachment. Aurora B^{Ipl1} generates unattached kinetochores through phosphorylation of the Ndc80 complex subunits, thereby reducing the affinity for microtubules (Figure 1-11G) (Khodjakov and Pines, 2010; Maresca and Salmon, 2010; Pinsky et al., 2006). These unattached kinetochores activate the SAC (described below) and allowing for correct attachment to take place.

While biorientation is the desired state, defects in any of the chromosome segregation machinery can result in the above-mentioned erroneous attachments. If these erroneous attachments go unresolved, unequal and improper forces act on segregating chromosomes. Therefore, resulting in incorrect segregation events such as micronuclei formation, lagging, non-disjunction, and unequal segregation of chromosomes. These segregation events result in varied fitness from the parent. Aneuploidy states often seen in cancers and fungal resistance. A dedicated surveillance mechanism in place in cells called the SAC correct for such errors (Lara-Gonzalez et al., 2012; Musacchio, 2015; Musacchio and Salmon, 2007).

Spindle assembly checkpoint (SAC)

The SAC monitors the bi-orientation of chromosomes and halts the progression of mitosis in cells to ensure the proper attachment, alignment, and the precise timing of sister chromatid separation (Figure 1-12) (Musacchio, 2015). The checkpoint proteins are conserved from yeast to humans (Hooff et al., 2017; Vleugel et al., 2012). Most checkpoint proteins are named **b**udding **u**ninhibited by **b**enzimidazole proteins (Bubs) or **m**itotic **a**rrest **d**eficient proteins (Mads) and are temporarily recruited to the kinetochore. The failure of checkpoint function in the presence of erroneous kinetochore-microtubule attachments results in segregation defects. So how do checkpoint proteins function?

Similar to other signaling pathways, the SAC comprises of a sensory apparatus consisting of Bub1, Bub3, Mps1, Mad1, and Mad2, that is recruited predominantly to Knl1^{Spc105}

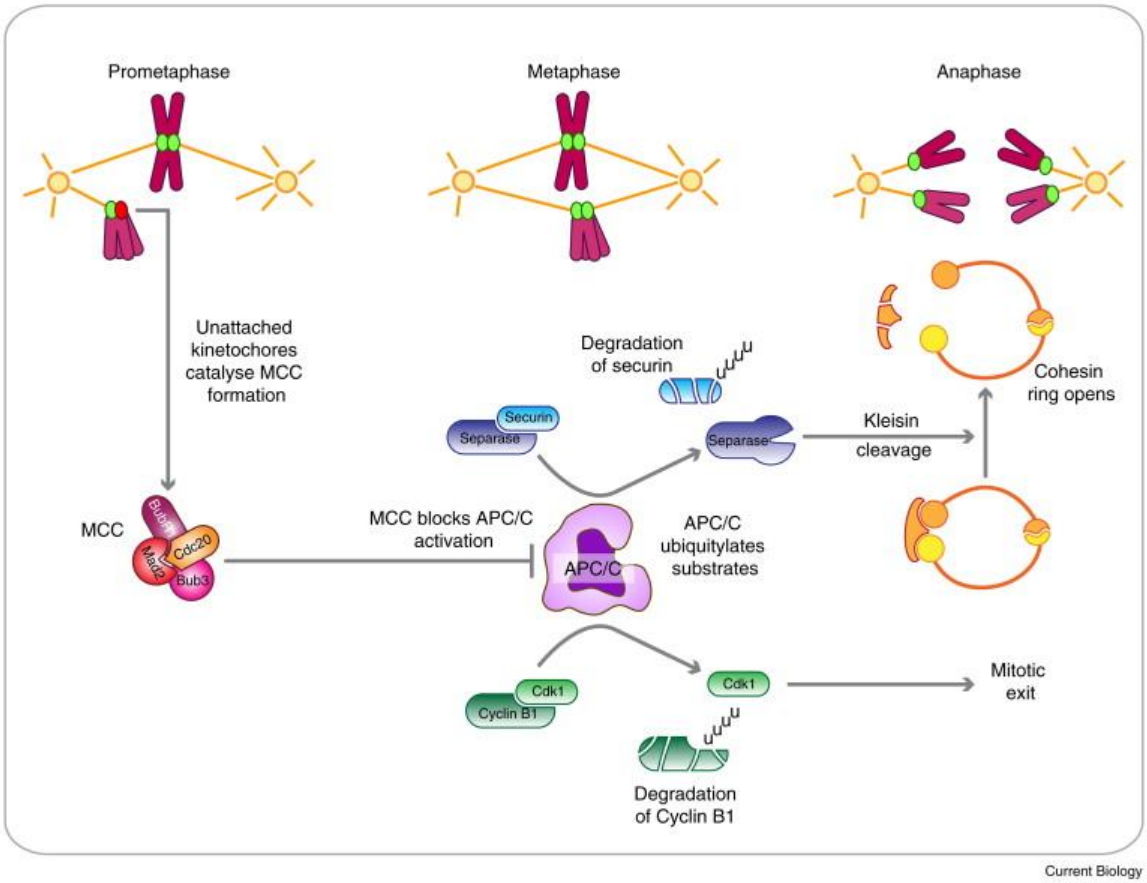

Figure 1-12: Schematic of spindle assembly checkpoint activity.

During the early stages of mitosis, prometaphase, unattached kinetochores catalyze the formation of the MCC, composed of BubR1/Mad3, Bub3, Mad2, and Cdc20, leading to inhibition of the APC/C. Once all the kinetochores are bioriented and aligned, the generation of the MCC halts, allowing the co-factor, Cdc20, to activate the APC/C, leading to the ubiquitylation and degradation of securin and cyclin B1. Degradation of securin frees separase. Active separase, in turn, cleaves the kleisin subunit, Scc1, of the cohesin ring structure, opening the ring and allowing sister chromatids to separate in anaphase. Meanwhile, the degradation of cyclin B1 inactivates Cdk1, leading to the mitotic exit. Adapted from (Lara-Gonzalez et al., 2012).

(Howell et al., 2004; Perpelescu and Fukagawa, 2011; Primorac et al., 2013; Shepperd et al., 2012; Silió et al., 2015; Varma and Salmon, 2012). The Ndc80 complex has been shown to play a role in Mps1 recruitment (Aravamudhan et al., 2015; Hiruma et al., 2015; Kemmler et al., 2009). These sensory subunits increase in concentration if erroneous attachments are detected and reduced if proper attachments are established (Figure 1-12). It is suggested that the checkpoint “acts as a rheostat rather than a toggle switch” (Collin et al., 2013). Thus, implying that the higher the number of unattached kinetochores, the more robust the SAC signal is.

The effector systems constitute of the **m**itotic **c**heckpoint **c**omplex (MCC), composed of BubR1/Mad3 (in fungi), Bub2, Cdc20, and Mad2, which targets the **a**naphase-**p**romoting **c**omplex or **c**yclosome (APC/C) (Chao et al., 2012; Liu and Zhang, 2016; Musacchio and Salmon, 2007). The APC/C, a ubiquitin ligase, targets two key substrates, cyclin B and securin, through polyubiquitination promotes their rapid degradation and triggers the exit from mitosis (Chang and Barford, 2014; Primorac and Musacchio, 2013). Thus, the MCC can inhibit the progression of mitosis by inhibiting the APC/C through the sequestering of its co-factor Cdc20 (Figure 1-12).

In between these two endpoints of the signaling pathway is Mad2, which acts as a catalyst towards the goal of the effector accumulation. In the popular model, the kinetochore localized SAC proteins detect the erroneous attachment and convert the Mad2 from the open form to the closed-form (De Antoni et al., 2005; Yang et al., 2008). The closed-form associates with the other MCC subunits to form an active MCC, which in turn inhibits the APC/C (Figure 1-12) (Lara-Gonzalez et al., 2012; Musacchio, 2015; Sacristan and Kops, 2015). Once the kinetochore attachments are satisfied, MCC is rapidly broken down through multiple mechanisms to release the arrest (Howell et al., 2001; Joglekar, 2016; Lara-Gonzalez et al., 2012; Musacchio, 2015).

Kinetochore assembly and dynamics

While the crystal structure and cryoEM studies give us a picture of contacts and interactions, the process of kinetochore organization is much more complex *in vivo*. It as yet remains difficult to examine the precise structure of the kinetochore *in vivo*. Thus, interdependency studies provide us a window to understand how the kinetochore is assembled and subsequently organized. Organisms have been described to undergo a varied mode of kinetochore assembly across evolution (Figure 1-13).

The kinetochore in budding yeast was found to be completely assembled all through the cell cycle, with the exception of a short duration in the S phase (Kitamura et al., 2007). While in most organisms, kinetochore establishment begins with CENP-A, in point centromere containing organisms such as *S. cerevisiae* kinetochore establishment begins with the CBF3 complex binding to the CDEIII element (Figure 1-13A). Studies have shown that the kinetochore in *S. cerevisiae*, although assembled on a given platform

throughout the cell cycle, is dynamics in nature. With the Ndc80 and Mis12^{MIND} complexes adding copies to the kinetochore in anaphase (Dhatchinamoorthy et al., 2017). Recently CENP-T^{Cnn1} was shown to reach a peak concentration at the kinetochore during anaphase (Bock et al., 2012). These results suggest that a distinct anaphase kinetochore configuration exists in budding yeasts.

The fission yeast, *S. pombe*, shares a similar kinetochore constitution throughout the cell cycle as in budding yeast except for Dam1 of Dam1 complex, which is kinetochore localized exclusively in M phase (Liu et al., 2005; Sanchez-Perez et al., 2005). Interdependency studies have established a hierarchal assembly of the kinetochore in both budding and fission yeast (Figure 1-13 A and B) (Hornung et al., 2014; Liu et al., 2005; Sanchez-Perez et al., 2005; De Wulf et al., 2003; Yamagishi et al., 2014). Interestingly, although the kinetochore is present all through the cell cycle in the pathogenic budding yeast *C. albicans*, the dependency of all subunits to all other subunits suggests that the kinetochore is assembled *en bloc* (Roy et al., 2011; Thakur and Sanyal, 2012).

In contrast, metazoans have been shown to undergo structural maturation of the kinetochore post-nuclear membrane breakdown (Brinkley and Stubblefield, 1966; McEwen et al., 1998; Roos, 1973). Numerous kinetochore protein components have been shown to undergo assembly and disassembly during mitosis on a platform of CCAN (Liu et al., 2006; Maiato, 2004; Musacchio and Desai, 2017). The regulation of the outer kinetochore was shown to be driven primarily by mitotic phosphorylation downstream of CDK1. Further, it was shown that the mitotic exclusive localization of the Ndc80 complex as a consequence of nuclear exclusion. Proteins of the KMN network reach a maximum intensity around metaphase, and disruption of the temporal regulation leads to chromosome segregation defects (Gascoigne and Cheeseman, 2013).

In CCAN deficient (except CENP-C) *D. melanogaster* system, precocious assembly of the outer kinetochore was prevented by the nuclear exclusion of Knl1^{Spc105}. It is suggested that the outer kinetochore assembly in the fly occurs independent of post-translational modifications and reach a peak concentration at anaphase (Przewloka et al., 2007; Venkei et al., 2012).

In summary, these studies aid in the understanding of the dynamics and organization of kinetochore assembly in space and time during mitosis. Additionally, understanding the

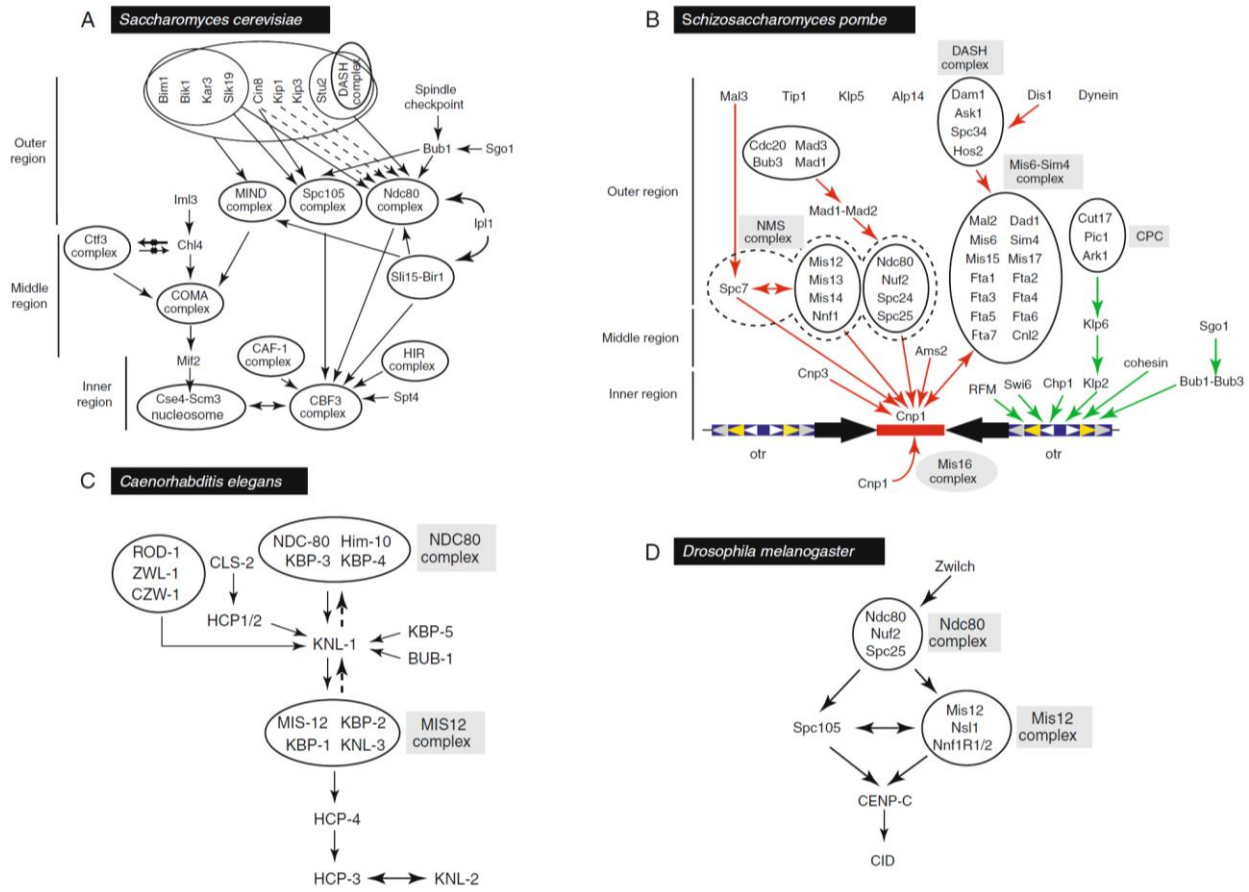

Figure 1-13: Assembly of nonvertebrate kinetochores.

(A) Assembly of the *S. cerevisiae* kinetochore. Kinetochore formation is initiated by the localization of the CBF3 complex onto a sequence defined point centromere. **(B)** Assembly of the *S. pombe* kinetochore. The red arrows indicate proteins that are recruited to the central core region, the green arrows those that are recruited to the outer repeats. Lines with double arrows symbolize protein interdependencies for localization to the centromere. **(C)** Assembly of the *C. elegans* kinetochore. The dashed lines represent partial recruitment dependencies. **(D)** Assembly of the *D. melanogaster* kinetochore. Nnf1R1 and Nnf1R2 are two Nnf1 homologs. This is adapted from (Fukagawa and De Wulf, 2009)

---

kinetochore organization assists in placing new/existing kinetochore players within the kinetochore assembly hierarchy (Jakopec et al., 2012; Schleiffer et al., 2012; Suzuki et al., 2018).

To understand the minimal subunit required to form a functional kinetochore tethering assays has proved to be a useful tool. In vertebrates, it was shown that CENP-C and CENP-T could independently form functional kinetochores at ectopic loci (Gascoigne et al., 2011; Hori et al., 2013). Tethering of CENP-A^{Cid} in *D. melanogaster* was sufficient to

nucleate the formation of a functional centromere-kinetochore structure (Mendiburo et al., 2011). Using an elegant assay wherein kinetochore proteins were tethered to replication-competent mini-chromosome Stefan Westermann, and colleagues described that as far down the kinetochore hierarchy as the Dam1 complex subunit, Ask1 was able to attach to the mitotic spindle and segregate the mini-chromosomes (Kiermaier et al., 2009; Schleiffer et al., 2012). Further, while the assembly of the kinetochore has been relatively well studied, there is a lack of studies addressing the process of disassembly, although PP1 has been implicated in certain vertebrate contexts (Gascoigne and Cheeseman, 2013). Thus identifying the process of kinetochore disassembly is an interesting area of future research.

Although it has been discovered that kinetochore complexes take several approaches to reach a functional kinetochore state, the goal to form accurate attachments with spindle microtubules remains a constant. Across evolution, it is not just the dynamics of assembly, but the conservation of the kinetochore subunits itself that is found to be varied. While the budding yeast and vertebrate systems discussed here have a conventional kinetochore, the recent availability of sequenced genomes from a large number of species has made it possible to predict kinetochore composition across eukaryotic evolution.

Kinetochore conservation across eukaryotes

Studies in budding yeast have suggested that tethering a microtubule-binding protein to chromatin, such as Ask1, is sufficient to facilitate mitotic chromosome segregation (Lacefield et al., 2009). The generated system is similar to the simple prokaryotic segregation systems, consisting of a handful of proteins to connect the DNA to the segregation machinery. Thus, why did eukaryotic systems that emerged from prokaryotic lineages result in increased complexity of the segregation apparatus? A recent *in silico* study suggested the origin of kinetochore proteins from prokaryotic lineages and was assisted by gene duplication (Tromer et al., 2019). Could the driving forces of kinetochore evolution in eukaryotes be identified from the analysis of unconventional systems harboring variations from known kinetochore models?

Insights into kinetochore composition and their conservation were initially gained through studies in vertebrate and yeast model systems (Figure 1-14A and C) (Baker et al., 1989; Bock et al., 2012; Cai and Davis, 1989; Cheeseman et al., 2004; Foltz et al., 2006; Kouprina et al., 1993; Lechner and Carbon, 1991; Meraldi et al., 2006; Musacchio and Desai, 2017; Obuse et al., 2004; Okada et al., 2006; Schleiffer et al., 2012; Spencer et al., 1990; De Wulf et al., 2003). *D. melanogaster* and *C. elegans* to this day remain distinct species with no members of the CCAN being identified except CENP-C (Figure 1-10) (Barth et al., 2014; Blumenthal, 2004; Cheeseman et al., 2004; Liu et al., 2016; Maddox et al., 2004; Przewloka et al., 2007; Richter et al., 2016). The *D. melanogaster* system additionally has undergone changes to its outer kinetochore, having lost Dsn1 and Zwint and gaining a paralog of Nnf1 (called Kmn1) (Liu et al., 2016).

In recent years with the availability of genome sequences and improved bioinformatic tools, the identification of unconventional kinetochores has been accelerated. The most striking example of this deviation from the standard kinetochore model presented in humans and budding yeast is that of the kinetoplastid kinetochore. In *Trypanosoma brucei*, a kinetoplastid, no homologs for any of the known kinetochore proteins, including CENP-A, CCAN, KMN network, and the Dam1 complex, have been identified (Akiyoshi and Gull, 2014). Instead, a novel set of kinetochores proteins have been discovered. It was suggested that some of the kinetochore proteins resembled that of the Ndc80 complex, although lacking the CH domain (D'Archivio and Wickstead, 2017). Remarkably not all Excavata species seem to have such a diverged kinetochore composition. *Giardia intestinalis* is predicted to have retained CENP-A and the KMN network. It would be fascinating to know what was the driving force was behind this change in kinetoplastids.

Interestingly a recent study has described the recurrent loss of CENP-A and CENP-C in insect species, possibly resulting in a transition to holocentricity (Drinnenberg et al., 2014, 2016). Amongst these Lepidoptera insects, CENP-T is suggested to play a major role in recruiting the Mis12 complex, although other CCAN proteins are shown to be required for the recruitment of the Ndc80 complex (Nuria Cortes-Silva et al., 2019). A similar phenomenon was reported in the fungal subphylum of Mucoromycotina, where a loss event involving CENP-A and CENP-C was observed, although the transition from monocentric to holocentriticity was not reported (Navarro-Mendoza et al., 2019). CENP-T is also speculated to play a dominant role in *Mucor sp.* Thus, further analysis of these

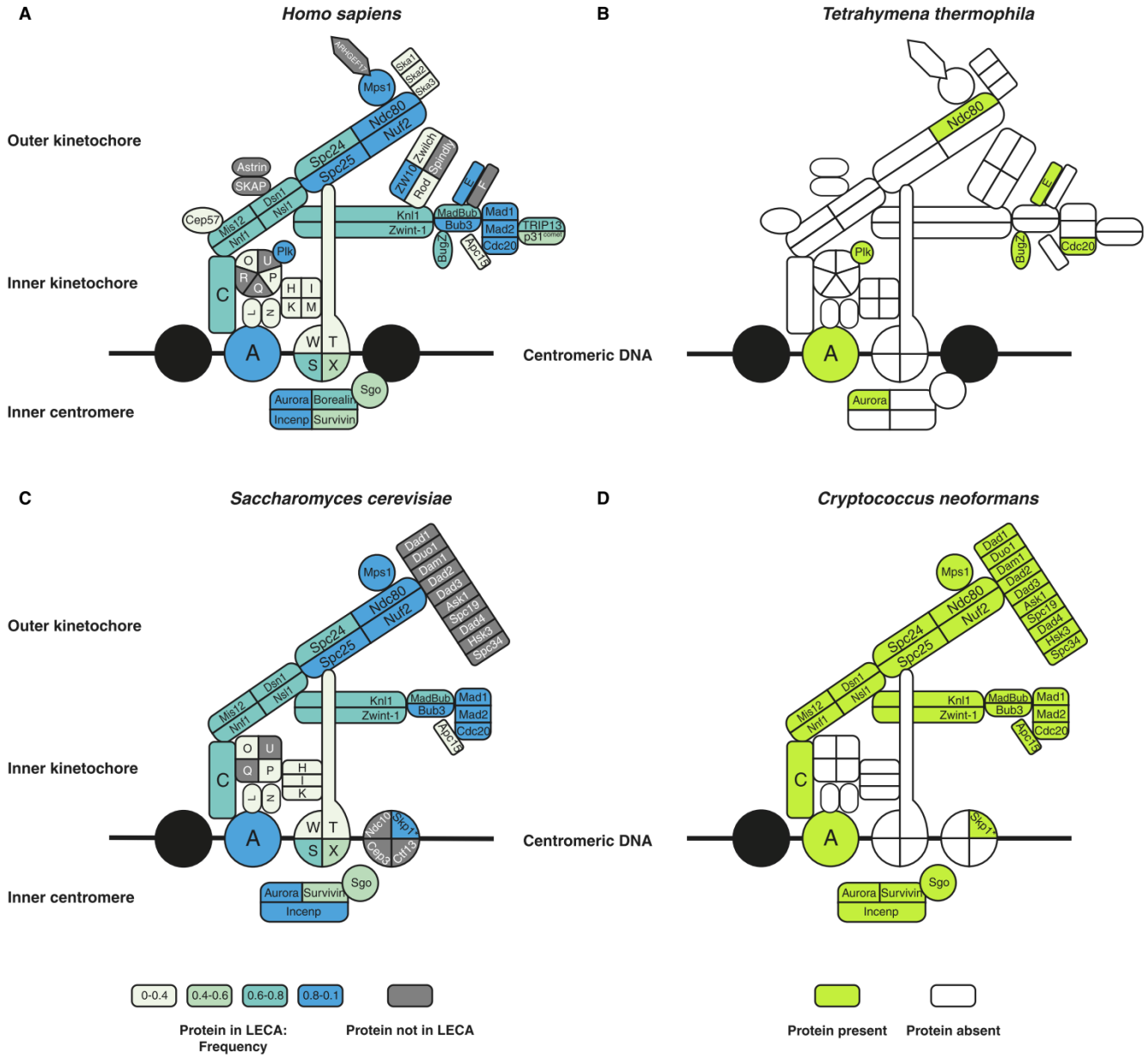

Figure 1-14: Kinetochores in the model and non-model systems.

(A-D) The colors of the proteins indicate if they were inferred to be present in LECA and their occurrence frequency across eukaryotes. **(A)** The human kinetochore. **(B)** The predicted kinetochore of *Tetrahymena thermophila* projected onto the human kinetochore. **(C)** The budding yeast kinetochore. Similar to the panel (B). **(D)** The predicted kinetochore of *C. neoformans* projected onto the budding yeast kinetochore. Adapted from (Hooff et al., 2017).

---

kinetochores is needed to understand their architecture and organization. An in-depth bioinformatic prediction of kinetochore conservation and origin of kinetochore proteins across eukaryotes was recently performed (Figure 1-14) (Hooff et al., 2017). These

findings implicate the outer kinetochore components to be more conserved than their inner kinetochore counterparts (Hooff et al., 2017; van Hooff et al., 2017; Tromer et al., 2019). Substantial *in vivo* studies to validate these findings are needed in the future. From these studies, it can be speculated that the conserved kinetochore composition observed in humans and budding yeast are an exception rather than the norm.

"The greater the diversity, the greater the perfection" – Thomas Berry

Despite the variation, all these organisms are predicted to undergo accurate chromosome segregation, which remains a constant. Thus, understanding the driving force for the variation would aid in understanding the key features of kinetochore function. Is it the limitations on force propagation, the formation of accurate kinetochore-microtubule attachments, or their structural propagation through the generations? With large diversity and the availability of rather genetically malleable systems, fungal systems present an excellent opportunity to explore this field of unconventional kinetochores.

Introduction to fungal systems

Fungi evolved close to a billion years ago, as suggested by analysis of the evolutionary rates, although strong archaeological evidence is scanty (Lücking et al., 2009). The advent of molecular phylogenetic analysis in the 1990s have greatly contributed to the understanding of fungal origins and evolution. Currently, true fungi that make up the fungal kingdom comprise of Blastocladiomycota, Chytridiomycota, Microsporidia, Glomeromycota, Neocallimastigomycota, Ascomycota and Basidiomycota (the latter two are combined in the subkingdom Dikarya) (Figure 1-15). Basidiomycota is suggested to have diverged from the well-studied fungal model systems of Ascomycotina around ~300 million years ago (Taylor TN, Krings M, 2015). It is suggested that there are currently ~120,000 species of fungi known (Blackwell, 2011; Hawksworth, 2001; Heitman et al., 2017). Ascomycota and Basidiomycota make up almost two-thirds and one-third of all known fungi, respectively, with a small fraction of known fungi belonging to other fungal phyla.

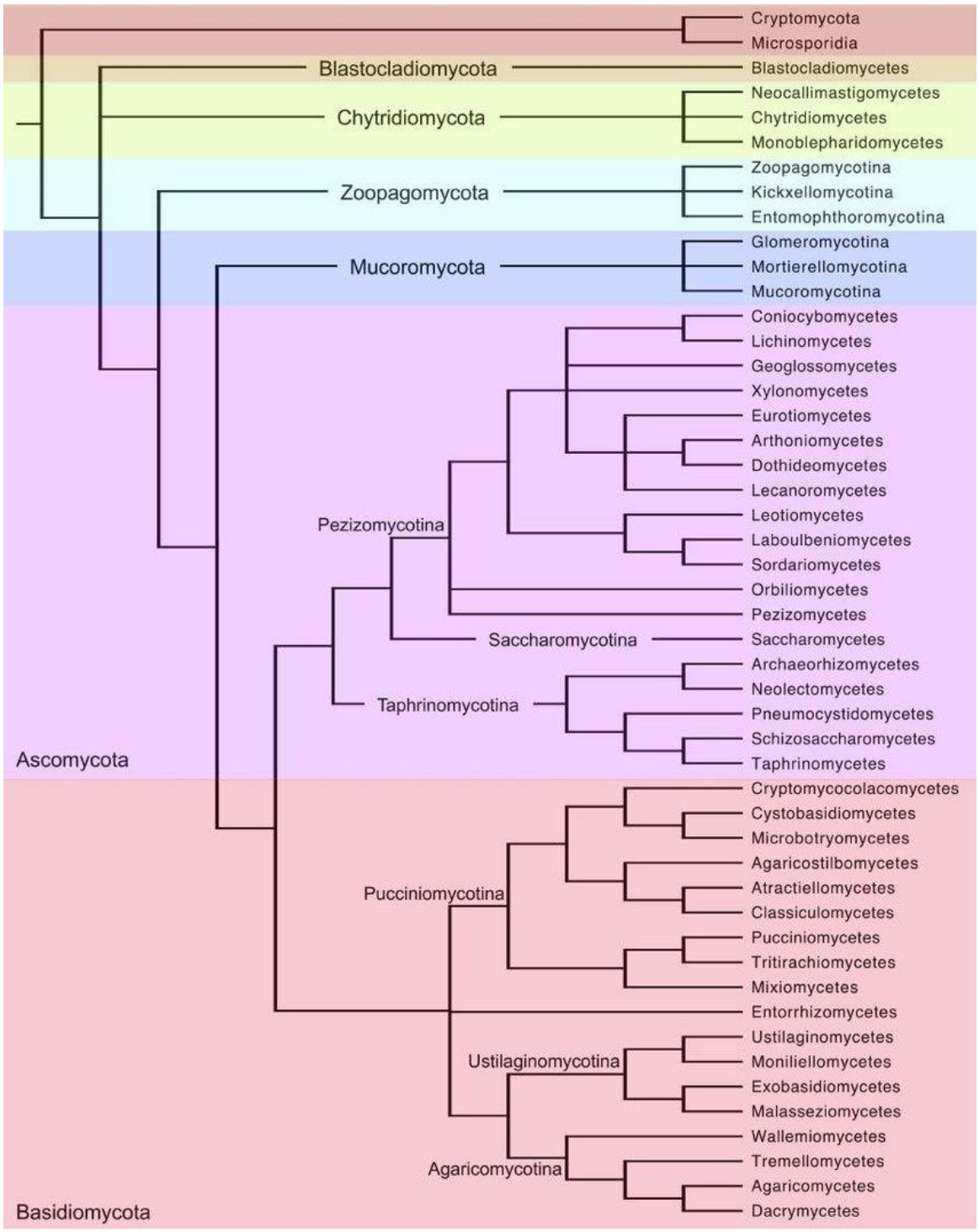

Figure 1-15: Summary of the advances in understanding fungal relationships in the genomic era.

The cladogram was derived from published multi-gene and genome-scale phylogenies. This is adapted from (Heitman et al., 2017).

Cryptococcus neoformans

Classification

Kingdom: Fungi

Subkingdom: Dikarya

Phylum: Basidiomycota

Sub-phylum: Agaricomycotina

Class: Tremellomycetes

Order: Tremellales

Genus: *Cryptococcus*

Species: *Cryptococcus neoformans var. grubii*

The genus *Filobasidiella* contains an approximate 38 *Cryptococcus* species. While only a few are pathogenic, they do constitute the pathogenic *Cryptococcus* species cluster. *Cryptococcus neoformans* is an opportunistic fungal pathogen that is found worldwide. The genome assembly of *C. neoformans var. grubii* was made available in 2014 (Janbon et al., 2014). The genome of 18.60 Mb contains 6941 protein-coding genes in 14 chromosomes. The haploid type strains of H99α and KN99 are used as wild-type strains for laboratory dissection.

Life cycle and sexual cycle

C. neoformans is often isolated in the haploid budding yeast form from patients or environmental sources such as pigeon guano, soil, decaying vegetables, and trees (Figure 1-16) (Lin, 2009). However, it has been observed that being a heterothallic basidiomycete fungus *C. neoformans* can undergo a dimorphic transition between the yeast and fungal forms (Figure 1-16). This transition can take place through two distinct pathways: monokaryotic fruiting and mating (Kozubowski and Heitman, 2012; Lin and Heitman, 2006). It was over four decades ago that mating in *C. neoformans* was discovered (Kwon-Chung, 1975, 1976). It involves the production of dikaryotic filaments upon the fusion of two opposite mating types, **a** and α. Following which it leads to the formation of the

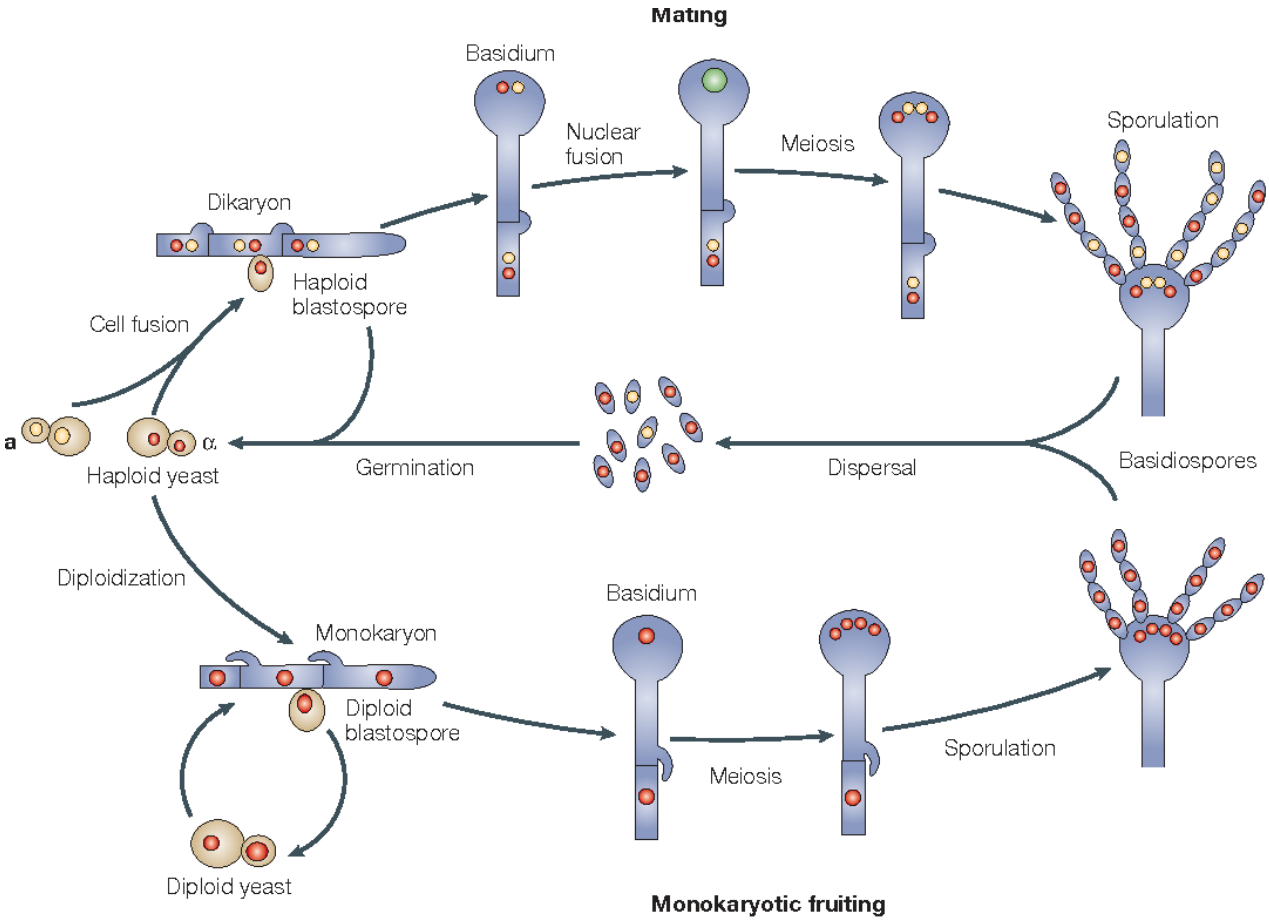

Figure 1-16: Model of the Cryptococcus neoformans life cycle.

Cell-cell fusion is triggered by peptide pheromones secreted by **a** and *α* cells in response to nutrient limitation. This involves the delay in nuclear fusion, resulting in dikaryon formation, which initiates filamentous growth. In the dikaryotic hyphae, the two parental nuclei migrate coordinately. As each septum forms to separate the cells, a clamp connection transfers one nucleus to the penultimate hyphal cell. At the stage of basidium development, the two nuclei fuse and undergo meiosis, producing four meiotic products. These products undergo mitosis and bud from the surface of the basidium producing chains of basidiospores. During the process of monokaryotic fruiting, cells of one mating type become diploid (*α*/*α*, **a**/**a**) cells, either through endoduplication or by nuclear fusion following the fusion of two cells. Diploid monokaryotic hyphae form rudimentary clamp connection, but these are not fused to the preceding cell. At the stage of basidium development, meiosis takes place, and haploid basidiospores are produced in four chains. Adapted from (Idnurm et al., 2005).

---

basidium wherein meiosis occurs to produce four chains of readily aerosolized basidiospores (Figure 1-16). *Cryptococcus* can undergo interspecies and intervarietal mating, although the viability of the formed basidiospores is reduced (Lengeler et al., 2001). Interestingly, it has been observed that the environmental and patient isolates have

predominantly been of the α mating-type (>98-99.9% average) (Kwon-chung and Bennett, 1978; Kwon-Chung et al., 1992).

C. neoformans strains under laboratory conditions have been observed to undergo monokaryotic fruiting, producing monokaryotic filaments and basidiospore formation following meiosis. While initially being suspected to be strictly haploid, mitotic, and asexual, monokaryotic fruiting has recently been shown to be a form of sexual reproduction taking place between strains of the same mating type (Figure 1-16) (Lin et al., 2005). α strains are predisposed to undergo monokaryotic fruiting, thus presenting an explanation as to why α strains are more abundant in nature (Wickes et al., 1996).

Dispersal of the formed basidiospores from mating or monokaryotic fruiting is suspected to be the most likely infectious candidate since they are around 2 μm, smaller than the ciliary action of the lung epithelial cells. It is also suspected that desiccated yeast (~3 μm) found in soil or nutrient-deprived condition are also likely to cause infections if they penetrate and lodge into the alveoli of the lung (Kozubowski and Heitman, 2012; Lin and Heitman, 2006). It was shown that *Cryptococcus* basidiospores are up to 100-fold more virulent than yeast cells, thus requiring far fewer spores to produce infection in mice (Sukroongreung et al., 1998)**.**

The pathogenic cycle and virulence factors

It was more than a century ago that *C. neoformans* was discovered as a human pathogen (Mitchell and Perfect, 1995). Around a million cases of Cryptococcal meningitis, infections are reported globally every year, resulting in more than 600,000 deaths occurring mostly in Sub-Saharan Africa (Park et al., 2009). Meningoencephalitis is the most common clinical manifestation of *Cryptococcus* infections. Infections particles of basidiospores or yeast cells are acquired by inhalation from an environmental source of pigeon guano, contaminated soil, or eucalyptus trees (Figure 1-17) (Callejas et al., 1998; Casadevall and Perfect, 1998; Granados and Castañeda, 2005). *Cryptococcus* infections have been reported in both animals and humans, but no animal-to-animal, animal-to-human, or human-to-human transmission has been documented. *Cryptococcus* infections begin with the colonization of the host respiratory tract where it can lay dormant and be asymptomatic for decades before its leads to a disease state or be cleared (Figure 1-17)

(Dromer et al., 1992; Garcia-Hermoso et al., 1999). Studies in children two-years or older in New York City suggested that most individuals have serological evidence of asymptomatic *C. neoformans* infections (Goldman et al., 2001). Often the dormant infectious particles get reactivated when the immunity of the host is compromised, under conditions such as immunosuppressants or predominantly in patients with AIDS. Upon reactivation, *Cryptococcus* particles disseminate hematogenous to cause a systemic infection. Local infections involving the urinary tract, prostate gland, lungs, joints, bones, skin, eyes or myocardium in addition to its affinity to infect the **c**entral **n**ervous **s**ystem (CNS) have been reported (Kozubowski and Heitman, 2012; Lin and Heitman, 2006; Martinez and Casadevall, 2007)**.**

The ability of *C. neoformans* to cross the blood-brain-barrier, thrive at 37˚C, the ability to form a polysaccharide capsule, and production of melanin is some of the

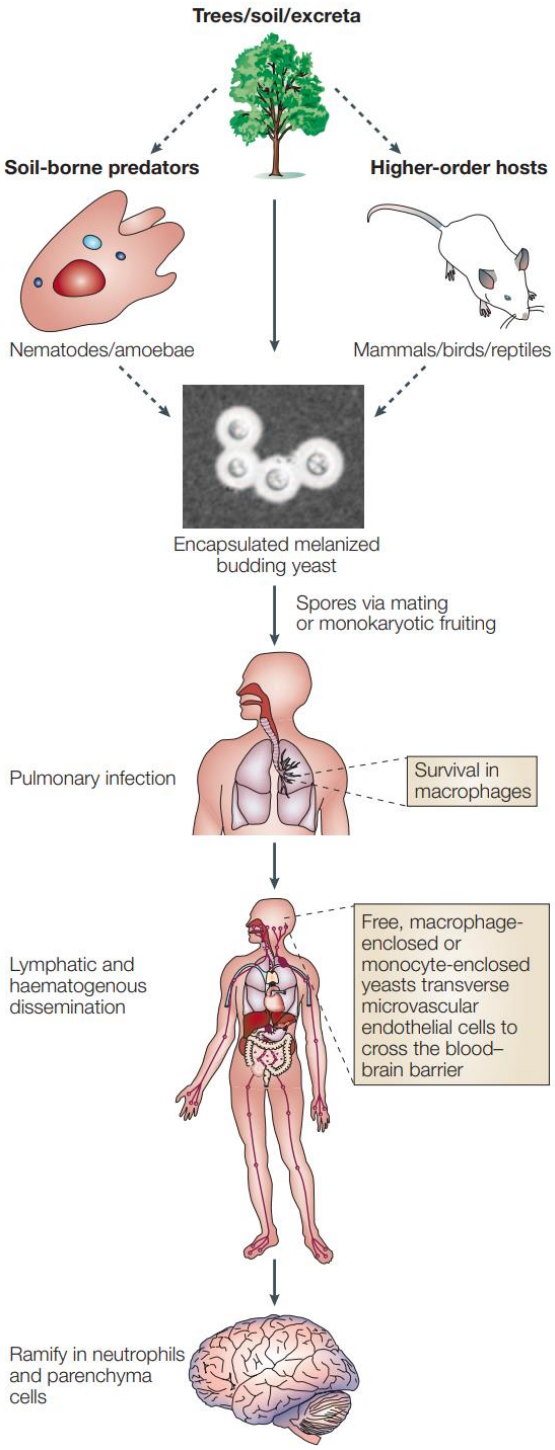

Figure 1-17: Virulence pathway of *Cryptococcus neoformans*.

C. neoformans survives in the environment within trees, soil, and bird guano. Here it can interact with wild animals or microbial predators, maintaining its virulence. When humans inhale desiccated yeast cells or spores a pulmonary form of the disease can be established. If the host is immunocompromised, *C. neoformans* can spread from the lungs and enter the CNS through the microcapillaries of the blood–brain barrier. CNS infections represent the most severe form of the disease. Adapted from (Idnurm et al., 2005).

factors that enable it to be the deadly pathogen it is today. It was observed that the *α* strains of *C. neoformans* are more virulent than the congenic **a** strain. *α* strains of *C. neoformans var. grubii* are also more likely to penetrate the CNS during coinfection with congenic **a** strain via the pulmonary route of inoculation (Nielsen et al., 2005).

The most common and fatal form of cryptococcosis is meningoencephalitis. The reason for *Cryptococcus* to exhibit neurotropism is an area of debate (Lin and Heitman, 2006). Besides humans, *Cryptococcus* can lead to infections in a wide range of wild and domesticated animals, although their clinical manifestations often differ from humans (Figure 1-16) (Casadevall and Perfect, 1998). Cryptococcosis is the most common clinical manifestation of fungal infections in cats (Sykes and Greene, 2011)

While *C. neoformans* is a fatal fungal pathogen, molecular details regarding its cell cycle are sparse. Aided by studies from our group and our collaborators, amongst others, have helped shed light on the molecular workings in this basidiomycetous budding yeast (Janbon et al., 2014; Kozubowski et al., 2013; Sutradhar et al., 2015; Takeo et al., 2004; Varshney et al., 2019; Yadav and Sanyal, 2018; Yadav et al., 2018b).

C. neoformans mitotic features

Nuclear and spindle dynamics

Labeling chromatin through a fluorescently tagged histone H4 helped us track the progression of the nuclear mass through the cell cycle. Two features of nuclear dynamics in *C. neoformans* stood out: an ~66% compaction of the chromatin mass during mitosis and the migration of the histone H4 tagged nucleus into the daughter bud wherein the nuclear division took place, with one half of the chromatin mass returning to the mother cell (Figure 1-20G) (Kozubowski et al., 2013). In other known budding yeast such as in *S. cerevisiae* and *C. albicans*, nuclear division takes place on the mother bud side of the bud-neck ring. *In silico* studies prompted us to examine **c**ytoplasmic **m**icro**t**ubules (cMTs) and dynein populations towards understanding this variation (Sutradhar et al., 2015). Through *in vivo* validation experiments, we propose than an increased number of cMTs or dynein population in the daughter cells of *C. neoformans* can assist in the migration of the nucleus into the daughter bud.

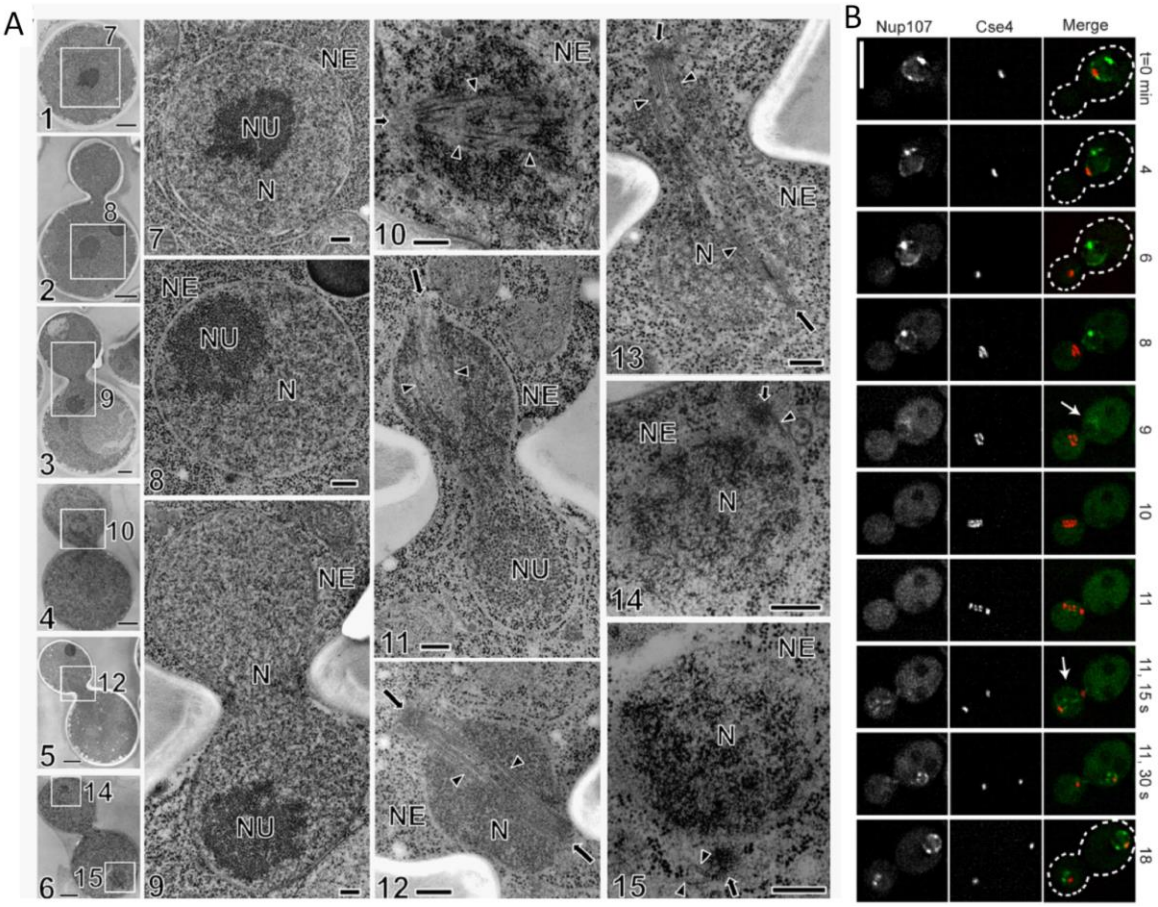

Figure 1-18: The nuclear envelope in *C. neoformans* breaks open partially during mitosis.

(A) The **t**ransmission **e**lectron **m**icroscopy (TEM) analysis of mitosis in *C. neoformans*. In images 2 to 6, the daughter cell is the one on top (smaller than the mother cell). Images: 1 and 7,G1-S phase; 2 and 8,G2 phase; 3 and 9, prophase; 4, 10, and 11, prometaphase; 5 and 12, metaphase; 13, anaphase; 6, 14, and 15, telophase. The **n**uclear **e**nvelope (NE) was intact at G1 through prophase, had broken near the spindle pole body (arrow) at prometaphase, and was closed at the end of telophase. **Nu**cleolus (NU) was visible at G1 through prophase, stayed in the mother cell at prometaphase, disappeared at metaphase, and reappeared after telophase. Spindle pole body resided on the nuclear envelope as one duplicated form at G1 through G2 phase, separated into two at prophase, entered the nuclear region by breaking the nuclear envelope at prometaphase, was located at the spindle poles at metaphase and anaphase, and was extruded back to the cytoplasm from the nuclear region at telophase. Microtubules (arrowheads) were distributed in the cytoplasm at G1 through prophase and appeared in the **n**ucleus (N) at prometaphase through the middle of telophase. **(B)** Time-lapse analysis of nuclear pore protein GFP-Nup107 and mCherry-Cse4. GFP-Nup107 was not present on the NE during metaphase (*t*-9 to 11.15 min), suggesting that NPCs disassembled at this stage. After genomic division, GFP-Nup107 was again visible on the NE, marking the reassembly of NPCs after mitosis. Bars, 1 μm (A [1 to 6]), and 250 nm (A [7 to 15]) and 5 μm B. (Kozubowski et al., 2013)

Another striking feature of mitosis in *C. neoformans* is that the nucleus experiences increased permeability on account of partial nuclear pore complex disassembly and a rupture of the nuclear membrane at the site of the clustered centromeres. Thus we concluded that *C. neoformans* experiences semi-open mitosis (Figure 1-18 A and B) (Kozubowski et al., 2013).

Centromere

Centromeres in *C. neoformans* were first predicted to be large regional. Long ORF free regions (~30 kb to 110 kb) abundant in retroelements and occurring once per chromosome (Janbon et al., 2014). These regions were found to be poorly transcribed and harbored full-length and truncated versions of Tcn1-Tcn6 retroelements (Figure 1-19). Within these regions, ChIP-seq of conserved kinetochore proteins, CENP-A^{Cse4,} and CENP-C^{Mif2}, revealed an ~20-40 kb regions of enrichment (Janbon et al., 2014; Yadav et al., 2018b). Through a comparative analysis of closely related *Cryptococcus* species, *Cryptococcus deuterogattii* having lost RNAi. It was suggested that the retention of full-length retroelements and consequently a longer centromere in the RNAi proficient species of *C. neoformans* and *Cryptococcus deneoformans* was a consequence of retroelement silencing, a phenomenon previously described in *C. neoformans* (Wang et al., 2010; Yadav et al., 2018b).

The identification of H3K9me2 and DNA methylation at centromeric regions of *C. neoformans* further suggested the presence of additional mechanisms to silence retroelements at the centromere (Dumesic et al., 2015; Huff and Zilberman, 2014).

Kinetochore

The kinetochore in *C. neoformans* was predicted by us and others to have a conserved KMN network and Dam1 complex at the outer kinetochore. While amongst the inner kinetochore it was suspected to retained only CENP-C^{Mif2} of the CCAN network, in addition to the centromeric histone H3 variant CENP-A^{Cse4} (Figure 1-10 and 1-13D) (van Hooff et al., 2017; Schleiffer et al., 2012; Sridhar et al., 2017). Our initial study observing kinetochore dynamics through fluorescent-tagged kinetochore proteins suggested there

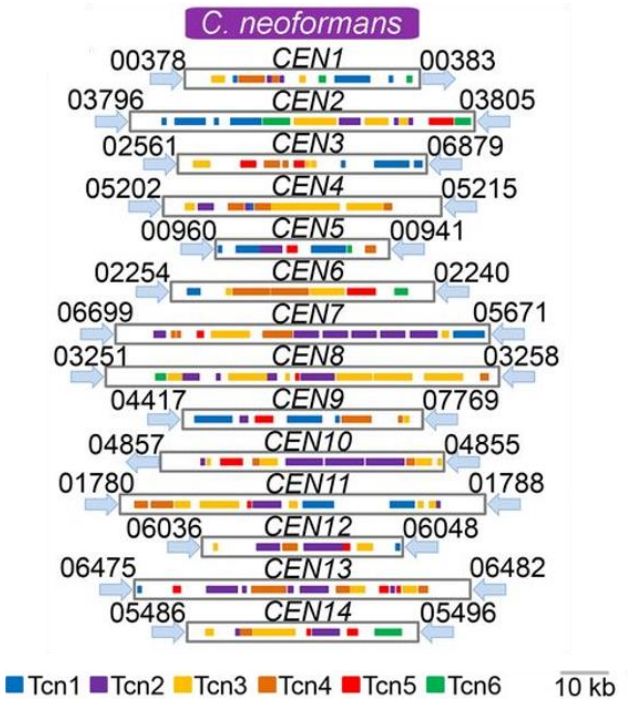

Figure 1-19: Organization of the kinetochore in *C. neoformans* strain H99.

Schematic shows the distribution of transposons across *C. neoformans* centromeres, Tcn1–Tcn6, occur at the centromeres of all 14 chromosomes of *C. neoformans* strain, H99. These transposon rich regions were identified as the largest ORF-free region on its respective chromosome and contain transposons or its footprints, which are clustered in these sites. Adapted from (Yadav et al., 2018b).

---

existed a step-wise assembly of outer kinetochore components (Figure 1-20G). The inner kinetochore components of CENP-A^{Cse4} and CENP-C^{Mif2} were observed to be localized to the kinetochore all through the cell cycle (Figure 1-20A and B). Proteins of the KMN network (referred to in figure 1-20 as a middle layer) were found to subsequently localize towards the onset of mitosis, followed by the Dam1 complex (Figure 1-20E).

The dynamics of disassembly were reversed with the Dam1 complex, followed by the KMN network proteins losing their kinetochore localization at anaphase (Figure 1-20F) (Kozubowski et al., 2013). Since the stages of the *C. neoformans* cell cycle were not marked, the precise timing of these events was not established. Further, the dynamic levels of kinetochore proteins through cell cycle progression were not evaluated. Additionally, though we had a gross idea of the step-wise assembly of kinetochore layers, the organization of sub-complexes was unexplored.

CENP-A^{Cse4} and CENP-C^{Mif2} localized to the kinetochore all through the cell cycle and were observed to be clustered during mitotic. To our surprise, the clustered centromeres

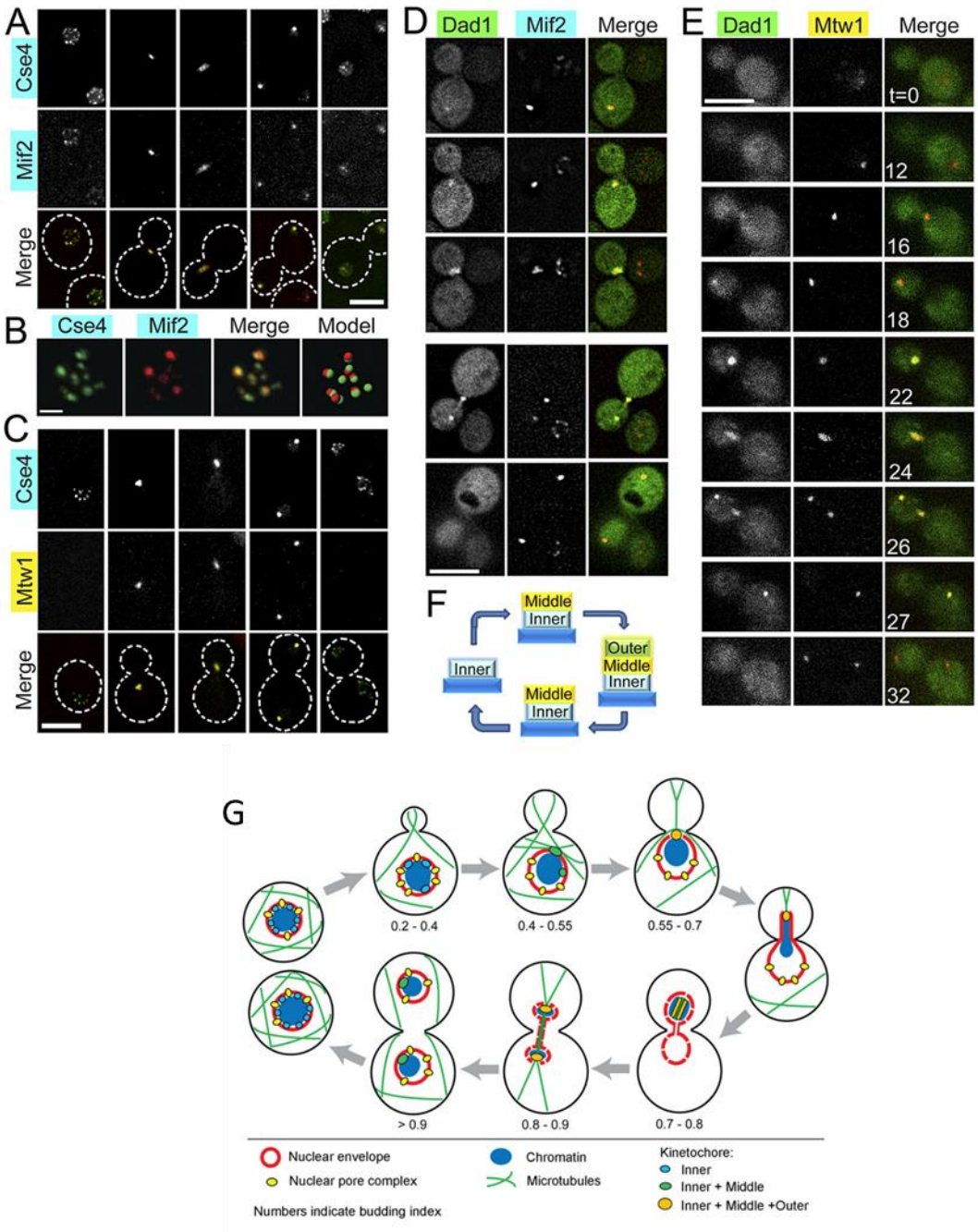

Figure 1-20: Ordered kinetochore assembly in *C. neoformans*.

(A) Two inner kinetochore proteins, GFP-CENP-A^{Cse4} and CENP-C^{Mif2}-mCherry, colocalized at all stages of the cell cycle. Both proteins colocalized as separate dots in unbudded cells (first column), small-budded cells (not shown), and soon after cytokinesis (last column) but remained clustered during mitosis (middle three columns). **(B)** A 3-dimensional (3-D) reconstruction based on Z-stack images of an unbudded cell shows a complete overlap of GFP-CENP-A^{Cse4} and CENP-C^{Mif2}-mCherry. **(C)** The KMN network protein Mis12^{Mtw1}-mCherry was not visible in cells where the inner kinetochore protein GFP-Cse4 was found as multiple non-clustered signals (the first and the last columns). However, Mis12^{Mtw1}-mCherry colocalized with clustered GFP-CENP-A^{Cse4} (middle three columns). **(D)** The outer kinetochore component GFP-Dad1 became visible before

mitosis when it colocalized with the inner kinetochore protein CENP-C^{Mif2}-mCherry in a single cluster. **(E)** Colocalization of the Dam1C protein (GFP-Dad1) and a KMN network (Mis12^{Mtw1}-mCherry) kinetochore protein showed that GFP-Dad1 was loaded onto the kinetochore later than Mis12^{Mtw1}-mCherry. GFP-Dad1 was visible during mitosis (*t*- 16 to 27 min) and disappeared soon after chromosome segregation, while Mis12^{Mtw1}-mCherry remained present (*t* -32 min). **(F)** Schematic showing ordered assembly of kinetochore proteins. The inner, middle (KMN network), and outer kinetochore protein names are highlighted in blue, yellow, and green, respectively. Bars, 5 μm (A, C, D, and E) and 1 μm (B). **(G)** The model is showing the clustering of centromeres, a gradual change in kinetochore architecture, and the nuclear envelope dynamics during the progression of the cell cycle in *C. neoformans*. (Kozubowski et al., 2013)

---

upon exiting mitosis unclustered and localized to the periphery of the nucleus (Figure 1-20A and C). These clustering-unclustering dynamics was unlike what was previously described for any budding yeast. Experiments suggested that these dynamics were under the influence of microtubules. *In silico* modeling suggested that the dynamics of clustering would not be possible within the biological time frames observed if not for coalescing of centromeres to a cluster by microtubules (Kozubowski et al., 2013; Sutradhar et al., 2015). Subsequent analysis suggested that Aurora B^{Ipl1} influenced cMTs and thereby delaying centromere clustering (Varshney et al., 2019).

Although several questions regarding kinetochore dynamics remain unanswered, these studies laid the groundwork for a more detailed analysis of kinetochore composition, organization, and dynamics presented in this thesis.

Previous work as part of my MS thesis

As a part of my Master's thesis (Shreyas Sridhar, MS thesis 2014), I had fluorescently tagged key proteins of the outer kinetochore that included Nuf2, Ndc80, and Knl1^{Spc105} of the KMN network, and Dad2 of the Dam1 complex in *C. neoformans*. These generated strains were subject to microscopic evaluation and were observed to localize to the kinetochore transiently. Towards the onset of mitosis, components of the KMN network localized first on to the inner kinetochore followed by Dam1 complex. Thus, we concluded that a step-wise assembly of the kinetochore exists in this organism (Figure 1-20). This study contributed to the initial characterization of the kinetochore in *C. neoformans* (Kozubowski et al., 2013).

To further understand the function and requirement of kinetochore subunits in this budding yeast, I generated and characterized conditional kinetochore mutants. The members tested of inner kinetochore proteins were CENP-A^{Cse4} and CENP-C^{Mif2}, of the outer kinetochore, were Mis12^{Mtw1} (Mis12 complex), Knl1^{Spc105} (KNL1 complex) and Nuf2 (Ndc80 complex) proteins of the KMN network, and the Dam1 complex proteins Dad1 and Dad2. To generate these conditional mutants, the gene promoters were replaced with the controllable *GAL7* promoter at their native loci (Ruff et al., 2009). When grown in media containing galactose as the only carbon source, the gene is expressed, and in the presence of glucose, the promoter expression is shut down (Figure 3-1). We characterized the repression dynamics of each gene and found that all tested proteins were essential for *C. neoformans* viability. Conditional mutants of CENP-A^{Cse4}, CENP-C^{Mif2}, Mis12^{Mtw1}, Nuf2, and Knl1^{Spc105,} although resulting in chromosome segregation errors, failed to elicit a SAC response. The Dam1 complex mutants, on the other hand, arrested in a large budded state upon repression. It was likely that the latter conditional mutants affected the scaffold required for the recruitment of the SAC proteins to the kinetochore. Thus, cells failed to elicit a SAC dependent cell cycle delay to correct for the segregation errors. Furthermore, we observed the transiently localized KMN network and the Dam1 complex proteins localized to kinetochores marked by CENP-A^{Cse4}, post-treatment of cells with microtubule depolymerizing drugs. Thus suggesting that kinetochore assembly in *C. neoformans* did not require the integrity of the mitotic spindle. However, for centromere clustering to take place, I showed that microtubules were required (Kozubowski et al., 2013). Following my MS thesis work, with the help of *in silico* modeling and *in vivo* validation, we determined that optimized microtubule catastrophe frequency was necessary to ensure centromere clustering in *C. neoformans* (Sutradhar et al., 2015). It was explained wherein for small catastrophe frequencies, longer microtubules inefficiently search for the MTOCs in the wrong directions leading to large clustering time. At high catastrophe frequency, microtubules are short and often fail to reach the target MTOC, and hence, clustering time is large (Sutradhar et al., 2015).

Following up on my MS thesis work, in this study, we utilize the fluorescent-tagged kinetochore strains to precisely determine their cell cycle dynamics in real-time. In addition, the conditional kinetochore mutants were used to determine the hierarchy of the kinetochore and, subsequently, the kinetochore receptor for a previously undescribed kinetochore protein.

The rationale of the study

Our motivation for this study stems from recent studies (van Hooff et al., 2017; Schleiffer et al., 2012; Sridhar et al., 2017) that utilized bioinformatics to suggest a variable inner kinetochore ensemble in certain model basidiomycetes species. *U. maydis* is predicted to have retained most components of the CCAN, while *C. neoformans* may have lost all CCAN components except CENP-C^{Mif2}. CCAN proteins are known to have critical functions at the kinetochore (Figure 1-6A). This raising the question of what the composition and organization of kinetochores across basidiomycete systems are when lacking evolutionarily conserved kinetochore protein complexes. In addition, *C. neoformans* could provide a good model system to address the contribution of Dsn1 autoinhibition towards driving the maintenance of multiple kinetochore linker pathways. This is especially intriguing since the kinetochore composition has been predicted to have retained a single kinetochore linker protein while retaining the autoinhibition mechanism mediated through Dsn1 (Figure 1-11). Details regarding precise kinetochore dynamics, composition, and organization, to the best of our knowledge, is not available for any fungal species outside ascomycetes.

Further, we asked if the loss of key kinetochore subunits in basidiomycetes be compensated for by previously undescribed kinetochore proteins? If so, could such candidates possibly serve as novel drug targets in pathogenic basidiomycete species, such as *C. neoformans*?

Our previous studies on understanding events of chromosome segregation in the basidiomycete budding yeast *C. neoformans* revealed more metazoan-like features of centromere dynamics and step-wise assembly of the inner and outer kinetochore layers. However, we did not address the organization and dynamics of kinetochore sub-complexes through the cell cycle.

With observed variations in kinetochore features coupled to possible differences in composition to the well-studied ascomycete systems, we asked what the kinetochore composition was across basidiomycetes in this thesis work. Further, using the *C. neoformans* system, we sought to address the composition, dynamics, and organization of the kinetochore in more detail.

Objectives of the study

The fundamental objective of this study was to gain a better understanding of the kinetochore ensemble through evolution. Towards this goal we sought to address the kinetochore composition, dynamics, and architecture in the basidiomycete and human pathogen *C. neoformans*.

Our initial objective was to utilize sensitive bioinformatic prediction tools to determine the conservation of kinetochore complexes through basidiomycete evolution. Subsequently, to validate our predictions, we will identify the kinetochore interactome in *C. neoformans.*

Following the description of the kinetochore interactome, we aim to address the cell cycle dynamics and assembly hierarchy of known kinetochore proteins. In the process, we will work towards developing and establishing microscopy-based markers to delineate cell cycle stages in *C. neoformans*.

Furthermore, from the identified kinetochore interactome, we hypothesize that there may exist previously undescribed kinetochore proteins. To test this, we will screen the obtained hits initially by a microscopic assay. Any promising hit/hits would be functionally characterized.

Results

Chapter 2 : Identification of the kinetochore interactome in *Cryptococcus neoformans.*

Multiple independent loss events of CCAN proteins in Basidiomycota

To have a comprehensive understanding of the kinetochore composition in the fungal phylum of Basidiomycota, we analyzed genomes to find putative kinetochore homologs using high confidence protein homology searches combined with predicted secondary and tertiary structures. We considered species representing 31 fungal orders across the three Basidiomycota sub-phyla (Pucciniomycotina, Ustilagomycotina, and Agaricomycotina). CENP-A^{Cse4}, the 16-member CCAN, and the 10-member KMN network were chosen for this study (Figure 2-1 and Appendix II). Our analysis indicates the robust conservation of the KMN network proteins across these basidiomycete species.

On the other hand, we observed that most CCAN proteins were recurrently lost across 23 basidiomycete orders (Figure 2-1 and Appendix II). In the sub-phylum of Agaricomycotina, the loss event may have occurred early at the time of the divergence of Wallemiales from other orders. While in two other sub-phyla of Pucciniomycotina and Ustilogamycotina, the loss of most CCAN subunits might have taken place at multiple independent occasions, as suggested by retention of these proteins in a few discrete orders (Figure 2-1 and Appendix II). Of the three known linker pathways, the inner kinetochore linker protein CENP-C^{Mif2} was the only uniformly conserved CCAN component present across basidiomycetes. Other known linker proteins, CENP-T^{Cnn1} and CENP-U^{Ame1,} were often observed to be lost together. Although the primary protein sequence conservation is low among CENP-T^{Cnn1} homologs, they share a typical protein architecture, an N-terminus α-helix composed of conserved hydrophobic residues and the CENP-T^{Cnn1} motif at the C-terminus (Figure 2-2). In the order Ustilaginales, a PITH domain spans the N-terminus of the CENP-T^{Cnn1} homolog, consisting of an α-helix composed of conserved hydrophobic residues (Figure 2-2). The CENP-C^{Mif2} linker pathway is the single known linker pathway in 23 of the 31 basidiomycete orders investigated. These results suggest that CCAN proteins, along with linker proteins, might have been lost on multiple independent occasions during basidiomycete evolution.

In vivo analyses of the kinetochore interactome validates our prediction of kinetochore structural components in *C. neoformans*

We subsequently sought to validate our predicted kinetochore composition using a

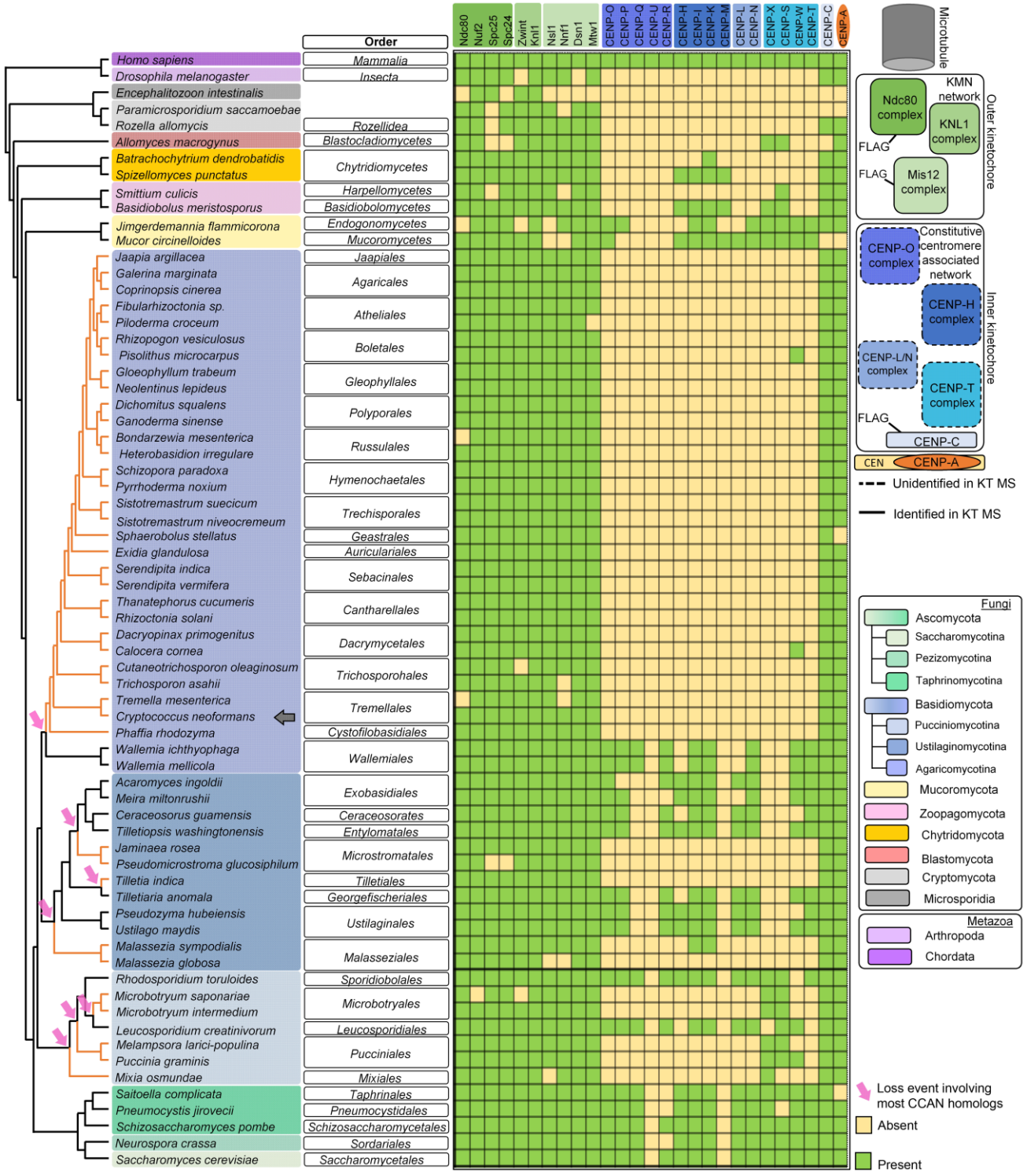

Figure 2-1: Recurrent loss of most CCAN components amongst basidiomycetes.

Conservation of kinetochore proteins across the species mentioned. A cladogram representing the relationship between the species is drawn, and each phylum/sub-phylum is color-coded. The presence or absence of respective kinetochore proteins is shown. Pink arrows indicate loss events of most CCAN proteins. FLAG labeling refers to proteins tagged in *C. neoformans* with 3xFLAG towards IP-MS identification of the kinetochore interactome. Solid and dashed lines representing protein complexes in the

kinetochore image refer to identified and unidentified complexes by our IP-MS experiment in *C. neoformans,* respectively.

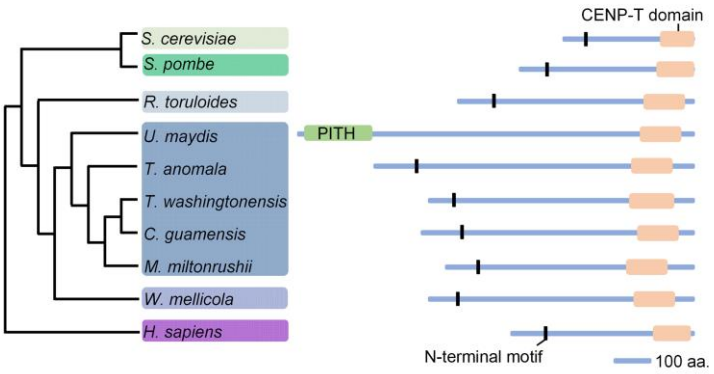

Figure 2-2: Domain architecture of identified CENP-T^{Cnn1} homologs amongst basidiomycetes.

Putative CENP-T homologs across basidiomycetes were identified as containing the conventional CENP-T^{Cnn1} motif at the C-terminus and an N-terminus α-helix containing hydrophobic residues. Phylum/sub-phylum is color-coded as mentioned in figure 2-1.

relatively well-studied basidiomycete yeast *C. neoformans.* To comprehensively determine the constitution of the kinetochore and its interactome *in vivo* we generated strains in which the endogenous genes of CENP-C^{Mif2}, Dsn1 (Mis12 complex) and Spc25 (Ndc80 complex) were replaced with a carboxy (C)-terminal 3xFLAG tagged version and confirmed their functionally in the haploid *C. neoformans* type-strain background of H99*α* (Figure 2-3Aand E and 6-1). **M**ass **s**pectrometry (MS) analysis was performed following FLAG **i**mmuno**p**recipitation (IP) of CENP-C^{Mif2}, Dsn1, and Spc25 from metaphase enriched cell population, mitotic index >90% (Figure 2-3B and C). All predicted CCAN and KMN network components were identified from each of the three FLAG purifications (Figure 2-3D and E and Appendix III). Identified KMN network components included previously unannotated ORFs coding for proteins of the Mis12 complex (Nsl1^{CNAG_04300}, Nnf1^{CNAG_04479}) and the KNL1 complex (Sos7^{CNAG_03715}) (Figure 2-3D). Except for CENP-C^{Mif2}, no components of the CCAN were identified (Figure 2-3D and Appendix III). This result further validates that *C. neoformans* retains a single known kinetochore linker pathway- the CENP-C^{Mif2} pathway, and lost other known linker pathways, mediated by CENP-T^{Cnn1} and CENP-U^{Ame1}.

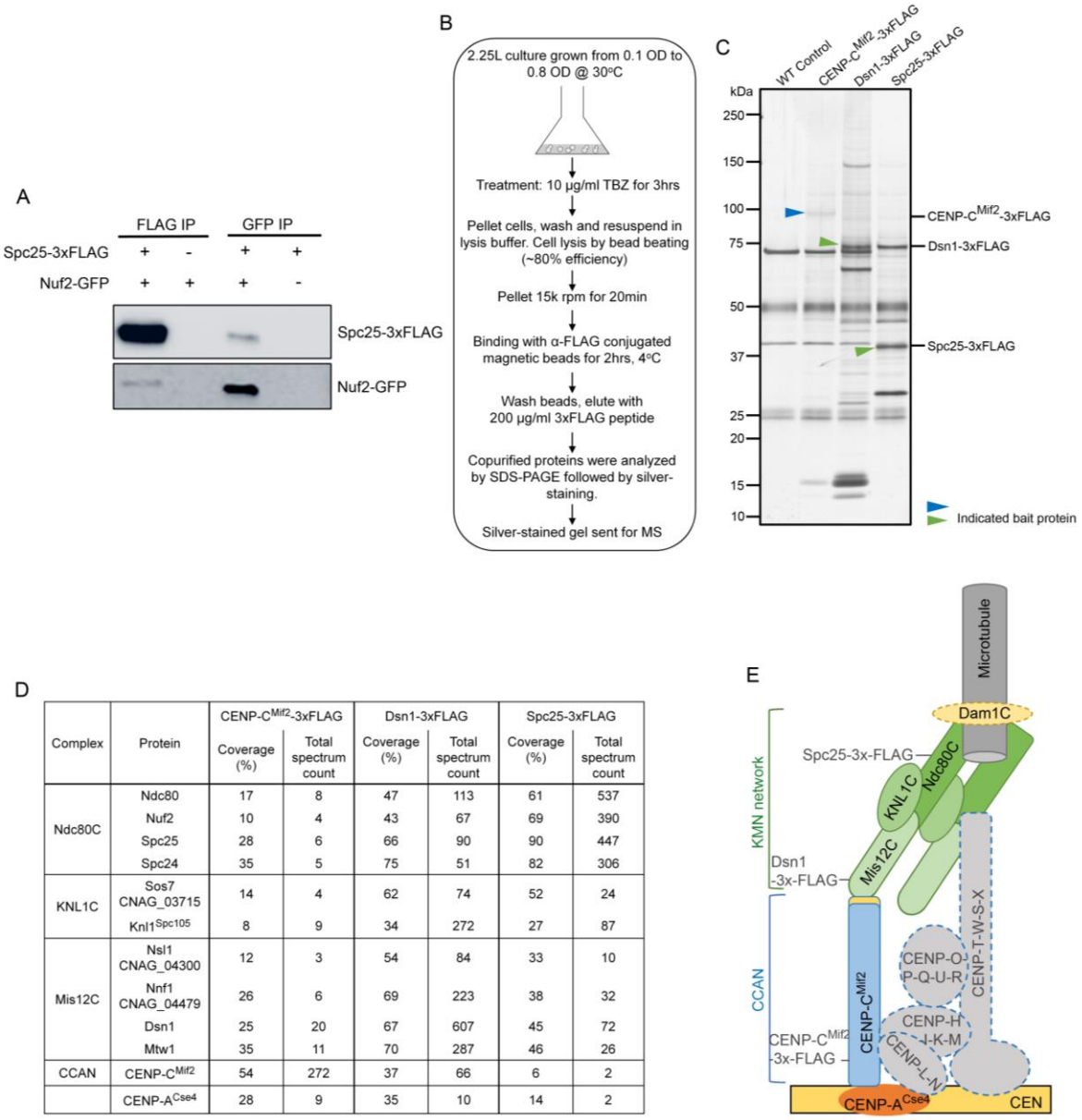

Complex	Protein	CENP-C^{Mif2}-3xFLAG		Dsn1-3xFLAG		Spc25-3xFLAG	
		Coverage (%)	Total spectrum count	Coverage (%)	Total spectrum count	Coverage (%)	Total spectrum count
Ndc80C	Ndc80	17	8	47	113	61	537
	Nuf2	10	4	43	67	69	390
	Spc25	28	6	66	90	90	447
	Spc24	35	5	75	51	82	306
KNL1C	Sos7 CNAG_03715	14	4	62	74	52	24
	Knl1^{Spc105}	8	9	34	272	27	87
Mis12C	Nsl1 CNAG_04300	12	3	54	84	33	10
	Nnf1 CNAG_04479	26	6	69	223	38	32
	Dsn1	25	20	67	607	45	72
	Mtw1	35	11	70	287	46	26
CCAN	CENP-C^{Mif2}	54	272	37	66	6	2
	CENP-A^{Cse4}	28	9	35	10	14	2

Figure 2-3: Identification of the kinetochore interactome in *C. neoformans*.

(A) Protein lysates were prepared from the mentioned strains. Kinetochore particles were purified using FLAG or GFP and analyzed by immunoblotting. **(B)** Outline of the protocol used for FLAG affinity purification. **(C)** A silver-stained gel shows kinetochore interacting proteins in the thiabendazole treated, M phase enriched cell population in *C. neoformans*. Proteins bound to each of the 3xFLAG tagged bait proteins were separated on a gradient PAGE gel. The left-most lane of the untagged control strain shows commonly found contaminating proteins in the single-step FLAG affinity purification elute. **(D)** List of kinetochore proteins with the percentage of amino acid sequence coverage and the number of total peptides specific to the corresponding protein obtained by MS analysis. **(E)** Model depicting the identified kinetochore proteins. Protein complexes of the CCAN in dashed lines filled with grey were not unidentified in the IP-MS. Affinity purified bait proteins are mentioned.

Screening of hits obtained as part of the kinetochore interactome

We next investigated whether there existed proteins with unknown kinetochore function compensating for the loss of CCAN subunits in *C. neoformans.* Having identified all known structural kinetochore components from each IP-MS experiment, we hypothesized that it was possible to identify previously undescribed kinetochore proteins from the common list of interactors obtained from CENP-C^{Mif2}, Dsn1 and Spc25 affinity purification experiments (Figure 2-4A). With this criteria, we categorized two sets of proteins: a) primarily conserved amongst basidiomycetes with no known function, and named them **b**asidiomycete **k**ine**t**ochore proteins (Bkts) (CNAG_01903^{Bkt1}, CNAG_03959^{Bkt2} and CNAG_02701^{Bkt3}) (Figure 2-4B) and b) known chromatin interacting proteins with uncharacterized kinetochore function (CNAG_01340^{Yta7} and all components of the Mcm complex (Mcm2-7) (Figure 2-4C). We used CNAG_03962^{Mcm6} as a representative test candidate for the Mcm complex. In the secondary screen, these five proteins were epitope-tagged at the native locus, each with a C-terminal V5-GFP in a strain background where a mCherry-tagged inner kinetochore, CENP-A^{Cse4} or CENP-C^{Mif2}, is expressed. Localization of Sos7^{CNAG_03715} was tested to validate our prediction of unannotated kinetochore proteins (Figure 2-4 D and 2-6A). Of the six tagged constructs, strains expressing the epitope-tagged construct could be obtained for five, except CNAG_02701^{Bkt3}. In a metaphase enriched population, the protein encoded by the Orf.CNAG_01903^{BKT1} was found to colocalize with CENP-A^{Cse4} at metaphase. No exclusive localization of other hits to the mCherry-tagged kinetochore markers was observed (Figure 2-4D). These observations suggested the Bkt1 may be a protein localized exclusively to the kinetochore.

Establishing microscopy-based markers to determine cell-cycle stages in *C. neoformans*

Having visualized the localization of the fluorescent-tagged protein hits in the metaphase phase, we sought to examine their localization in the other cell cycle stages. Before addressing this, we worked to establish microscopy-based markers to determine the stages of the cell cycle in *C. neoformans*. We utilized PCNA (**P**roliferating **C**ell **N**uclear **A**ntigen), an established marker of S phase and cell proliferation in several systems, as

A

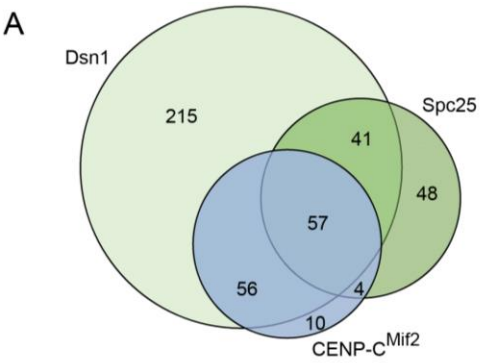

B

Proteins of unknown function

Orf	Given name	CENP-C^{Mif2}-3xFLAG		Dsn1-3xFLAG		SPC25-FLAG		Domains present	Domain function
		% coverage	peptides	% coverage	Peptides	% coverage	Peptides		
CNAG_01903	Bkt1	46	120	46	120	47	212	FHA domain	Phosphopeptide recognition
CNAG_03959	Bkt2	65	17	65	17	73	27	NA	NA
CNAG_02701	Bkt3	17	10	17	10	15	6	BAG domain	Modulators of chaperone activity

C

Predicted chromatin binding proteins with no known function at the kinetochore

Orf	Given name	CENP-C^{Mif2}-3xFLAG		Dsn1-3xFLAG		SPC25-FLAG		Domains present
		% Coverage	peptides	% coverage	Peptides	% coverage	Peptides	
CNAG_01340	Yta7	15	39	31	228	12	21	ATPase, bromodomain
CNAG_03962	Mcm6	13	17	51	60	15	16	DNA helicase

D

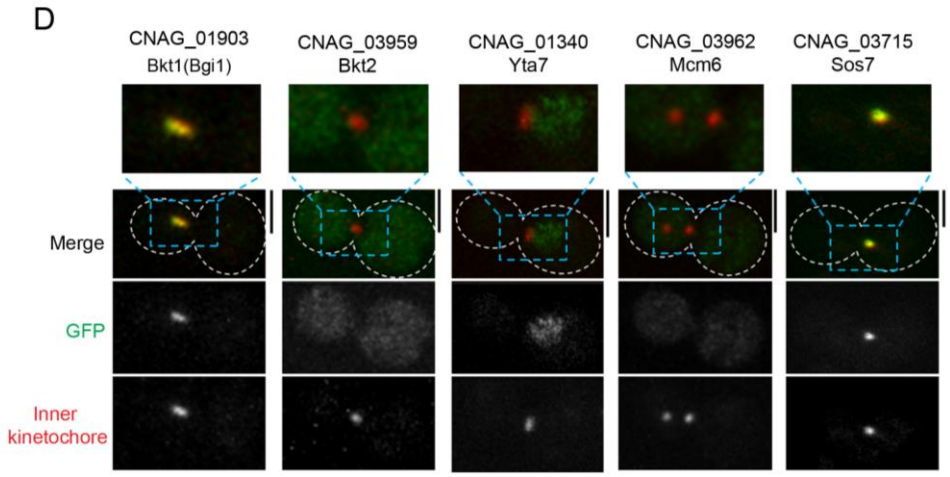

Figure 2-4: Identification of Bkt1 as a putative kinetochore protein in C. neoformans.

(A) Venn diagram of identified interacting proteins. Peptide threshold of 95%, protein threshold of 99%, and a minimum identification of 2 unique peptides are the parameters used to select an interacting protein. Circles in green indicate components of the KMN network, Dsn1, and Spc25, while members of the CCAN, CENP-C^{Mif2}, are shown in a blue circle. **(B)** List of common interacting proteins with no known function. These protein hits showed conservation primarily across basidiomycetes and were identified in CENP-C^{Mif2}, Dsn1, and Spc25 FLAG affinity-purified eluates. Predicted domains and possible domain functions are listed. **(C)** Tabulation of proteins known to bind chromatin with no strong association with kinetochore proteins and identified as interacting partners in CENP-C^{Mif2}, Dsn1, and Spc25 FLAG affinity purifications. **(D)** Micrographs of *C. neoformans* cells at metaphase expressing C-terminally tagged GFP proteins identified by the screen mentioned above. Kinetochores are marked by a mCherry tagged inner kinetochore proteins, CENP-C^{Mif2} or CENP-A^{Cse4}. Scale bar, 3 μM.

---

one of the cell-cycle markers (Landberg and Roos, 1991; Morris and Mathews, 1989; Strzalka and Ziemienowicz, 2011). PCNA was expressed as a fusion protein with GFP and expressed under the histone H3 promoter.

PCNA was previously described to localize as punctate structures in S phase across various systems (Pohler et al., 2005; Schönenberger et al., 2015; Strzalka and Ziemienowicz, 2011). With this as the starting point, the time-frame wherein GFP-PCNA was observed to exhibit punctate-like structures were designated as S phase in *C. neoformans* (Figure 2-5). PCNA is chromatin-bound exclusively during the S phase to carry out its DNA replication role (Strzalka and Ziemienowicz, 2011). Previously we have established that *C. neoformans* undergo semi-open mitosis (Kozubowski et al., 2013). Therefore, the period wherein chromatin unbound GFP-PCNA was observed to diffuse into the cytoplasm was labeled as M phase (Figure 2-5). The cell cycle interval between PCNA's punctate localization in the S phase to its cytoplasmic diffusion in the M phase was designated as G2. Meanwhile, the ensuing stage following the reestablishment of nuclear permeability, at the end of M phase, until the subsequent punctate localization in S phase was designated as G1 (Figure 2-5). The average budding index of cells at various cell cycle stages was designated.

Having established cell cycle stages based on the observed dynamics of PCNA, histone H4 dynamics were overlaid. We observed that the events of nuclear migration into the daughter cell, chromatin condensation, and the uniform diffusion of GFP-PCNA signal across the cell due to semi-open mitosis coincided. Further, an increase in the histone H4-mCherry signal was seen during the S phase, coinciding with punctate PCNA

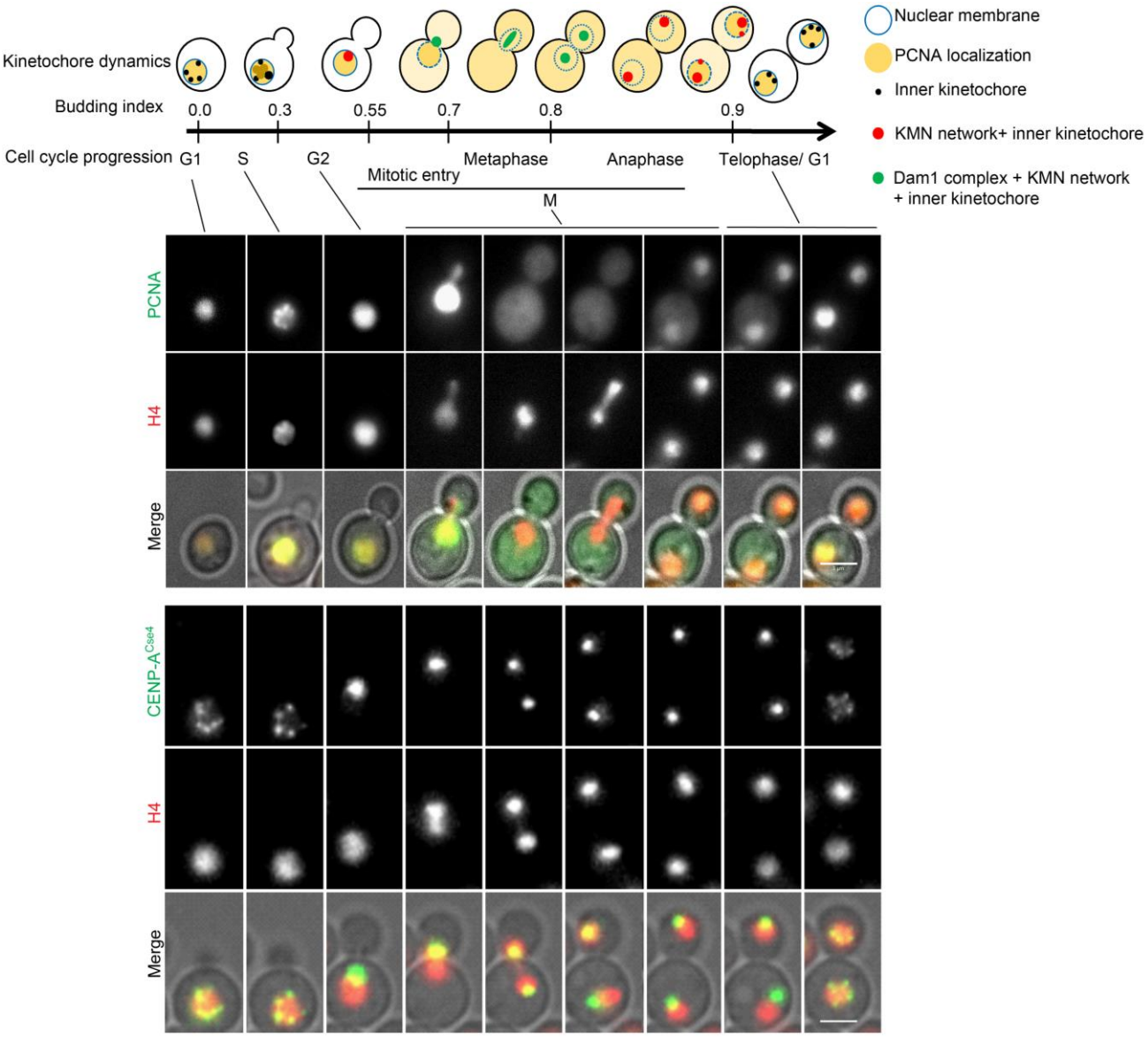

Figure 2-5: Graphical summary of cell cycle markers used to determine cell cycle stages in C. neoformans.

(Top) Schematic summary of mitotic features determined. Budding index mentioned is an approximate daughter bud: mother bud diameter ratio observed in log phase growing cells. *(Bottom)* PCNA and histone H4 dynamics were used to establish stages of the *C. neoformans* cell cycle. CENP-A^{Cse4} dynamics were recognized in the stages labeled by histone H4.

---

localization. Centromere clustering, marked by the centromere marker CENP-A^{Cse4}, was observed to occur in G2. Unclustering of kinetochores was observed at telophase/G1. These observations, in addition to our previously described cell cycle events (Kozubowski et al., 2013), are summarized (Figure 2-5) and used to define cell cycle stages in the following sections.

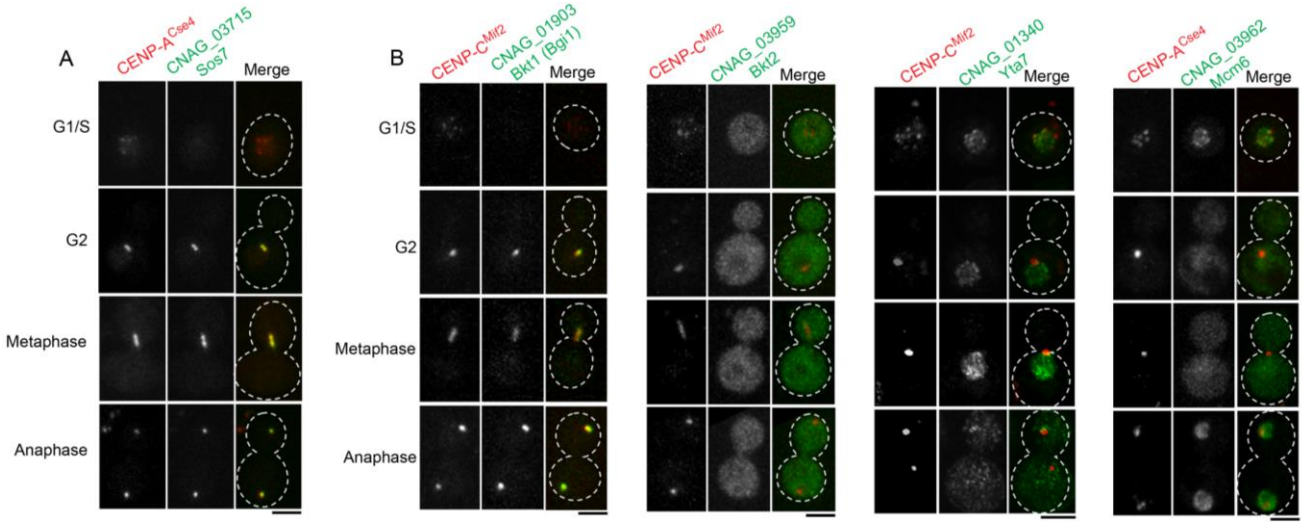

Figure 2-6: Localization of fluorescently tagged candidate proteins through the cell cycle.

(A) Sos7 localization across cell-cycle stages. mCherry-CENP-A^{Cse4} marks the kinetochore. Scale bar, 3 µm. **(B)** Localization of C-terminal tagged GFP constructs across mentioned interphase and mitotic stages. CENP-C^{Mif2}-mCherry or CENP-A^{Cse4}-mCherry marks the kinetochores. Scale bar, 3 µm.

A novel basidiomycete kinetochore protein (Bkt), Bridgin (Bgi1) is identified

On establishing a microscopy-based criterion to determine cell cycle stages, we examined the localization pattern of the fluorescently tagged hits. Bkt1^{CNAG_01903} signals appeared in G2 and found to co-localize with CENP-C^{Mif2} until the end of the M phase (Figure 2-6B). Other protein hits did not show exclusive kinetochore localization, although some puncta of Yta7 and Mcm6 co-localized transiently with the inner kinetochore marker at the G1/S stage of the cell cycle (Figure 2-6B). Based on the localization of the protein hits, Bkt1^{CNAG_01903} was taken forward as a likely candidate kinetochore protein. Considering its identified function through this study, we refer to Bkt1 as “bridgin” (Bgi1) henceforth.

Summary

In this chapter, our initial objective was to identify the conservation and composition of the kinetochore in basidiomycetes. Towards this, using sensitive *in silico* pipelines we predicted kinetochore homologs among 31 orders across 3 basidiomycete sub-phylum to

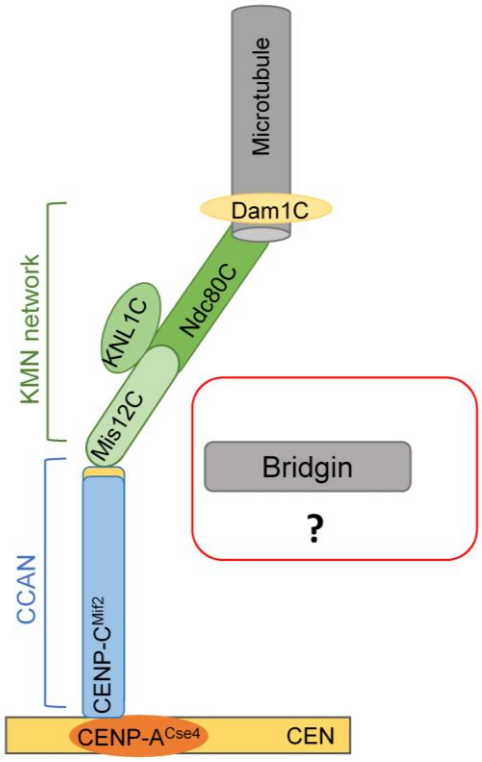

Figure 2-7: Bridgin, a putative kinetochore protein.

Bridgin was found to localize to the kinetochore from G2 until the end of the M phase. However, how and where it localized to at the kinetochore remains unknown.

---

find that CCAN proteins except CENP-C^{Mif2} are recurrently lost. Further, we found that proteins of the outer kinetochore KMN network were well conserved. Using the basidiomycete and human fungal pathogen *C. neoformans* we identify the kinetochore interactome through IP-MS of three kinetochore proteins (CENP-C^{Mif2}, Dsn1, and Spc25) and validate the retention of only CENP-C^{Mif2} of the CCAN. All components of the KMN network were also identified, including the previously unannotated ORFs of Nsl1^{CNAG_04300}, Nnf1^{CNAG_04479,} and Sos7^{CNAG_03715}. From the interactome we also identified a previously undescribed set of proteins we call **B**asidiomycete **k**inetochore **p**roteins (Bkts). Additionally several proteins with undescribed kinetochore function including the Mcm 2-7 complex were identified. To verify these novel kinetochore interactors we screened CNAG_01903^{Bkt1}, CNAG_03959^{Bkt2}, CNAG_02701^{Bkt3}, CNAG_01340^{Yta7} and CNAG_03962^{Mcm6} using a microscopy assay. Furthermore, using PCNA, histone H4 and CENP-A^{Cse4} we establish microscopy-based criteria to determine

the cell-cycle stages in *C. neoformans*. With these markers established, we identify a previously undescribed protein coded by the ORF. CNAG_01903^{Bkt1} to localize to the kinetochore, albeit in a cell-stage specific manner. We name the protein " bridgin (Bgi1)". With these findings, we subsequently question if bridgin is indeed a kinetochore protein and if so how and where does it localize? Further, we also ask as to what function bridgin performs at the kinetochore in *C. neoformans*?

Chapter 3 : Functional characterization of the putative kinetochore protein bridgin (Bgi1)

Assembly hierarchy of sub-complexes at the kinetochore

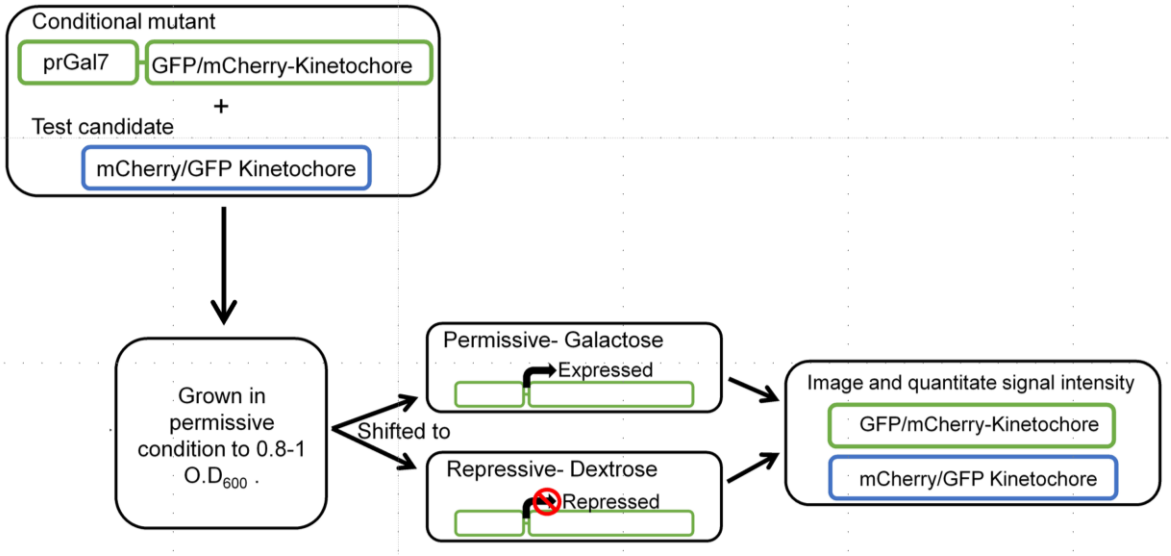

Figure 3-1: Schematic of microscopy-based kinetochore interdependency assay.

Schematic of the experimental design to determine localization interdependency amongst kinetochore sub-complexes.

Previously we have observed that bridgin localized exclusively to the kinetochore (Figure 2-6). We subsequently investigated where amongst the kinetochore hierarchy bridgin localized to. Our previous study suggested a step-wise assembly of the kinetochore, yet no sequential assembly of kinetochore sub-complexes was established in *C. neoformans* (Kozubowski et al., 2013). Thus, using a microscopy-based interdependency analysis (Figure 3-1), we determined the hierarchy of the identified protein sub-complexes (CENP-A^{Cse4}, CENP-C^{Mif2}, KNL1 complex, Mis12 complex, Ndc80 complex, and the Dam1 complex) that constitute the kinetochore in *C. neoformans* (Figure 3-2 and 2-3E).

We observe that the Mis12 complex and Ndc80 complex influence the stability of each other at the kinetochore (Figure 3-2B and C). The Dam1 complex (Figure 3-2H-J) and KNL1 complex (Figure 3-2D-G) independently require the Mis12 complex-Ndc80 complex platform for kinetochore recruitment (Figure 3-2B-C). Further, the Ndc80 complex demands the presence of the kinetochore protein CENP-C^{Mif2} for its localization (Figure 3-2A). Additional representative proteins from the various complexes were used to validate these results. The performed interdependencies are tabulated (Figure 3-3A) and summarized in a schematic (Figure 3-3B).

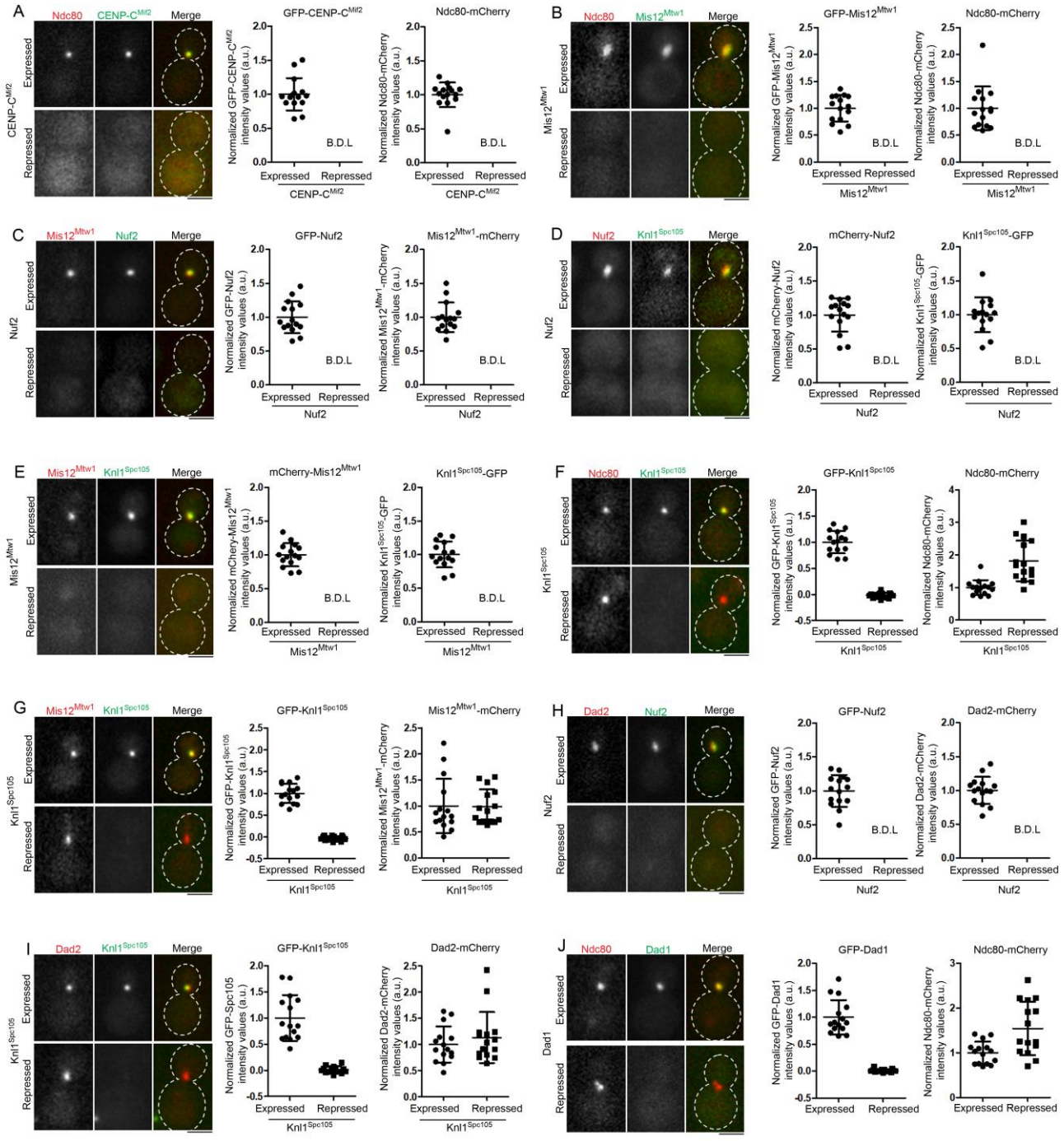

Figure 3-2: Kinetochore localization interdependencies of protein sub-complexes in C. neoformans.

(A-J) Kinetochore proteins were fluorescently labeled in a kinetochore conditional mutant. Normalized intensities of the tagged kinetochore proteins were measured under conditions of expression and repression of the conditional kinetochore mutant. The strong influence of the conditional kinetochore protein on the test protein resulted in signals that were below detectable levels (B.D.L). *N* = 15 for the expressed and repressed conditions. Error bars, s.d. Scale bar, 3 μm. **(A)** The dependency of Ndc80 (Ndc80 complex) on CENP-C^{Mif2}. **(B)** The dependency of Ndc80 (Ndc80 complex) on Mis12^{Mtw1} (Mis12 complex). **(C)** The dependency of Mis12^{Mtw1} (Mis12 complex) on Nuf2

(Ndc80 complex). **(D)** The dependency of Knl1^{Spc105} (KNL1 complex) on Nuf2 (Ndc80 complex). **(E)** The dependency of Knl1^{Spc105} (KNL1 complex) on Mis12^{Mtw1} (Mis12 complex). **(F)** The dependency of Ndc80 (Ndc80 complex) on Knl1^{Spc105} (KNL1 complex). **(G)** The dependency of Mis12^{Mtw1} (Mis12 complex) on Knl1^{Spc105} (KNL1 complex). **(H)** The dependency of Dad2 (Dam1 complex) on Nuf2 (Ndc80 complex). **(I)** The dependency of Dad2 (Dam1 complex) on Knl1^{Spc105} (KNL1 complex). **(J)** The dependency of Ndc80 (Ndc80 complex) on Dad1 (Dam1 complex).

A

			Depletion of kinetochore protein							
	Kinetochore sub-complex		CENP-A	CENP-C	Mis12C	Ndc80C	KNL1C	Dam1 complex		
		KT protein	CENP-A^{Cse4}	CENP-C^{Mif2}	Mis12^{Mtw1}	Nuf2	Knl1^{Spc105}	Dad1	Dad2	Ask1
Kinetochore protein localization upon depletion	CENP-A	CENP-A^{Cse4}	-	N.D.	+	+	+	+	N.D.	N.D.
	CENP-C	CENP-C^{Mif2}	-	-	+	+	+	+	N.D.	N.D.
	Mis12C	Mis12^{Mtw1}	-	-	-	-	+	+	N.D.	N.D.
	Ndc80C	Ndc80	-	-	-	-	+	+	N.D.	N.D.
	KNL1C	Knl1^{Spc105}	N.D.	N.D.	-	-	-	N.D.	+	N.D.
	Dam1 complex	Dad1	-	N.D.	-	N.D.	N.D.	-	-	N.D.
		Dad2	-	-	N.D.	-	+	-	-	-
		Ask1	N.D.	N.D.	N.D.	N.D.	N.D.	N.D.	N.D.	-

(+) : retains localization **(-)** : loss in localization N.D. : not determined

B

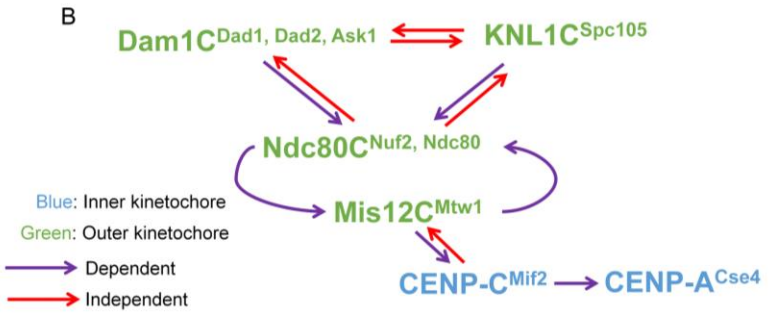

Figure 3-3: The kinetochore hierarchy.

(A) Table summarizing the kinetochore interdependencies tested. Symbols in red highlight the shown interactions. **(B)** Schematic of interdependencies observed across kinetochore sub-complexes at the *C. neoformans* kinetochore.

Bridgin is recruited via multiple outer kinetochore KMN network receptors

Having established the hierarchy of sub-complexes at the kinetochore, we subsequently determined how bridgin was recruited to the kinetochore. Interdependency analyses

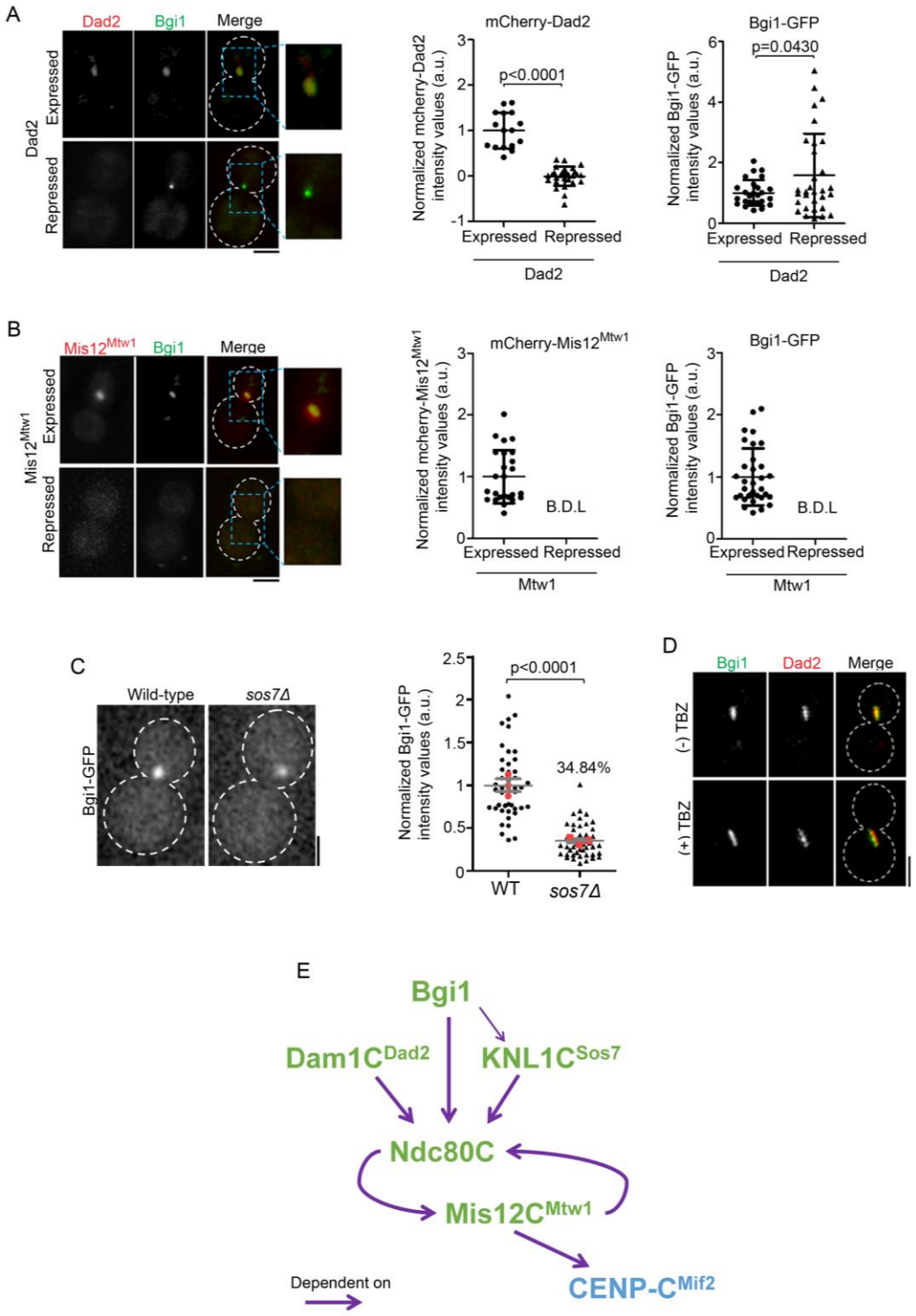

Figure 3-4: Bridgin is recruited by multiple receptor sites at the outer kinetochore KMN network.

(A) (*Left*) Bridgin localization signals in representative cells in the presence and absence of Dad2. *(Right)* Levels of Dad2 and bridgin signals upon Dad2 expression and repression are quantified. For Dad2 measurements, *N* = 16 and *N* = 29 or Dad2 expressed and repressed conditions, respectively. For Bgi1-GFP measurements, *N* = 26 and *N* = 31 for Dad2 expressed and repressed conditions, respectively. *P*-value was

determined using the two-tailed t-test. Error bars, s.d. **(B)** Normalized intensities of Mis12^{Mtw1} and bridgin under conditionals of Mis12^{Mtw1} expression and repression. The strong influence of Mis12^{Mtw1} kinetochore protein on bridgin resulted in signals that were below detectable levels (B.D.L). Scale bar, 3 µm. *N* = 25 and *N* = 33 for Mis12^{Mtw1} and bridgin, respectively. Error bars, s.d. **(C)** Bridgin signal intensities at the kinetochore were measured in WT and *sos7Δ* cells. Red dots indicate the mean bridgin signal intensities of three independent transformants. Error bars, s.e.m. *P*-value was determined using the two-tailed t-test. *N* = 45. Scale bar, 2 µm. **(D)** Representative cells illustrate the non-reliance of bridgin on an intact mitotic spindle for kinetochore localization. (+) TBZ cells were treated with 10 µg/ml thiabendazole (TBZ) for 3 h. Scale bar, 3 µm **(E)** Schematic describes the observed localization interdependency of kinetochore protein complexes at the *C. neoformans* kinetochore. The direction of the purple arrow corresponds to the dependence of one complex on the indicated protein complex. Protein complexes indicated in green or blue correspond to the outer or inner kinetochore, respectively.

---

suggested bridgin localizes to the kinetochore independent of Dad2 (Dam1 complex) (Figure 3-4A). On the other hand, bridgin localization at the kinetochore wholly and partially (~65%) depended on Mis12^{Mtw1} (Mis12 complex) (Figure 3-4B) and Sos7 (Knl1 complex) (Figure 3-4C), respectively. Further, bridgin's kinetochore localization is independent of spindle integrity (Figure 3-4D). These results suggest that there may be multiple binding sites for the recruitment of bridgin at the outer kinetochore KMN network, downstream of the KNL1 complex and Mis12 complex-Ndc80 complex platform (Figure 3-4E).

Bridgin reaches a peak concentration at the kinetochore during anaphase

To understand how bridgin dynamics is regulated during cell cycle progression, we analyzed bridgin signal intensities at the kinetochore. Bridgin localized to the kinetochore starting from G2 until telophase/G1 (Figure 3-5A-E). Additional copies of bridgin are added to the kinetochore during mitosis, reaching a peak immediately at the onset of anaphase. At this stage, bridgin intensity attains an average of ~150% of metaphase intensity (Figure 3-5B, E, and F). The dynamic intensities of transiently localized kinetochore proteins of the KMN network, Mis12^{Mtw1}, Nuf2, and Knl1^{Spc105}, and the subunits of the Dam1 complex, Dad1, and Dad2, were measured (Figure 3-6). The KMN network proteins localized concomitantly to the kinetochore during G2 and persisted until

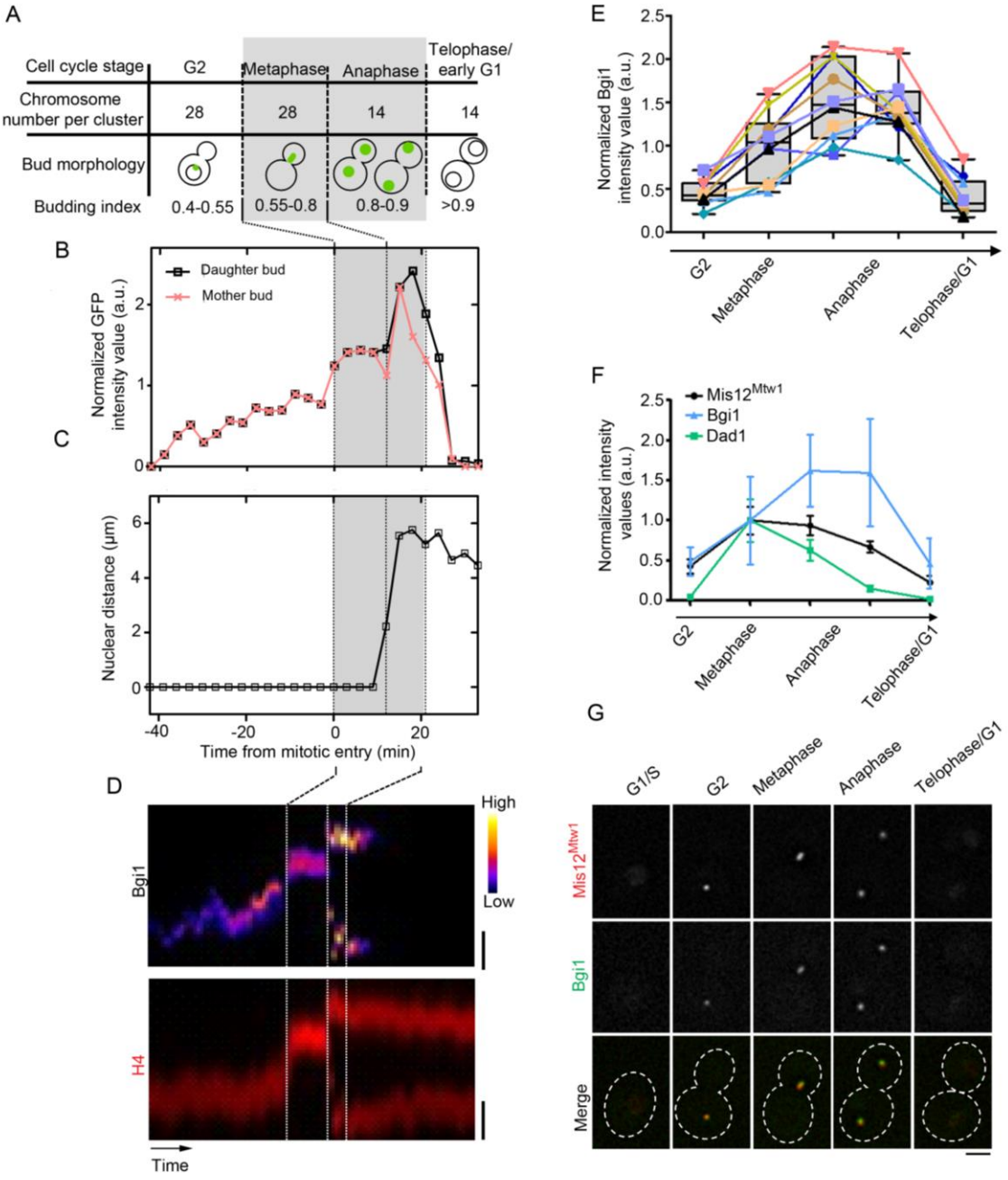

Figure 3-5: Bridgin localizes to the kinetochore, starting from G2 to the end of the M phase.

(**A)** Expected chromosome number per kinetochore cluster in the haploid type-strain H99*α* and spatial location of bridgin with corresponding budding index are tabled. **(B)** Signal intensity measurements of bridgin from the G2 phase until the subsequent G1 phase are shown in a plot at an interval of 3 min. The event of mitotic entry is referred to as time 0. **(C)** A cell is considered to have exited anaphase when nuclear distances have reached their maxima. **(D)** A kymograph of the corresponding tabulated bridgin signals. Time interval represented, 1 min for a total of 100 min. Scale bar, 2 μm. **(E)** A normalized intensity plot of bridgin signals from G2 until telophase in ten cells. Error bars, standard deviation (s.d.). **(F)**. Comparison of protein levels of bridgin, and representative proteins of the outer kinetochore. *N* = 5 each kinetochore protein. Error bars, s.d. **(G)** Co-

localization of Bgi1-GFP signals in cells at the various stages of the cell cycle with Mis12^{Mtw1} in an asynchronous culture. Scale bar, 3 µm.

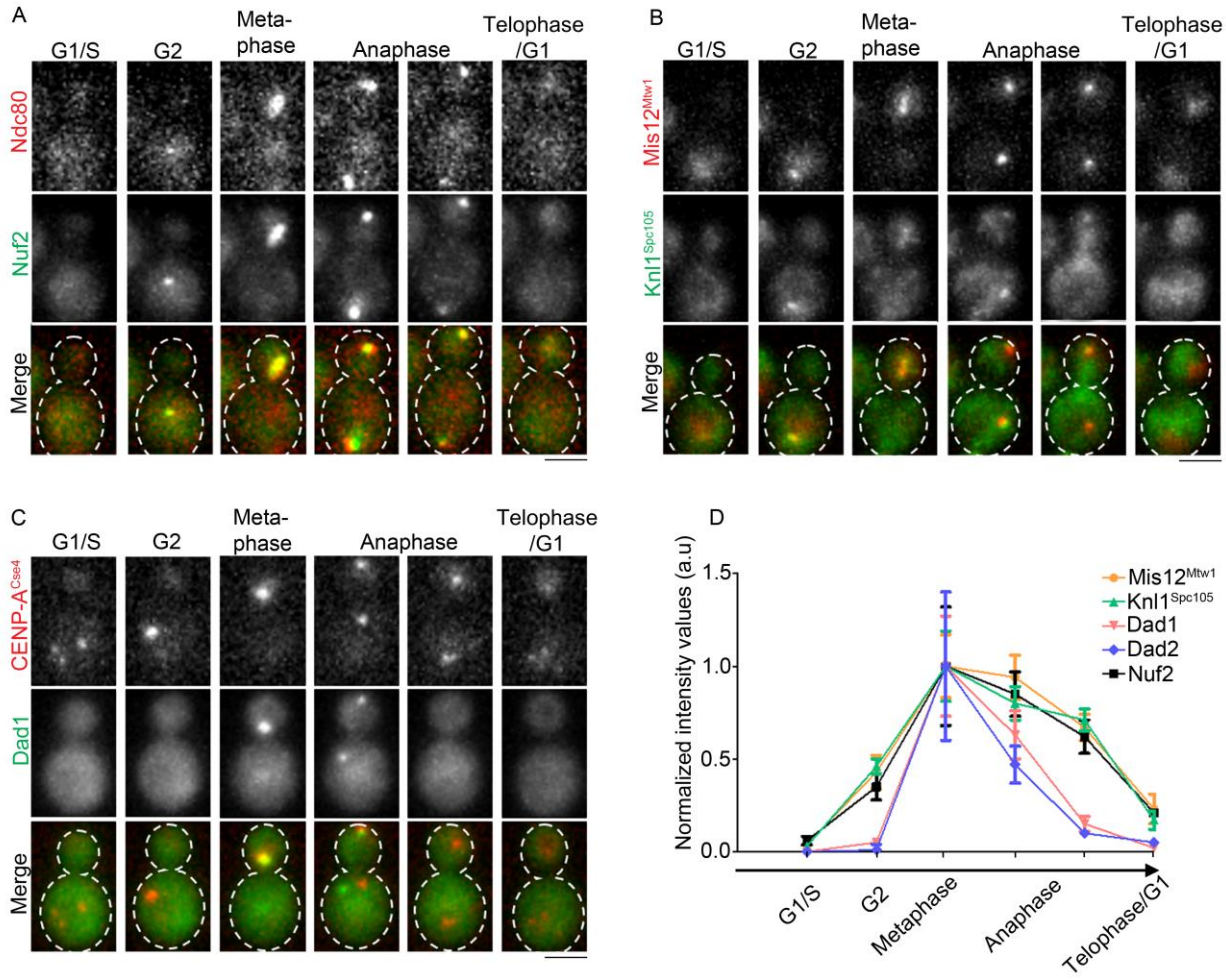

Figure 3-6: Dynamics of kinetochore proteins through the cell cycle.

(A-C) Representative images of fluorescently tagged kinetochore proteins followed through the cell cycle. **(A)** Nuf2 and Ndc80, components of the Ndc80 complex. **(B)** Knl1^{Spc105} and Mis12^{Mtw1} of the KNL1 complex and Mis12 complex, respectively. **(C)** Dam1 complex component Dad1 and the centromeric histone H3 variant CENP-A^{Cse4}. **(D)** Tabulation of kinetochore intensities in 5 cells across the mentioned cell cycle stages. Error bars, s.d. Scale bar, 3 µm

telophase/G1, reaching the maximum signal intensity during metaphase (Figure 3-6A and B). The Dam1 complex proteins Dad1 and Dad2 localized post-mitotic onset exclusively, reaching peak intensity at metaphase and reducing sharply, almost to an undetectable level in late anaphase (Figure 3-6C and D). Thus, KMN network proteins and bridgin

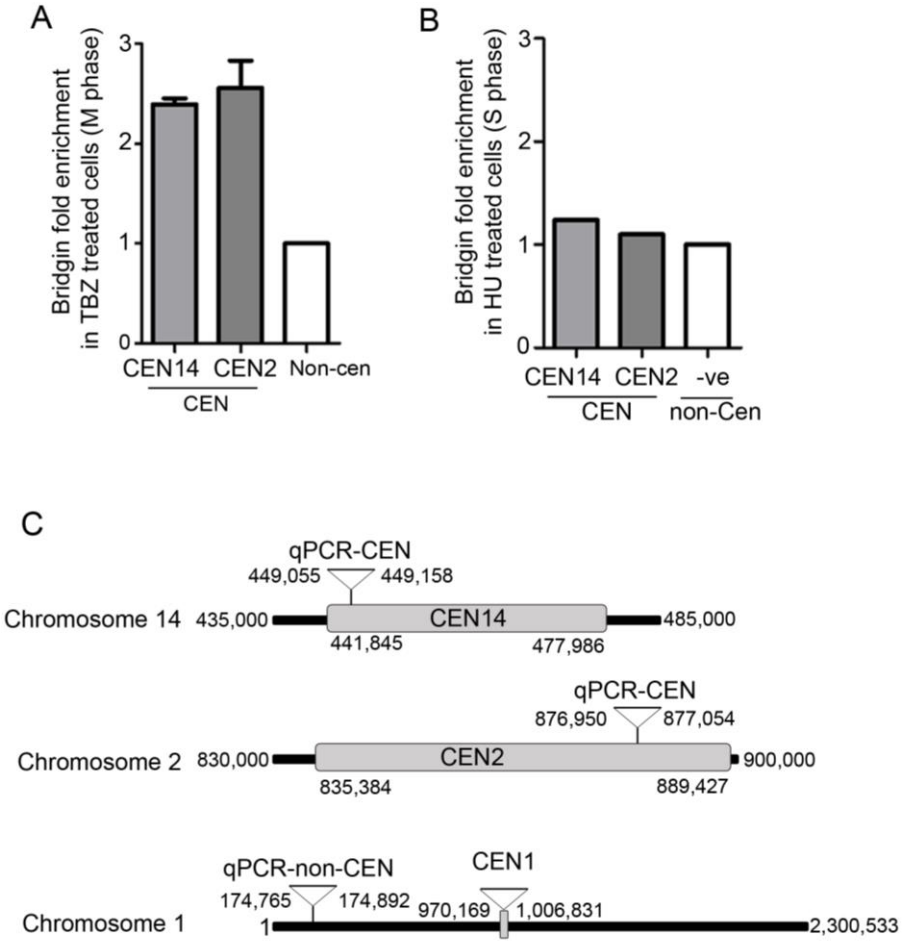

Figure 3-7: Bridgin localizes at the centromere during the M phase.

(A and B) Measurement of levels of bridgin at the kinetochore in M phase **(A)** and S phase **(B)** cells by cross-linked ChIP-**q**uantitative **p**olymerase **c**hain **r**eaction (qPCR). Centromeres (14,2) and control non-centromeric regions were amplified by specific primers to determine its levels at the centromere. *N* = 3. Error bars, s.d. **(B)** ChIP enrichment of bridgin in HU treated (200mM, 3h) cells arrested in early S phase. **(C)** Schematic is representing the location of utilized qPCR primers.

---

reached peak kinetochore intensities at distinct times, metaphase and anaphase, respectively (Figure 3-5F).

Analysis of bridgin localization in an asynchronous population further validated the cell cycle-stage specific kinetochore localization, which was similar to the outer kinetochore protein Mis12^{Mtw1} (Figure 3-5G). Chromatin immunoprecipitation assays validated these microscopic observations. Bridgin could be localized at the centromeric loci in an M phase enriched cell population but not in S phase cells (Figure 3-7A-C). Supporting a cell cycle stage-specific kinetochore localization of bridgin.

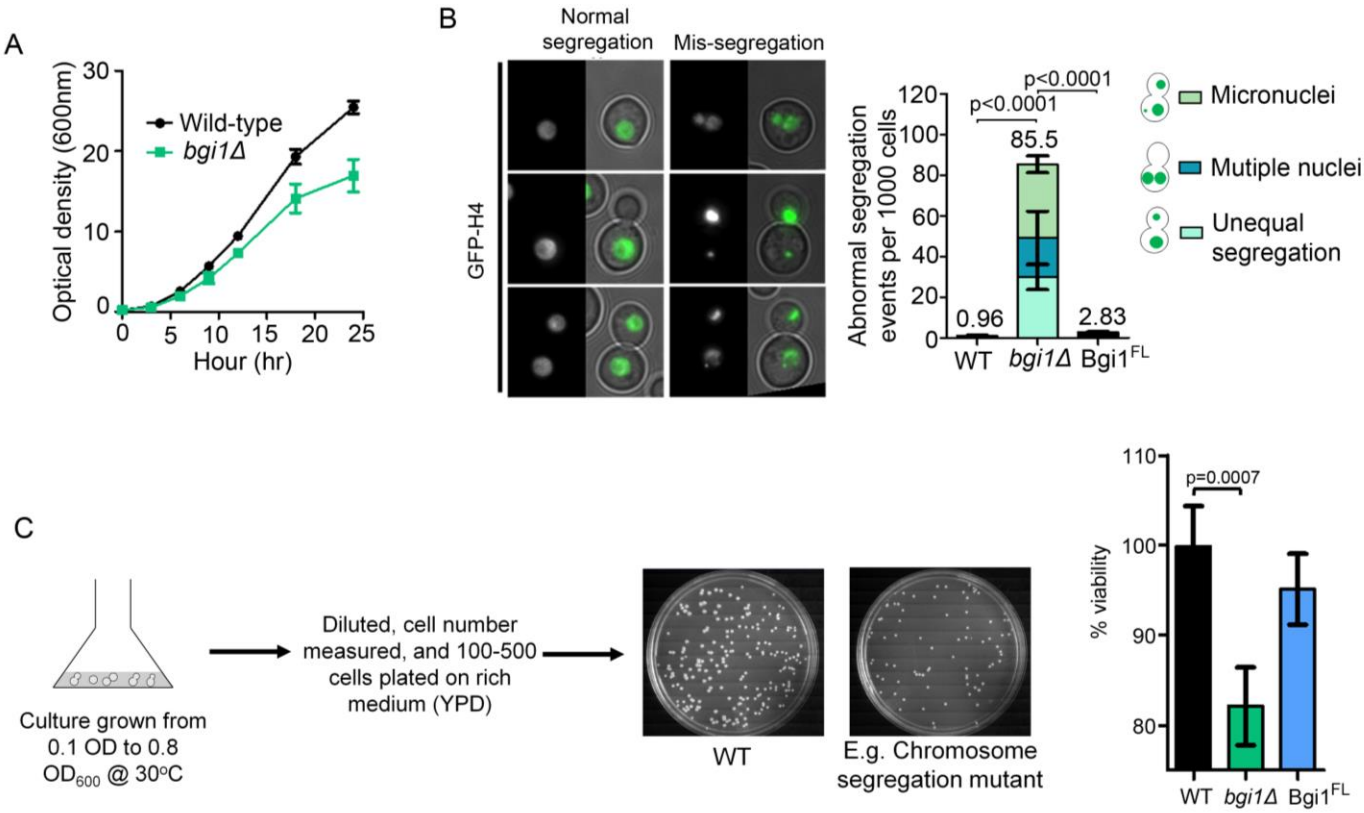

Figure 3-8: Bridgin is required for mitotic fidelity.

(A) Growth curve of the WT strain H99*α* and bridgin null mutant (*bgi1Δ*) cells. *N* = 3. **(B)** *(Left)* Representative events scored as normal, or chromosome missegregation events are mentioned. The presence of multiple nuclei in a single cell, unequal segregation amongst daughter cells, and formation of micronuclei were considered as missegregation events. *(Right)* The rate of abnormal nuclear segregation events was measured using GFP-H4 in WT, *bgi1Δ,* and bridgin full-length re-integrant (FL) strains. The number of cells examined was >3000, *N* = 3. Error bars, s.d. *P*-value was determined using a two-tailed t-test. **(C)** *(Left)* Schematic of the experimental design to estimate cell viability. *(Right)* The **c**olony-**f**orming **u**nit (CFU) was counted after 48 h at 30°C and tabulated. Error bars, s.d. *N* = 3. *P*-value determined using the two-tailed t-test.

Exclusive localization and enrichment at the kinetochore and dependence on the outer kinetochore KMN network proteins of bridgin strongly implicate that bridgin is as an outer kinetochore protein. Further, taking into consideration the interdependency with the outer kinetochore proteins and the localization dynamics, we conclude that bridgin localizes onto the KMN platform at the kinetochore.

Bridgin is important for accurate kinetochore-microtubule interaction

Bridgin-null (*bgi1Δ*) strains were generated to characterize the function of bridgin as a kinetochore protein. *bgi1Δ* cells exhibited reduced growth rates (Figure 3-8A), and ~20% loss in viability as compared to WT (Figure 3-8C). These mutant cells also displayed an ~90-fold increase in the gross missegregation rate as compared to WT, which may account for the reduced viability in *bgi1Δ* (Figure 3-8B). Gross missegregation events of chromosomes are an under-representation of overall chromosome loss rates. *bgi1Δ* defects were complemented by the reintegration of the full-length bridgin gene ($Bgi1^{FL}$) expressed under its native promoter (Figure 3-8B and C).

Defective kinetochore-microtubule attachments are a consequence of bridgin loss (*bgi1Δ*).

We subsequently examined how *bgi1Δ* affected cell cycle progression. For this, previously determined microscopic markers to determine cell cycle stages used (Figure 2-5). While WT cells spent an average of 18 min in M phase, *bgi1Δ* cells showed a delay in M phase, spending an ~30 min (an under-representation since ~10% of cells failed to exit M phase arrest even after >50 min) (Figure 3-9A). No significant change was observed for the time spent in other cell cycle stages (Figure 3-9A). While the total cell cycle time was not statistically significant between WT and *bgi1Δ,* a delay of around 11 min on average was observed (Figure 3-9B). Within the M phase, the delay was found to occur prior to anaphase onset, suggestive of a SAC dependent delay (Figure 3-9C). *bgi1Δ cells* exhibited unattached chromosomes, lagging chromosomes, and micronuclei formation defects upon live-cell analysis, suggesting that inaccurate kinetochore-microtubule attachments occurred (Figure 3-9D-G).

mad2Δ in the background of *bgi1Δ* alleviated the M phase delay (Figure 3-9C), but the double mutants were conditionally synthetic lethal upon treatment of the microtubule poison thiabendazole (2 μg/ml) or under conditions of spindle insult (14˚C and 37˚C) (Figure 3-10). Based on these observations, we conclude that bridgin is important for accurate kinetochore-microtubule interactions and that *bgi1Δ* cells elicit a prolonged SAC response in its absence to correct for erroneously kinetochore-microtubule attachments.

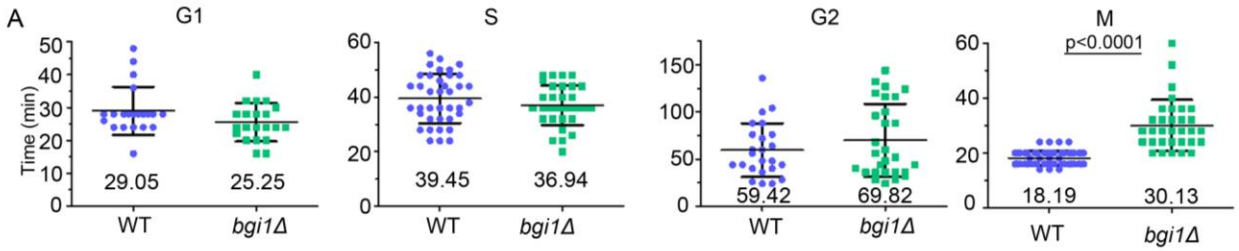
A
G1
S
G2
M
Time (min)
29.05
25.25
39.45
36.94
59.42
69.82
18.19
30.13
p<0.0001
WT
bgi1Δ

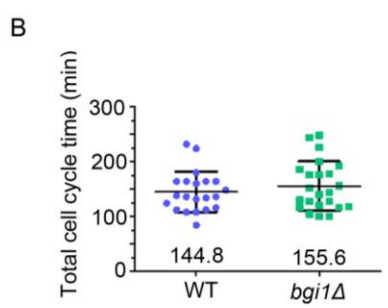
B
Total cell cycle time (min)
144.8
155.6
WT
bgi1Δ

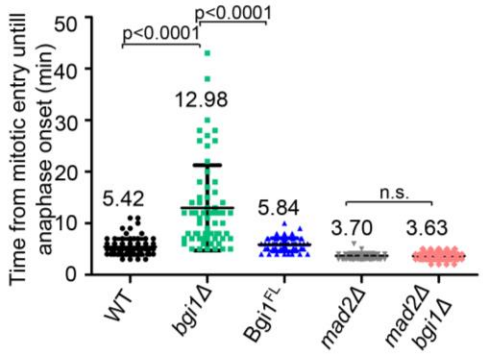
C
Time from mitotic entry untill anaphase onset (min)
p<0.0001
p<0.0001
12.98
5.42
5.84
n.s.
3.70
3.63
WT
bgi1Δ
Bgi1FL
mad2Δ
mad2Δ bgi1Δ

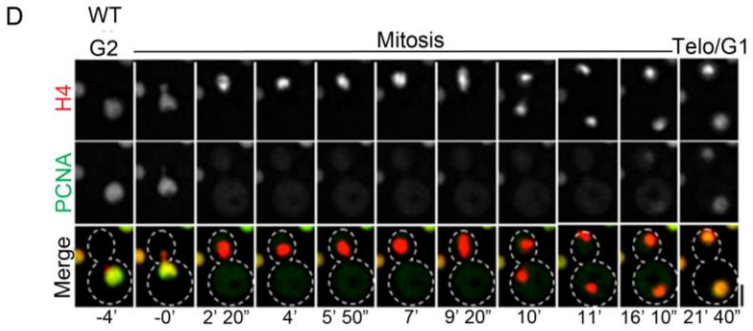
D
WT
G2
Mitosis
Telo/G1
H4
PCNA
Merge
-4'
-0'
2' 20"
4'
5' 50"
7'
9' 20"
10'
11'
16' 10"
21' 40"

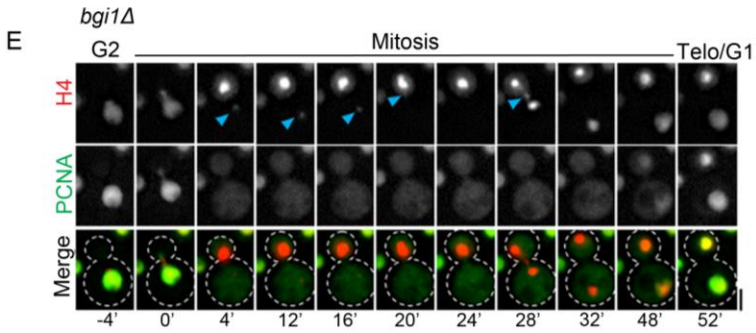
E
bgi1Δ
G2
Mitosis
Telo/G1
H4
PCNA
Merge
-4'
0'
4'
12'
16'
20'
24'
28'
32'
48'
52'

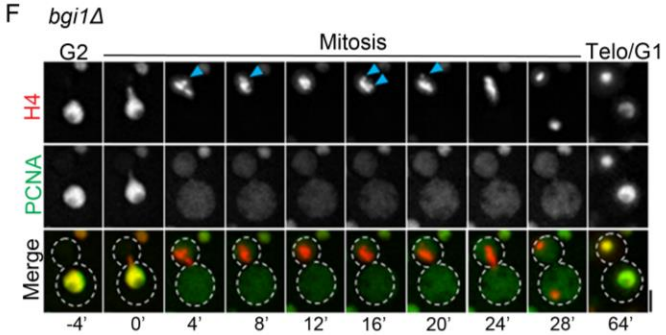
F
bgi1Δ
G2
Mitosis
Telo/G1
H4
PCNA
Merge
-4'
0'
4'
8'
12'
16'
20'
24'
28'
64'

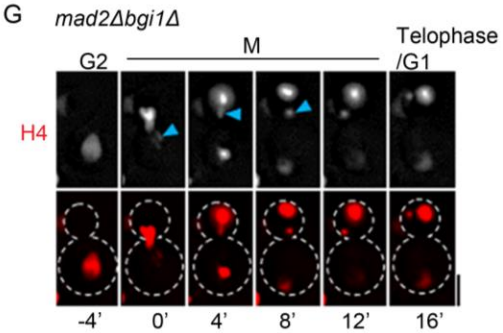
G
mad2Δbgi1Δ
G2
M
Telophase /G1
H4
-4'
0'
4'
8'
12'
16'

Figure 3-9: Loss of bridgin results in mad2 mediated mitotic arrest.

(A) Comparison of cell cycle stage-specific timing between WT and *bgi1Δ*. The mean of the measured times is mentioned. WT *N* = 21,38,24 and 52 in G1, S, G2, and M phases, respectively. *bgi1Δ N* = 21, 34, 28, and 32 in G1, S, G2, and M phases, respectively. Error bars, s.d. *P*-value determined using the two-tailed t-test. **(B)** Total cell cycle time was determined by live-cell analysis using cell cycle events marked by a nuclear protein PCNA and a chromatin-associated protein H4. Error bars, s.d. WT: *N* = 21, *bgi1Δ*: *N* = 23. *P*-value determined using the two-tailed t-test. **(C)** Time from the mitotic entry to anaphase onset was quantified and plotted for each strain as indicated. Diffusion of a nuclear marker PCNA coincided with the migration of the nucleus into the daughter cell, indicating entry into semi-open mitosis. Nuclear distance >1 µm was considered as the entry into anaphase. Mean of WT (*N* = 88), *bgi1Δ* (*N* = 64), Bgi1FL (*N* = 61), *mad2Δ* (*N* = 67) and *mad2Δ bgi1Δ* (*N* = 56) were measured as indicated. Error bars, s.d. *P*-value was determined using the two-tailed t-test. Not significant, n.s. **(D-G)** Representative time-lapse images of **(D)** WT**, (E and F)** *bgi1Δ***,** and **(G)** *mad2Δbgi1Δ* cells. The onset of mitosis was considered as *t* = 0. Cell cycle stages were scored for either by PCNA localization or chromatin condensation (H4-mCherry) and nuclear migration into the daughter bud. **(E)** Blue arrows point to an unattached chromosome at the mitotic onset and a lagging chromosome at anaphase. Scale bar, 2 µm. **(F)** Blue arrows indicate a chromosome that is separated from the compact chromatin mass in prometaphase, as seen in WT. Scale bar, 2 µm. **(G)** Blue arrows point to an unattached chromosome that results in a micronuclei formation. Scale, 3 µm.

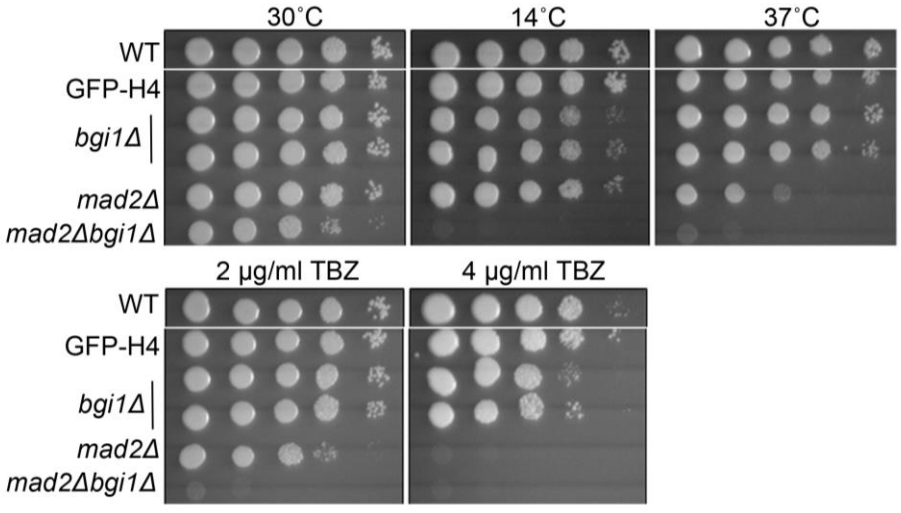

Figure 3-10: Defective kinetochore-microtubule attachments are a consequence of bridgin loss (*bgi1Δ*).

10-fold dilutions starting from $2x10^5$ cells were spotted for WT, GFP-H4, *bgi1Δ*, *mad2Δ*, and *mad2Δ bgi1Δ* are shown.

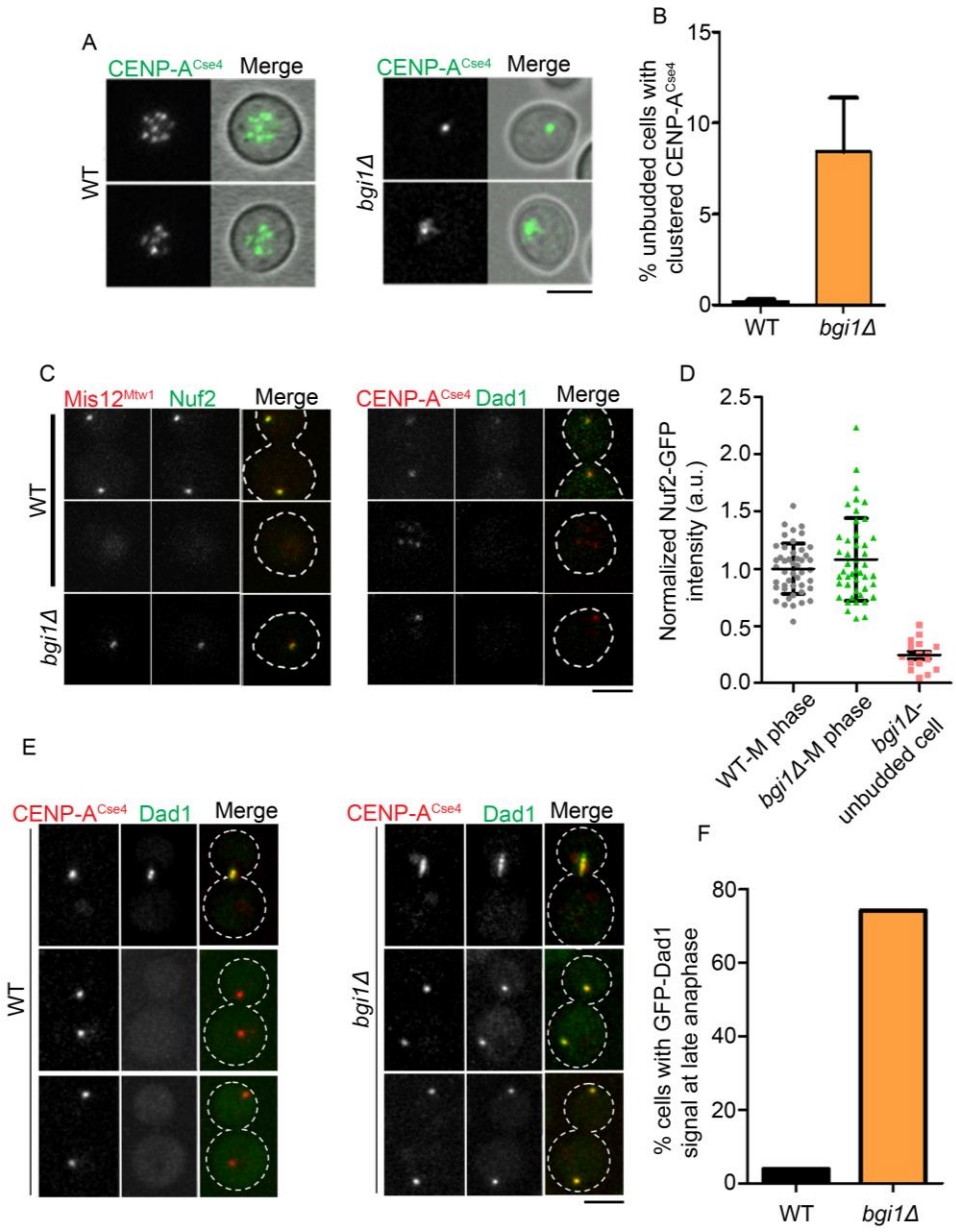

Figure 3-11: Bridgin loss effects kinetochore dynamics in *C. neoformans*.

(A) Representative images of GFP-CENP-A^{Cse4} localization in unbudded cells of WT and *bgi1Δ.* Scale, 3 μm. **(B)** Quantitation of the % population of unbudded cells with clustered kinetochore signals. *N* = 3. The number of cells counted is >200 for each experiment. Error bars, s.d. **(C)** Representative images of altered KMN network and Dam1 complex dynamics. Scale, 3 μm. **(D)** Quantitation of Nuf2-GFP signal in unbudded cells. *N* = 46, 45, and 26 for WT M-phase, *bgi1Δ* M-phase, and unbudded cells, respectively. Error bars, s.d. **(E)** Representative images of the Dam1 complex protein Dad1 dynamics in M phase. Scale, 3 μm. **(F)** Tabulation of the number of later anaphase cells with persistent GFP-Dad1 punctate signal. The number of cells counted is >100.

Loss of bridgin effects centromere clustering and kinetochore disassembly

C. neoformans centromeres undergo clustering from an unclustered state in G2, which persists until telophase/G1 of the cell cycle. We observed ~8% of the unbudded cell population (G1/S) to exhibit clustered centromeres phenotype in *bgi1Δ*, which was close to none in WT (Figure 3-11A and B). Is the outer kinetochore disassembly also affected in these unbudded cells? Our analysis revealed that the outer kinetochore KMN network, marked by Nuf2 and Mis12^{Mtw1}, persisted in these unbudded cells, although at lower intensities (Figure 3-11C and D). However, no Dam1 complex signal was observed in these unbudded cells (Figure 3-11C). However, interestingly in *bgi1Δ*, ~80% of cells in late anaphase retained Dam1 complex signal, while it observed in 4% of WT cells (Figure 3- 11E and F). Thus, loss of bridgin was found to alter the disassembly dynamics of the Dam1 complex.

The altered disassembly dynamics associated with cells lacking bridgin suggest an overall delay in kinetochore disassembly. It is to be tested if the delay in kinetochore disassembly is linked to centromere clustering. Furthermore, the mechanism(s) by which bridgin sheds influence on kinetochore disassembly dynamics and centromere clustering is to be studied in the future.

Summary

With the observation that bridgin localizes to the kinetochore, our aim was to understand how and where it localizes to at the kinetochore and its subsequent function. Towards this goal, in this chapter, we begin with determining the hierarchy of protein sub-complexes at the kinetochore. Not surprisingly, the outer kinetochore components required the inner kinetochore subunits for their localization. However at the outer kinetochore the Ndc80-Mis12 complexes directed the recruitment of other outer kinetochore components. Placing bridgin in this hierarchy, we observed that its kinetochore localization required the Mis12 complex and to a less extent, the KNL1 complex component Sos7. This observation in addition to ChIP enrichment of bridgin at the centromere and bridgin kinetochore localization being independent of spindle integrity, led us to conclude that

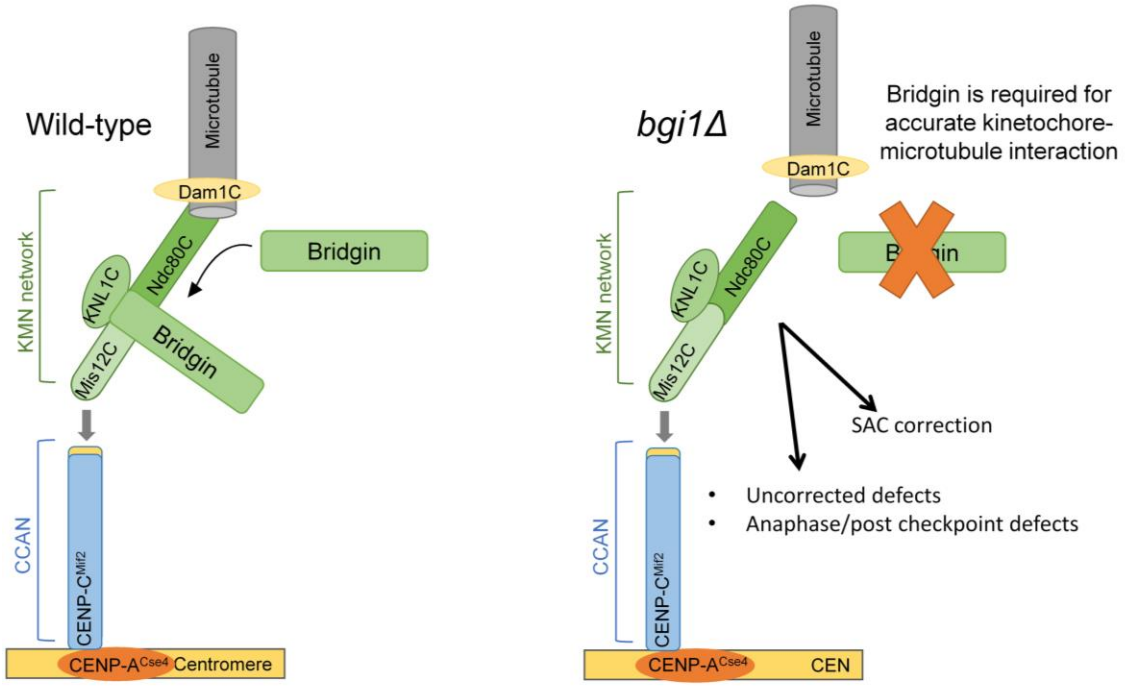

Figure 3-12: Schematic of bridgin recruitment to the kinetochore and its subsequent role.

(Left) Bridgin was found to be recruited to the kinetochore downstream of the outer kinetochore KMN network. *(Right)* In the absence of bridgin, inaccurate kinetochore-microtubule attachments result in a SAC dependent cell cycle delay in the M phase. An ~90-fold increase in the rate of missegregation defects is observed, a possible consequence of uncorrected defects or defects that manifest post-SAC.

---

bridgin is an outer kinetochore protein. Analysis of bridgin levels at the kinetochore suggest a concomitant loading with other KMN network components at G2. Additional bridgin molecules were added during mitosis reaching a peak during anaphase, unlike other outer kinetochore proteins that reached an intensity maximum during metaphase.

To assess bridgin function, *bgi1Δ* strains were generated. These null mutant cells exhibited increased chromosome missegregation defects of ~90-fold. We addressed the observed missegregation phenotype to be a consequence of compromised kinetochore-microtubule attachments in *bgi1Δ*. Furthermore, we also noticed that bridgin was also found to influence the disassembly and clustering-unclustering dynamics of the *C. neoformans* kinetochore. With these exciting outcomes, we next asked as to how bridgin carries out its influence on the formation of accurate kinetochore-microtubule attachments?

Chapter 4 : Structure-function analysis of the outer kinetochore protein bridgin

Bridgin is directed to the kinetochore through its FD and the USD

We sought to understand how bridgin carries out its role at the kinetochore. Bridgin is a 1295-amino acid (aa) long protein, in which aa1-124 forms a fork-head associated domain (FD, a phosphopeptide recognition domain), and aa161-164 possibly forms an unconventional PP1 docking site. The rest of the protein is predicted to be largely unstructured (Figure 4-1A). The aa1005-1295 C-terminal region is predicted to have a pI of 11.20, and we refer to this region as the basic domain (BD). The unstructured domain (USD) was defined as a region spanning aa125-1004, which was acidic with a pI of 4.65 (Figure 4-1A) and contained 13 repeats with a consensus motif rich in acidic residues (Figure 4-1B and Appendix IV). Domain deletion constructs were generated as described in Figure 4-1C, wherein the domain deletion is expressed under its native promoter with an N-terminal 3xFLAG-GFP epitope tag. The cassettes were reintegrated into *bgi1Δ* cells expressing H4-mCherry (Figure 4-1D) to obtain strains expressing truncated bridgin proteins with various domains deleted, as mentioned in Figure 4-1C.

Microscopic estimation of GFP signal intensities of the bridgin derivatives and the $Bgi1^{FL}$ suggested that the FD and USD regions were able to localize independently of each other at the kinetochore, albeit to different extents of ~20% and ~40% of the WT level, respectively (Figure 4-1E and F). Localization of $Bgi1^{BD\Delta}$ at the kinetochore was not significantly different from that of WT (Figure 4-1E and F). Further, lack of kinetochore localization by the BD suggested it was not involved in kinetochore localization of bridgin. Thus the localization analysis using various truncated mutants suggest that bridgin can make multiple contacts at the kinetochore through its FD and USD. Consistent with the observation that bridgin is recruited downstream to multiple outer kinetochore proteins (Figure 3-4B, C, and E).

The basic domain of bridgin is dispensable for its localization but indispensable for its function.

To define the domains necessary for bridgin function, we scored for complementation of the *bgi1Δ* phenotype at 37˚C, due ease of scoring owing to enhancement in the population of M phase delayed cells (Figure 4-2A), and cell growth assays under conditions altering microtubule dynamics (Figure 4-2C). Partial complementation of phenotype was

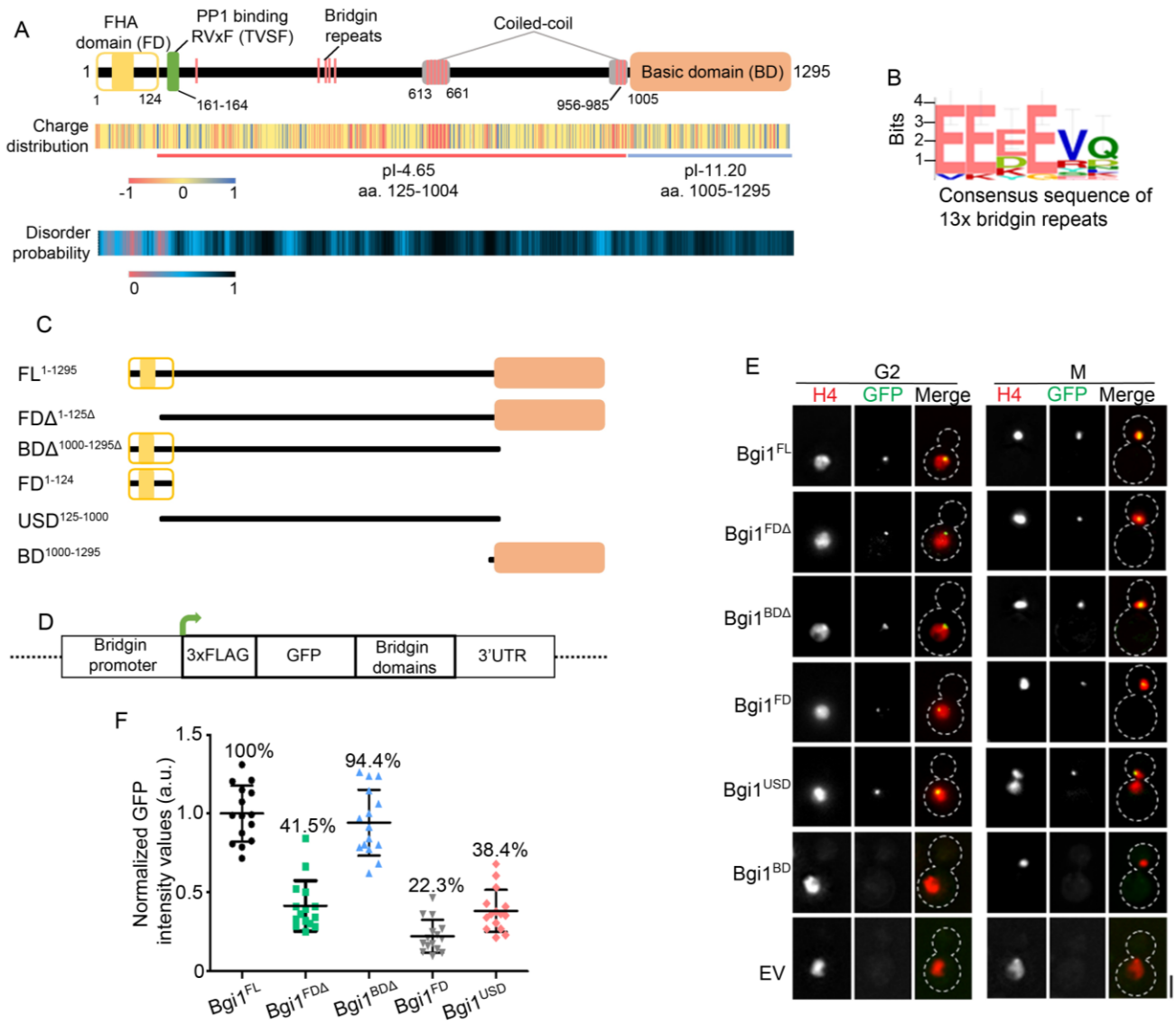

Figure 4-1: Kinetochore recruitment and positioning of bridgin via multiple receptor sites.

(A) Schematic describing predicted features of bridgin protein. Charge distribution of amino acid residues was predicted with a window size of 2 using EMBOSS charge. The disorder probability of bridgin was calculated using IUPRED2A. **(B)** The motif for bridgin repeats was identified using MEME suit with the alignment of the 13 identified bridgin repeats, of 8-amino acid in length. **(C)** Schematic of generated domain deletion constructs of bridgin. Constructs were generated with a 3xFLAG-GFP tag at the amino-terminus. **(D)** Schematic of the bridgin domain deletion construct cassette. Not to scale. **(E)** Representative cells in G2 and M phase showing localization of bridgin or its derivatives and the **e**mpty control **v**ector (EV). Bridgin constructs were integrated into the *bgi1Δ* strain. Nuclear localization was scored for using the chromatin marker histone H4. Scale bar, 3 µm. **(F)** Bridgin signal intensities were measured in 15 mitotic cells prior to anaphase onset. Percent intensity values normalized to FL have been mentioned.

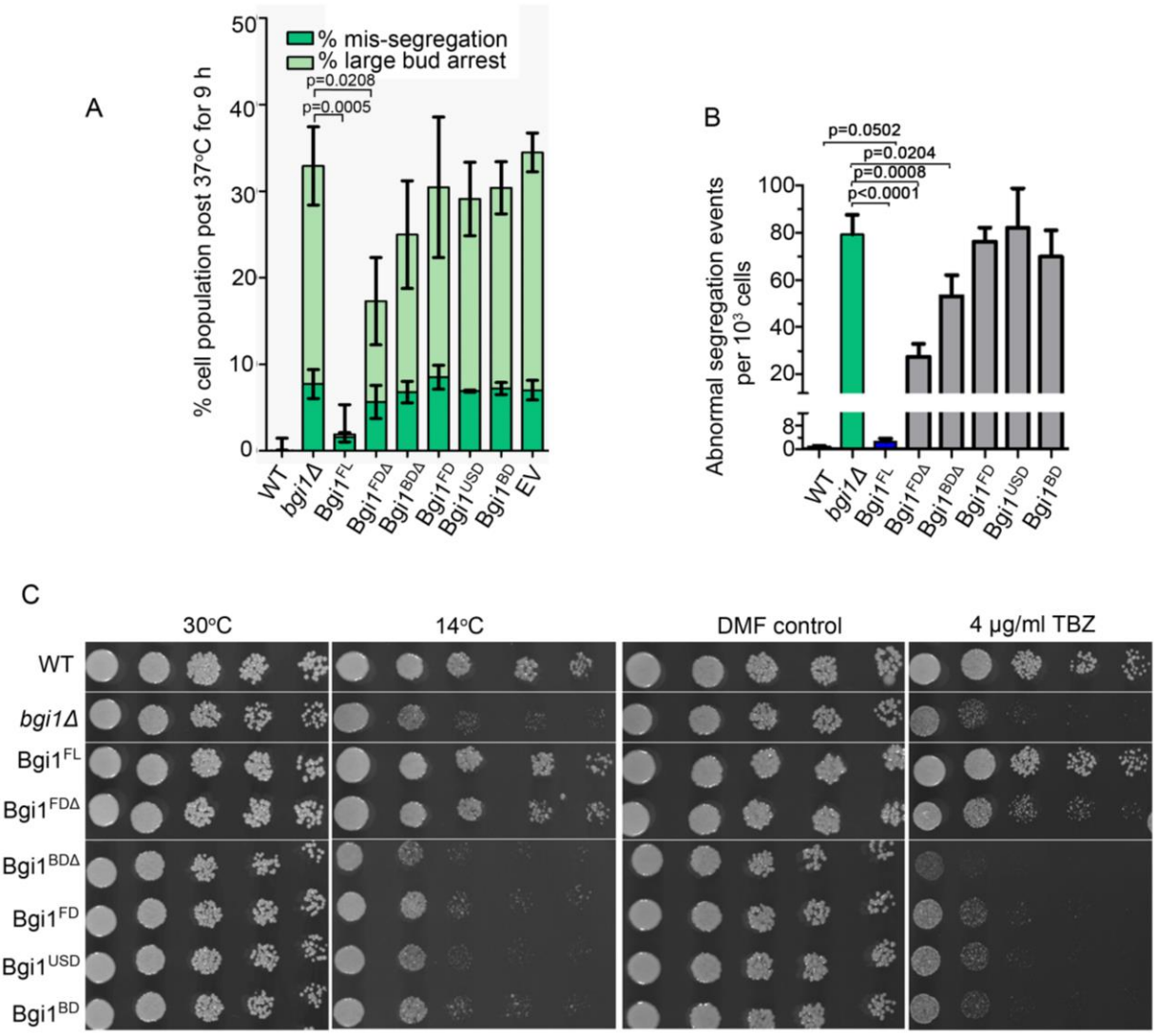

Figure 4-2: Kinetochore localization is insufficient for bridgin function.

(A) The extent of complementation by truncated proteins of bridgin was measured. H4-mCherry was localized in bridgin protein derivatives, lacking various domains, in a *bgi1Δ* strain background. Cells were grown at 30˚C until log phase and transferred to 37˚C. Indicated cell populations were measured 9 h post-incubation at 37˚C. All values were normalized to WT. Defects in nuclear segregation were measured, as mentioned in Fig 3b. Error bars, s.d. The number of cells examined was >1000, *N* = 3 for each indicated strain. **(B)** The Rate of abnormal segregation defect was measured for each of the strains mentioned and normalized to events per 10^3. The number of cells examined was > 2000. *N* = 3. Error bars, s.d. *P*-value determined using the two-tailed t-test. **(C)** Cells of varying numbers $2x10^4$, $2x10^3$, 200, 100, and 50 cells were spotted on plates as indicated. Plates were incubated at the indicated temperatures for 2, 3 or 7 days for 30˚C and DMF control, 30˚C with 4 µg/ml TBZ and 14˚C, respectively.

observed for the $Bgi1^{FD\Delta}$ mutant, exhibiting reduced kinetochore localization while retaining the BD. No significant complementation was obtained for any of the other

domain deletion constructs, including the Bgi1$^{BD\Delta}$, that localized to the kinetochore similar to Bgi1^{FL} levels (Figure 4-2A and C). Bgi1^{FL} was able to suppress the *bgi1Δ*phenotype significantly (Figure 4-2A and C). Comparable results were observed for the rate of missegregation events at 30˚C, albeit weak complementation was observed for Bgi1$^{BD\Delta}$ (Figure 4-2B). Taken together, all domains, including BD, which is not related to kinetochore localization of bridgin, are critical for the function of bridgin.

SAC activity, spindle dynamics, and gross kinetochore composition are unaffected in the absence of bridgin.

To identify how bridgin effects kinetochore-microtubule attachments and the role of BD thereof, we first tested if SAC activity was compromised. WT and *bgi1Δ* cells in the presence of a microtubule depolymerization drug, arrested with equal efficiency (Figure 4-3A and B). Subsequently, to test the influence of bridgin on spindle dynamics, time taken from early to late anaphase, a stage spindle is highly dynamic, was measured. Time taken was observed to be ~3 min for both WT and *bgi1Δ* (Figure 4-3C). Further, to test if bridgin loss effected the gross composition of the kinetochore, Nuf2 (Figure 4-3D), Knl1^{Spc105} (Figure 4-3E), Mis12^{Mtw1} (Figure 4-3F) and CENP-A^{Cse4} (Figure 4-3G), levels at the kinetochore was quantitated and found to be consistent with WT levels in *bgi1Δ*. Thus, these factors were ruled out as possible reasons for defective kinetochore-microtubule attachments associated with *bgi1Δ* mutants.

Interaction of bridgin with chromatin may require its carboxy-terminal basic domain (BD)

To address the role of the BD towards bridgin function, FLAG affinity purification of Bgi1^{FL} (using 150 mM KCl and a more stringent condition of 300 mM KCl) and Bgi1$^{BD\Delta}$ (150 mM KCl) was performed. The samples were subsequently subject to mass spectrometry analysis (Figure 4-4A and Appendix V). A comparison of the relative abundance of specific interactors obtained within Bgi1^{FL} and Bgi1$^{BD\Delta}$ suggested an enrichment of chromatin interacting proteins in Bgi1^{FL} affinity purification over Bgi1$^{BD\Delta}$ (Figure 4-4B *top*). While kinetochore proteins were relatively more abundant as interactors in Bgi1$^{BD\Delta}$ over Bgi1^{FL} affinity purifications (Figure 4-4 *bottom*). Proteins of

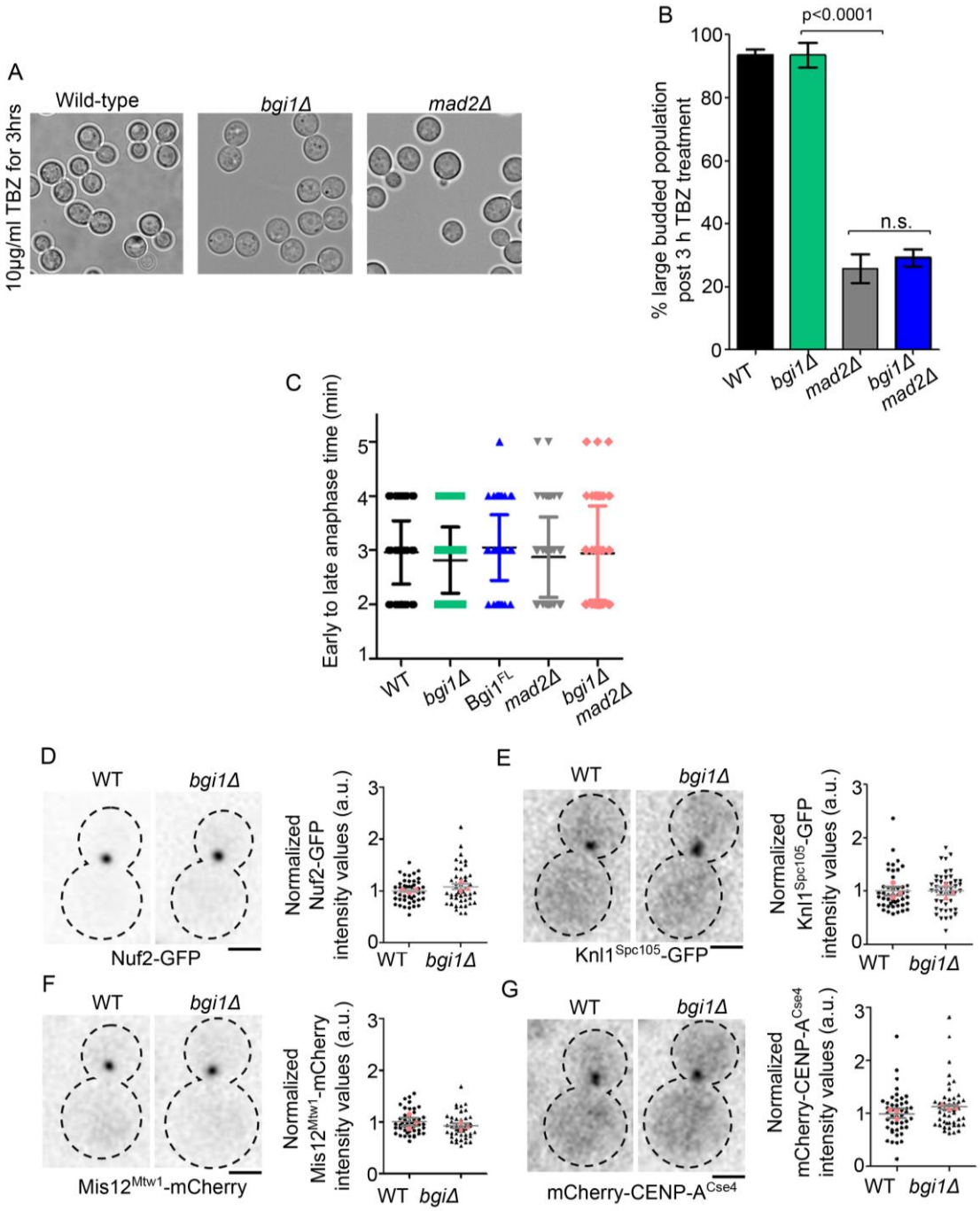

Figure 4-3: Bridgin does not affect SAC activity, spindle dynamics, and gross kinetochore composition.

(A and B) WT, *bgi1Δ,* and *mad2Δ* cells were treated for 3 h with 10 µg/ml of thiabendazole (TBZ). **(A)** Representative bright-field micrographs of WT, *bgi1Δ,* and *mad2Δ* cells. **(B)** The percentage of large budded cells was determined by scoring for cells with a budding index of >0.55. Error bars, s.d. >300 cells for each of the strains used were measured. *N* = 3. *P*-value determined using the two-tailed t-test. **(C)** Measurement of time spent in anaphase for WT, *bgi1Δ*, *mad2Δ*, and *mad2Δbgi1Δ* cells. Cells were considered to have entered anaphase if their kinetochore distances were >1 µm or if the leading edge of the chromatin marker histone H4 were >1 µm. Late anaphase was defined as stages when kinetochore distances reached a maximum. *N* =

88, 64, 61, 67 and 56 respectively for WT, *bgi1Δ*, Bgi1^{FL}, *mad2Δ* and *mad2Δbgi1Δ*. Error bars, s.d. **(D-G)** Measurement of the kinetochore protein intensity in WT and *bgi1Δ* cells. The kinetochore intensity values in representative cells of WT and *bgi1Δ* are shown as inverted greyscale images. Signal intensity was measured in 45 cells across 3 independent transformants. Red symbols denote the means of each independent transformant. Scale bar, 2 µm. *P*-value determined using the two-tailed t-test. **(D)** Nuf2-GFP **(E)** Knl1^{Spc105}-GFP **(F)** Mis12^{Mtw1}-mCherry **(G)** mCherry-CENP-A^{Cse4}.

---

the KMN network was among the top hits in Bgi1$^{BD\Delta}$ (Figure 4-4 and Appendix V). Thus, further promoting bridgin as an outer kinetochore protein interacting with the KMN network. Additionally, identification of CENP-A^{Cse4} as an interactor in the Bgi1^{FL} IP-MS data suggests an interaction of bridgin with centromeric chromatin as previously suggested (Figure 3-7A).

Based on the observation that chromatin interacting proteins are more enriched in the Bgi1 construct containing the BD, Bgi1^{FL}, we hypothesized that the BD might interact with chromatin. Through co-immunoprecipitation experiments, histone H4 was found to associate with Bgi1^{FL} (150 mM) and to a reduced extent with inner kinetochore protein CENP-C^{Mif2} (Figure 4-4C). No detectable association of histone H4 was obtained with outer kinetochore proteins (Dsn1, Spc25, and Spc34) or Bgi1$^{BD\Delta}$ (Figure 4-4C). These results led us to hypothesize that bridgin-chromatin interaction requires the bridgin basic domain and is not a consequence of bridgin receptor assembly, the outer kinetochore KMN network, onto centromeric chromatin.

The carboxy-terminal basic domain of bridgin displays non-specific interaction with DNA/chromatin *in vitro*

We tested the possibility of interactions between bridgin BD and chromatin *in vitro* by **e**lectrophoretic **m**obility **s**hift **a**ssay (EMSA) (Figure 4-5A). It was observed that the Bgi1^{BD} was necessary and sufficient to interact with DNA (Figure 4-5B). Analysis of Bgi1^{BD} binding to DNA of varying lengths and GC content suggested no particular preference for binding. Similar results were obtained for the Bgi1^{FL} (Figure 4-5D). Non-specific Bgi1^{BD}-DNA interactions were further strengthened by the observation that the Bgi1^{BD}-22 nt oligo complex could be competed out by adding a molar-excess of 63 nt oligo or poly(dI-dC) (Figure 4-5E).

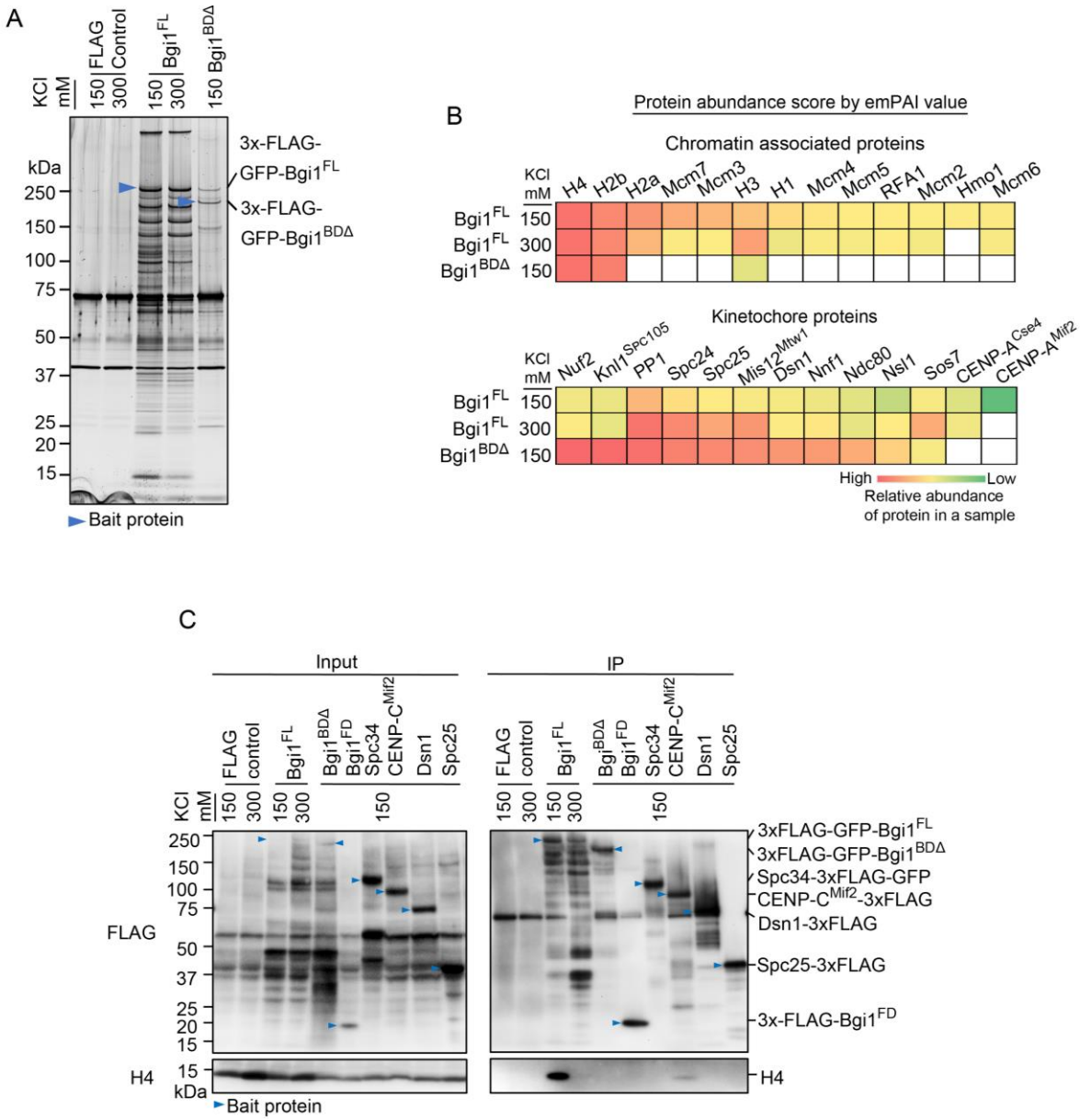

Figure 4-4: The basic carboxy terminus of bridgin may interact with chromatin *in vivo*.

(a) The silver-stained gel used to visualize bridgin interacting proteins. Blue arrows indicate the bait protein on each lane as applicable. Lysates for the immunoprecipitation experiment were prepared from a G2/M cell population that was enriched by treatment with 10 µg/ml of TBZ for 3 h. Two left lanes show common contaminating proteins obtained in the single-step 3xFLAG affinity purification. **(b)** List of chromatin-associated and kinetochore proteins obtained as interactors from bridgin affinity purification. Top 10 known chromatin-associated proteins obtained in FL 150 mM affinity purification *(top)* and known kinetochore proteins obtained in BDΔ 150 mM affinity purification *(bottom)* were arranged in ascending order from left to right based on relative abundance scores across each IP. The scores are based on emPAI values obtained for interacting proteins across affinity purifications. **(c)** Proteins from 3xFLAG tagged strains were extracted, and affinity purifications were performed with FLAG antibodies. Interacting proteins were

eluted with 3xFLAG peptides, and blots were probed with FLAG and histone H4 antibodies. Bait protein bands are indicated.

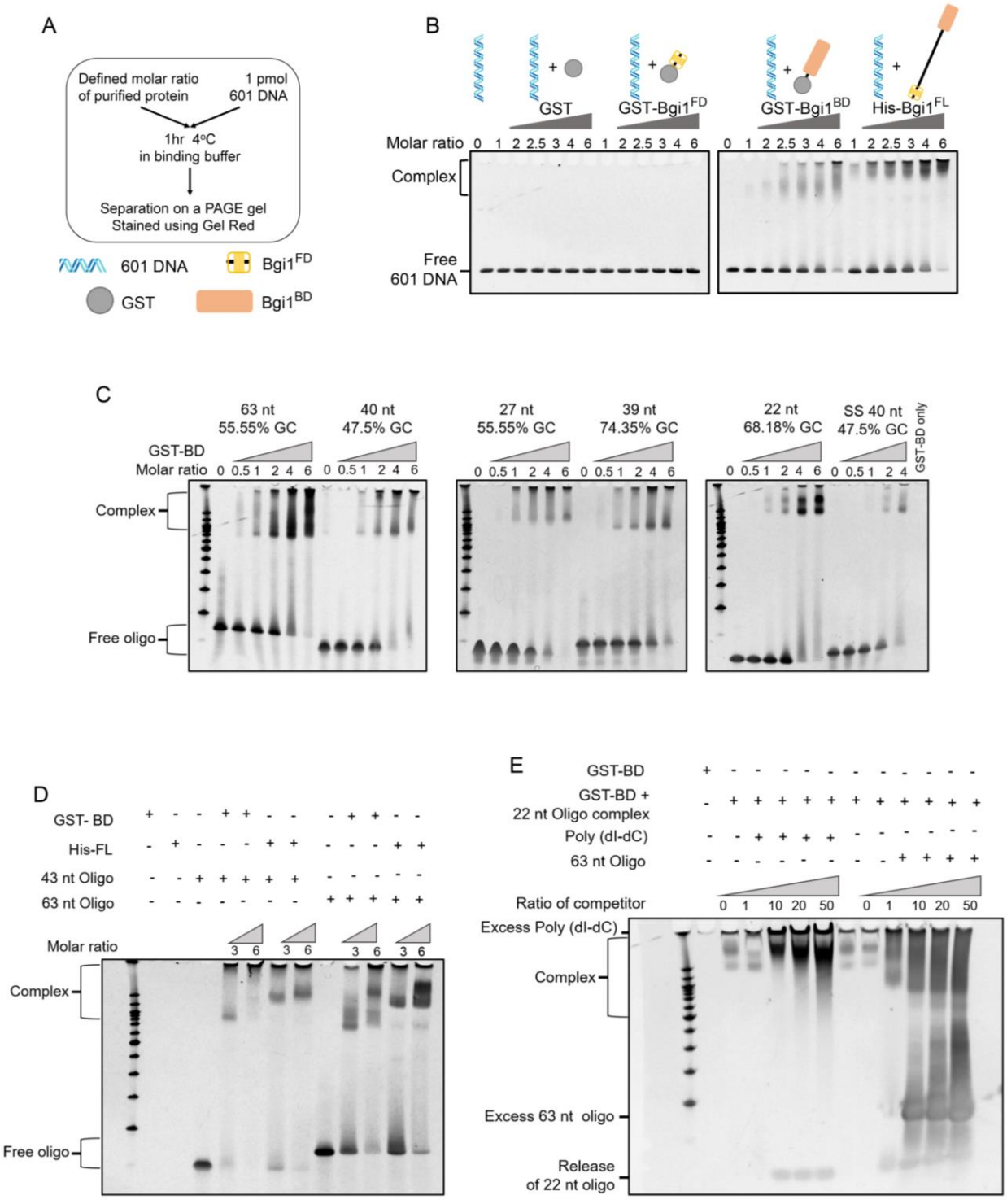

Figure 4-5: The DNA binding domain of bridgin is necessary and sufficient for non-specific DNA binding *in vitro.*

(A) Experimental design of electrophoretic mobility shift assays (EMSA) performed with 601 DNA. **(B-E)** EMSA samples were separated on a PAGE gel after incubation and stained with Gel Red for visualization. **(B)** EMSA of Bgi1 with 601 DNA. **(C)** Bgi1^{BD} interaction with DNA of varying lengths and GC content. **(D)** Comparison of Bgi1^{BD} and Bgi1^{FL} binding abilities to varying oligos. **(E)** Competition assay using Bgi1^{BD}. The complex formed with Bgi1^{BD} and a 22 nt oligo competed with poly (dI-dC) and a 63 nt oligo.

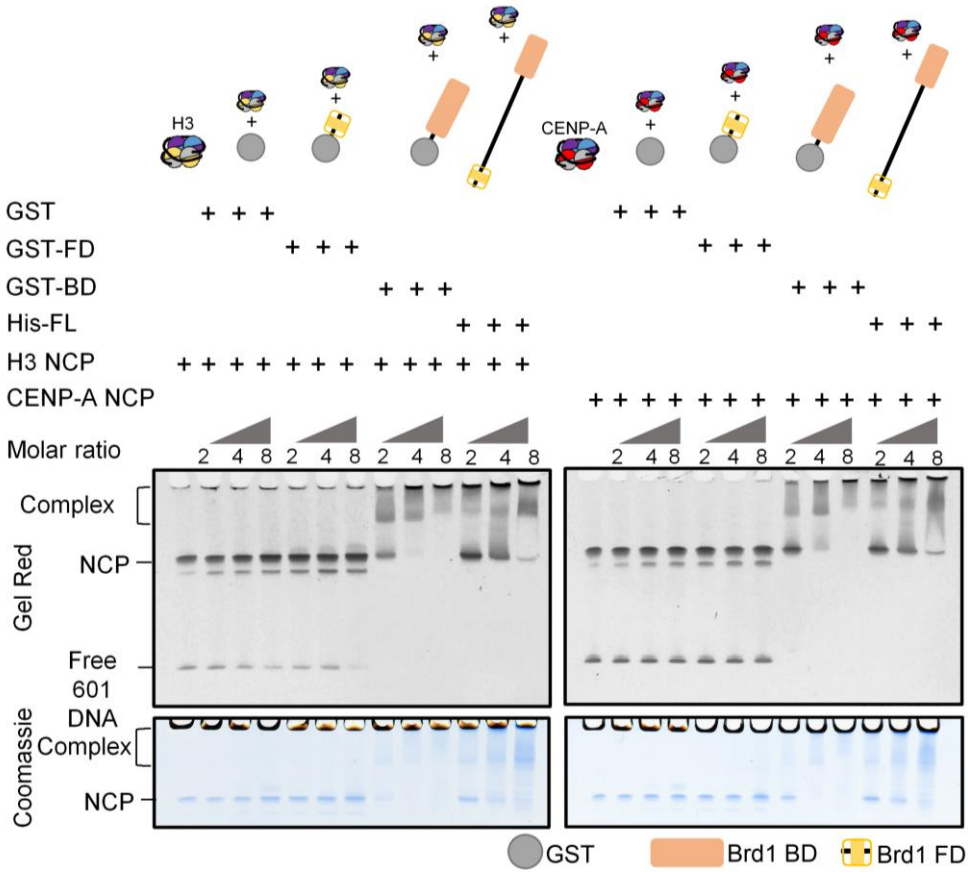

Figure 4-6: Bridgin can interact with nucleosomes of varying compositions *in vitro*.

EMSA performed with reconstituted chicken histone H3 and human CENP-A nucleosomes. Approximately 1 µM of reconstituted nucleosomes was incubated with the mentioned molar ratio of purified protein for 1 h at 4˚C. Samples were separated on a PAGE gel and stained with Gel Red, followed by Coomassie.

We next tested the possibility of interaction between Bgi1^{BD} and chromatin and observed that both Bgi1^{BD} and Bgi1^{FL} interacted with nucleosomes of varying compositions (Figure 4-6). These observations indicated that the DNA binding basic domain was necessary and sufficient for non-specific interaction with DNA/chromatin.

Bridgin basic domain (BD) is sufficient for *in vivo* non-specific interaction with chromatin

We observed non-specific bridgin-chromatin interactions *in vitro*. To test this, we hypothesized that if additional regulators existed *in vivo* to restrict bridgin BD localization to centromeric chromatin, over-expression (OE) of bridgin would not alter its localization (Figure 4-7A and B). On the contrary, we observed that localization of bridgin upon OE was transformed with respect to the native expressed protein, and localization of bridgin no longer was observed as a punctum (Figure 4-7C). Instead, Bgi1 overlapped with chromatin marked by histone H4 (Figure 4-7D), indicating that bridgin can interact with DNA/chromatin non-specifically *in vivo* as well. No microtubule-like signal or localization of Bgi1-OE outside chromatin, marked by histone H4, was observed. Thus, we ruled out the possibility of the outer kinetochore protein bridgin in binding to microtubules.

We further used the over-expression strategy as an assay to determine the DNA binding ability of bridgin domain deletion mutants *in vivo* (Figure 4-7A). PCNA was used as a negative control for chromatin binding in mitosis, as nuclear-localized but chromatin unbound PCNA pool diffused into the cytoplasm during mitosis on account of nuclear-pore complex disassembly (Figure 4-7D). While $Bgi1^{FL}$-OE localization was observed to overlap with H4-mCherry, $Bgi1^{BD\Delta}$-OE was restricted to a punctum. Supporting the notion that bridgin localizes to the kinetochore through FD and USD, a punctum for both constructs, $Bgi1^{FD,}$ and $Bgi1^{USD}$, were observed (Figure 4-7D). Further, the localization of $Bgi1^{BD}$ was found to be similar to $Bgi1^{FL}$. Thus, these observations suggested that the BD was necessary and adequate to bind chromatin *in vivo,* and the loss of BD in the over-expression constructs was sufficient to restrict bridgin localization to the kinetochore puncta (Figure 4-7D).

Considering that bridgin was recruited to the outer kinetochore downstream of the KMN network, it was surprising that bridgin BD binds to chromatin. Nevertheless, increased enrichment of DNA from the $Bgi1^{FL}$ over $Bgi1^{BD\Delta}$ in the native-ChIP suggested that bridgin, through its BD, interacts with DNA when kinetochore localized (Figure 4-8).

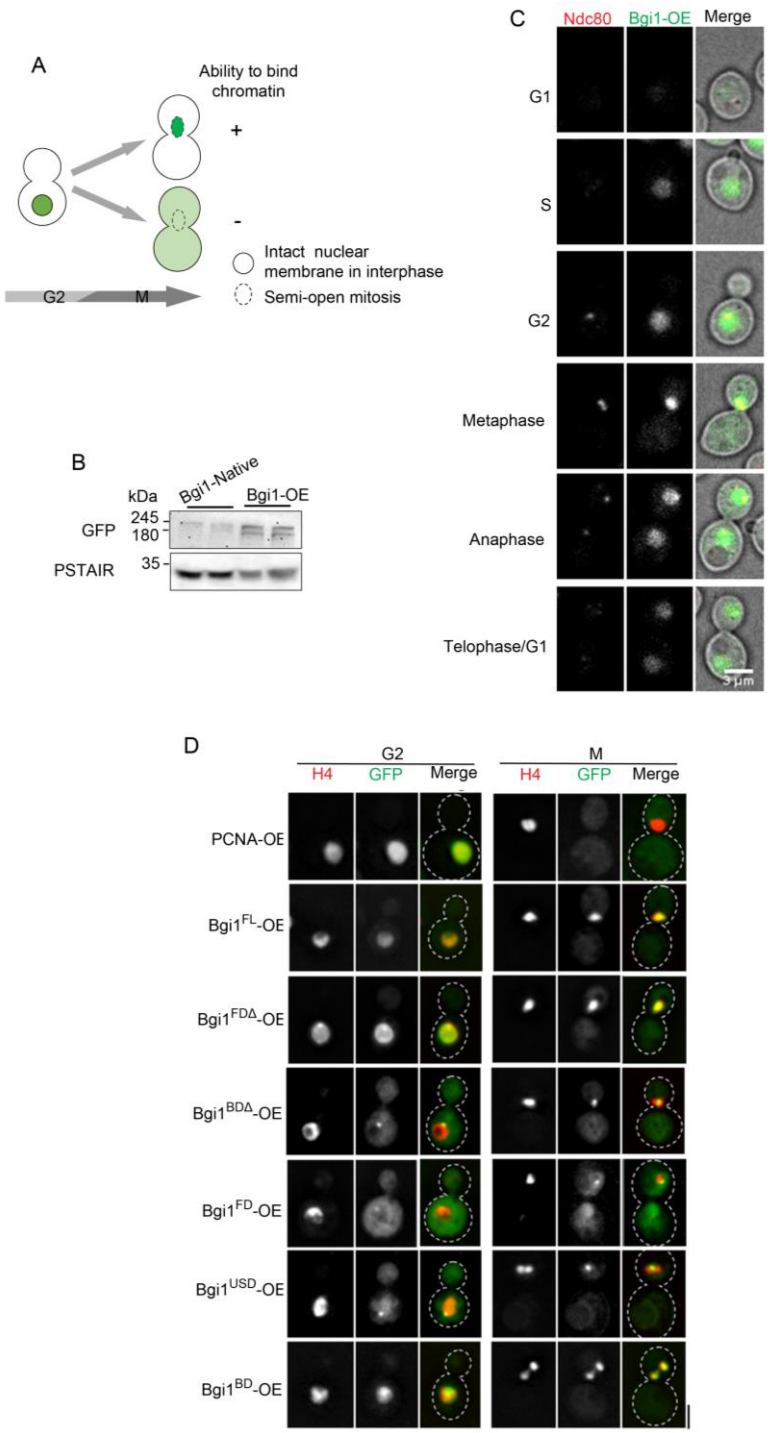

Figure 4-7: BD of bridgin is sufficient for interaction with chromatin *in vivo*.

(A) Schematic showing chromatin-bound proteins would colocalize with the nuclear marker H4-mCherry in metaphase while free nuclear proteins diffuse into the cytoplasm following the entry into mitosis. **(B)** Whole-cell protein levels of bridgin when expressed under the native or *GAL7* promoter construct. **(C)** Visualization of bridgin localization through the cell cycle by fluorescence microscopy when expressed under the OE promoter construct. Outer kinetochore protein Ndc80 was used to mark the kinetochore. **(D)** Visualization of Bgi1^{OE} constructs. GFP-Bgi1^{OE} constructs were transformed into the

H4-mCherry *bgi1Δ* strain. Representative images of cells in the G2 and M phases are shown. Scale bar, 3 µm.

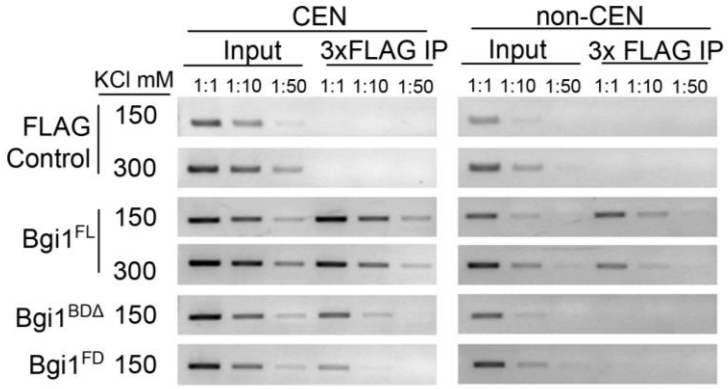

Figure 4-8: Increased enrichment of DNA by native-ChIP of Bgi1^{FL}

Native ChIP of 3xFLAG-GFP bridgin protein derivatives. G2/M cells were enriched and lysed using bead beating. FLAG affinity purification was performed as in Figure 4-4A**.** DNA was isolated from the elute, and PCR was set with two centromere and non-centromere primers. Dilutions of eluted DNA and input of 1:1, 1:10, and 1:50 were used.

Basic nature of the DNA binding basic domain of bridgin is vital for its function

We show that bridgin loss does not alter previously described chromatin marks of H3K9me2 (Figure 4-9A) and CpG methylation (Figure 4-9B) at *C. neoformans* centromeres, towards understanding the consequence of bridgin binding to DNA.

To summarize our findings, we observe that bridgin localizes to the kinetochore through the FD and USD, and its interaction with DNA/chromatin through its BD is essential for its function. However, it is still unclear how BD influences the bridgin's function. We hypothesize two possibilities: a) interaction of BD with other proteins at chromatin is essential for bridgin function or b) the ability of BD to interact with DNA is adequate for bridgin's function. To distinguish these possibilities, we performed a domain-swap experiment. Replacing the BD$^{1005\text{-}1295}$ of bridgin with an amino acid stretch of similar properties (length: ~300aa., unstructured, non-specific DNA binding ability with a charge: ~pI of 10) found in the basic region (BD)$^{2937\text{-}3256}$ of the human *KI67* gene

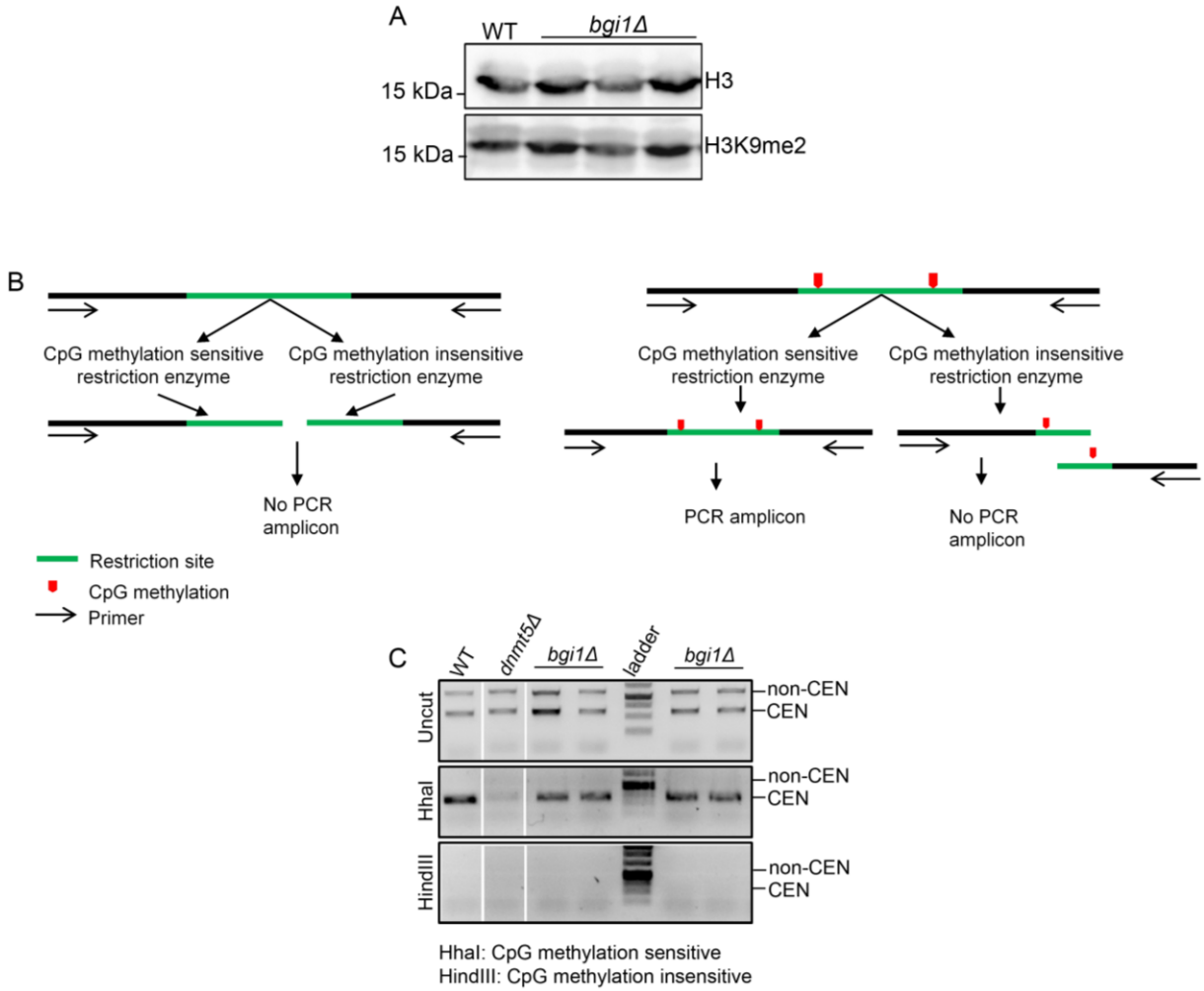

Figure 4-9: H3K9me2 and DNA methylation marks associated with the centromere is not altered in *bgi1Δ*

(A) Immunoblot analysis of the whole-cell pool of H3K9me2 levels in WT and *bgi1Δ* cells. **(B)** Detection of CpG methylation by Dnmt5 in WT and *bgi1Δ*. Schematic of the restriction enzyme-PCR based assay used to assess the methylation status at the centromere. **(C)** Restriction enzyme HindIII is insensitive, while HhaI is sensitive to CpG methylation. Genomic DNA was isolated and digested with either HindIII or HhaI, and primers flanking the restriction site is used to estimate relative levels of digested genomic DNA, a read-out for levels of CpG methylation at the locus. The amount of HhaI PCR amplicon is proportional to the level of CpG methylation in comparison to WT.

(Figure 4-10A). Ki67 was previously shown to bind non-specifically to DNA (MacCallum and Hall, 2000) and functions as a surfactant by coating chromosomes during mitosis(Cuylen et al., 2016). We confirmed that Ki67 $BD^{2937-3256}$ binds to DNA non-specifically in *C. neoformans* using the overexpression assay (Figure 4-10B).

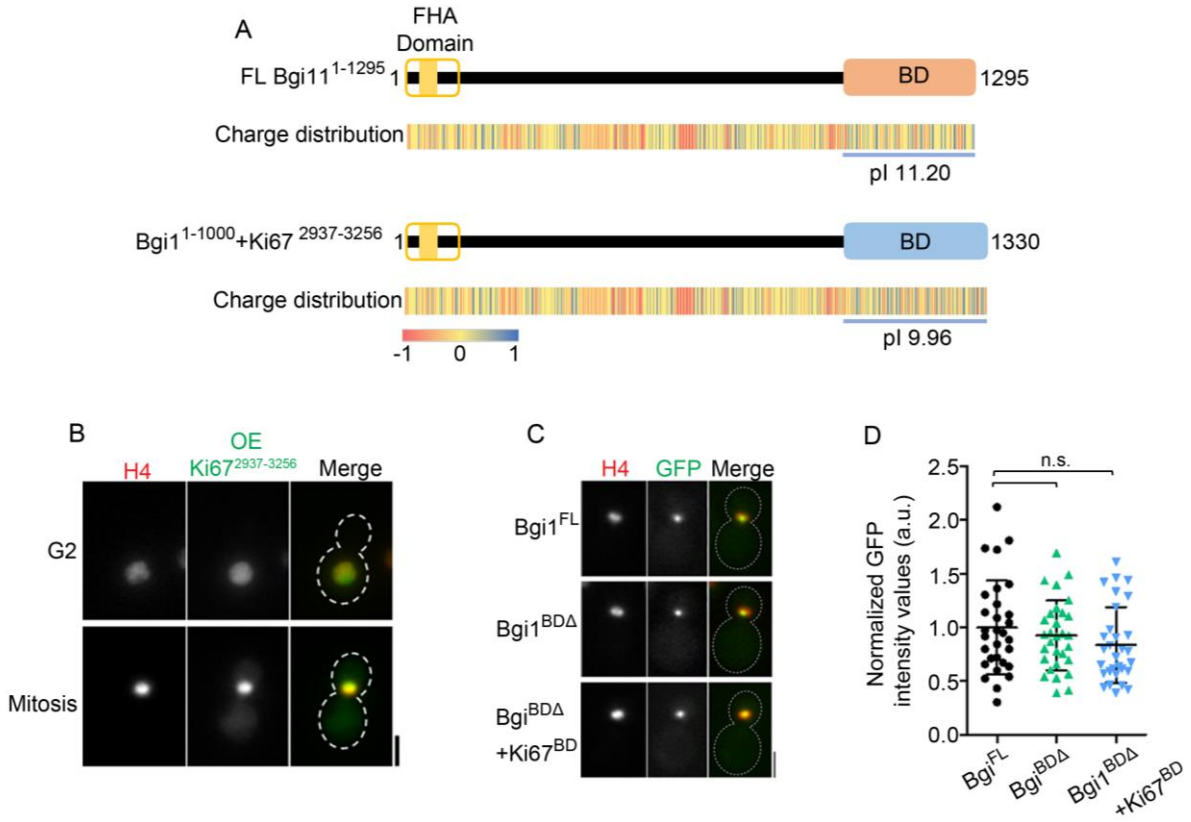

Figure 4-10: Ki67 basic region can bind to chromatin in C. neoformans.

(A) Schematic representation of bridgin in which its basic domain aa1005-1295 with a pI of 11.2, was replaced with the basic DNA binding domain from HsKi67, aa2937-3256 that exhibits a pI of 9.96. **(B)** Localization of GFP -Ki67 BD^{OE} at G2 and mitosis. Chromatin is marked using H4-mCherry. Scale bar, 3 µm. **(C)** Representative micrographs of $Bgi1^{FL}$, $Bgi1^{BD\Delta}$, and $Bgi1^{BD\Delta}$+$Ki67^{BD}$ expressed in *bgi1Δ* cells expressing H4-mCherry. Scale bar, 3 µm. **(D)** Quantitation of GFP-Bgi1 signals in 30 cells. Not significant (n.s.). *P*-value was determined using the two-tailed t-test. Scale bar, 3 µm.

$Bgi1^{FL}$, $Bgi1^{BD\Delta}$, and $Bgi1^{BD\Delta}$+$Ki67^{BD}$ were expressed under the native bridgin promoter as described for other domain deletion constructs and were found to localize to the kinetochore with similar intensities when integrated into a *bgi1Δ* background strain (Figure 4-10C and D). Weak complementation was observed for $Bgi1^{BD\Delta}$ over *bgi1Δ* (Figure 4-11A and B). On the other hand, the $Bgi1^{BD\Delta}$+$Ki67^{BD}$ construct was able to complement defects observed in *bgi1Δ* and the $Bgi1^{BD\Delta}$ mutants. The $Bgi1^{BD\Delta}$+$Ki67^{BD}$ phenotype was non-significant from the FL (Figure 4-11A and B). These observations were additionally validated by the spotting growth assay (Figure 4-11C).

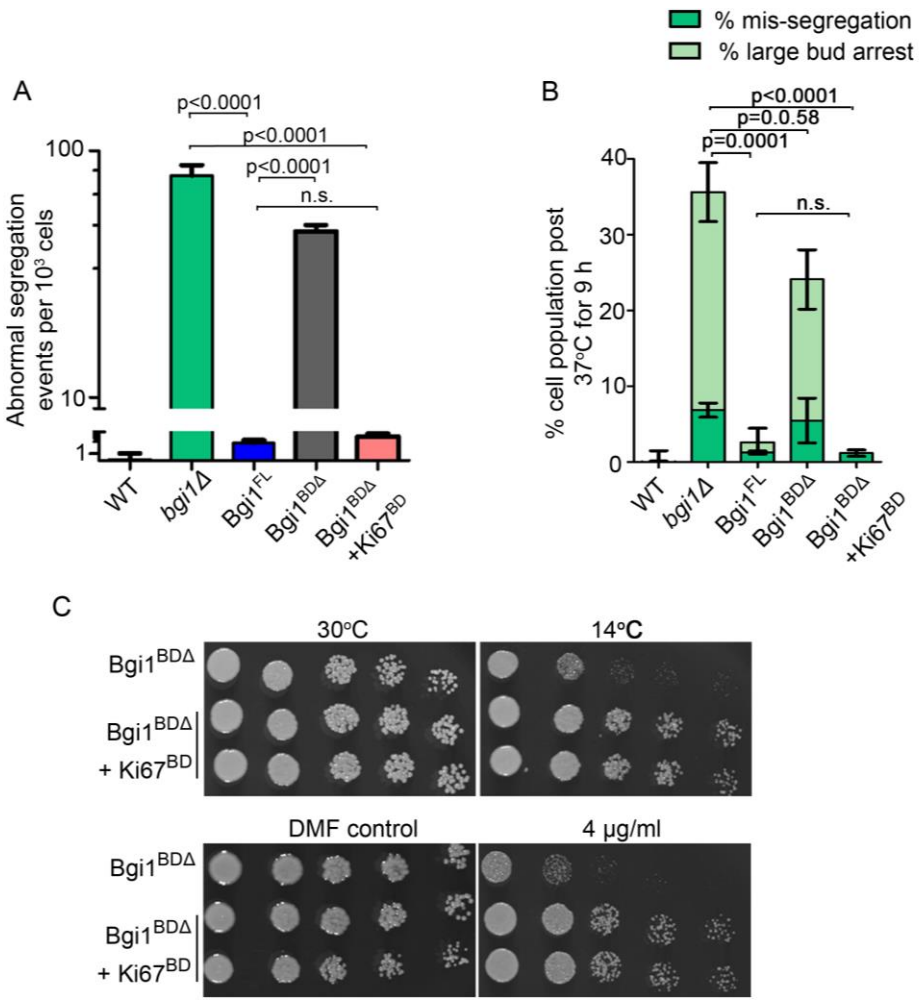

Figure 4-11: Bgi1BDΔ+Ki67BD chimera can complement the Bgi1BD defect.

(A) The extent of complementation by $Bgi1^{FL}$, $Bgi1^{BD\Delta}$, or basic domain swap bridgin constructs was measured. The number of missegregation events per 1000 cells was estimated. Cells were grown to early log phase (0.8-1 OD_{600}) at 30˚C, and abnormal segregation events were scored using the chromatin marker H4-mCherry. Error bars, s.d. >1000 for each mentioned strain were measured. *N* = 3. *P*-value determined using the two-tailed t-test. **(B)** Complementation of *bgi1Δ* phenotype by $Bgi1^{FL}$, $Bgi1^{BD\Delta}$, and $Bgi1^{BD\Delta}$+$Ki67^{BD}$ protein derivatives was measured by assessing their phenotype post-incubation of cells to 37ºC for 9 h. Error bars, s.d. The number of cells examined was >1000, *N* = 3 for each indicated strain. *P*-value was determined using the two-tailed t-test. **(C)** Cells of varying numbers $2x10^4$, $2x10^3$, 200, 100, and 50 were spotted on YPD without TBZ and YPD containing 4 µg/ml TBZ. Plates were incubated at the indicated temperatures for 2, 3 or 7 days for 30˚C and DMF control, 30˚C 4 µg/ml TBZ and 14˚C respectively.

While we cannot rule entirely out the contribution of amino and/or middle region of bridgin, independent of its kinetochore localization capacity, towards bridgin function, we propose that bridgin links the outer kinetochore to centromeric chromatin. This is based

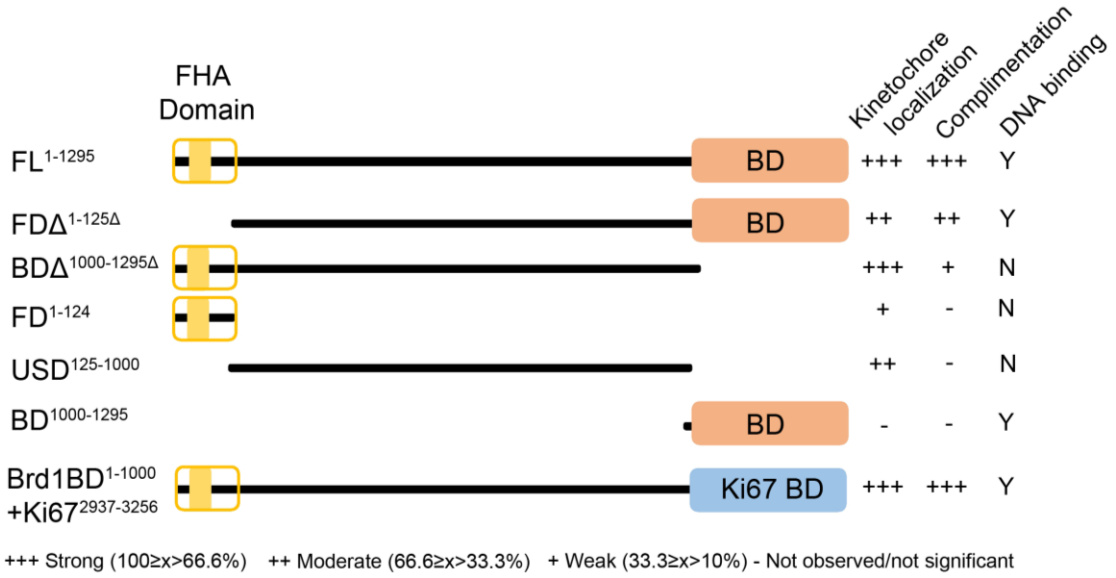

Figure 4-12: Summary of functional analysis of the bridgin protein derivatives truncated for various domains based on their kinetochore localization, functional complementation, and ability to bind DNA *in vivo*.

on the ability of bridgin to simultaneously localize to the outer kinetochore through the KMN network and to bind to chromatin (Figure 5-1).

Summary

With the identification of bridgin as a previously undescribed outer kinetochore protein in *C. neoformans*, we work to address how bridgin carries out its function in maintaining mitotic fidelity in this chapter. We generated bridgin domain deletion mutants and tested their ability to localize to the kinetochore, followed by their ability to complement the phenotype of *bgi1Δ*. We find that its FD and USD synergistically mediate bridgin kinetochore localization. Although being a requisite, kinetochore localization of bridgin mutants is not sufficient for bridgin function. We rule out the influence of bridgin on SAC, spindle dynamics and gross kinetochore composition. Through biochemical approaches, we learned that the Bgi1^{BD} could interact with chromatin. Using *in vitro* EMSA assays, we find that Bgi1^{BD} is necessary and sufficient for interaction with DNA and reconstituted nucleosomes. The nature of Bgi1^{BD}-chromatin interactions was identified to be non-specific under *in vitro* and *in vivo* assay conditions.

Further, bridgin was observed not to affect the total pool of H3K9me2 or the DNA methylation mark at the centromere. Subsequently, to address how Bgi1^{BD}-chromatin interaction facilitated bridgin function, we performed a domain swap experiment with the chromatin interacting *Hs*Ki67^{BD}. Our findings from this experiment suggest that the ability of the Bgi1^{BD} to interact with chromatin, critical for bridgin function, is a property of its basic nature and not reliant on its protein sequence. To conclude, we suggest that the interaction of bridgin basic domain with centromeric chromatin is a consequence of its specific recruitment to the outer kinetochore.

Chapter 5 : Discussion

As a step towards understanding the evolution of kinetochore organization and composition, we chose to identify and study the kinetochore interactome of the human pathogen and a basidiomycete yeast *C. neoformans.* During the study, we identified a novel outer kinetochore protein that we termed as "bridgin" in *C. neoformans*. Our experiments strongly indicate the absence of most known CCAN proteins, except CENP-C^{Mif2}, and the presence of all KMN network proteins in this system. This result also validates our bioinformatic prediction and reveals a single known linker pathway from centromeric chromatin to the outer kinetochore, reminiscent of the fruit fly, *D. melanogaster,* and the nematode, *C. elegans,* kinetochores (Barth et al., 2014; Drinnenberg et al., 2016; Hooff et al., 2017; Liu et al., 2016; Richter et al., 2016). Identification of bridgin, as the name suggests, functions as a new linker protein, since we observed that it binds to the outer kinetochore and centromeric DNA simultaneously, analogous to previously described linker proteins CENP-C^{Mif2} (Dimitrova et al., 2016; Milks et al., 2009; Petrovic et al., 2016) and CENP-T^{Cnn1} (Bock et al., 2012; Hori et al., 2008; Schleiffer et al., 2012) (Figure 5-1).

The presence of multiple kinetochore linker pathways is critical, to varying extents, in overcoming Dsn1 inhibition (Hara et al., 2018; Kim and Yu, 2015; Lang et al., 2018). Unlike the single linker protein (CENP-C) containing kinetochore such as that of *D. melanogaster* (Liu et al., 2016; Venkei et al., 2012), *C. neoformans* retains the Dsn1 autoinhibitory domain (Figure 5-2A and 2-1). Although a recent study suggests Nnf1 to be the Dsn1 homolog is *D. melanogaster*, we were unable to identify the presence of the Dsn1 autoinhibitory domain in the suggested homolog (van Hooff et al., 2017). Through our findings, we propose a role of bridgin towards linking the outer kinetochore by its recruitment and interaction with multiple KMN network proteins and chromatin, thereby promoting accurate kinetochore-microtubule attachments in *C. neoformans* (Figure 5-1).

An inability of the BD to localize specifically to the kinetochore and non-reliance of bridgin on sequence specificity for BD function endorses the hypothesis that binding of the basic domain of bridgin to chromatin is a consequence of specific kinetochore recruitment (Figure 5-1). Rather unique to bridgin as a linker protein is a fact that its kinetochore localization is dependent on conserved KMN network proteins, Sos7 (KNL1 complex), and Mis12 complex-Ndc80 complex platform (Figure 3-4A-C). CENP-T homologs require other CCAN proteins for its kinetochore localization (Basilico et al., 2014; Carroll et al., 2010; Lang et al., 2018) and bind non-specifically to DNA *in vitro.*

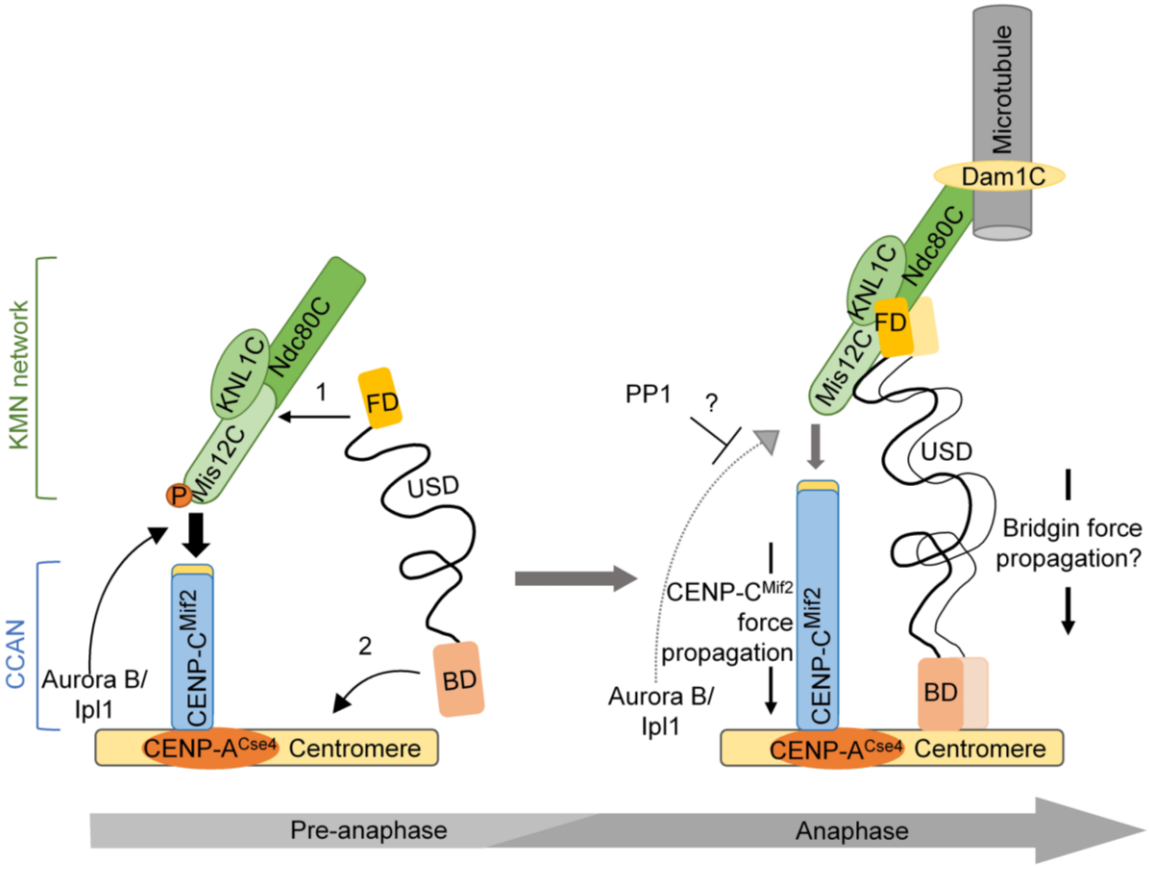

Figure 5-1: Schematic representation of bridgin dynamics and function.

A model describing bridgin as a kinetochore protein connecting the outer KMN network, through its FD and USD, and directly to DNA via its basic DNA binding domain. Restricted interaction of bridgin with DNA in WT cells is a possible consequence of outer kinetochore specific recruitment prior to its interaction with centromeric chromatin.

CENP-T^{Cnn1} was shown to increase the stability of a mini-chromosome, possibly due to its ability to recruit the Ndc80 complex, as suggested in a recent study (Lang et al., 2018; Schleiffer et al., 2012). CENP-T was shown to recruit the KMN network when ectopically tethered in metazoans (Gascoigne et al., 2011; Hara et al., 2018; Kim and Yu, 2015). Bridgin does not appear to influence the recruitment of outer kinetochore proteins (Figure 4-3D-G), further supported by the lack of Ndc80 mislocalization upon recruitment of bridgin to ectopic sites (Figure 4-7C).

Bridgin levels at the kinetochore reach a peak at anaphase (Figure 3-5B, E, and F), a time when Aurora B^{Ipl1}-mediated phosphorylation is suggested to be countered by the phosphatase activity of PP1. A sharp reduction of AuroraB^{Ipl1} localization at the

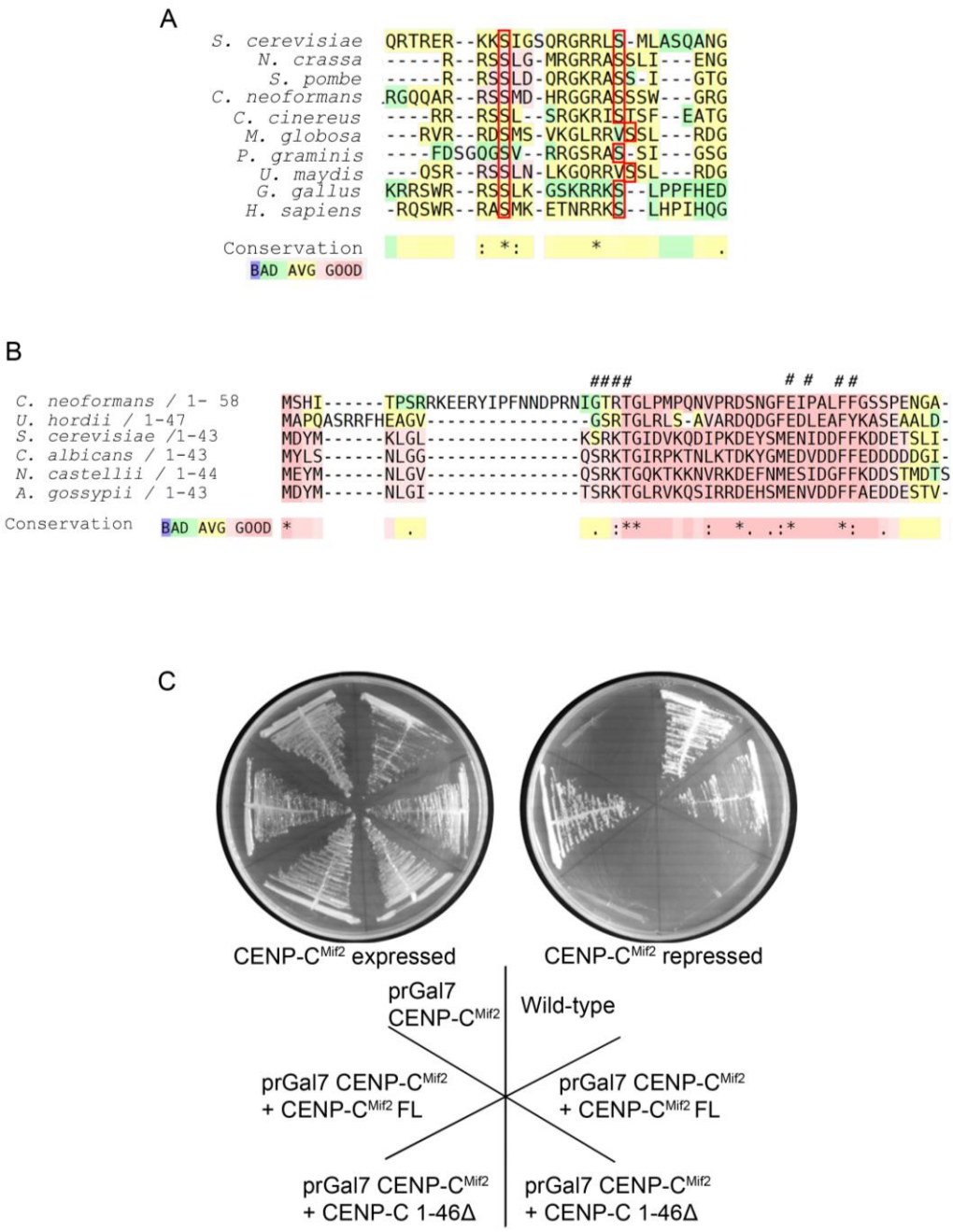

Figure 5-2: Conservation of the Dsn1 basic motif and the CENP-C^{Mif2}-Mis12^{Mtw1} interaction domain.

(A) Sequence alignment of the Dsn1 basic motif encompassing the two Aurora B^{Ipl1} kinase phosphorylation sites across species are highlighted in the red box. Alignment and visualization were performed using T-coffee. **(B)** Alignment of the described CENP-C^{Mif2}-Mis12^{Mtw1} interacting motif in CENP-C^{Mif2}. # represent CENP-C^{Mif2} residues important for CENP-C^{Mif2}-Mis12^{Mtw1} interaction, as shown in *S. cerevisiae*. **(C)** Essentiality of the CENP-C^{Mif2} N-terminus for growth in *C. neoformans.* The CENP-C^{Mif2} conditional mutant was complemented with either the FL or the aa 1-46Δ.

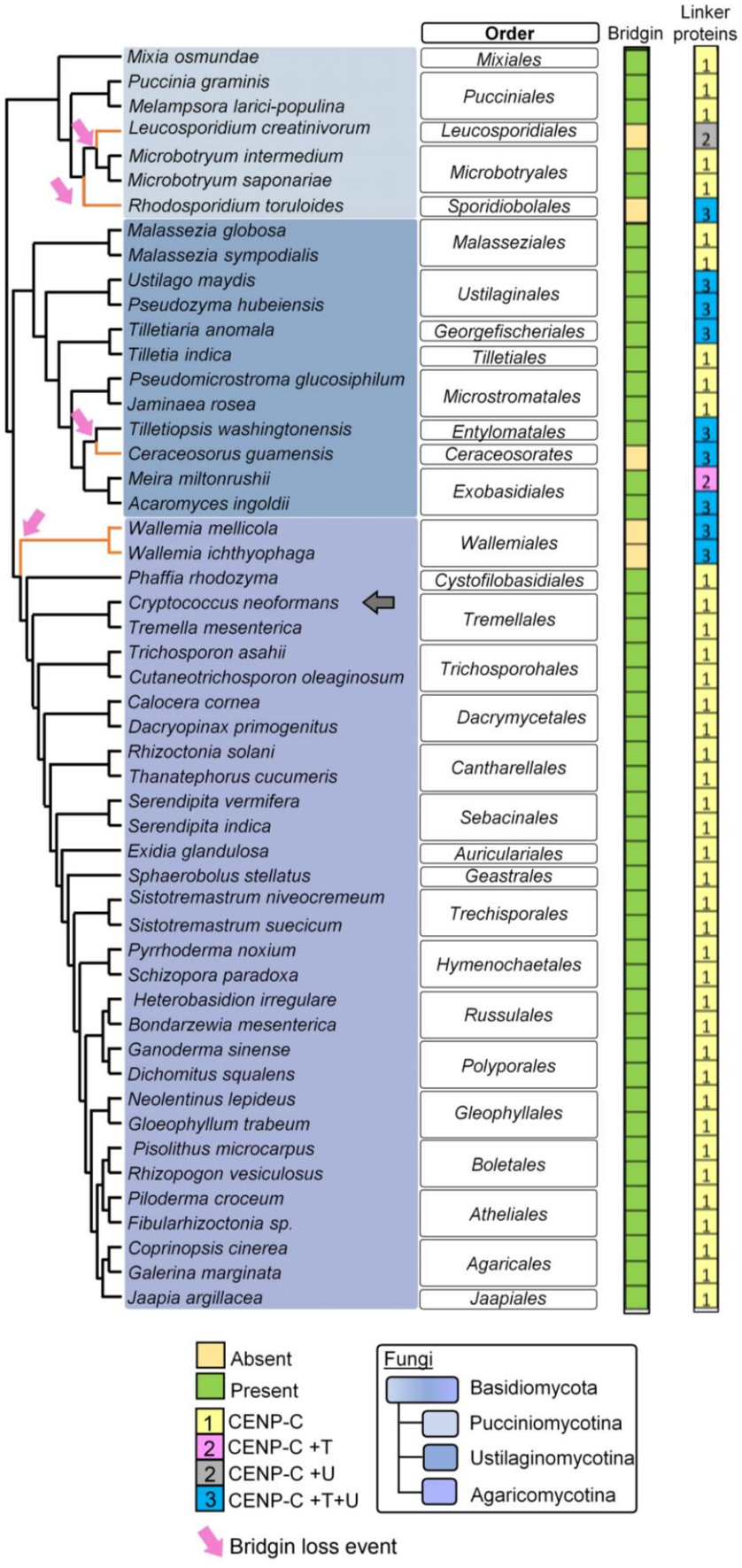

Figure 5-3: Conservation of linker proteins across basidiomycetes.

Identification of bridgin homologs across the fungal phylum of Basidiomycota. The presence or absence of a bridgin homologs is represented. The number of identified linker pathways is mentioned and color-coded to represent the linker pathway(s) present. Grey arrow points to *C. neoformans.*

kinetochore in anaphase (Varshney et al., 2019) and essentiality of CENP-C^{Mif2} N-terminus are observed in *C. neoformans* (Figure 5-2B and C). Taken together, we propose that the kinetochore architecture alters during the metaphase-anaphase transition and the bridgin linker pathway functions to reinforce/stabilize the outer kinetochore. Thus, an important question we must address in the future is whether the presence of Dsn1 autoinhibition can provide a constraint driving evolution/maintenance of multiple outer kinetochore linker pathways required for outer kinetochore reinforcement in organisms with monocentric chromosomes.

Outer kinetochore proteins are found to be more conserved than their inner kinetochore counterparts, including linker proteins, across eukaryotes (D'Archivio and Wickstead, 2017; Hooff et al., 2017) (Figure 2-1). Thus, additional KMN-recruited linker pathways like the bridgin-pathway may provide cells with an effective alternative towards outer kinetochore reinforcement. Bridgin homologs are identified across all basidiomycete sub-phylum (Figure 5-3 and Appendix VI). Strikingly, an inability to identify bridgin homologs in specific orders correlates with the presence of multiple known linker pathways (Figure 5-3 and Appendix VI). It would be worth investigating whether the presence of multiple linker pathways may have allowed for flexibility in the retention of specific linker pathways in basidiomycetes. Genome sequencing of a greater number of distinct basidiomycetes will help address if any correlation exists. It would be intriguing to recognize the contribution of the multiple linker pathways in organisms like *U. maydis,* which retained CENP-T^{Cnn1} and CENP-C^{Mif2}, in addition to bridgin.

The identification of bridgin homologs in the basal ascomycetes of the class Pneumocystidales, such as in *Pneumocystis jirovecii* (causative organism of pneumonia), and Taphrinales, and further, identification of bridgin-like proteins outside fungi may suggest a more ancient origin of the protein (Figure 5-4). In metazoans, a protein with bridgin-like architecture (N-terminal FHA domain, a PP1 docking site, an unstructured central region containing repeats and a basic C-terminus), was found to code for Ki67, a component of the mitotic chromosome periphery (Figure 5-4) (Cuylen et al., 2016).

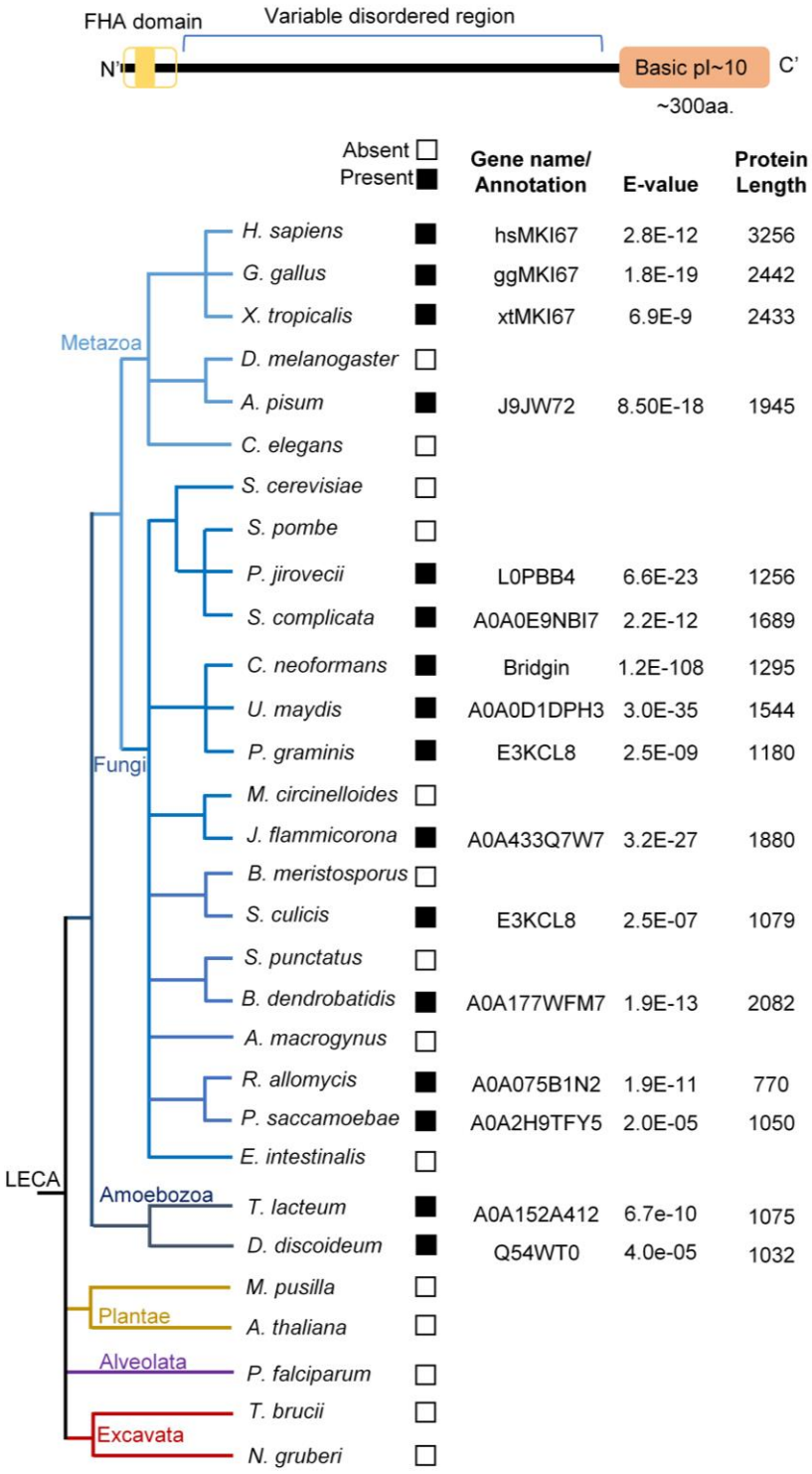

Figure 5-4: Identification of bridgin-like proteins across eukaryotes.

Parameters considered to identify bridgin homologs include the FHA domain within the first ~200 amino acids followed by a variable-length disordered region and a C-terminus of ~300 residues with an isoelectric point of ~10.

The role of bridgin-like proteins outside metazoans is not known and would be interesting to look into.

Future perspectives

In this study, we have identified a previously undescribed putative linker protein in *C. neoformans,* bridgin. Towards carrying forward these findings, forthcoming experiments will have to reveal how bridgin's outer kinetochore recruitment and DNA/chromatin binding are regulated. Does recognition of a phosphorylated residue by the Bgi1 FHA domain influence accumulation of bridgin towards anaphase? *In vitro* biochemical reconstitution experiments followed by *in vivo* mutational studies may shed light on the precise mechanism of recruitment by the kinetochore interacting partners of Bgi1.

The basic domain of bridgin is interspersed with a large number of serine and threonine sites. Could it be possible that its phosphorylation could alter the charge and reduce affinity for DNA post its function in mitosis? The DNA binding ability of Ki67 is suggested to be regulated by phosphorylation, wherein its hyperphosphorylated form has been shown not to bind DNA (Endl and Gerdes, 2000; MacCallum and Hall, 1999).

Following bridgin's ability to interact with the outer kinetochore and centromeric chromatin simultaneously, it is imperative to understand the extent of its ability to bear load at the kinetochore. We propose to address this exciting question using a FRET-based assay (Suzuki et al., 2016) and/or coupled with utilizing the Talin-Rod system, as shown in *D. melanogaster,* to measure load (Ye et al., 2016).

Going further, towards understanding bridgin biology, we would like to address if bridgin has additional functions at the kinetochore, for example, the regulation of disassembly dynamics of the kinetochore through the recruitment of PP1. The process of kinetochore disassembly is rather poorly understood, and studies have suggested a role for PP1 in metazoans (Gascoigne and Cheeseman, 2013; Hara and Fukagawa, 2018). Could bridgin recruit PP1 through its non-canonical PP1 docking site to influence kinetochore disassembly, resulting in the altered dynamics we observed in *bgi1Δ* (Figure 3-11)? Since other studied ascomycetous yeasts exhibit a mature kinetochore throughout the cell cycle *C. neoformans* is a good model organism to study kinetochore disassembly dynamics.

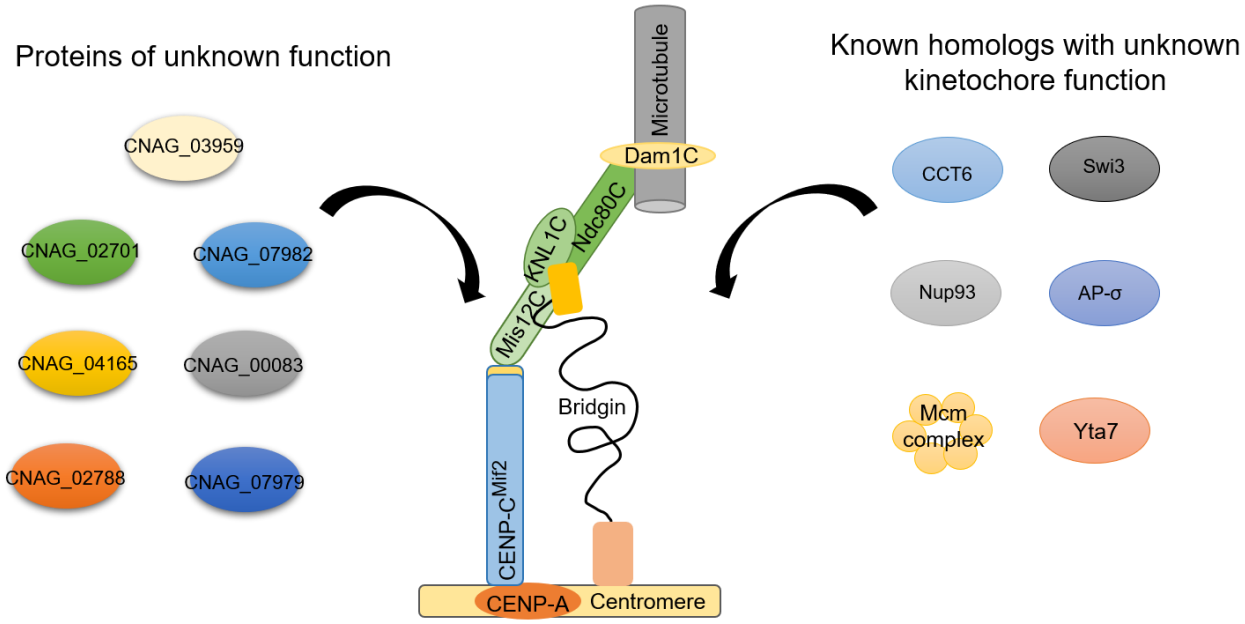

Figure 5-5: Resolving the function of components identified as part of the kinetochore interactome.

The *C. neoformans* kinetochore has retained the conserved outer kinetochore KMN network and Dam1 complex, only CENP-C^{Mif2} of the CCAN and centromeric histone CENP-A^{Cse4}. In this study, we have identified a previously undescribed outer kinetochore linker protein bridgin. Additionally, we have identified several proteins as part of the kinetochore interactome and whose function at the proteinaceous bridge is as yet unknown.

Further, we identified all predicted kinetochore proteins from each of the kinetochore IPs. Our IP-MS also identified previously known accessory proteins that more closely associated with specific kinetochore layers such as Mps1 in the Spc25 IP (Ndc80 complex) and Scm3 in the CENP-C^{Mif2} IP, to a lesser extent in Dsn1 IP. These results have given us the confidence to discover additional proteins with unknown functions at the kinetochore. Although we have mentioned a few of the common interactors in Figure 2-4 B and C, several other protein-specific interactors were also obtained (Figure 5-5). Future studies screening some of the obtained interactors may shed light on additional players at the kinetochore and giving us a comprehensive outlook on kinetochore composition and architecture in the basidiomycete *C. neoformans*.

It is of interest to note that we failed to obtain the Dam1 complex proteins as interactors from any of the performed IP-MS. We have previously shown (Shreyas Sridhar, MS thesis) that the Dam1 complex co-localization with other kinetochore proteins is retained upon using conditions similar to the IP-MS protocol (10 µM TBZ for 3 h). Could it be

possible that the outer kinetochore architecture is altered in *C. neoformans*? We hope further studies on non-conventional model systems like *C. neoformans* will help reveal conserved fundamental principles of the kinetochore architecture and its organization.

Chapter 6 : Materials and methods

Reagents generated

Yeast strains, plasmids, and primers

A list of strains and plasmids used in the study can be found in Table 6-1 and Table 6-2, respectively. Primers used to generate the strains are mentioned in Table 6-3.

Media, growth conditions and transformation

Conditional kinetochore mutant strains were grown on 1 % yeast extract, 2 % peptone, and 2 % galactose (YPG). All other strains were grown in 1 % yeast extract, 2 % peptone, and 2 % dextrose (YPD). YPD and YPG cultures were grown at 30˚C maintaining 180 rpm unless mentioned otherwise. Strains were retained on YPD/YPG solidified with 2% agar and stored at 4˚C or -80˚C in 15% glycerol. Yeast strains are based on the haploid type strain H99*α* or KN99**a** and generated by the standard biolistics procedure as previously described (Kozubowski et al., 2013). Generated native tagging and *GAL7* promoter (Davidson et al., 2000; Ruff et al., 2009) replacement cassettes were excised from the plasmid construct, over-expression cassettes were linearized by appropriate restriction enzymes, and deletion cassettes were generated by overlap PCR and transformed into *C. neoformans* strains of appropriate background by biolistic transformation. In brief, a single colony of the *C. neoformans* strain was inoculated into 5 ml of YPD/YPG and incubated at 30˚C for ~15 h with shaking, 180 rpm. The grown culture was pelleted at 4000 rpm for 5 min and the supernatant was discarded. Cells were resuspended in 500 µl of autoclaved water. From this cell suspension, 200 µl was spread on YPD/YPG + 1M sorbitol containing agar plates. Plates were allowed to dry in the hood for ~15-20 min. During this time DNA preparation was undertaken. The carrier gold bead stock (0.6 µm, BioRad), suspended in 50% glycerol (60 mg/ml) and stored at 4˚C, was kept for vortexing (~10-15 min). 10 µl of the gold bead mixture was added to a microfuge tube containing 2-3 µg of DNA and mixed well. To this 10 µl of $CaCl_2$ and 2 µl of 1 M spermidine free base (Sigma-Aldrich) was added, vortexed for a minute and allowed to incubate at RT for 5 min. The mixture was pelleted by spinning the microfuge tube for 6-7 s at 13,000 rpm, following which the supernatant was discarded. The

obtained pellet was resuspended in 500 µl of 100% ethanol by vortexing for ~15 s and again pelleted. The DNA-gold bead pellet was subsequently resuspended in 10 µl of 100% ethanol and spotted on to the center of ethanol sterilized microcarrier membranes. The spot was allowed to dry before using using it for biolistic transformation.

The prepared sorbitol plates with spread cells were placed 2 levels below the microcarrier membrane in the chamber of the PSD-1000/He™ Biolistics system (BioRad). Rupture disks (1350 psi, BioRad) were placed in the rupture disk holder and the biolistic machine was turned on as per manufacturer's instructions (BioRad). The chamber of the biolistics machine was allowed to reach a vacuum of ~26 inches of Hg before bombarding cell with the prepared DNA-gold bead mixture. Following this, the sorbitol plates were removed from the chamber and incubated at 30˚C for 4-5 h. The cells were then scraped from the plates using ~1 ml of water. The cell suspension was plated on YPD/YPG agar selection plates containing either 200 µg/ ml of G-418 (Sigma-Aldrich), 100 µg/ml of nourseothricin (clonNAT, Werner BioAgents) or 300 µg/ml of hygromycin (HiMedia). Transformants were obtained 3-5 days post-incubation of plates at 30˚C. Obtained transformants were patched on secondary plates containing the respective selection drug. Only transformants that grew on secondary plates were used for subsequent experiments.

Yeast strain construction and cloning

Screening constructs to tag genes with V5-GFP

To generate the V5-GFP screening constructs for *BKT1*, *BKT2*, *BKT3*, *MCM6*, and *YTA7*, ~1 kb of the gene body upstream of the stop codon and 3'-UTR was PCR amplified. This amplicon contained overhangs complementary to pRS426 (Sikorski and Hieter, 1989). Additionally, the V5-GFP-NAT sequence was PCR amplified. The three fragments, in addition to a linearized pRS426 plasmid, were transformed into the *S. cerevisiae* strain BY4742. DNA from the obtained *S. cerevisiae* transformants was transformed into *Escherichia coli* towards obtaining the plasmid DNA. The following plasmid was confirmed to contain the required fusion product post isolation from *E. coli* and sequenced for validation. Following this, the epitope tagging cassettes were released from

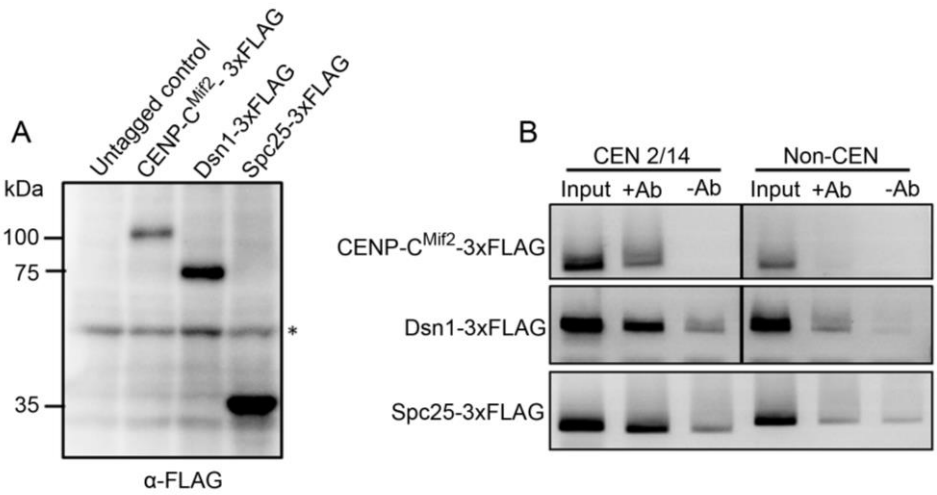

Figure 6-1: Expression and functional characterization of 3xFLAG tagged kinetochore proteins.

(A) Western blot analysis of whole-cell extract containing 3xFLAG-tagged kinetochore proteins. **(B)** ChIP assays to functionally validate the 3xFLAG-tagged kinetochore proteins. Location of CEN and non-CEN primers were as mentioned in Figure 3-7

the plasmid and transformed. The transformants were screened by PCR and validated by fluorescence microscopy.

Conditional mutants and GFP/mCherry tagged kinetochore proteins.

PCR and Southern blot analysis was used to confirm the conditional kinetochore mutant strains of CENP-A^{Cse4}, CENP-C^{Mif2}, Mis12^{Mtw1}, Nuf2, Knl1^{Spc105}, Dad1 and Dad2. GFP/mCherry tagged kinetochore protein strains were validated by PCR. The generation and validation of these strains were described in my MS thesis (Shreyas Sridhar, MS thesis 2014). To obtain strains for the evaluation of kinetochore assembly hierarchy, the tagged kinetochore constructs were transformed into the kinetochore conditional mutant strains. The obtained transformants were validated by microscopic screening.

Kinetochore FLAG-tagged strains and their functional confirmation

C-terminal 3x-FLAG tag constructs of CENP-C^{Mif2}, Dsn1, and Spc25 were generated by overlap PCR. ~1 kb upstream of the stop codon and 3’ UTR end were amplified and

fused to the amplified marker gene (hygromycin B, *HygB*) with the 3x-FLAG tag at its 5' end by overlap PCR.

The overlap cassettes were transformed into appropriate *C. neoformans* strains. The integration of the 3x-FLAG cassettes at the native locus of the respective genes was confirmed by PCR. The expression of the constructs was visualized by western blot, and the functional validity of the tagged constructs was analyzed by ChIP assays (Figure 6-1).

BRIDGIN and *SOS7* deletion strains

Cassettes to generate the bridgin-null strains were created by overlap PCR. 1006 bp of the 5'-UTR and 1098 bp of the 3' UTR of CNAG_01903 were amplified and ligated using PCR with either the amplified marker gene for G-418 resistance (*NEO*) or *HygB*. PCR was used to confirm the generation of *bgi1Δ*.

Overlap PCR was used to generate the *SOS7* deletion cassette. An 1136 bp sequence upstream of the start codon and 1241 bp downstream of the stop codon was amplified and ligated to *NEO*. The obtained overlap cassette was transformed into *C. neoformans* and subsequently screened using PCR.

Bridgin domain deletion and chimeric bridgin-Ki67 construct generation

To express bridgin domain deletions under its native promoter, plasmids pSS59 and pSS 61 were generated. They contained 424 bp of the *BGI1* promoter sequence, taken as the sequence from the stop codon of the previous gene and the start codon of *BGI1*. The promoter was amplified and cloned at the SacI and NcoI site of the GFP-NAT plasmid (pVY7), replacing the histone H3 promoter (CNAG_06745). The reverse primer encodes the 3xFLAG sequence. To generate pSS59, the *GFP* sequence was removed by NcoI, and BamHI digestion followed by blunting the DNA ends by Klenow fragment and subsequent ligation.

Sequences of bridgin domain deletions were subsequently PCR amplified and cloned into pSS59 or pSS61 at the BamHI and SpeI sites to yield N-terminal tagged 3xFLAG or

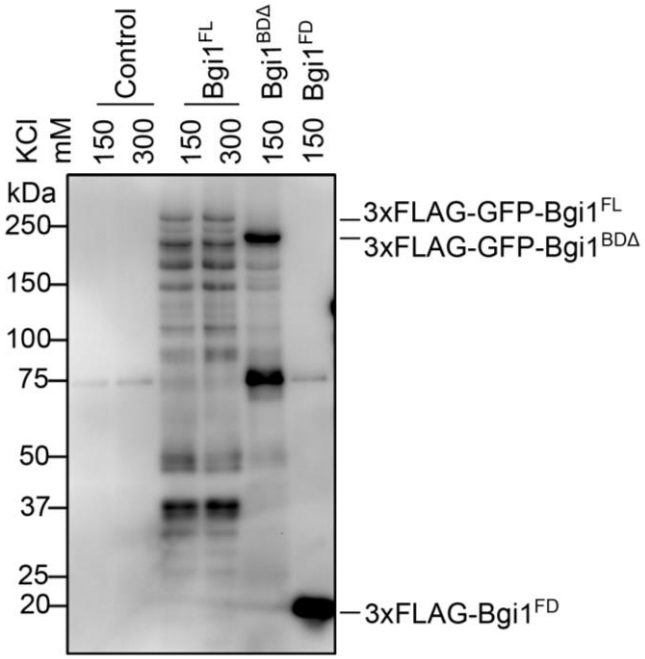

Figure 6-2: Western blot analysis of bridgin domain deletion mutants used for affinity purifications.

Whole-cell lysates of untagged WT and strains containing bridgin reintegration constructs were separated on an SDS-PAGE and immune-blotting was performed.

3xFLAG-GFP constructs which would be expressed under the native *BGI1* promoter.

To generate *BGI1*$^{BD\Delta}$+ *KI67*^{BD}, overlap PCR was used to ligate the two gene fragments together and subsequently cloned into pSS61 at BamHI and SpeI sites. *KI67* was amplified from the plasmids generously sent to us by Daniel W Gerlich (Institute of Molecular Biotechnology, Vienna)

The generated plasmid constructs were subsequently linearized using AatII and transformed into *C. neoformans.* Expression of the generated constructs used for affinity purification was scored by western blot analysis (Figure 6-2)

BRIDGIN and *KI67* over-expression (OE) constructs

To generate the OE constructs, the gene fragments of *BRIDGIN* and *KI67* were amplified using the primers previously mentioned to generate domain deletions, in the previous section. The amplified gene products were subsequently cloned into the pCIN19 plasmid (obtained from the Alspaugh lab), which contains histone H3 (CNAG_06745) promoter

driving the expression of GFP, at the BamHI and SpeI site. The generated plasmid was linearized using PmlI and transformed. The genome integrated cassette would express the gene with an N-terminal GFP tag. These strains were confirmed by microscopic screening for GFP expression in the transformants.

General methods

Homolog detection

All searches were carried out using the NCBI non-redundant protein database or the UniProtKB database. Searches for kinetochore homologs were initially carried out using iterative HMMER (Potter et al., 2018) jackhammer searches (E-value $\leq 10^{-3}$) with Pfam models for the mentioned kinetochore proteins. Available models of both yeast and metazoan kinetochore homologs were considered. Obtained hits were validated by performing reciprocal HMMER searches. The secondary structure of obtained hits was validated using Jpred4 and tertiary structure prediction using HHpred (Zimmermann et al., 2018) and/or Phyre2 (Kelley et al., 2015). Protein sequences that were unable to produce hits upon reciprocal searches or failed to conform to expected secondary and tertiary structures were discarded.

Further searches were performed with the same criteria using identified homologs phylogenetically closest to the species in question. Species considered in the study are mentioned in Appendix II. When homologs were not identified from a specific strain, an obtained homolog from another strain of the same species was considered, since some of the considered organisms did not have well assembled genomes. If multiple splice variants were identified the longest splice variant was mentioned. Obtained hits when possible was validated through BLAST searches with the *in vivo* identified homologs of *C. neoformans.* Known kinetochore homologs from *S. cerevisiae, S. pombe, D. melanogaster,* and *H. sapiens* were used to draw the matrix of kinetochore homologs.

Towards identifying homologs of bridgin, the conserved FHA domain was taken as the bait for subsequent iterative HMMER jackhammer searches. Obtained hits were further screened for overall protein architecture (N-terminus FHA domain, an unstructured central region containing repeats and a basic C-terminus, Figure 5-4). Disorder

probability was predicted using IUPred2A (Mészáros et al., 2018) and pI of the basic C-terminus was predicted using ProtParam (Gasteiger et al., 2005). Amongst the pucciniomycetes *Exidia glandulosa* and *Sistotremastrum suecicum* the basic C-terminus is ~150 aa. in contrast to ~300 aa. in other organisms.

Using published multi-gene and genome-scale phylogenetic data from The Fungal Kingdom (Heitman et al., 2017), JGI MycoCosm (Grigoriev et al., 2014) and Interactive **T**ree **o**f **L**ife (iTOL) v4 (Letunic and Bork, 2019) the cladograms were drawn showing the relationship amongst the considered species.

Protein affinity purification and native chromatin immunoprecipitation (n-ChIP).

An overnight culture was inoculated at 0.1 OD_{600} into fresh YPD. Grown until ~0.7 OD_{600} and treated with 10 µg/ml of **t**hia**b**enda**z**ole (TBZ) for 3 h. Cells were harvest, washed once in water followed by one wash with binding buffer BB150 (25 mM HEPES pH 8.0, 2 mM $MgCl_2$, 0.1 mM EDTA, 0.5 mM EGTA, 0.1 % NP-40, 150 mM KCl, 1x complete EDTA-free protease inhibitor [Roche], 1x PhosStop [Roche] and 15 % glycerol). Cells were resuspended in binding buffer (100 OD_{600}/ml). Bead beating was performed to lyse the cell suspension until ~80 % cell lysis was obtained. Lysates were centrifuged at 15k rpm for 20 min, and the supernatant was collected. The extracted cell lysate was incubated with anti-FLAG M2 antibodies (Sigma) conjugated to Dynabeads™ M-280 sheep anti-mouse IgG (ThermoFisher Scientific) for 2 h at 4˚C, under constant rotation. Unbound proteins were collected as flow-through, and proteins bound to antibody-conjugated beads were washed five times with BB150 w/o glycerol. Invert mixing was followed during each wash. Bound proteins were eluted in BB150 w/o glycerol + 200 µg/ml of 3xFLAG peptide (Sigma). Two elutes of ~½ volume each of initial bead volume was taken and pooled.

About 1 µg of anti-FLAG M2 antibody was conjugation to 10 µl of Dynabeads™ M-280 sheep anti-mouse IgG (ThermoFisher Scientific) in 1x **p**hosphate-**b**uffered **s**aline (PBS), pH 7.4, and incubation for 1 h at **r**oom **t**emperature (RT). Washed twice with 1x PBS and resuspended in PBS. This anti-FLAG conjugated beads were used for the lysate prepared from 100 OD_{600} culture. Affinity purification samples that were processed subsequently

for **m**ass **s**pectrometry (MS) was started from a 2.25 L culture, yielding ~4500 OD_{600} cells. 300 mM KCl, where mentioned in experiments, was used throughout the affinity purification experiment as part of the binding buffer yielding BB300. For GFP affinity purification, GFP-Trap agarose beads (ChromoTek) were used. Bound proteins were eluted by boiling the beads for 10 min in 1x sample loading buffer (SLB, 50 mM Tris-HCl pH 6.8, 2% SDS, 0.05% bromophenol blue, 10% glycerol, 5% 2-Metcaptoethanol) and the supernatant was collected. Other steps of the affinity purification protocol were kept the same as mentioned above.

For n-ChiP, lysate preparation, affinity purification, and isolation of the bound proteins were performed as mentioned above. DNA from the elute and input sample was extracted using the MagExtractor clean-up kit (TOYOBO). PCR for the identical dilution of input and IP was set-up using centromere 14 primers (5'-GGTGATGCTACCTCGGT-3' and 5'-CCCGACGACTGTATCAGTTA-3') and non-centromere control primers (5'-GATCAAGTATAGGCGAAGG-3' and 5'-CATCTCTTATTCCCACTTCTACTC-3') located on the gene body of CNAG_00063, ~825 kb away from the centromere on chromosome 1.

Immunoblot analysis.

For whole-cell lysates, 3 OD cells were harvested and resuspended in 15% TCA overnight. 500 µl 0.5 mm glass beads were added, and samples were vortexed for a total time of 15min, with intermittent cooling on ice. Centrifuged at 13k rpm for 10 min, and the obtained pellet was washed twice with 100% acetone, air-dried, and resuspended in 1x SLB and boiled for 10min. Samples were separated on an SDS-PAGE and transferred onto Immobilon-P (Merck).

For figures 2-3A, 4-7B, 4-9A, and 6-1A, primary antibody and secondary antibody dilutions were made in skim milk. Proteins bound by antibodies were detected with Clarity western ECL (BioRad) and visualized with Versadoc (BioRad). For figure 4-4C and 6-2, primary and secondary antibody dilution was prepared in Signal Enhancer Hikari (Nacalai tesque). ChemiDoc Touch (Bio-Rad) was used to visualize proteins reacting with antibody in the presence of the substrate ECL Prime (GE Healthcare). ImageJ (Abràmoff et al., 2005; del Valle et al., 2015) and Image lab (BioRad) was used to

visualize and process images. Antibodies used are tabulated and can be found later in the section.

Mass spectrometry (MS).

Affinity purified samples were separated on an SDS-PAGE followed by silver staining. Isolated samples from the stained gel were Trypsin digested. Samples were subject to nano LC-MS-MS as described previously (Oya et al., 2019). Using the MASCOT ver2.6.2 search engine in Proteome Discoverer 2.1.1.21 and 2.2.0.388 (ThermoFisher Scientific), the obtained spectra peaks were assigned using the UniProt proteome database for *C. neoformans* H99*α* database (ID: UP000010091 20171201downloaded (7340 sequences)). Fragment tolerance 0.80 Da (Monoisotropic), parent tolerance 10 PPM (Monoisotropic), fixed modification of +57 on C (carbamidomethyl), variable modification of +16 on M (oxidation) and +42 on Peptide N-terminus (acetyl) and allowing for a maximum of 2 missed cleavages for CENP-C^{Mif2}, Dsn1 and Spc25 and 3 missed cleavages for bridgin samples. The obtained results were visualized using Scaffold 4.8.9 (Proteome Software). A minimum threshold for peptide (95%), and protein (99%) in addition to the identification of a minimum of two unique peptides were considered as hits after normalization with untagged control spectra. Identified protein hits from CENP-C^{Mif2}, Dsn1, Spc25, and their untagged controls can be found in Appendix III.

To relatively quantitate proteins obtained within each of the experiments, $Bgi1^{FL}$ 150 mM, $Bgi1^{FL}$ 300 mM, and $Bgi1^{BD\Delta}$ 150 mM, **e**xponentially **m**odified **p**rotein **a**bundance **i**ndex (emPAI) (Ishihama et al., 2005) values were determined using Scaffold 4.8.9 (Proteome Software). Higher the emPAI score, the more abundant the protein is in the mixture. Hits were arranged in descending order of their obtained emPAI scores. Appendix V summarizes the identified interacting protein hits from $Bgi1^{FL}$, $Bgi1^{BD\Delta}$, and their untagged control IPs.

Cross-linked Chromatin immunoprecipitation and quantitative real-time PCR.

ChIP assays were performed with some modification of previously described protocols (Dubin et al., 2010; Sanyal et al., 2004). To begin, 100 ml of culture strain was grown until ~1 OD_{600}. Cross-linking was performed for 20 min using formaldehyde to a final concentration of 1% and incubated at RT with intermittent mixing. The reaction was quenched by the addition of 2.5 M glycine and further incubated for 5 min. Fixed cells were harvested by centrifugation and resuspended in 9.5 ml of deionized water, followed by the addition of 0.5 ml of 2-Mercaptoethanol and incubated at 30˚C for 60 min at 180 rpm. Cells were pelleted and resuspended in 10 ml spheroplasting buffer (1 M sorbitol, 0.1 M sodium citrate, and 0.01 M EDTA) containing 40 mg of lysing enzyme from *Trichoderma harzianum* (Sigma). Spheroplasts were washed once with 15 ml each of the following buffers, 1) 1x PBS 2) Buffer I (0.25% Triton X-100, 10 mM EDTA, 0.5 mM EGTA, 10 mM Na-HEPES pH 6.5) and 3) Buffer II (200 mM NaCl, 1 mM EDTA, 0.5 mM EGTA, 10 mM Na-HEPES pH 6.5). Following which the spheroplasts were resuspended in 1 ml of extraction buffer (50 mM HEPES pH 7.4, 1% Triton X-100, 140 mM NaCl, 0.1% Na-Deoxycholate, 1 mM EDTA) and sonicated to shear chromatin using a Bioruptor (Diagenode) for 30 cycles of 30 s on and 30 s off bursts at high-intensity setting. Sheared chromatin was isolated in the supernatant fraction after centrifugation for 15 min at 13k rpm. Average chromatin fragment sizes ranged from 200-500 bp. 100 µl, $1/10^{th}$ the volume, of the chromatin fraction, was kept for input DNA preparation, the remaining chromatin volume was divided into two halves of 450µl each for (+) antibody and (-) antibody. For (+) antibody, 20 µl of GFP-Trap agarose beads (ChromoTek) and 20 µl of blocked agarose beads (ChromoTek) were added to (-). The tubes were incubated for 8 h to overnight on a rotator at 4˚C. Following which the supernatant was isolated as flow-through, and the beads were washed twice with low salt buffer (0.1% SDS, 1% Triton X-100, 2 mM EDTA, 20 mM Tris-Cl pH 8.0 and 150 mM NaCl), twice with high salt buffer (0.1% SDS, 1% Triton X-100, 2 mM EDTA, 20 mM Tris-Cl pH 8.0 and 500 mM NaCl), once with LiCl buffer (50 mM LiCl, 1% NP40, 1% deoxycholate, 1 mM EDTA and 10 mM Tris-Cl pH 8.0) and twice with Tris-EDTA (10 mM Tris-Cl pH 8.0 and 1 mM EDTA). Bound chromatin was eluted in two 250 µl elution using elution buffer. All three fractions (SM, (+) and (-)) were de-crosslinked (mixed with 20 µl of 5 M NaCl and incubated at 65˚C for 8 h to overnight), Proteinase K treated (10 µl of 0.5M EDTA, 20 µl of 1 M Tris-HCl pH 6.8, 40 mg Proteinase K was added to the solution and incubated for up to 2 h at 45˚C) and DNA was isolated using phenol: chloroform

extraction followed by ethanol precipitation. Isolated DNA was air-dried and dissolved in 25 µl of de-ionized water containing 25 µg/ml of RNase (Sigma).

All three samples (SM, (+) and (-)) were subject to PCR and Real-time quantitative PCR. The reaction mixture was set up using the iTaq™ universal SYBR green Supermix (BioRad) with 1 µl of the undiluted (+), (-) DNA samples, and SM (diluted 1:50). CN1 (CEN 14)- 5'-CCATCCAGTTCTTGCTTGAG-3' 5'-GCAAGGAATGTGTTGTCTGG-3' and CN3 (CEN 2)-5'-CAGACCCTTCCTTCAGCCG-3' 5'-TGGCAAGGAGTCGTCAGCG-3' was used to estimate centromeric enrichment levels and non-centromeric primer set NC3 5'-GATCAAGTATAGGCGAAGG-3' 5'-ATCTCTTATTCCCACTTCTACTC-3' located ~825 kb away from the centromere on chromosome 1 was used to normalize and obtained fold enrichment. Values were plot using GraphPad Prism.

Fluorescence microscopy and analysis.

Overnight cultures grown in YPD were sub-cultured into fresh YPD at 0.1 OD_{600} and grown until 0.4-0.6 OD_{600}. Cells were isolated, washed twice in 1x PBS, and mounted on slides. Images for Figure 2-6B (CNAG_01340) were acquired using the Airyscan mode in the Zeiss LSM 880 confocal system equipped with an Airyscan module, 63x Plan Apochromat 1.4 NA. Z-stacks were obtained at an interval of 166 nm, 488/516 and 561/595 nm excitation/emission wavelengths were used GFP and mCherry respectively. Airyscan images were processed using Zen (Zeiss) and visualized in ImageJ (Abràmoff et al., 2005; del Valle et al., 2015). Images for Figure 2-4D and Figures 2-6B were acquired in the Zeiss LSM 880 confocal system equipped with GaAsp photodetectors. Z-stacks were obtained at an interval of 300 nm, 488 and 561 nm excitation was used for GFP and mCherry respectively, and emission between 490-553 nm and 571-651 nm was captured. Images are represented as maximum-intensity projections.

Live-cell microscopy, images for kinetochore quantitation, and microscopy-based assays were acquired using the Zeiss Axio Observer 7, equipped with Definite Focus.2, Colibri 7 (LED light source), TempController 2000-2 (PECON), 100x Plan Apochromat 1.4 NA objective, pco.edge 4.2 sCMOS and Andor iXon Ultra 897 electron-multiplying CCD (charge-coupled device). Zen 2.3 (blue edition) was used for image acquisition and

controlling all hardware components. Filter set 92 HE with excitation 455-483 nm and 583-600 nm for GFP and mCherry, respectively, and corresponding emission was captured at 501-547 and 617-758 nm. To limit the time taken for an image, a complete Z-stack was obtained for each channel before switching.

For live-cell microscopy, an overnight culture was grown in YPD was sub-cultured into fresh YPD at ~0.1 OD_{600} and grown for 2-3 generations until 0.4-0.8 OD_{600}. Cells were harvested, washed in 1x PBS, and resuspended in synthetic complete media with 3% dextrose. Cells were mounted onto an agarose pad (3% dextrose, 3% agarose in synthetic complete media) and sealed with petroleum jelly. Images were captured at time intervals of 1, 2, or 4 min, as appropriate, with an EM gain of 300 and Z interval of 300 nm. Z-stack projection of images is represented.

To study kinetochore interdependency, conditional strains were grown overnight in YPG, sub-cultured at 0.2 $OD_{600,}$ and grown until 0.8-1 OD_{600}. Cells were washed and resuspended in 1x PBS. Following which cells were inoculated into YPD (repressive) and YPG (permissive) at 0.1 OD_{600}. Images were acquired after 6, 12, 15, 18, 9, and 18 h for CENP-C^{Mif2}, $Mis12^{Mtw1}$, Nuf2, $Knl1^{Spc105}$, Dad1, and Dad2, respectively. Z-stack was obtained at an interval of 300 nm. Single Z slice representing the maximum intensity of the tagged kinetochore proteins was represented. Quantitation of kinetochore signal was performed from large budded cells (budding index 0.55-0.90).

To estimate the population of large-bud and cells with segregation defects, cells were grown until early-log phase 0.8-1 OD_{600} after sub-culture from an overnight culture. Imaged using the above mentioned sCMOS camera with a Z-interval of 300 nm. Cells with a budding index of >0.55 were considered as large bud cells in mitosis. Chromatin marked with a tagged H4 construct was used to observe missegregation events.

Images for the over-expression assay of bridgin strains are representative maximum intensity projection images.

For live-cell quantitation of kinetochore signal, signal intensity was measured after the projection of Z-stacks. Kinetochore signal measurement in interdependency assays and *bgi1Δ* background were measured from the in-focus Z plane exhibiting the most intense signal. Background signal measured from a region neighboring the kinetochore measured signal in the same plane of the equal area was subtracted from the measured kinetochore intensity and normalized to the appropriate control and plot using GraphPad Prism 5.00

(GraphPad software). All acquired images were processed in ImageJ (Abràmoff et al., 2005; del Valle et al., 2015). For images wherein brightness and contrast were modified the settings were applied uniformly across the entire image.

Budding index calculation

Budding index of a cell is defined as the ratio obtained by:

$$Diameter\ of\ daughter\ cell / Diameter\ of\ mother\ cell$$

The diameter of the daughter and mother cell was measured along the mother-daughter axis using the line tool in ImageJ (Abràmoff et al., 2005).

Generation of recombinant proteins

GST, GST-Bgi1^{FD} (residues 1-130), and GST-Bgi1^{BD} (residues 1000-1295) were expressed from pGEX-6P-1 (GE Healthcare) in the Rosetta2 (DE3) *E. coli* strain (Merck). GST and GST-BD were induced for expression using 1 mM IPTG for 3 h at 37˚C. GST-FD was induced for expression overnight at 16˚C using 0.2 mM IPTG. Cells were harvested and lysed in lysis buffer (20 mM HEPES pH 7.5, 300 mM NaCl, 1 mM EDTA, 0.5 mM TECP, 1x complete EDTA-free protease inhibitor (Roche)) and 1x PBS with 1x complete EDTA-free protease inhibitor (Roche) for GST and GST-Bgi1^{FD} (Figure 6-3A). GST fusion proteins were affinity purified using Glutathione sepharose 4b beads (GE Healthcare) and eluted using 20 mM glutathione. GST-Bgi1^{FD} and GST-Bgi1^{BD} were further purified using anion exchange chromatography. The column was equilibrated using 20 mM Tris-HCl pH 7.5, 1 mM DTT. Elution gradient of 5-75% NaCl was achieved using 20 mM Tris-HCl pH 7.5, 1 M NaCl, 1 mM DTT (Figure 6-3B and C). Relevant fractions were pooled, concentrated in Amicon-Ultra (Merck), frozen in liquid nitrogen, and stored at -80˚C.

His-Bgi1^{FL} was expressed in SF9 cells. Cells were resuspended and lysed in binding buffer (20 mM Tris-HCl pH 8.0, 500 mM NaCl, 5 mM Imidazole). His-Bgi1^{FL} was affinity purified with Ni-NTA agarose (GE Healthcare), eluted with 20 mM Tris-HCl pH 8, 500 mM NaCl, 500 mM Imidazole. Purified protein was dialyzed against buffer

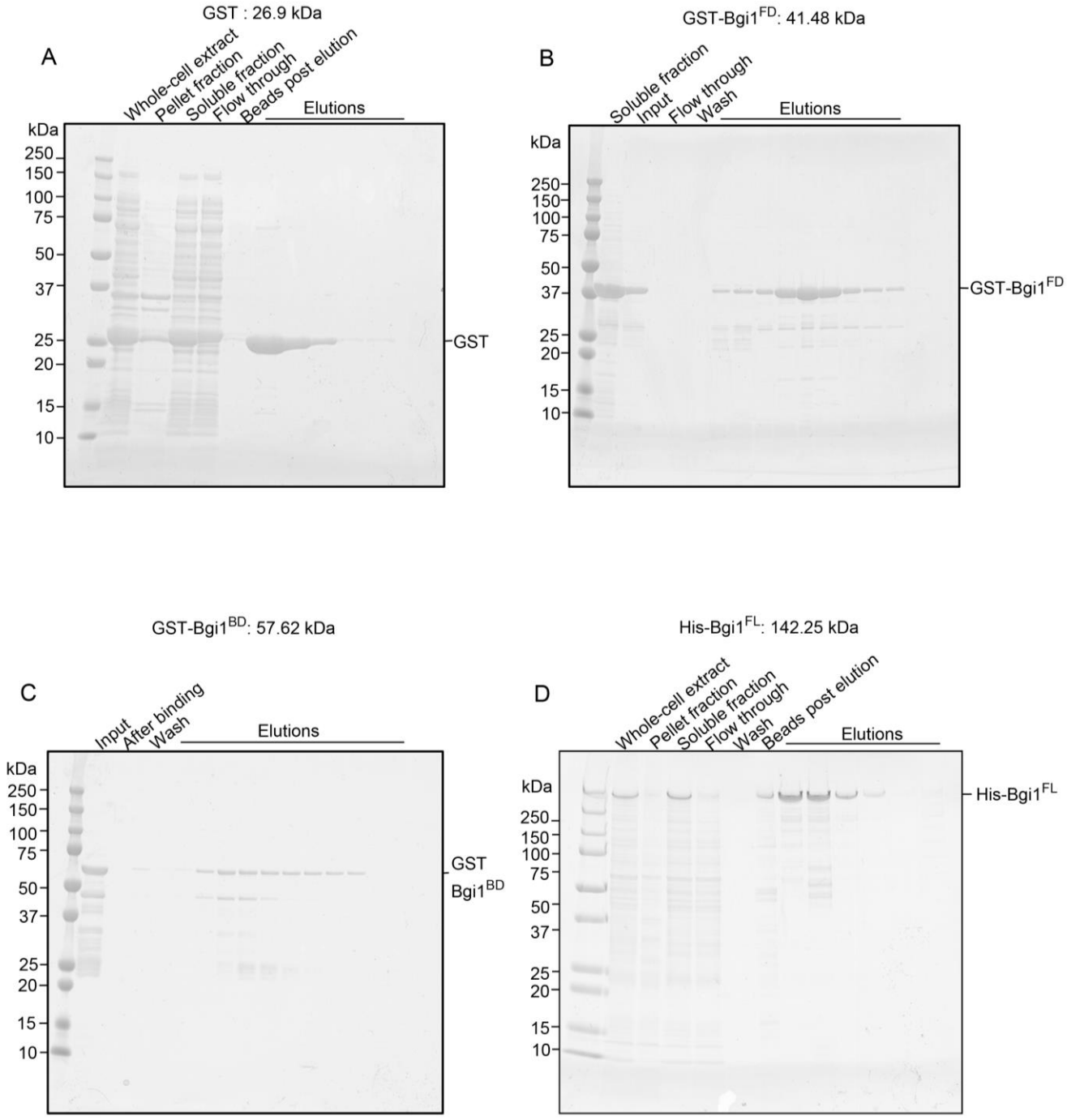

Figure 6-3: Purification of recombinant bridgin proteins.

(A) Single-step affinity purification of GST. **(B)** Affinity purification, followed by anion exchange chromatography, was performed for Bgi1^{FD}. **(C)** Affinity purification, followed by anion exchange chromatography, was performed for Bgi1^{BD}. **(D)** Single-step affinity purification was performed for Bgi1$^{FL.}$

containing Tris-HCl pH 7.5, 1 mM DTT, and 100 mM NaCl (Figure 6-3D). Samples were concentrated using Amicon-Ultra (Merck), frozen in liquid nitrogen, and stored at -80˚C. The absence of contaminating DNA was confirmed in all recombinant protein samples.

Viability assay

An overnight culture was inoculated into fresh YPD medium at 0.1 OD_{600} and grown to ~0.8 OD_{600}. The cell number was measured, followed by dilution of the cell suspension. 100-500 cells were subsequently plated on YPD solidified using 2% agar and grown for 2 days at 30˚C. The number of colonies formed was measured and plot as normalized values to the WT strain.

Serial dilution growth analysis.

Cells were grown overnight, inoculated into fresh YPD at 0.2 $OD_{600,}$ and grown until 0.8-1 OD_{600}. Following which cells were isolated and made up to 2 OD_{600}/ml in 1x PBS. Further dilutions were made as indicated in 1x PBS. 2 µl of the cell suspension was transferred onto appropriate agar plates as mentioned and incubated for 2 days for 30˚C and 30˚C + DMF control and 2 µg/ml TBZ, 3 days for 30˚C + 4 µg/ml TBZ and 37˚C and 7 days for 14˚C.

Electrophoretic mobility shift assays.

Purified recombinant proteins of mentioned molar ratio were incubated with 601 DNA (2.5 pMoles) or 1 pM of reconstituted nucleosomes in binding buffer (20 mM Tris pH 7.5, 100 mM NaCl, 5% glycerol and 1 mM DTT). Incubated for 1 h at 4˚C and separated on a PAGE gel, stained with GelRed, and visualized using a gel documentation system. Further, the gels were stained with Coomassie to visualize the protein complexes and imaged using a scanner.

Estimation of DNA methylation.

Genomic DNA was isolated from overnight cultures of WT and *bgi1Δ*, using a modified glass bead protocol (Ruff et al., 2009). In brief, cells were suspended in a microfuge tube containing 500 µl of lysis buffer (50 mM Tris-HCl pH 7.5, 20 mM EDTA and 1% SDS) and 250 µl of glass beads. Cells were disrupted by vortexing for 5 min and centrifuged for 1 min at 13k rpm. To the supernatant, 275 µl of 7 M, ammonium acetate was added and incubated at 65˚C for 5 min and rapidly chilled on ice for 5 min. 500 µl of chloroform was added, mixed, and centrifuged at 13k rpm for 3 min. The supernatant containing DNA was precipitated with isopropanol, washed with 70% ethanol, dried, and resuspended in 50 µl deionized water.

The isolated genomic DNA was digested separately with CpG methylation-sensitive (HhaI) or insensitive (HindIII) restriction enzymes overnight with a no enzyme (uncut) control reaction. The digested DNA was diluted 1:50 and used for PCR amplification. Primer sets for PCR amplification of the centromeric region (5'-AGTCTCGTGTGGCTATGATT-3' and 5'-GGATCTGCTTGACAGTGTCA-3') and non-centromeric regions (5'-CCAACCGAAGCCCAAGACAA-3' and 5'-TTGAAGGATGATCCGGCCGA-3') were used. Obtained PCR products were subsequently separated by agarose gel electrophoresis using a 1% agarose gel and visualized by EtBr staining.

Statistics and reproducibility.

P-values were assessed by unpaired, two-tailed *t*-test using GraphPad Prism 5.00 (GraphPad software). Error bars represent standard deviation (s.d.) or standard error of the mean (s.e.m.), as mentioned for each experiment. *N* for each experiment is mentioned in the figure legends.

Antibodies used

Primary antibodies

Antibody	Species	Source	Catalog no	Assay and dilution
α-H3K9me2	Mouse	Abcam	ab1220	Immunoblot, 1:2000
α-PSTAIR	Mouse	Abcam	10345	Immunoblot, 1:5000
α-GFP	Mouse	Roche	11814460001	Immunoblot, 1:3000
α-H4	Mouse	(Hayashi-Takanaka et al., 2015)	CMA400	Immunoblot, 1:5000
α-FLAG M2	Mouse	Sigma	F3165	Immunoblot, 1:5000
α-pan histone H3	Rat	(Kimura et al., 2008)	140-1G1	Immunoblot, 1:3000

Secondary antibodies

Antibody	Species	Source	Catalog no	Assay and dilution
α-Mouse	Goat	Bangalore genei	HO06	Immunoblot, 1:10000
HRP-conjugated α-mouse IgG	Rabbit	Jackson ImmunoResearch	315-035-003	Immunoblot, 1:15000
HRP-conjugated α-Rat IgG	Goat	Jackson ImmunoResearch	112-035-003	Immunoblot, 1:15000

Table 6-1: Strain list

Strain name	Genotype	Reference
H99*α*	*MATα (Wild type)*	(Toffaletti et al., 1993)
KN99**a**	*MAT***a** *(Wild type)*	(Nielsen et al., 2003)
SHR894	*MATα CENP-C^{MIF2}::CENP-C^{MIF2}-3xFLAG-HygB*	This study
SHR824	*MATα DSN1::DSN1-3xFLAG-HygB, NUF2::NUF2-GFP-NAT, MIS12^{MTW1}:: MIS12^{MTW1}-mCherry-NEO*	This study
SHR861	*MATα SPC25::SPC25-3xFLAG-HygB*	This study
SHR823	*MATα SPC25::SPC25-3xFLAG-HygB, NUF2::NUF2-GFP-NAT, MIS12^{MTW1}:: MIS12^{MTW1}-mCherry-NEO*	This study
SHR845	*MAT***a** *SOS7::GAL7p-SOS7-HYGB, K99::mCherry-CENP-A-NEO (pLKB74)*	This study
SHR876	*MAT***a** *BGI1::BGI1-V5-GFP-NAT, CENP-C^{MIF2}:: CENP-C^{MIF2}-mCherry-NEO*	This study
SHR897	*MAT***a** *CENP-C^{MIF2}:: CENP-C^{MIF2}-mCherry-NEO, BKT2::BKT2-V5-GFP-NAT*	This study

SHR842	*MAT***a** *CENP-C^{MIF2}:: CENP-C^{MIF2}-mCherry-NEO, YTA7::YTA7-V5-GFP-NAT*	This study
SHR905	*MAT***a** *KN99::mCherry- CENP-A^{CSE4}-NEO (pLKB74), MCM6::MCM6-V5-GFP-NAT*	This study
SHR870	*MATα BGI1::BGI1-V5-GFP-NAT*	This study
SHR516	*MAT***a** *Mis12^{MTW1}:: Mis12^{MTW1}-mCherry-NEO, NUF2::NUF2-GFP-NAT*	(Kozubowski et al., 2013)
CNVY120	*MAT***a** *KN99::GFP-DAD1-NAT (pVY2), KN99:: CENP-A^{CSE4}-mCherry-NEO*	(Kozubowski et al., 2013)
CNV119	*MATα H99::GFP-DAD1-NAT (pVY2), DAD2::DAD2-mCherry-NEO*	(Kozubowski et al., 2013)
SHR772	*MAT***a** *MIS12^{MTW1}:: MIS12^{MTW1}-mCherry-NEO, KNL1^{SPC105}:: KNL1^{SPC105}-GFP-NAT*	This study
SHR869	*MAT***a** *MIS12^{MTW1}:: MIS12^{MTW1}-mCherry-NEO, BGI1::BGI1-V5-GFP-NAT*	This study
SHR906	*MATα DAD2::GAL7p-mCherry-DAD2-HygB, BGI1::BGI1-V5-GFP-NAT*	This study
SHR907	*MAT***a** *MIS12^{MTW1}::GAL7p-mCherry- MIS12^{MTW1}-HygB, BGI1::BGI1-V5-GFP-NAT*	This study
SHR908	*MATα BGI1::BGI1-V5-GFP-NAT, sos7Δ::NEO*	This study
SHR909	*MAT***a** *Dad2::DAD2-mCherry-NEO, BGI1::BGI1-V5-GFP-NAT*	This study
SHR720	*MAT***a** *NDC80::NDC80-mCherry-NEO, CENP-C^{MIF2}::GAL7p-GFP- CENP-C^{MIF2}-HygB*	This study
SHR724	*MAT***a** *NDC80::NDC80-mCherry-NEO, Mis12^{MTW1}::GAL7p-GFP- MIS12^{MTW1}-HygB*	This study
SHR732	*MAT***a** *MIS12^{MTW1}:: MIS12^{MTW1}-mCherry-NEO, NUF2::GAL7p-GFP-NUF2-HygB*	This study
SHR910	*MATα KNL1^{SPC105}:: KNL1^{SPC105}-GFP-NAT, NUF2::GAL7p-mCherry-NUF2-HygB*	This study
SHR768	*MATα KNL1^{SPC105}:: KNL1^{SPC105}-GFP-NAT, MIS12^{MTW1}::GAL7p-mCherry- MIS12^{MTW1}-HygB*	This study
SHR911	*MAT***a** *DAD2::DAD2-mCherry-NEO, NUF2::GAL7p-GFP-NUF2-HygB*	This study
SHR767	*MATα KNL1^{SPC105}:: KNL1^{SPC105}-GFP-NAT, Dad2::GAL7p-mCherry-DAD2-HygB*	This study

SHR713	*MAT***a** *NDC80::NDC80-mCherry-NEO, DAD1::GAL7p-GFP-DAD1-HygB*	This study
SHR706	*MATα H99::GFP-DAD1-NAT (pVY2), CENP-A^{Cse4}::GAL7p-mCherry- CENP-A^{Cse4}-HygB*	This study
SHR754	*MATα H99::GFP-DAD2-NAT (pSS09),CENP-A^{Cse4}::GAL7p-mCherry- CENP-A^{Cse4}-HygB*	This study
SHR786	*MAT***a** *CENP-C^{MIF2}:: CENP-C^{MIF2}-mCherry-NEO, CENP-A^{Cse4}::GAL7p-GFP- CENP-A^{Cse4}-HygB*	This study
SHR792	*MAT***a** *MIS12^{MTW1}:: MIS12^{MTW1}-mCherry-NEO,CENP-A^{Cse4}::GAL7p-GFP- CENP-A^{Cse4}-HygB*	This study
SHR795	*MAT***a** *NDC80::NDC80-mCherry-NEO, CENP-A^{Cse4}::GAL7p-GFP- CENP-A^{Cse4}-HygB*	This study
SHR755	*MAT***a** *MIS12^{MTW1}:: MIS12^{MTW1}-mCherry-NEO, CENP-C^{MIF2}::GAL7p-GFP- CENP-C^{MIF2}-HygB*	This study
SHR721	*MAT***a** *Dad2::DAD2-mCherry-NEO, CENP-C^{MIF2}::GAL7p-GFP-CENP-C^{MIF2}-HygB*	This study
SHR760	*MATα H99::GFP-DAD1-NAT (pVY2), MIS12^{MTW1}::GAL7p-mCherry- MIS12^{MTW1}-HygB*	This study
SHR725	*MAT***a** *KN99::mCherry- CENP-A^{CSE4}-NEO (pLKB74), MIS12^{MTW1}::GAL7p-GFP- MIS12^{MTW1}-HygB*	This study
SHR726	*MAT***a** *CENP-C^{MIF2}:: CENP-C^{MIF2}-mCherry-NEO, MIS12^{MTW1}::GAL7p-GFP- MIS12^{MTW1}-HygB*	This study
SHR729	*MAT***a** *KN99::mCherry- CENP-A^{CSE4}-NEO (pLKB74), NUF2::GAL7p-GFP-NUF2-HygB*	This study
SHR731	*MAT***a** *CENP-C^{MIF2}:: CENP-C^{MIF2}-mCherry-NEO, NUF2::GAL7p-GFP-NUF2-HygB*	This study
SHR806	*MAT***a** *NDC80::NDC80-mCherry-NEO, KNL1^{SPC105}::GAL7p-GFP- KNL1^{SPC105}-HygB*	This study
SHR808	*MAT***a** *MIS12^{MTW1}:: MIS12^{MTW1}-mCherry-NEO, KNL1^{SPC105}::GAL7p-GFP- KNL1^{SPC105}-HygB*	This study
SHR788	*MAT***a** *Dad2::DAD2-mCherry-NEO, KNL1^{SPC105}::GAL7p-GFP-KNL1^{SPC105}-HygB*	This study
SHR789	*MAT***a** *KN99::mCherry- CENP-A^{CSE4}-NEO (pLKB74), KNL1^{SPC105}::GAL7p-GFP- KNL1^{SPC105}-HygB*	This study
SHR797	*MAT***a** *CENP-C^{MIF2}:: CENP-C^{MIF2}-mCherry-NEO, KNL1^{SPC105}::GAL7p-GFP- KNL1^{SPC105}-HygB*	This study

SHR711	*MAT***a** *KN99::mCherry- CENP-A^{CSE4}-NEO (pLKB74), DAD1::GAL7p-GFP-DAD1-HygB*	This study
SHR712	*MAT***a** *MIS12^{MTW1}:: MIS12^{MTW1}-mCherry-NEO, DAD1::GAL7p-GFP-DAD1-HygB*	This study
SHR805	*MAT***a** *Dad2::DAD2-mCherry-NEO, DAD1::GAL7p-GFP-DAD1-HygB*	This study
SHR758	*MAT***a** *CENP-C^{MIF2}:: CENP-C^{MIF2}-mCherry-NEO, DAD1::GAL7p-GFP-DAD1-HygB*	This study
SHR761	*MATα H99::GFP-DAD1-NAT (pVY2), DAD2::GAL7p-mCherry-DAD2-HygB*	This study
SHR809	*MAT***a** *Dad2::DAD2-mCherry-NEO, ASK1::GAL7p-GFP-ASK1-HygB*	This study
SHR867	*MATα bgi1Δ::NEO*	This study
SHR838	*MAT***a** *bgi1Δ::HygB*	This study
SHR830	*MATα H99::GFP-H4-NAT (pLKB35), bgi1Δ::HygB*	This study
SHR832	*MAT***a** *H4::H4-mCherry-NEO, bgi1Δ::HygB*	This study
SHR873	*MAT***a** *H4::H4-mCherry-NEO, KN99::GFP-PCNA-NAT (pSS60)*	This study
SHR912	*MAT***a** *bgi1Δ::HygB, KN99::3xFLAG-GFP-BGI1-NAT*	This study
SHR879	*MAT***a** *H4::H4-mCherry-NEO, bgi1Δ::HygB, KN99::3xFLAG-GFP-BGI1-NAT (pSS62)*	This study
SHR854	*MAT***a** *H4::H4-mCherry-NEO, KN99::GFP-PCNA-NAT (pSS60)*	This study
SHR734	*MATα mad2Δ::NEO,*	This study
SHR866	*MATα mad2Δ::NEO, bgi1Δ::HygB, H4::H4-GFP-NAT*	This study
SHR741	*MAT***a** *H4::H4-mCherry-NEO, mad2Δ::NEO*	This study
SHR913	*MAT***a** *H4::H4-mCherry-NEO, bgi1Δ::HygB, bgi1Δ::3x-FLAG-GFP-BGI1 FDΔ-NAT (pSS63)*	This study
SHR880	*MAT***a** *H4::H4-mCherry-NEO, bgi1Δ::HygB, bgi1Δ::3x-FLAG-GFP-BGI1 BDΔ-NAT (pSS64)*	This study
SHR915	*MAT***a** *H4::H4-mCherry-NEO, bgi1Δ::HygB, bgi1Δ::3x-FLAG-GFP-BGI1 FD-NAT (pSS65)*	This study
SHR916	*MAT***a** *H4::H4-mCherry-NEO, bgi1Δ::HygB, bgi1Δ::3x-FLAG-GFP-BGI1 USD-NAT (pSS66)*	This study
SHR917	*MAT***a** *H4::H4-mCherry-NEO, bgi1Δ::HygB, bgi1Δ::3x-FLAG-GFP-BGI1 BD-NAT (pSS67)*	This study
SHR918	*MAT***a** *H4::H4-mCherry-NEO, bgi1Δ::HygB, bgi1Δ::3x-FLAG-GFP-NAT (pSS61)*	This study

CNVY121	*MAT***a** *H4::H4-mCherry-NEO*	(Kozubowski et al., 2013)
SHR903	*MAT***a** *MIS12^{MTW1}:: MIS12^{MTW1}-mCherry-NEO, NUF2::NUF2-GFP-NAT, bgi1Δ::HygB*	This study
SHR904	*MAT***a** *MIS12^{MTW1}:: MIS12^{MTW1}-mCherry-NEO, KNL1^{SPC105}:: KNL1^{SPC105}-GFP-NAT, bgi1Δ::HygB*	This study
SHR902	*MAT***a** *KN99::GFP-DAD1-NAT (pVY2), KN99::CENP-A^{CSE4}-mCherry-NEO, bgi1Δ::HygB*	This study
SHR919	*MAT***a** *bgi1Δ::HygB, bgi1Δ::3x-FLAG-FD-NAT (pSS77)*	This study
SHR858	*MAT***a** *NDC80::NDC80-mCherry-NEO, BGI1::GAL7p-GFP-BGI1-HygB*	This study
SHR893	*MATα SPC34::SPC34-3xFLAG-GFP-NAT*	This study
SHR895	*MAT***a** *H4::H4-mCherry-NEO, bgi1Δ::HygB, KN99::H3p-GFP-BGI1-NAT (pSS68)*	This study
SHR920	*MAT***a** *H4::H4-mCherry-NEO, bgi1Δ::HygB, KN99::H3p-GFP-BGI1-FDΔ-NAT (pSS69)*	This study
SHR921	*MAT***a** *H4::H4-mCherry-NEO, bgi1Δ::HygB, KN99::H3p-GFP-BGI1-BDΔ-NAT (pSS70)*	This study
SHR922	*MAT***a** *H4::H4-mCherry-NEO, bgi1Δ::HygB, KN99::H3p-GFP-BGI1-FD-NAT (pSS71)*	This study
SHR923	*MAT***a** *H4::H4-mCherry-NEO, bgi1Δ::HygB, KN99::H3p-GFP-BGI1-USD-NAT (pSS72)*	This study
SHR924	*MAT***a** *H4::H4-mCherry-NEO, bgi1Δ::HygB, KN99::H3p-GFP-BGI1-BD-NAT (pSS73)*	This study
SHR925	*MAT***a** *H4::H4-mCherry-NEO, KN99::H3p-GFP-BGI1-NAT (pSS74)*	This study
SHR926	*MAT***a** *H4::H4-mCherry-NEO, bgi1Δ::HygB, MAT a H4::H4-mCherry-NEO, bgi1Δ::HygB, bgi1Δ::3x-FLAG-GFP-(BDΔ+HsKI67BD)-NAT (pSS75)*	This study
SHR826	*MATα CENP-C^{MIF2}::GAL7p-GFP- CENP-C^{MIF2}-HygB, H99::H3p-mCherry-CENP-C$^{MIF2\ 1\text{-}46\Delta}$-NEO (pSS104)*	This study
SHR828	*MATα CENP-C^{MIF2}::GAL7p-GFP- CENP-C^{MIF2}-HygB, H99::H3p-mCherry-CENP-C$^{MIF2\text{-}FL}$-NEO (pSS103)*	This study

Table 6-2: Plasmid list

Plasmid name	Description	Reference
pCIN19	*Histone H3p (CNAG_06745)-GFP-NAT*	Alspaugh lab
pSS59	*BGI1-3xFLAG-NAT in pBlueScriptII KS(-)*	This study
pSS61	*BGI1p-3xFLAG-GFP-NAT in pBlueScriptII KS(-)*	This study
pSS78	*BGI1-V5-GFP-NAT in pRS426*	This study
pSS85	*GAL7p-GFP-SOS7-HygB in pBlueScriptII KS(-)*	This study
pSS79	*BKT2-V5-GFP-NAT in pRS426*	This study
pSS81	*BKT3-V5-GFP-NAT in pRS426*	This study
pSS80	*YTA7-V5-GFP-NAT in pRS426*	This study
pSS82	*MCM6-V5-GFP-NAT in pRS426*	This study
pSS13	*GAL7p-GFP- CENP-C^{MIF2}-HygB pBlueScriptII KS(-)*	Shreyas Sridhar MS thesis 2014
pSS14	*GAL7p-GFP- MIS12^{MTW1}- HygB pBlueScriptII KS(-)*	Shreyas Sridhar MS thesis 2014
pSS07	*GAL7p-GFP-NUF2- HygB pBlueScriptII KS(-)*	Shreyas Sridhar MS thesis 2014
pSS24	*GAL7p-mCherry-NUF2- HygB pBlueScriptII KS(-)*	Shreyas Sridhar MS thesis 2014
pSS19	*GAL7p-GFP- MIS12^{MTW1}- HygB pBlueScriptII KS(-)*	Shreyas Sridhar MS thesis 2014
pSS27	*GAL7p-GFP-KNL1^{SPC105}- HygB pBlueScriptII KS(-)*	This study
pSS21	*GAL7p-mCherry-DAD2- HygB pBlueScriptII KS(-)*	Shreyas Sridhar MS thesis 2014
pSS04	*GAL7p-GFP-DAD1- HygB pBlueScriptII KS(-)*	Shreyas Sridhar MS thesis 2014
pSS05	*GAL7p-mCherry-CENP-A^{Cse4}- HygB pBlueScriptII KS(-)*	Shreyas Sridhar MS thesis 2014
pSS16	*GAL7p-GFP-CENP-A^{Cse4}- HygB pBlueScriptII KS(-)*	Shreyas Sridhar MS thesis 2014
pSS19	*GAL7p-mCherry- MIS12^{MTW1}- HygB pBlueScriptII KS(-)*	Shreyas Sridhar MS thesis 2014
pSS114	*GAL7p-GFP-ASK1- HygB pBlueScriptII KS(-)*	This study
pSS84	*BGI1^{FL} in pSS59 (BamHI/SpeI)*	This study

pSS62	*BGI1^{FL} in pSS61 (BamHI/SpeI)*	This study
pSS63	*BGI1$^{FD\Delta}$ in pSS61 (BamHI/SpeI)*	This study
pSS64	*BGI1$^{BD\Delta}$ in pSS61 (BamHI/SpeI)*	This study
pSS65	*BGI1^{FD} in pSS61 (BamHI/SpeI)*	This study
pSS66	*BGI1^{USD} in pSS61 (BamHI/SpeI)*	This study
pSS67	*BGI1^{BD} in pSS61 (BamHI/SpeI)*	This study
pSS76	*BGI1^{FL} in pSS59 (BamHI/SpeI)*	This study
pSS58	*SPC34-3xFLAG-HygB in pBlueScriptII KS(-)*	This study
pSS86	*BGI1^{FD} in pGEX6P1*	This study
pSS87	*BGI1^{BD} in pGEX6P1*	This study
pSS89	*6xHis-BGI1 in pFASTBacHTA*	This study
pSS87	*GAL7p-GFP-BGI1-HygB in pBlueScriptII KS(-)*	This study
pSS68	*BGI1^{FL} (BamHI/SpeI) in pCIN19*	This study
pSS69	*BGI1$^{FD\Delta}$ (BamHI/SpeI) in pCIN19*	This study
pSS70	*BGI1$^{BD\Delta}$ (BamHI/SpeI) in pCIN19*	This study
pSS71	*BGI1^{FD} (BamHI/SpeI) in pCIN19*	This study
pSS72	*BGI1^{USD} (BamHI/SpeI) in pCIN19*	This study
pSS73	*BGI1^{BD} (BamHI/SpeI) in pCIN19*	This study
pSS74	*HsKi67^{BD} (BamHI/SpeI) in pCIN19*	This study
pSS75	*BGI1$^{BD\Delta}$+HsKI67^{BD} in pSS61 (BamHI/SpeI)*	This study
pSS103	*Histone H3p (CNAG_06745)-mCherry- CENP-C$^{MIF2\text{-}FL}$-NEO*	This study
pSS104	*Histone H3p (CNAG_06745)-mCherry- CENP-C$^{MIF2\text{-}1\text{-}46\Delta}$-NEO*	This study

Table 6-3: Primer list

Name	Sequence (5'------3')	Description
SHR17	CAACGAGCTCGGTAAAAGGTCACCAGTAGCAG	Generation of *GAL7p-GFP/mCherry-CENP-A^{Cse4}*
SHR18	ATAGTATTGCGGCCGCATTCCTTCCGATTGTTTCG	
SHR19	CAGCAAGCTTATGGCAAGAACAGTAACGAGC	
SHR20	GTAGCTCGAGCATGATTGTCACCCTCTTTGC	
SHR03	GTGCGAGCTCGCTAGCTTCTCCAAGATGGGTGTCACG	Generation of *GAL7p-GFP-DAD1*
SHR04	GTGAGAATGCGGCCGCCTTGGAGTGCTAGTTTTCCTGC	
SHR05	ATGTCTTTATCAAGACCATCGAATGCCTACGATGC	
SHR06	GTGCGGTACCGAGCTCATGCCTATGAAGTCCAGC	
SHR72	AGCTTGAGCTCCTTCGAGATATACAGCTCC	
SHR73	TTTAAGCGGCCGCCACTCGAGAGTTACAGTG	

SHR74	CATCAAGCTTGGTGGTATGTCCCGTCCATCAATAGAAATG	Generation of *GAL7p-mCherry-DAD2*
SHR75	AACTCTCGAGGTGAGATAGGGTTGAAGGAGC	
SHR64	AGCTGAGCTCCAAATCCACAACATCTGAAATACG	Generation of *GAL7p-GFP/mCherry-MIS12^{MTW1}*
SHR65	AAATTTGCGGCCGCGAACGTAGAGACGATTATGAATGC	
SHR66	GCTGTTAACGGTGGTATGGTCCCGAGGAAGCCAG	
SHR67	AGGTCCTCGAGCATTGGCAAGCTAACTAAATTAATGGAACG	
SHR68	AGCTGAGCTCCAAGTCTCTTGTCGACATCTCTCC	Generation of *GAL7p-GFP-CENP-C^{MIF2}*
SHR69	TTATTAGCGGCCGCGTTGAAGATGTTCTGGAGAAGTGC	
SHR70	AACCCAAGCTTATGTCCCACATAACACCCTCAAGA	
SHR71	TCGTCTCGAGCTTTCCATCTGCTTGCTTCTTTGG	
SHR50	GACTGAGCTCCTTGCACTCTTACAGAAGCCTCC	Generation of *GAL7p-GFP/mCherry-NUF2*
SHR51	TCACATGCGGCCGCGATTGCTGAATGCAAATGCAG	
SHR52	GACTAAGCTTATGTCGCAGCAGAATCGCAG	
SHR53	GACTGGTACCGATTTCAAGCTGTGTGACGATACG	
SHR112	AATGCGAGCTCTCTGTACCAGATAGTCACCAC	Generation of *GAL7p-GFP-KNL1^{SPC105}*
SHR113	ATATATATGCGGCCGC AATATGCTCGGTTAACTGCTG	
SHR114	TAGTCAAGCTTATGTCTTTAGCAGCTCGCTC	
SHR115	TCTAGGTACCGTTTCGAGTTGCTGTAGCTG	
SHR104	TGATGAGCTCACGATAATCGAACACAAGG	Generation of *GAL7p-GFP-ASK1*
SHR105	TATATAATGCGGCCGCTGTGATATTCTCAATACAGTGT	
SHR106	GGAGTTACCATGTCCAACGACGACAACC	
SHR107	TAATGGTACCGAATTTCATGGTCACAGGTGG	
SHR179	CTACTCTTACAGGCAAGTTGGAG	*KNL1^{SPC105}-GFP* tagging
SHR180	CTCGCCCTTGCTCACCATACTGGAGTACCTTGCACCGA	
SHR181	TCGGTGCAAGGTACTCCAGTATGGTGAGCAAGGGCGAG	
SHR182	CCTTGTAACCATCCATACAACCTAGGATGTGAGCTGGAGAGC	
SHR183	GCTCTCCAGCTCACATCCTAGGTTGTATGGATGGTTACAAGG	
SHR184	CTCTGGTGATACACTCAAGGAC	
SHR77	TCGTGAGCTCGTCTCAACAATTTGGTTACTGATCAAGG	Generation of *mad2Δ* cassette
SHR78	AGGACACTAGTTTCGTGGGGTAGAAACTGGAAG	
SHR81	TTTAAAGCGGCCGCGTAATATTATCTAGTTCAACGTTCACG	
SHR80	ACCCTTAGATCTGTGAATTCCTTTTATCCATTTTCC	
SHR389	GTCAGAGCTCCTCACAACATAAGACATCG	Generation of *GAL7p-GFP-SOS7*
SHR390	ATATATGCGGCCGCAGATCCAATATTACTACTATACGG	
SHR391	GTCAAAGCTTGCTGGTGCAGGAATGGAACCCTCTATGACG	
SHR392	GTCACTCGAGGTTTGAGCTTCAACCAG	
SHR374	GATGTTGAGAGAAGTGATGGAGG	Tagging of *DSN1* with 3xFLAG
SHR450	CTACTTGTCATCGTCATCCTTGTAGTCGATGTCATGATCTTTATAATCACCGTCATGGTCTTTGTAGTCTTCCCTCTCCGGCCTA	

SHR452	CGACTACAAGGATGACGATGACAAGTAGCTAGTAACGGCCGCCA	
SHR377	CAATTGTAACCATCGTCATTAACACCAGTGTGATGGATATCTGCAGA	
SHR378	TCTGCAGATATCCATCACACTGGTGTTAATGACGATGGTTACAATTG	
SHR379	GATGGCATTTCGCTAACCAC	
SHR367	GTATGTGTCGACGTATGACCT	
SHR451	CTACTTGTCATCGTCATCCTTGTAGTCGATGTCATGATCTTTATAATCACCGTCATGGTCTTTGTAGTCTTTACCCAAAGCCAATTG	Tagging of *SPC25* with 3xFLAG
SHR370	GCACTCAAAAATGTTACAAATACAGTCCAGTGTGATGGATATCTGCAGA	
SHR371	TCTGCAGATATCCATCACACTGGACTGTATTTGTAACATTTTTGAGTGC	
SHR372	CATCGTCATGCCAATCGTG	
SHR493	GAAGAATGGTAGAGCAAGG	Tagging of *CENP-C*^{MIF2} with 3xFLAG
SHR511	CTTGTCATCGTCATCCTTGTAGTCGATGTCATGATCTTTATAATCACCGTCATGGTCTTTGTAGTCTCCAGCACCTCTCCTACTCTTCCCCTTAC	
SHR494	ACCCATTCATACCTTCTTTCTCAGTGTGATGGATATCTGCAGA	
SHR495	TCTGCAGATATCCATCACACTGAGAAAGAAGGTATGAATGGGT	
SHR496	CACCAGATAGAAAGAGTCTAGG	
SHR513	CGACGGTATCGATAAGCTTGATATCGAGATGTACGAGGAAGAAGAGG	Tagging of *BGI1* with V5-GFP
SHR514	GAGACCAAGGAGAGGGTTGGGGATAGGCTTACCAGCACCCTTCCTACTCCTGGTTGTCCT	
SHR515	GCACCTATCTTACAACATCCACTATCAGGATGTGAGCTGGAGAGC	
SHR516	GCTCTCCAGCTCACATCCTGATAGTGGATGTTGTAAGATAGGTGC	
SHR517	CGGCCGCTCTAGAACTAGTCAGAGGAAGGAACCTTGGATG	
SHR518	CGACGGTATCGATAAGCTTGATATCCAATGGAGCTCTCCAGATGTC	Tagging of *YTA7* with V5-GFP
SHR519	GAGACCAAGGAGAGGGTTGGGGATAGGCTTACCAGCACCATCGTTTTTCCAACTATTAACCTCTTTG	
SHR520	AAACGCCATGCTAACAACAAAATGAGGATGTGAGCTGGAGAGC	
SHR521	GCTCTCCAGCTCACATCCTCATTTTGTTGTTAGCATGGCGTTT	
SHR522	CGGCCGCTCTAGAACTAGTCTCCATCTTCGTTCATTCACGC	
SHR523	CGACGGTATCGATAAGCTTGATATCCAGTCAGGGAAGATTTGACGTG	

SHR524	GAGACCAAGGAGAGGGTTGGGGATAGGCTTACCAGCACCCTCGTCACCACCGAACAC	Tagging of *BKT2* with V5-GFP
SHR525	GCATTAGTGTGGCTTCTTGATTCAGGATGTGAGCTGGAGAGC	
SHR526	GCTCTCCAGCTCACATCCTGAATCAAGAAGCCACACTAATGC	
SHR527	CGGCCGCTCTAGAACTAGTCATTCAAGGTAGCACATAAAGTTGAC	
SHR533	CGACGGTATCGATAAGCTTGATATCACTGCTGAGAGGAGCTGTG	Tagging of *BKT3* with V5-GFP
SHR534	GAGACCAAGGAGAGGGTTGGGGATAGGCTTACCAGCACCGATCATTTCGTAACCTTCATCTTTTGC	
SHR535	CGCTATACTACCTTAAGTTTAACCGTAGGATGTGAGCTGGAGAGC	
SHR536	GCTCTCCAGCTCACATCCTACGGTTAAACTTAAGGTAGTATAGCG	
SHR537	CGGCCGCTCTAGAACTAGTCCAACACACAAATTATCAAGGATTCC	
SHR453	CGACGGTATCGATAAGCTTGATATCGATCTTCGTCAGCATCTAGCTC	Tagging of *SPC34* with 3xFLAG-GFP
SHR454	TATAATCACCGTCATGGTCTTTGTAGTCAGCTCCATCTGCAAATCTAACCCTACCC	
SHR455	GGTATACAGTTAGATCAAGGAGGATACAGGATGTGAGCTGGAGAGC	
SHR456	GCTCTCCAGCTCACATCCTGTATCCTCCTTGATCTAACTGTATACC	
SHR457	CGGCCGCTCTAGAACTAGTCAAATAACATGACGTGACGGAC	
SHR538	CGACGGTATCGATAAGCTTGATATCGCTCCAGAGGTATATTCGATACG	Tagging of *MCM6* with V5-GFP
SHR539	GAGACCAAGGAGAGGGTTGGGGATAGGCTTACCAGCACCTGCGGGAATAGAAGAAGATAAATCTG	
SHR540	GGAACAGCGGGAAATGCAAGGATGTGAGCTGGAGAGC	
SHR541	GCTCTCCAGCTCACATCCTTGCATTTCCCGCTGTTCC	
SHR542	CGGCCGCTCTAGAACTAGTCGAACCCTGCTCAAGTCG	
SHR560	GGTAAGCCTATCCCCAACCCTCTCCTTGGTCTCGACAGCACCGGTGCTATGGTGAGCAAGGGCGAG	Common V5-GFP primer
SHR548	GCTCAGAGGTCACATACAGG	Generation of *sos7Δ* cassette
SHR564	CTGCAGATATCCATCACACTGGAGGTCAAAGATGGGTAAATAGC	
SHR565	GCTATTTACCCATCTTTGACCTCCAGTGTGATGGATATCTGCAG	
SHR551	GCTGTCCACTTTCGAAGGTCAGTGTGCTGGAATTCGC	
SHR552	GCGAATTCCAGCACACTGACCTTCGAAAGTGGACAGC	
SHR553	CATTATTGGAGATGTCTGAAGCG	
SHR582	CGACGGTATCGATAAGCTTGATATCCCAGAAGGATAGAGTCCTCTG	Generation of *GAL7p*-

SHR583	CTCACATCCTCGCAGCTTTTCGTTGCAAGTCAGC	*GFP/mCherry-BGI1*
SHR584	GCTGACTTGCAACGAAAAGCTGCGAGGATGTGAG	
SHR585	CTCTCGTCAAACTCTTGCATGGCACCAGCGTACAGCTCGTCCATGCCG	
SHR586	CGGCATGGACGAGCTGTACGCTGGTGCCATGCAAGAGTTTGACGAGAG	
SHR587	CGGCCGCTCTAGAACTAGTGTTACTGTCAATTGAGGAAGC	
SHR600	CTAGCTTGGCAATAGTGTAGCAG	Generation of *bgi1Δ* cassette
SHR601	CTGCAGATATCCATCACACTGGGTTGCTGTTTGTATAGCGAGTC	
SHR602	GACTCGCTATACAAACAGCAACCCAGTGTGATGGATATCTGCAG	
SHR603	GCACCTATCTTACAACATCCACTATCCAGTGTGCTGGAATTCGC	
SHR604	GCGAATTCCAGCACACTGGATAGTGGATGTTGTAAGATAGGTGC	
SHR605	CAGAGGAAGGAACCTTGGATG	
SHR611	AGTCGGATCCGCCGCTGGTGCCATGCAAGAGTTTGACGAGAG	Generation of domain deletion constructs expressed under native or H3 promoter
SHR612	ATATATACTAGTCAAGTACTCGCCACTTATCACTC	
SHR613	AGTCGGATCCGCCGCTGGTGCCTGGACCTATGGAAGATGCT	
SHR614	ATATATACTAGTCTATCTTACAACATCCACTATCCATTATCATTAAGCATCTTCCATAGGTCCA	
SHR615	ATATATACTAGTCTATCTTACAACATCCACTATCCATTATCATTATAGTTGAACCTGAAAAGCTTTTTC	
SHR616	AGTCGGATCCGCCGCTGGTGCCGAGATCGAAGAGAAGGGTAAAG	
SHR715	CCTCAGTGTGGCCTGGGGCACCAGCCTCATCTTGCTCCTGCAC	Generation of fusion protein of Bgi1$^{BD\Delta}$ and HsKi67^{BD}
SHR716	GTGCAGGAGCAAGATGAGGCTGGTGCCCCAGGCCACACTGAGG	
SHR676	ATATATACTAGTCTATCTTACAACATCCACTATCCATTATCATTACCAAATATCTTCACTGTCCCTATG	
SHR677	AGTCGGATCCCCAGGCCACACTGAGG	Over-expression of Hs*KI67^{BD}*
SHR561	ATATATACTAGTGGTGCTGGAGCCATGTCCCACATAACACCCTC	Generation of CENP-C^{Mif2} reintegration cassettes
SHR562	ATATATACTAGTGGTGCTGGAGCCGCGTTATTCTTTGGCTCATCCC	
SHR563	ATATATGCGGCCGCCAGCGACACTCGTTCG	
SHR729	CTGAGGATCCATGCAAGAGTTTGACGAGAG	Tagging BGI1^{FD} with GST for recombinant protein purification
SHR730	CTGAGTCGACTTAATCTTCCATAGGTCCATAGTTG	

SHR731	CTGAGGATCCATCGAAGAGAAGGGTAAAGG	Tagging *BGI1*^{BD} with GST for recombinant protein purification
SHR733	ATATATGCGGCCGCTTACTTCCTACTCCTGGTTGTC	
VYP75	AGTCTCGTGTGGCTATGATT	Centromeric DNA methylation
VYP76	GGATCTGCTTGACAGTGTCA	
VYP79	CCAACCGAAGCCCAAGACAA	Non-centromeric DNA methylation
VYP80	TTGAAGGATGATCCGGCCGA	

Appendix

Appendix I- List of abbreviations and acronyms

˚C	-	Degree Celsius
µg	-	Microgram
µl	-	Microliter
aa	-	Amino acid
APC/C	-	Anaphase-promoting complex or cyclosome
ARS	-	Autonomously replicating sequence
N-terminus	-	Amino-terminus
BD	-	Basic domain
bp	-	Base pair
BLAST	-	Basic Local Alignment Search Tool
BKT	-	Basidiomycete kinetochore protein
BUB	-	Budding uninhibited by benzimidazole
C-terminus	-	Carboxy-terminus
CATD	-	CENP-A targeting domain
CCAN	-	Constitutive Centromere Associated Network
CDE	-	Centromeric DNA element
ChIP	-	Chromatin immunoprecipitation
ChIP-qPCR	-	ChIP-quantitative polymerase chain reaction
CEN	-	Centromere
Non-CEN	-	Non-centromere
CNS	-	Central nervous system
DMF	-	Dimethylformamide
DNA	-	Deoxyribonucleic Acid
EDTA	-	Ethylenediaminetetraacetic Acid
EGTA	-	Ethylene glycol-bis(β-aminoethyl ether)-N,N,N′,N′-tetraacetic acid
EMSA	-	Electrophoretic mobility shift assay
FD	-	Fork-head associated domain
FRET	-	Förster resonance energy transfer
G-418	-	Genticin-418
GDP	-	Guanosine diphosphate
GFP	-	Green fluorescent protein
GTP	-	Guanosine triphosphate
h	-	Hour
Hyg	-	Hygromycin
IP	-	Immunoprecipitation
kb	-	kilobase

KMN network	-	KNL1, Mis12, NDC80 complex network
M	-	Molar
MAD	-	Mitotic arrest deficient
MAPs	-	Microtubule-associated proteins
MCC	-	Mitotic checkpoint complex
MCM	-	Mini chromosome stability
mg	-	Milligram
min	-	Minute
ml	-	Millilitre
mM	-	Millimolar
MS	-	Mass-spectrometry
MT	-	Microtubule
MTOC	-	Microtubule organizing center
N	-	Normal
NAT	-	Nourseothricin
NCP	-	Nucleosome Core Particle
NE	-	Nuclear envelope
NPC	-	Nuclear pore complex
NU	-	Nucleolus
PCNA	-	Proliferation cell nuclear antigen
PLK1	-	Polo-like kinase 1
OD_{600}	-	Optical density at 600 nM
ORF	-	Open reading frame
PBS	-	Phosphate buffered saline
PCR	-	Polymerase chain reaction
rpm	-	Revolutions per minute
RT	-	Room temperature
s	-	Second
SAC	-	Spindle assembly checkpoint
SDS	-	Sodium dodecyl sulphate
SLB	-	Sample loading buffer
SPB	-	Spindle pole body
USD	-	Unstructured domain
UTR	-	Untranslated region

Appendix II-List of kinetochore homologs

Organism	CENP-A	CENP-C	CENP-T	CENP-W	CENP-S	CENP-X
Mixia osmundae	G7E9P5	G7DW28				G7E2N8
Puccinia graminis f. sp. tritici	E3JV97	H6QPD2		E3KAK6	E3JQT5	E3KHN0
Melampsora larici-populina	F4R5S6	F4R433			F4RWE9	F4RQY9
Leucosporidium creatinivorum	A0A1Y2FVV3	A0A1Y2EM16		A0A1Y2FYM4	A0A1Y2EX15	
Microbotryum intermedium	A0A238F3R0	A0A238FDF6			A0A238F2J2	A0A238FHJ6
Microbotryum saponariae	A0A2X0LQ22	A0A2X0M4P9			A0A2X0KCZ3	A0A2X0LAV3
Rhodosporidium toruloides	M7X4Z3	M7X596	M7XJJ5		A0A2T0A3W5	A0A2T0AI48
Ustilago maydis	A0A0D1BW46	A0A0D1E8Y7	A0A0D1DP16	A0A0D1D1F8		
Pseudozyma hubeiensis	R9P9G8	R9P2Y1	R9P1M7			
Malassezia globosa	A8PWP4	A8PQY9				
Malassezia sympodialis	A0A1M8A1W5	A0A1M8ABY3				
Tilletiopsis washingtonensis	A0A316Z1M5	A0A316ZLC4	A0A316Z3D1	A0A316Z378		
Meira miltonrushii	A0A316VBX8	A0A316VKE0	A0A316VJ52	A0A316V933		
Acaromyces ingoldii	A0A316YT03	A0A316YS18	A0A316YP96	A0A316YYK0		
Tilletiaria anomala	A0A066WNL5	A0A066W8P5	A0A066WRD5	A0A066WII0		
pseudomicrostroma glucosiphilum	A0A316U930	A0A316U9X5				
Jaminaea rosea	A0A316UZM6	A0A316UU94				
Tilletia indica	A0A177TI60	A0A177TQA4				
Ceraceosorus guamensis	A0A316W0C6	A0A316W2A4	A0A316W9B0			
Wallemia mellicola	I4Y9D3	I4YE81	I4Y8Y2	I4YEJ2		
Wallemia ichthyophaga	R9AE00	R9AL52	R9AAJ0	R9AHT8		
Phaffia rhodozyma	A0A0F7SSH2	A0A0F7STL1				
Cryptococcus neoformans	J9VFS1	J9VX29				
Tremella mesenterica	A0A4Q1BGX1	R7SBY4				
Trichosporon asahii var. asahii	J4UFA7	J4UI38				
Cutaneotrichosporon oleaginosum	A0A0J0XSZ0	A0A0J0XDI8				
Calocera cornea	A0A165HUZ5	A0A165EL90		A0A165IGA5		
Dacryopinax primogenitus	M5GEW7	M5GGA7				
Exidia glandulosa	A0A165QXI9	A0A166AY16				
Serendipita vermifera	A0A0C2X7I3	A0A0C3B6F4				
Serendipita indica	G4TK51	G4T8Y7				
Rhizoctonia solani	*X8JRC7*	A0A0A1UJU4				
Thanatephorus cucumeris	*M5BL97*	*A0A0B7F0D6*				
Sistotremastrum niveocremeum	*A0A164ZQA5*	*A0A164TLB7*				
Sistotremastrum suecicum	A0A166BX56	A0A166GXV6				
Sphaerobolus stellatus		A0A0C9ULG3				
Pyrrhoderma noxium	*A0A286UMK6*	*A0A286UW90*				
Schizopora paradoxa	*A0A0H2REA8*	*A0A0H2S4Q9*				
Neolentinus lepideus	*A0A165P0Q3*	*A0A165RL39*				
Gloeophyllum trabeum	S7QJ88	S7QHN6				
Ganoderma sinense	A0A2G8STN0	A0A2G8RS81				
Dichomitus squalens	R7SHT0	A0A4Q9QCP7				
Heterobasidion irregulare	W4KH44	W4KMG4				
Bondarzewia mesenterica	A0A4S4MA74	A0A4S4M8U5				
Coprinopsis cinerea	A8NXR9	A8NDW9				
Galerina marginata	A0A067TKG8	A0A067T1B7				
Piloderma croceum	A0A0C3BWG1	A0A0C3FQ52				
Fibularhizoctonia sp.	A0A166VQP7	A0A166GIG9				
Pisolithus microcarpus	A0A0D0A7K3	A0A0C9ZYA3		A0A0C9YTM0		
Rhizopogon vesiculosus	A0A1J8QWF2	A0A1J8QBH2				
Jaapia argillacea	A0A067QBW2	A0A067QCJ6				
Saccharomyces cerevisiae	P36012	P35201	P43618	Q2V2P8	Q3E835	Q3E829
Neurospora crassa	Q7RXR3	Q7RV28	Q7SEQ6	F5HD67	Q1K7Q5	Q7SC05
Schizosaccharomyces pombe	Q9Y812	Q9USR9	Q9HGK9	G2TRL2	O74807	O74896
Pneumocystis jirovecii	A0A0W4ZJU2	A0A0W4ZMH7	L0PES2	A0A0W4ZQ96		A0A0W4ZTV6
Saitoella complicata		A0A0E9N9E8	A0A0E9NS05	A0A0E9NA34	A0A0E9NL70	A0A0E9NME3
Allomyces macrogynus	*A0A0L0SPU9*				*A0A0L0SJR2*	*A0A0L0SDH2*
Encephalitozoon intestinalis				E0SAD5		
Basidiobolus meristosporus	*A0A1Y1Y3G1*	*A0A1Y1Z2A3*				*A0A1Y1XT29*
Smittium culicis	*A0A1R1Y034*	*A0A1R1YGT1*				
Spizellomyces punctatus	A0A0L0HUW6	A0A0L0H916			A0A0L0HRB0	
Batrachochytrium dendrobatidis	F4P4R3	F4PCQ2			F4P3E2	
Mucor circinelloides f. lusitanicus			A0A168MHP9	A0A162R5Z1	A0A168LR49	A0A162TPX3
Jimgerdemannia flammicorona	A0A433D8Y3 /	A0A433DDI3	A0A433D5L6	A0A433BAB8	A0A433CWE9	A0A433Q2J2
Rozella allomycis	A0A075AWL4	A0A0L0T820				
Paramicrosporidium saccamoebae						
Homo sapiens	P49450	Q03188	H3BTR4	Q5EE01	Q8N2Z9	A8MT69
Drosophila melanogaster	Q9V6Q2	Q9VHP9				

Organism	CENP-L	CENP-N	CENP-H	CENP-I	CENP-K	CENP-M
Mixia osmundae						
Puccinia graminis f. sp. tritici						
Melampsora larici-populina						
Leucosporidium creatinivorum	A0A1Y2G1C6	A0A1Y2ER80		A0A1Y2FX86	A0A1Y2D6E4	A0A1Y2D6E4
Microbotryum intermedium						
Microbotryum saponariae						
Rhodosporidium toruloides	M7XDR7	M7WGR0	M7WD46	M7WTK9	M7WV79	M7WV79
Ustilago maydis	A0A0D1CVM7	YU309	A0A0D1DX98	A0A0D1DXU8	A0A0D1DU34	A0A0D1DU34
Pseudozyma hubeiensis	R9P554	R9P5Z8	R9NVN9	R9NYD4	R9PCN5	R9PCN5
Malassezia globosa						
Malassezia sympodialis				A0A1M8A6Z2	A0A1M8A301	A0A1M8A301
Tilletiopsis washingtonensis	A0A316Z746	A0A316ZBI6	A0A316Z443	A0A316Z6E9	A0A316Z6U5	A0A316Z6U5
Meira miltonrushii		A0A316VKX3	A0A316VAH4	A0A316VDN5	A0A316VPK6	A0A316VPK6
Acaromyces ingoldii	A0A316YTY0	A0A316Z0B3	A0A316YYQ5	A0A316YVQ9	A0A316YD75	A0A316YD75
Tilletiaria anomala	A0A066VXX4	A0A066VG45		A0A066VVK2	A0A066VIV3	A0A066VIV3
pseudomicrostroma glucosiphilum						
Jaminaea rosea						
Tilletia indica						
Ceraceosorus guamensis	A0A316VTF2	A0A316VSE4		A0A316VP28	A0A316VV51	A0A316VV51
Wallemia mellicola		I4YJ43		A0A4T0MY12	I4YEX8	I4YEX8
Wallemia ichthyophaga		R9AGB9		R9AB10	R9AAE9	R9AAE9
Phaffia rhodozyma						
Cryptococcus neoformans						
Tremella mesenterica						
Trichosporon asahii var. asahi						
Cutaneotrichosporon oleaginosum						
Calocera cornea						
Dacryopinax primogenitus						
Exidia glandulosa						
Serendipita vermifera						
Serendipita indica						
Rhizoctonia solani						
Thanatephorus cucumeris						
Sistotremastrum niveocremeum						
Sistotremastrum suecicum						
Sphaerobolus stellatus						
Pyrrhoderma noxium						
Schizopora paradoxa						
Neolentinus lepideus						
Gloeophyllum trabeum						
Ganoderma sinense						
Dichomitus squalens						
Heterobasidion irregulare						
Bondarzewia mesenterica						
Coprinopsis cinerea						
Galerina marginata						
Piloderma croceum						
Fibularhizoctonia sp.						
Pisolithus microcarpus						
Rhizopogon vesiculosus						
Jaapia argillacea						
Saccharomyces cerevisiae	P38265	P38907	Q12262	Q12748	P47167	P47167
Neurospora crassa	V5IM47	Q7RY00	Q7S057	Q1K7M1	Q7SCU2	Q7SCU2
Schizosaccharomyces pombe	O36024	Q9C0W0	O94261	P87227	O94494	O94494
Pneumocystis jirovecii	L0PES1	A0A0W4ZWC7	L0PG58	L0PGI3	L0PB71_PNEJ8	L0PB71_PNEJ8
Saitoella complicata	A0A0E9NBA3	A0A0E9NGD5	A0A0E9NE62	A0A0E9NGX2	A0A0E9NJZ4	A0A0E9NJZ4
Allomyces macrogynus						
Encephalitozoon intestinalis						
Basidiobolus meristosporus			A0A1Y1Y8Z8	A0A1Y1ZB45	A0A1Y1XP72	A0A1Y1XP72
Smittium culicis						
Spizellomyces punctatus			A0A0L0HRS8		A0A0L0H4Y9	A0A0L0H4Y9
Batrachochytrium dendrobatidis					A0A177WYW1	A0A177WYW1
Mucor circinelloides f. lusitanicus	A0A168GZ11	A0A0C9MSE6	A0A168NSX4	A0A168J4Z7	A0A168INL0	A0A168INL0
Jimgerdemannia flammicorona		A0A433PYD8		A0A433QW52	A0A433P5J3	A0A433P5J3
Rozella allomycis						
Paramicrosporidium saccamoebae						
Homo sapiens	Q8N0S6	Q96H22	Q9H3R5	Q92674	Q9BS16	Q9BS16
Drosophila melanogaster						

Organism	CENP-O	CENP-P	CENP-Q	CENP-U	CENP-R	Mis12
Mixia osmundae						G7DVW9
Puccinia graminis f. sp. tritici						E3JT89
Melampsora larici-populina						F4RR42
Leucosporidium creatinivorum	A0A1Y2EL28	A0A1Y2FU67	A0A1Y2FKX1	A0A1Y2FH42		A0A1Y2FV98
Microbotryum intermedium						A0A238FF93
Microbotryum saponariae						A0A2X0L6H3
Rhodosporidium toruloides	M7XY45	M7XMW8	A0A0K3CAB9	M7WK14		M7X1N8
Ustilago maydis	A0A0D1DW01	A0A0D1EBM7		A0A0D1DY09		A0A0D1DVB6
Pseudozyma hubeiensis	R9NWJ2	R9P5Z7		R9P6I6		R9P9Y3
Malassezia globosa						A8PX04
Malassezia sympodialis						M5EJX5
Tilletiopsis washingtonensis	A0A316Z4B9	A0A316Z0Q6		A0A316Z9Q4		A0A316ZDA6
Meira miltonrushii	A0A316VJT6	A0A316V0V2				A0A316V7J8
Acaromyces ingoldii	A0A316YVM4	A0A316YWZ1		A0A316YPA5		A0A316YS36
Tilletiaria anomala	A0A066WNY2	A0A066WK83		A0A066VS55		A0A066WRB1
pseudomicrostroma glucosiphilum						A0A316UCW0
Jaminaea rosea						A0A316UWG5
Tilletia indica						A0A177T8T5
Ceraceosorus guamensis	A0A316VW09	A0A316VR75		A0A316VSV6		A0A316VRI3
Wallemia mellicola	I4YDT9	I4YDQ5	A0A4T0LAA9	I4Y7S9		I4YA27
Wallemia ichthyophaga	R9ACM8	R9AGP4	I4YIS9	R9AN95		R9AEH1
Phaffia rhodozyma						A0A0F7SUG0
Cryptococcus neoformans						J9VR34
Tremella mesenterica						A0A4Q1BNK5
Trichosporon asahii var. asahi						J5T6K1
Cutaneotrichosporon oleaginosum						A0A0J0XQ63
Calocera cornea						A0A165JE42
Dacryopinax primogenitus						M5FQV5
Exidia glandulosa						A0A165H0R8
Serendipita vermifera						A0A0C3AXX6
Serendipita indica						G4T5M6
Rhizoctonia solani						X8JJ86
Thanatephorus cucumeris						L8WK01
Sistotremastrum niveocremeum						A0A165A665
Sistotremastrum suecicum						A0A166I9J6
Sphaerobolus stellatus						A0A0C9V664
Pyrrhoderma noxium						A0A286UFD3
Schizopora paradoxa						A0A0H2R4G0
Neolentinus lepideus						A0A165NWA1
Gloeophyllum trabeum						S7Q1D7
Ganoderma sinense						A0A2G8RZB4
Dichomitus squalens						A0A4Q9NGG0
Heterobasidion irregulare						W4JRF4
Bondarzewia mesenterica						A0A4S4LPU7
Coprinopsis cinerea						A8N8I8
Galerina marginata						A0A067T9T8
Piloderma croceum						
Fibularhizoctonia sp.						A0A166AT23
Pisolithus microcarpus						A0A0C9Z8L8
Rhizopogon vesiculosus						A0A1J8RC98
Jaapia argillacea						A0A067PG00
Saccharomyces cerevisiae	Q06675	Q02732	P53298	P38313		P39731
Neurospora crassa	Q10290	Q7S720	Q1K8Y3	Q7SGV7		Q7RYV6
Schizosaccharomyces pombe	Q7SFQ0	Q9US26	O74844	O94643		Q9Y738
Pneumocystis jirovecii	L0PGW4	L0PAY6	L0PDD7	A0A0W4ZQ33		L0PGL6
Saitoella complicata	A0A0E9NIE2	A0A0E9NCJ7	A0A0E9NE68	A0A0E9NHF8		A0A0E9NJ94
Allomyces macrogynus						A0A0L0TFF2
Encephalitozoon intestinalis						
Basidiobolus meristosporus						A0A1Y1YTD6
Smittium culicis						A0A1R1XR82
Spizellomyces punctatus						A0A0L0H5E6
Batrachochytrium dendrobatidis						A0A177WUB4
Mucor circinelloides f. lusitanicus	A0A168L447					A0A162QTX2
Jimgerdemannia flammicorona	A0A433AVQ4	A0A433QBH6		A0A433D2H8		A0A433ADX6
Rozella allomycis						A0A075AWR8
Paramicrosporidium saccamoebae						A0A2H9TQ31
Homo sapiens	Q9BU64	Q6IPU0	Q7L2Z9	Q71F23	Q13352	Q9H081
Drosophila melanogaster						Q9VS01

Organism	Dsn1	Nnf1	Nsl1	Knl1	Zwint
Mixia osmundae	G7DTX3	G7E0B5		G7E8S4	G7DWC1
Puccinia graminis f. sp. tritici	E3JZA3	E3KFY6	E3L1S1	E3JT36	E3KUE7
Melampsora larici-populina	F4REE3	F4RJ33	F4RS41	F4RH85	F4R626
Leucosporidium creatinivorum	A0A1Y2C2C3	A0A1Y2C482	A0A1Y2FXA7	A0A1Y2ERD0	A0A1Y2G486
Microbotryum intermedium	A0A238FC02	A0A238F8V0	A0A238F2S3	A0A238FH77	A0A238FSS6
Microbotryum saponariae	A0A2X0NLV0	A0A2X0MY78	A0A2X0L5S8		A0A2X0NB71
Rhodosporidium toruloides	M7WL51	M7WV95	M7WLC9	M7WNI6	M7WL68
Ustilago maydis	A0A0D1DSE4	A0A0D1CST2	A0A0D1C5E9	A0A0D1E8A4	A0A0D1E7F1
Pseudozyma hubeiensis	R9P9M6	R9NX20	R9P7W0_PSEHS	R9P5V9	R9P4V2
Malassezia globosa	A8PUV8			A8Q201	A8Q7V3
Malassezia sympodialis	A0A1M8A8I8	A0A1M8A5K2	A0A1M8AAW6	M5EKW6	M5EQU2
Tilletiopsis washingtonensis	A0A316ZG04	A0A316Z2C8	A0A316ZD30	A0A316ZGT3	A0A316ZAI3
Meira miltonrushii	A0A316VSG4	A0A316V8T3	A0A316VI39	A0A316VP20	A0A316V2V5
Acaromyces ingoldii	A0A316YU71	A0A316YHL1	A0A316YQ84	A0A316YMZ5	A0A316YSX8
Tilletiaria anomala	A0A066WG04	A0A066VV05	A0A066VUY3	A0A066WG66	A0A066W2L0
pseudomicrostroma glucosiphilum	A0A316U8S8	A0A316U0E1	A0A316U0Y0	A0A316UCY6	A0A316U419
Jaminaea rosea	A0A316U8S8	A0A316UYE7	A0A316UJJ2	A0A316UXR1	A0A316UY39
Tilletia indica	G4T7Q3	A0A177TZK0	A0A177TA45	A0A177TJ56	A0A177TDF9
Ceraceosorus guamensis	A0A316W0F1	A0A316VV78	A0A316VRV9	A0A316W190	A0A316VUJ2
Wallemia mellicola	I4Y9Q3	I4YFY1	I4YJP6	I4Y9V7	I4YBH7
Wallemia ichthyophaga	R9AEV7	R9AGT0	R9APA9	R9AET8	R9APM0
Phaffia rhodozyma	A0A0F7SHW1	A0A0F7SVW2	A0A0F7SP84	A0A0F7SSF4	A0A0F7SKB2
Cryptococcus neoformans	J9VVR5	J9VX48	J9VUF4	J9W032	J9VIH9
Tremella mesenterica	A0A4Q1BH80		A0A4V3XGD2	A0A4Q1BNF4	A0A4Q1BGL0
Trichosporon asahii var. asahi	J6F847		K1V4X0	J5QYW9_TRIAS	J5Q385J5Q385
Cutaneotrichosporon oleaginosum	A0A0J0XGB0	A0A0J1AZ27	A0A0J0XXS8	A0A0J0XXP2	
Calocera cornea	A0A165DW81	A0A165JZG9	A0A165E2H2	A0A165EZH0	A0A165K0V2
Dacryopinax primogenitus	M5GGA1	M5FWB8	M5G907	M5FU62	M5FTA8
Exidia glandulosa	A0A165DWU1	A0A165MZU9	A0A166A683	A0A165PST1	A0A166AL44
Serendipita vermifera	A0A0C3AUC8	A0A0C2X3K2	A0A0C3AAS2	A0A0C3BQ11	A0A0C3B760
Serendipita indica	G4T7Q3	G4TK10	G4T6G8	G4TA55	G4T7P5
Rhizoctonia solani	A0A0A1UIJ0	A0A0A1UL15	X8JES0	X8JP29	X8JNR1
Thanatephorus cucumeris	A0A0B7FAM2	M5BPV1	L8X3Q4	A0A0B7FPX8	M5BM11
Sistotremastrum niveocremeum	A0A164TYP6	A0A164VY18	A0A165ANC6	A0A164XPD0	A0A164ZY73
Sistotremastrum suecicum	A0A166AXS4	A0A166HZR3	A0A166C2K7	A0A166J8Y5	A0A166FDK2
Sphaerobolus stellatus	A0A286U9Z8	A0A485KMY1	A0A0C9U1F6	A0A0C9US15	A0A0C9VM41
Pyrrhoderma noxium	A0A286U9Z8	A0A286UJZ4	A0A286US23	S8EGZ5	A0A286U5B2
Schizopora paradoxa	A0A0H2R143	A0A0H2SPY1	A0A0H2SDE0	A0A0H2SF93	A0A0H2RHU5
Neolentinus lepideus	A0A165R4H4	A0A165SGM2	A0A165USL2	A0A165RIA0	A0A165RCK8
Gloeophyllum trabeum	S7PYT6	S7RPZ2	S7RVE0	S7S548	S7PWQ7
Ganoderma sinense	A0A2G8SNI0	A0A2G8RV54	A0A2G8S9M7	A0A2G8SB11	A0A2G8RTP7
Dichomitus squalens	R7SR18	R7STU8	A0A4Q9P353	A0A4Q9QBR2	A0A4Q9N0M6
Heterobasidion irregulare	W4KCG5	W4K0M3	W4KJR7	W4KQB8	W4K943
Bondarzewia mesenterica	A0A4S4LYW8	A0A4S4LU15	A0A4Q1BE91	A0A4S4M8S3	A0A4S4LQH2
Coprinopsis cinerea	A8P3A5	A8N991	A8NGL4	A8N175	A8NCV3
Galerina marginata	A0A067SEY7	A0A067TBQ6	A0A067TE53	A0A067TNQ6	A0A067TDJ0
Piloderma croceum	A0A0C3F6N5	A0A0C3C0T2	A0A0C3F891	A0A0C3G059	A0A0C3GJA8
Fibularhizoctonia sp.	A0A166JCB1	A0A166TEV3	A0A166NCZ1	A0A166AWE7	A0A166WL22
Pisolithus microcarpus	A0A0C9Y9U3	A0A0C9Y7U8	A0A0C9ZMN8	A0A0C9XUD8	A0A0C9Y9D7
Rhizopogon vesiculosus	A0A1J8QXK8	A0A1J8PU02	A0A1J8Q3B8	A0A1J8Q321	A0A1J8Q1K0
Jaapia argillacea	A0A067PD49	A0A067P6S1	A0A067PZT6	A0A067PUB3	A0A067Q3R2
Saccharomyces cerevisiae	P40568	P47149	Q12143	P53148	Q04431
Neurospora crassa	Q1K7T2	U9W5A0	Q7S5A3	Q7SFZ1	Q7SE89
Schizosaccharomyces pombe	Q9UUB5	Q09858	Q9P6M3	O59757	U3H042
Pneumocystis jirovecii	A0A0W4ZD36	L0P9V1	L0PGC1	L0PA06	A0A0W4ZL57
Saitoella complicata	A0A0E9NKP9	A0A0E9NSQ4	A0A0E9NAN2	A0A0E9NPH0	A0A0E9NSB0
Allomyces macrogynus	A0A0L0RWZ4	A0A0L0S6A1	A0A0L0RZ83	A0A0L0S3J4	A0A0L0S303
Encephalitozoon intestinalis				E0S8Q0	E0S616
Basidiobolus meristosporus	A0A1Y1XSZ3	A0A1Y1Z0A9	A0A1Y1Y167	A0A1Y1Z644	A0A1Y1XL41
Smittium culicis	A0A1R1YNI6		A0A1R1YR45	A0A1R1XUY3	A0A1R1XKH1
Spizellomyces punctatus	A0A0L0HN30	A0A0L0HKU3	A0A0L0HV19	A0A0L0HRB8	A0A0L0HV79
Batrachochytrium dendrobatidis	F4P8M5	F4P541	F4PAP7	A0A177WP16	F4NU44
Mucor circinelloides f. lusitanicus	A0A168PFG4				A0A168K1L8
Jimgerdemannia flammicorona	A0A433DFD3	A0A433A2T6		A0A433D481	
Rozella allomycis	A0A075AZR2	A0A075ARP0	A0A4P9YLE6	A0A075AYJ2	A0A4P9Y9Y2
Paramicrosporidium saccamoebae	A0A2H9TPG1		A0A2H9TQ63	A0A2H9TGG7	A0A2H9TPY3
Homo sapiens	Q5JW54	Q6P1K2	Q96IY1	Q8NG31	O95229
Drosophila melanogaster		Q7JZC9	Q9VYX4	Q9VPB2	

Organism	Spc24	Spc25	Nuf2	Ndc80
Mixia osmundae	G7E4T6	G7E0N5	G7DTI5	G7E2U9
Puccinia graminis f. sp. tritici	E3K761	A0A180GXK3	E3KK41	E3KAZ6
Melampsora larici-populina	F4R2Y1	F4S1R2	F4SE35	F4RKL3
Leucosporidium creatinivorum	A0A1Y2FZI5	A0A1Y2FZI5	A0A1Y2FZP1	A0A1Y2FW48
Microbotryum intermedium	A0A238F8M1	A0A238FHA8	A0A238FQ42	A0A238FF02
Microbotryum saponariae	A0A2X0MXN3	A0A2X0MBP8	A0A2X0LDQ4	A0A2X0L4R5
Rhodosporidium toruloides	M7X462	M7X5N5	M7WYS0	A0A0K3CC27
Ustilago maydis	A0A0D1CZS3	A0A0D1C3Q2	A0A0D1DVI0	A0A0D1CZX4
Pseudozyma hubeiensis	R9P5W4	R9NYU4	R9PEW9	R9PC57
Malassezia globosa	A8Q2U9	A8Q4C1	A8Q9N5	A8Q1A7
Malassezia sympodialis	M5E9A1	M5EB06	M5ECW4	A0A1M8ABU6
Tilletiopsis washingtonensis	A0A316ZL55	A0A316ZGH2	A0A316Z9K4	A0A316ZDV6
Meira miltonrushii	A0A316VLQ8	A0A316VJM1	A0A316VM49	A0A316V8N0
Acaromyces ingoldii	A0A316YWC4	A0A316YMT1	A0A316YPQ7	A0A316YR50
Tilletiaria anomala	A0A066V7D8	A0A066W8Y3	A0A066V592	A0A066WRE0
pseudomicrostroma glucosiphilum			A0A316U7J7	A0A316UE71
Jaminaea rosea	A0A316UQ14	A0A316UP49	A0A316UUR3	A0A316UVW3
Tilletia indica	A0A177TQM6	A0A177TLX0	A0A177TTQ5	A0A177TPZ5
Ceraceosorus guamensis	A0A316W4J9	A0A316VQ99	A0A316VMS6	A0A316W478
Wallemia mellicola	A0A2H3J7Y4	I4Y7I6	I4YCF2	I4YC13
Wallemia ichthyophaga	R9ABS2	A0A4T0G0P7	R9AFR0	R9AP10
Phaffia rhodozyma	A0A0F7SWU3	A0A0F7ST96	A0A0F7SPC7	A0A0F7SJL8
Cryptococcus neoformans	J9VGT1	J9VMC1	T2BQM3	J9VMS7
Tremella mesenterica	A0A4Q1BAZ6	A0A4Q1BSY5	A0A4Q1BUF8	
Trichosporon asahii var. asahi	K1WIL6	J4U7S0	J5TJS5	K1W9J7
Cutaneotrichosporon oleaginosum	A0A0J0XPB0	A0A0J0XSH4	A0A0J0XUX3	A0A0J0XFK1
Calocera cornea	A0A165ECZ9	A0A165GVM9	A0A165K5G1	A0A165IEH2
Dacryopinax primogenitus	M5GGL3	M5G5E6	M5GEV0	M5GAH8
Exidia glandulosa	A0A165GF84	A0A166BFU0	A0A165DME5	A0A165N4W2
Serendipita vermifera	A0A0C2WXQ5	A0A0C3BLN6	A0A0C3B9C4	A0A0C3BFH3
Serendipita indica	G4TR20	G4U2N9	G4TM46	G4TET1
Rhizoctonia solani	X8JW54	X8JNX3	A0A0A1UK11	A0A074SD24
Thanatephorus cucumeris	A0A0B7F7N1	A0A0B7FQR4	A0A0B7F5U0	M5BJI5
Sistotremastrum niveocremeum	A0A165AGF1	A0A164R4P1	A0A165AN31	A0A165AG99
Sistotremastrum suecicum	A0A166IWW4	A0A166HM21	A0A0C9TW85	A0A166IX45
Sphaerobolus stellatus	A0A0C9UM51	A0A0C9VDQ3	A0A0C9TW85	A0A0C9VZX4
Pyrrhoderma noxium	A0A286UXQ9	A0A286UA41	A0A286UCM8	A0A286UUF8
Schizopora paradoxa	A0A0H2S0Z8	A0A0H2RV79	A0A0H2RV59	A0A0H2R849
Neolentinus lepideus	A0A165UQN8	A0A165S685	A0A165VM34	A0A165RPU9
Gloeophyllum trabeum	S7QG87	S7QPC3	S7RIS1	S7QHI1
Ganoderma sinense	A0A2G8RQM8	A0A2G8S4Y6	A0A2G8RQB9	A0A2G8RQL9
Dichomitus squalens	A0A4Q9MW69	R7SSZ6	A0A4Q9QFZ7	A0A4Q9QEC3
Heterobasidion irregulare	W4KJK3	W4JZP6	W4KIF0	W4KJL1
Bondarzewia mesenterica	A0A4S4LQU7	A0A4Q1BSY5	A0A4S4LE82	
Coprinopsis cinerea	A8NHD3	A8N117	A8N2G7	A8NGW6
Galerina marginata	A0A067TS68	A0A067T0K3	A0A067TDV7	A0A067T0M4
Piloderma croceum	A0A0C3FM20	A0A0C3FRG2	A0A0C3CDB2	A0A0C3BU51
Fibularhizoctonia sp.	A0A166JHL9	A0A165X6Q4	A0A166SYK9	A0A166JGE7
Pisolithus microcarpus	A0A0C9Z0X4	A0A0C9Z8P8	A0A0C9YIM3	A0A0C9YQ03
Rhizopogon vesiculosus	A0A1J8Q1Z5	A0A1J8Q554	A0A1J8QIP5	A0A1J8QF65
Jaapia argillacea	A0A067PXN6	A0A067PJC7	A0A067Q316	A0A067PXW9
Saccharomyces cerevisiae	Q04477	P40014	P33895	P40460
Neurospora crassa	Q7S8M2	Q873B7	Q7S9H0	Q96U60
Schizosaccharomyces pombe	Q9UST6	Q10430	Q10173	Q10198
Pneumocystis jirovecii	L0PFA9	L0PFD6	L0PEI6	L0PBK8
Saitoella complicata	A0A0E9N888	A0A0E9NFF2	A0A0E9NAI0	A0A0E9ND58
Allomyces macrogynus			A0A0L0SDT4	A0A0L0SNR7
Encephalitozoon intestinalis		Q8SU30	E0S942	
Basidiobolus meristosporus	A0A1Y1XXT9	A0A1Y1Y094	A0A1Y1XMR3	A0A1Y1Y5U3
Smittium culicis	A0A1R1YG65		A0A1R1YTW3	A0A1R1XH11
Spizellomyces punctatus	A0A0L0HS79		A0A0L0HV03	A0A0L0HDG7
Batrachochytrium dendrobatidis	F4NZ95		F4PDC9	A0A177WR61
Mucor circinelloides f. lusitanicus	A0A168IDC1		A0A168GV79	A0A168IM48
Jimgerdemannia flammicorona	A0A433Q9I9		A0A433A0E5	
Rozella allomycis	A0A075AXU2		A0A4P9YEJ1	A0A075AWW8
Paramicrosporidium saccamoebae			A0A2H9TGI0	A0A2H9TLJ1
Homo sapiens	K7EJH0		B1AQT3	O14777
Drosophila melanogaster	Q9V3V7		Q9VM45	Q9VYB1

Appendix III-Kinetochore IP-MS

Alternate ID	Total spectrum count H99 untagged	Total spectrum count CENP-C^{Mif2}-3xFlag	Total spectrum count Dsn1-3xFlag	Total spectrum count Spc25-3xFlag
CNAG_02578	625	427	444	90
CNAG_07635	0	8	126	584
CNAG_00680	1	4	72	395
CNAG_02193	6	8	107	489
CNAG_03484	0	21	706	77
CNAG_07414	89	84	114	40
CNAG_00423	0	6	61	310
CNAG_06087	0	9	296	90
CNAG_06125	25	69	122	88
CNAG_01903	0	9	138	58
CNAG_04157	0	12	306	26
CNAG_05391	0	272	72	2
CNAG_01648	0	52	210	59
CNAG_04479	0	5	236	33
CNAG_06746	1	41	81	19
CNAG_01340	0	34	189	1
CNAG_01117	1	37	67	40
CNAG_00334	23	65	125	53
CNAG_06150	13	13	41	61
CNAG_01727	38	152	201	111
CNAG_06443	16	29	30	21
CNAG_04300	0	3	85	6
CNAG_06840	3	5	13	19
CNAG_03715	0	5	76	21
CNAG_02974	13	19	37	28
CNAG_06101	11	25	59	68
CNAG_02129	2	13	36	27
CNAG_05918	12	10	35	31
CNAG_01890	6	11	11	25
CNAG_01984	19	11	12	22
CNAG_06919	0	22	62	1
CNAG_05465	2	4	32	3
CNAG_01148	0	20	83	4
CNAG_00785	1	10	48	13
CNAG_06377	5	15	28	12
CNAG_05750	5	6	13	18
CNAG_06208	4	5	9	32
CNAG_05199	4	12	15	19
CNAG_03891	11	12	10	23
CNAG_00848	4	8	3	46
CNAG_00777	22	18	21	13
CNAG_05976	0	12	77	0
CNAG_07561	4	2	7	17
CNAG_04640	2	3	9	26
CNAG_03577	6	11	18	17
CNAG_00809	0	21	41	4
CNAG_03944	1	21	23	12
CNAG_04348	0	10	85	0
CNAG_05235	11	7	8	13
CNAG_00116	2	6	15	10
CNAG_03962	0	13	48	1
CNAG_06747	1	9	33	2
CNAG_01840	0	14	38	13
CNAG_04762	3	10	28	11
CNAG_03706	0	0	40	10
CNAG_06699	6	6	12	11
CNAG_06545	0	0	57	0
CNAG_05555	2	3	25	10
CNAG_05884	0	4	18	10
CNAG_03341	0	12	39	0
CNAG_03959	1	18	14	5
RPS0	2	12	20	13
CNAG_06475	22	16	12	20
CNAG_03072	5	1	2	14
RPS1	5	9	16	7
CNAG_02209	0	5	57	0
CNAG_07361	13	8	9	5
CNAG_04441	1	9	9	6
CNAG_01577	3	3	6	21
CNAG_04584	0	13	18	10
CNAG_01558	6	5	8	10
CNAG_01480	2	7	11	7
CNAG_04609	0	9	30	8
CNAG_00417	3	1	10	12
CNAG_02943	0	7	18	11
CNAG_01726	0	0	52	0
CNAG_01167	0	13	23	1
CNAG_03787	0	5	20	18
CNAG_06474	12	11	11	21
CNAG_04788	0	24	21	0
CNAG_00741	1	1	19	9
CNAG_00640	1	4	8	3
NIP1	0	1	3	2
CNAG_01976	2	9	8	9
CNAG_07445	0	1	7	12
CNAG_03225	6	3	4	11
CNAG_06626	0	3	46	0
CNAG_06770	5	1	5	13
CNAG_00483	6	9	14	9
CNAG_00099	0	8	28	1
CNAG_06182	0	10	29	0
CNAG_07347	0	4	12	11
CNAG_02437	0	1	41	0
CNAG_01750	29	122	154	90
CNAG_01224	1	3	14	3
CNAG_03053	2	1	5	10
CNAG_03780	2	5	6	13
CNAG_06683	0	1	44	0
CNAG_01638	5	2	4	0
CNAG_02545	7	5	8	8
CNAG_04726	0	5	12	9
CNAG_00083	0	0	30	0
CNAG_01641	0	4	25	0
CNAG_01144	1	16	22	2
CNAG_02051	0	9	26	0
CNAG_02134	0	13	24	4
CNAG_02936	0	0	7	1
CNAG_05070	1	6	7	4
CNAG_02234	0	1	17	3
CNAG_02331	0	3	8	5
CNAG_01334	0	7	31	0
CNAG_01990	2	2	7	5
CNAG_01264	1	9	11	12
CNAG_02928	0	1	14	7
CNAG_03767	0	13	24	0
CNAG_00305	1	9	13	5
CNAG_00649	1	3	6	15
CNAG_05825	0	3	24	2
CNAG_06113	4	0	2	10
CNAG_00672	0	3	5	8
CNAG_05725	3	4	7	6
CNAG_00091	4	1	0	12
CNAG_04304	0	7	16	4
CNAG_06118	0	2	6	0
CNAG_00656	0	2	14	4
CNAG_01573	0	0	2	0
CNAG_00779	0	4	7	9

CNAG_06745	0	8	52	6	CNAG_00260	1	4	4	2
CNAG_06447	0	0	8	7	CNAG_00930	0	0	2	5
CNAG_01896	5	0	0	8	CNAG_02948	0	2	11	4
CNAG_03000	3	2	1	7	CNAG_03358	1	1	0	3
CNAG_00034	0	2	5	4	CNAG_04365	0	0	24	0
CNAG_07362	0	2	32	0	CNAG_00065	4	1	3	7
CNAG_05179	2	3	8	8	CNAG_05556	2	4	5	3
CNAG_07676	2	6	23	0	CNAG_05699	0	0	4	0
CNAG_02144	0	3	12	3	CNAG_04698	0	4	5	4
CNAG_06535	0	4	20	0	CNAG_02263	0	6	9	6
CNAG_05904	1	8	4	7	CNAG_01145	0	4	14	0
CNAG_07494	0	6	18	0		0	0	16	0
CNAG_01991	2	4	1	7	CNAG_06646	1	3	4	5
CNAG_05762	1	6	8	6	CNAG_06754	0	7	10	0
TIF32	0	2	10	5	CNAG_04209	0	2	4	0
CNAG_03602	0	1	37	0	CNAG_07363	0	3	4	4
CNAG_03886	0	0	31	0	CNAG_06811	1	0	0	9
CNAG_03637	0	15	17	0	CNAG_05661	0	0	17	0
CNAG_00565	0	2	7	9	CNAG_01000	6	6	0	1
CNAG_05800	0	5	7	4	CNAG_00700	0	1	1	5
CNAG_03251	2	2	5	6	CNAG_04799	1	2	3	5
CNAG_01300	2	4	7	7	CNAG_02257	0	3	7	5
CNAG_04370	0	0	28	0	CNAG_03435	0	3	11	2
CNAG_02100	0	2	7	0	CNAG_03285	0	1	12	0
CNAG_00992	0	0	4	8	CNAG_01863	0	1	15	0
CNAG_04445	3	2	9	6	CNAG_02218	0	12	7	0
CNAG_00061	3	1	1	6	CNAG_03554	0	1	9	1
CNAG_04776	0	2	9	7	FRR1	2	2	4	3
CNAG_02982	0	1	27	0	CNAG_06847	1	0	2	4
CNAG_04851	0	2	8	4	CNAG_04052	0	4	14	0
MET3	0	0	7	7	CNAG_02457	0	4	9	2
CNAG_00232	2	2	5	7	CNAG_07630	0	3	14	0
CNAG_02182	2	2	4	5	CNAG_07979	0	3	10	0
CNAG_03283	0	2	7	6	CNAG_01428	0	0	0	2
CNAG_03722	3	4	8	9	CNAG_05753	1	2	7	3
CNAG_03322	1	1	6	6	CNAG_00678	0	5	8	1
CNAG_00063	0	7	11	2	CNAG_01170	1	1	6	4
TIF35	0	5	13	4	CNAG_04969	0	0	15	4
CNAG_07108	0	6	4	4	CNAG_03824	0	4	4	4
CNAG_06576	1	0	0	4	CNAG_06095	0	0	9	2
CNAG_00626	4	3	5	4	CNAG_02507	0	1	6	0
CNAG_02843	5	3	1	5	CNAG_07373	0	0	0	1
CNAG_04362	0	9	10	3	CNAG_00655	1	3	8	2
CNAG_05232	0	5	11	4	CNAG_01137	1	1	1	7
CNAG_01884	0	0	8	1	CNAG_03263	1	3	1	4
TIF34	0	3	12	5	CLU1	0	2	7	5
CNAG_01842	0	0	23	0	CNAG_03168	0	0	2	0
CNAG_00716	4	0	3	8	CNAG_05683	4	2	0	5
CNAG_03409	0	6	13	0	CNAG_03645	0	0	12	0
CNAG_04981	0	5	18	8	CNAG_02816	0	2	10	2
CNAG_00747	1	5	7	4	CNAG_01388	0	0	2	2
CNAG_00988	0	4	8	9	CNAG_03142	2	0	0	5
CNAG_02923	2	5	4	3	CNAG_07925	0	0	5	1
CNAG_02285	1	2	4	6	CNAG_01820	0	0	0	7
CNAG_02701	0	2	8	0	CNAG_06697	0	0	0	1
CNAG_04601	0	0	2	8	CNAG_06109	2	0	0	6
CNAG_02994	1	0	0	6	CNAG_06335	0	3	14	0
CNAG_07941	8	7	12	3	CNAG_06313	0	0	2	5
CNAG_04883	1	4	3	6	CNAG_02025	0	4	6	0
CNAG_07839	1	1	3	3	CNAG_03299	0	1	11	4
CNAG_04068	0	0	5	9	CNAG_06605	0	1	6	2
CNAG_02981	0	4	16	1	CNAG_06231	0	1	5	1
CNAG_06687	0	2	19	0	CNAG_02315	0	0	0	1
CNAG_03739	1	3	9	2	CNAG_00886	3	0	0	4
CNAG_03482	2	1	2	3	CNAG_01253	3	4	1	3
CNAG_04513	0	6	9	0	CNAG_05814	0	0	2	6
CNAG_05525	0	4	3	6	CNAG_04021	0	1	3	5
CNAG_01361	0	11	5	3	CNAG_01655	0	1	7	4
NAT10	0	1	14	0	CNAG_03725	0	1	1	4
CNAG_03892	3	1	1	3	CNAG_03596	0	0	0	5
CNAG_01153	0	4	4	4	CNAG_04803	0	0	5	8

CNAG_01023	0	2	14	0	CNAG_07982	0	4	10	0
CNAG_04708	0	2	14	0	CNAG_02166	0	0	9	0
CNAG_02761	0	0	0	2	CNAG_04770	0	1	9	0
CNAG_02458	0	1	5	2	CNAG_03057	0	0	10	0
CNAG_01628	2	1	1	2	CNAG_06361	0	0	1	1
CNAG_04895	1	6	1	7	CNAG_04904	0	0	1	6
CNAG_03124	0	0	17	0	CNAG_03771	0	4	10	0
CNAG_05437	2	0	0	2	CNAG_00960	0	3	8	0
CNAG_05218	0	2	3	6	CNAG_03627	4	4	1	6
CNAG_03813	0	3	3	1	CNAG_03658	1	1	1	0
CNAG_00641	0	2	12	0	CNAG_00072	0	2	1	5
CNAG_05932	0	0	4	3	CNAG_01291	0	3	2	2
CNAG_01182	0	4	4	2	CNAG_06563	0	4	3	1
CNAG_07746	1	2	1	4	CNAG_04487	3	3	2	1
CNAG_01102	2	1	2	3	CNAG_03510	0	0	1	5
CNAG_02485	1	0	4	4	CNAG_03790	0	2	4	0
CNAG_05101	0	0	17	0	CNAG_01780	0	1	8	0
CNAG_03507	0	0	2	5	CNAG_04220	0	4	9	0
CNAG_01390	0	0	0	1	CNAG_05752	0	1	9	0
CNAG_02673	0	0	0	5	ERB1	0	0	13	0
CNAG_07487	0	0	0	2	CNAG_05980	0	0	0	6
CNAG_03606	0	0	17	0	CNAG_01179	0	1	10	0
CNAG_03734	0	1	4	0	CNAG_01120	0	0	0	1
CNAG_02359	0	2	2	3	CNAG_01454	0	1	10	0
CNAG_02710	0	2	5	1	CNAG_01332	0	0	1	1
CNAG_02726	1	2	1	3	CNAG_01951	0	0	7	1
CNAG_06630	0	1	7	3	CNAG_05105	0	3	5	4
CNAG_05759	0	0	0	0	CNAG_00418	0	0	3	2
CNAG_06075	2	0	0	7	CNAG_03198	0	1	5	2
CNAG_01744	0	0	8	4	CNAG_02148	1	1	0	5
CNAG_04484	0	0	6	2	CNAG_01395	0	2	1	2
CNAG_03983	2	1	0	1	CNAG_01211	0	5	3	1
CNAG_03064	0	0	2	0	CNAG_06157	4	6	3	0
CNAG_05701	0	0	0	3	CNAG_04176	0	0	2	0
CNAG_01733	0	0	9	2	CCP1	1	0	0	1
CNAG_02330	0	0	3	4	CNAG_02714	0	1	0	1
COII	0	1	3	4	ADK1	0	0	0	3
CNAG_02435	0	1	8	0	CNAG_05269	0	1	7	0
CNAG_01740	0	2	3	2	CNAG_06370	0	0	3	2
CNAG_02801	2	2	1	1	CNAG_02326	0	3	6	3
CNAG_02754	1	1	1	1	CNAG_04906	0	5	5	0
CNAG_00509	0	2	8	2	CNAG_00448	0	2	5	0
CNAG_03621	5	3	1	8	CNAG_03040	0	0	0	5
CNAG_01563	0	0	18	0	CNAG_02421	1	3	1	4
CNAG_00812	0	1	11	0	CNAG_02099	0	0	0	1
CNAG_04637	0	0	0	3	CNAG_06112	0	0	1	3
CNAG_02091	0	0	0	0	PIM1	0	2	1	2
CNAG_02788	0	2	14	0	CNAG_08022	2	5	7	0
CNAG_01052	0	0	0	3	CNAG_01236	0	2	6	0
CNAG_06472	0	0	14	0	CNAG_00665	0	2	5	2
CNAG_01168	0	1	12	0	TPS2	0	1	2	5
CNAG_06748	0	1	11	0	CNAG_03904	0	2	9	1
CNAG_05844	1	4	3	1	CNAG_00681	0	2	5	0
CNAG_03303	2	3	3	3	CNAG_03655	0	0	7	0
CNAG_07558	1	1	1	2	CNAG_03458	0	1	3	0
HOG1	0	2	7	1	CNAG_04071	0	5	7	0
CNAG_04990	0	2	7	2	CNAG_00372	0	3	7	0
CNAG_01414	0	3	6	2	CNAG_06220	1	0	0	0
CNAG_05602	0	0	2	1	CNAG_03418	0	0	3	4
CNAG_05935	0	0	2	3	CNAG_05102	0	0	8	0
CNAG_02520	0	4	7	0	CNAG_00935	0	0	0	1
CNAG_00139	1	0	0	2	CNAG_06367	0	0	10	0
CNAG_01745	0	2	7	0	CNAG_03853	1	1	2	1
CNAG_00100	0	0	0	4	CNAG_00256	0	1	2	2
CNAG_01413	0	3	4	3	CNAG_00771	0	0	2	0
CNAG_02133	1	0	0	1	CNAG_00482	0	3	2	0
CNAG_01019	3	0	0	3	CNAG_04163	0	0	0	0
CNAG_00984	2	0	2	4	INT6	0	1	4	0
CNAG_02880	0	1	0	4	CNAG_02810	0	1	7	1
CNAG_07864	0	2	6	0	CNAG_00058	0	0	3	1
CNAG_07740	0	0	0	1	CNAG_05552	0	2	5	0

CNAG_04286	0	1	4	1	CNAG_01981	0	0	1	3
CNAG_04066	0	0	0	1	CNAG_04082	0	1	1	4
CNAG_07411	0	0	2	0	CNAG_07863	0	0	3	0
CNAG_00088	0	3	5	3	CNAG_03861	0	0	0	1
CNAG_01276	0	1	5	1	CNAG_00136	0	0	0	3
CNAG_01152	0	0	8	2	CNAG_04605	0	0	5	0
CNAG_06005	0	0	7	0	CNAG_03563	0	2	4	0
CNAG_01140	0	0	8	0	CNAG_01958	0	0	0	1
CNAG_07590	0	2	6	0	CNAG_03876	0	1	2	0
CNAG_03747	0	1	2	1	CNAG_04694	0	2	6	0
CNAG_03814	0	1	2	2	CNAG_01146	0	0	4	0
CNAG_07660	2	0	2	1	CNAG_04313	0	0	0	0
CNAG_07851	1	1	1	1	CNAG_05151	0	0	3	0
CNAG_00534	1	1	1	3	CNAG_04165	0	2	2	0
CNAG_06633	0	1	1	2	CNAG_02672	0	1	7	0
CNAG_04327	0	0	0	6	CNAG_01251	0	0	8	0
CNAG_03641	0	0	1	3	CNAG_03591	0	0	6	0
CNAG_07004	0	0	1	4	CNAG_04044	0	0	5	0
CNAG_00774	0	0	1	2	CNAG_05597	0	2	3	1
CNAG_04460	0	3	6	1	CNAG_03301	2	1	1	1
CNAG_04196	0	0	6	0	CNAG_06723	0	1	1	3
CNAG_06096	0	0	3	1	CNAG_03175	3	2	4	0
CNAG_03777	0	0	8	0	CNAG_01049	1	1	2	1
CNAG_04148	0	1	8	0	CNAG_00781	0	1	4	1
CNAG_01813	0	2	5	4	CNAG_03931	0	1	3	2
CNAG_01879	0	0	5	3	CNAG_00337	0	3	6	0
CNAG_02748	0	0	2	3	CNAG_03375	0	1	0	1
CNAG_02290	0	4	8	0	CNAG_07322	0	0	4	1
CNAG_02382	0	0	6	0	CNAG_01274	0	0	2	2
CNAG_00879	0	0	0	5	CNAG_00006	0	1	1	2
CNAG_00108	0	0	6	0	CNAG_02113	0	0	1	4
CNAG_04062	0	0	9	0	CNAG_02338	0	0	0	1
CNAG_02301	0	0	8	0	CNAG_06068	0	1	4	0
CNAG_01159	0	1	7	0	CNAG_07756	1	1	0	0
CNAG_05936	0	1	10	0	CNAG_07439	0	0	6	0
CNAG_03603	0	0	10	0	CNAG_01293	0	1	3	0
CNAG_06412	0	0	7	0	CNAG_05351	0	0	2	3
CNAG_03513	0	0	11	0	CNAG_03270	0	0	0	2
CNAG_01959	0	0	6	0	CNAG_04577	0	0	0	3
CNAG_05839	1	1	1	4	CNAG_01400	1	0	0	1
CNAG_02925	2	2	2	0	CNAG_06585	0	0	2	0
CNAG_05221	1	9	33	2	CNAG_00441	0	0	0	0
CNAG_00092	0	1	1	3	CNAG_05198	0	2	5	0
CNAG_02916	1	0	2	3	CNAG_06373	0	2	4	0
CNAG_05462	1	0	3	2	CNAG_04259	0	0	5	0
CNAG_03612	0	0	0	2	CNAG_06766	0	0	5	0
CNAG_04679	0	2	5	0	CNAG_03267	0	0	4	0
CNAG_01204	0	0	1	3	CNAG_01270	0	0	4	2
CNAG_02110	0	0	4	1	CNAG_02991	0	0	0	0
CNAG_03459	0	0	4	0	CNAG_04179	0	0	0	1
CNAG_00111	0	1	5	0	CNAG_07511	0	0	7	0
CNAG_06908	0	0	1	1	CNAG_00057	0	0	0	3
CNAG_03205	0	0	8	0	CNAG_06734	0	3	4	0
CNAG_04899	0	0	6	0	CNAG_06007	0	0	5	0
CNAG_01360	0	3	5	0	CNAG_00775	0	0	4	0
CNAG_03246	0	1	8	0	CNAG_01790	0	0	6	0
CNAG_01187	0	1	7	0	CNAG_04395	0	0	6	0
CNAG_05789	0	2	3	0	CNAG_05571	0	0	4	0
CNAG_02762	0	0	0	1	CNAG_06685	0	0	5	0
CNAG_02722	0	0	0	1	CNAG_05068	1	0	1	2
CNAG_05422	0	0	8	0	CNAG_07427	0	1	2	1
CNAG_04828	0	7	30	4	CNAG_07778	0	1	1	1
CNAG_01586	1	1	1	2	CNAG_05240	0	1	2	1
CNAG_06779	0	2	1	3	CNAG_01833	1	1	0	0
CNAG_04668	0	2	0	2	CNAG_04219	1	0	0	2
CNAG_06900	0	0	0	3	CNAG_03916	0	0	0	1
CNAG_02671	2	0	5	0	CNAG_06153	0	1	4	1
CNAG_04194	0	1	2	1	CNAG_01035	0	0	2	0
CNAG_06144	0	0	0	1	CNAG_02230	0	0	5	1
CNAG_03416	0	0	0	3	CNAG_06906	0	0	0	2
CNAG_03320	0	3	1	2	CNAG_06351	0	0	0	0

CNAG_05847	0	0	0	0	CNAG_04319	0	0	2	0
CNAG_04765	0	0	1	0	CNAG_03186	0	2	2	0
CNAG_06088	0	0	0	3	CNAG_06273	0	0	5	0
CNAG_01486	0	0	4	1	CNAG_01307	0	0	0	0
CNAG_06333	0	1	3	0	CNAG_01902	0	1	2	0
CNAG_00280	0	0	4	0	CNAG_03347	0	0	3	1
CNAG_01404	0	0	0	2	CNAG_02434	0	0	0	1
CNAG_04156	0	1	4	0	CNAG_04190	0	1	3	0
CNAG_03023	0	0	7	0	CNAG_03674	0	0	0	2
CNAG_05153	0	0	6	0	CNAG_06160	0	0	2	0
CNAG_03266	0	0	0	3	CNAG_05013	0	0	2	0
CNAG_00514	0	0	5	0	CNAG_06287	0	0	0	1
CNAG_05359	0	0	4	0	CNAG_03038	0	0	0	1
CNAG_04840	0	0	4	0	CNAG_07965	0	0	0	2
CNAG_03815	3	3	0	0	CNAG_07878	0	0	3	0
CNAG_01819	0	2	6	0	CNAG_04790	0	0	6	0
CNAG_01316	0	3	4	0	cyn1	0	0	0	0
CNAG_00450	0	0	0	1	CNAG_04709	0	1	4	0
CNAG_00705	0	0	5	0	CNAG_02404	0	0	0	0
CNAG_02502	0	0	7	0	CNAG_02035	0	0	0	0
CNAG_06126	0	0	5	0	CNAG_05308	0	0	1	0
CNAG_06170	1	0	1	1	CNAG_00055	0	0	2	0
CNAG_03566	1	1	0	1	CNAG_02890	0	0	5	0
CNAG_05688	1	1	1	2	CNAG_01132	0	0	6	0
CNAG_04934	0	1	3	1	CNAG_01751	1	2	1	1
CNAG_04028	0	0	2	2	CNAG_03298	0	0	1	1
CNAG_02736	0	0	2	1	CNAG_04985	0	0	0	2
CNAG_04678	0	2	3	1	CNAG_02500	1	0	0	0
CNAG_04973	0	0	3	1	CNAG_06288	0	1	2	0
CNAG_02367	0	0	2	1	CNAG_02917	0	0	3	0
CNAG_02760	1	3	0	0	CNAG_06421	1	0	0	0
CNAG_05909	1	0	1	1	CNAG_05031	0	0	1	3
CNAG_00894	0	0	0	1	CNAG_06849	0	0	1	2
CNAG_01101	0	1	2	0	CNAG_07552	0	0	2	0
CNAG_04666	0	0	5	0	CNAG_03007	0	0	0	2
CNAG_06001	0	0	2	1	CNAG_02901	0	1	2	0
CNAG_01005	1	0	0	1	CNAG_04687	0	0	2	0
CNAG_06716	0	1	2	0	CNAG_00326	0	0	0	1
CNAG_01446	1	0	0	3	CNAG_04175	0	1	3	0
CNAG_02350	0	2	4	0	CNAG_00622	0	0	0	1
CNAG_07719	0	0	5	1	CNAG_07374	0	0	4	0
NOP7	0	1	3	0	CNAG_03245	0	0	0	2
CNAG_04510	0	0	2	0	CNAG_08025	0	2	1	0
CNAG_00457	0	0	0	1	CNAG_02418	0	0	1	2
CNAG_00793	0	0	3	0	CNAG_04450	0	0	3	0
CNAG_02426	0	1	3	0	TRM82	0	1	3	0
CNAG_00176	0	0	0	1	CNAG_00019	0	0	0	2
CNAG_00990	0	0	0	3	CNAG_04499	0	0	0	0
CNAG_03584	0	0	3	0	CNAG_03961	0	0	2	0
CNAG_01189	0	0	3	0	CNAG_01650	0	1	3	0
CNAG_05475	0	0	3	0	CNAG_05497	0	0	0	1
CNAG_02918	0	0	0	1	CNAG_03058	0	0	0	1
CNAG_05409	0	1	6	0	CNAG_01355	0	2	2	0
CNAG_01564	0	1	7	0	CNAG_03098	0	0	0	0
CNAG_03677	0	0	0	1	CNAG_01309	0	0	1	0
CNAG_06260	0	0	2	0	CNAG_03486	0	0	0	0
CNAG_05650	0	0	3	0	CNAG_01952	0	1	2	0
CNAG_07593	0	0	6	0	CNAG_02858	1	0	0	0
CNAG_05398	0	0	0	0	CNAG_02232	0	1	3	0
CNAG_05521	0	0	0	0	CNAG_00636	0	1	4	0
CNAG_00706	0	0	6	0	CNAG_06798	0	0	6	0
CNAG_01438	0	0	7	0	CNAG_06864	0	0	0	0
CNAG_05134	0	0	1	2	CNAG_00606	0	0	4	0
CNAG_02267	0	1	2	0	CNAG_07957	0	0	3	0
CNAG_04378	0	0	1	1	CNAG_03389	0	0	4	0
CNAG_06106	0	2	2	1	CNAG_04802	0	0	4	0
CNAG_03447	0	2	2	0	CNAG_05623	0	0	0	0
CNAG_00703	0	0	0	3	CNAG_02020	0	0	2	0
CNAG_02492	0	2	1	0	CNAG_03724	0	0	3	0
CNAG_00046	0	2	2	0	CNAG_04048	0	0	5	0
CNAG_00533	0	1	4	1	CNAG_05131	0	0	3	0

CNAG_00764	0	0	5	0
CNAG_05642	0	0	3	0
CNAG_05069	0	1	1	2
CNAG_04817	0	0	1	1
CNAG_00062	0	1	2	0
CNAG_05596	0	0	1	1
CNAG_01198	0	2	1	1
CNAG_06279	0	1	1	1
CNAG_00067	0	1	2	2
CNAG_05434	0	0	2	1
CNAG_06453	0	0	0	1
CNAG_03809	0	1	4	0
CNAG_02817	0	0	1	3
CNAG_03457	0	0	0	2
CNAG_03319	0	1	2	0
CNAG_01376	0	1	2	0
CNAG_03316	0	0	0	0
CNAG_06980	0	0	4	0
CNAG_03106	0	2	2	0
CNAG_05907	0	0	0	2
CNAG_02150	2	0	1	0
CNAG_01799	0	0	0	0
CNAG_05788	0	0	0	0
VAD1	0	0	2	0
CNAG_06638	0	0	0	1
CNAG_01363	0	0	3	0
CNAG_00808	0	0	2	0
CNAG_06772	0	1	4	0
CNAG_01837	0	0	2	0
CNAG_06916	0	0	2	0
CNAG_05886	0	0	0	1
CNAG_04716	0	0	0	0
CNAG_01531	0	0	2	0
CNAG_03356	0	0	2	0
CNAG_01859	0	1	4	0
CNAG_03153	0	0	0	0
CNAG_04207	0	0	0	0
CNAG_01423	0	0	2	0
CNAG_07914	0	0	3	0
CNAG_07637	0	0	2	0
CNAG_05393	0	0	3	0
CNAG_05755	0	0	3	0
CNAG_04800	0	0	3	0
CNAG_00581	0	0	0	0
CNAG_01025	0	0	2	0
CNAG_00603	0	0	4	0
CNAG_00677	0	0	3	0
CNAG_00845	0	0	4	0
CNAG_03956	0	0	4	0
CNAG_00605	0	0	0	0
YTM1	0	0	2	0
URA5	0	0	0	1
CNAG_00829	0	0	0	1
CNAG_04002	0	1	2	0
CNAG_06764	0	0	1	1
CNAG_06327	0	0	3	0
CNAG_05228	0	1	2	0
CNAG_04284	0	0	0	2
CNAG_06141	0	0	0	0
CNAG_00707	0	0	0	2
CNAG_05638	0	0	0	1
CNAG_06767	0	0	0	1
CNAG_02891	1	0	0	0
CNAG_02751	0	0	1	0
CNAG_03317	0	0	3	0
CNAG_05689	0	0	2	0
CNAG_03297	0	0	3	0
CNAG_05787	0	0	2	0
CNAG_03826	0	0	2	0
CNAG_00142	0	0	2	0
CNAG_01271	0	0	3	0

CNAG_07720	0	0	0	0
CNAG_05979	0	0	2	0
CNAG_03920	0	0	0	0
CNAG_06905	0	0	0	0
CNAG_02686	0	0	2	0
CNAG_05530	0	0	0	0
CNAG_03332	0	0	3	0
CNAG_05349	0	0	2	0
CNAG_03672	0	0	2	0
CNAG_02378	0	0	2	0
CNAG_02240	0	0	2	0
CNAG_01284	0	0	2	0
CNAG_05473	0	0	2	0
NOG2	0	0	2	0
CNAG_04571	0	0	2	0
CNAG_01644	0	0	2	0
CNAG_06028	0	0	2	0
CNAG_07924	0	0	2	0
CNAG_00512	0	0	3	0
CNAG_03781	0	0	3	0
CNAG_06948	0	0	3	0
CNAG_03143	0	0	0	0
CNAG_01909	0	0	4	0
CNAG_06295	0	0	4	0
CNAG_00810	0	0	3	0
CNAG_00713	0	0	2	0
CNAG_03667	0	0	0	0
CNAG_07352	0	0	0	0
CNAG_05568	0	0	0	0
CNAG_01664	0	1	3	0
CNAG_00316	0	0	0	1
CNAG_02692	0	0	2	1
CNAG_02335	0	0	0	1
CNAG_02265	0	0	1	0
CNAG_04951	0	0	0	1
CNAG_06168	0	0	1	0
CNAG_05645	0	0	2	0
CNAG_00040	2	0	0	0
CNAG_07745	0	0	0	1
CNAG_07859	0	0	2	0
CNAG_04604	0	0	0	0
CNAG_02712	0	0	2	0
CNAG_00089	0	0	3	0
CNAG_05905	0	0	3	0
CNAG_03300	0	0	2	0
CNAG_01437	0	0	2	0
CNAG_05968	0	0	0	0
CNAG_03203	0	2	0	0
CNAG_00575	0	2	0	4
CNAG_01060	0	0	0	0
CNAG_00356	0	0	0	0
CNAG_02738	0	0	2	0
CNAG_07567	0	0	2	0
CNAG_03001	0	0	2	0
CNAG_02084	0	0	0	0
CNAG_05925	0	0	2	0
CNAG_06511	0	0	0	0
CNAG_06489	0	0	0	0
CNAG_00499	0	0	2	0
TIF6	0	0	2	0
CNAG_05339	0	0	0	0
CNAG_03941	0	0	2	0
CNAG_03705	0	0	0	0
CNAG_00770	0	0	2	0
CNAG_02903	0	0	0	0
CNAG_06102	0	0	0	25
CNAG_02489	0	0	1	0
CNAG_03427	0	0	0	0
CNAG_04514	0	1	0	0
CNAG_02511	0	0	0	0

Appendix IV-Bridgin repeat sequences

Start amino acid	*p*-value	Upstream	Consensus sequence	Downstream
2	1.21E-04	E	EEDEVQ	E
2	1.21E-04	E	EEDEVQ	E
2	1.21E-04	E	EEDEVQ	E
4	2.93E-04	DEY	EEYEVQ	
2	1.15E-03	E	EEEEVQ	E
2	1.15E-03	E	EEEEVQ	E
2	1.95E-03	E	EEKEVD	L
2	2.14E-03	E	EEKESD	D
2	8.67E-03	E	EKEERN	P
3	1.20E-02	TE	EEEEYL	
1	4.36E-02		EEEEEQ	KE
1	4.93E-02		EEEGVE	EL
2	6.16E-02	E	VEEERK	P

Appendix V- Bridgin IP-MS

Alternate ID	FLAG_ Control 150mM	FLAG_ Control 300mM	Bgi1^{FL} 150mM	Bgi1^{FL} 300mM	Bgi1$^{BD\Delta}$ 150mM
CNAG_02578	548	776	708	493	784
CNAG_01903	17	0	1034	1285	128
CNAG_07414	216	193	163	140	113
CNAG_00334	39	52	203	265	83
CNAG_04227	4	0	10	3	0
CNAG_06125	16	31	62	73	46
CNAG_01648	2	13	157	109	20
CNAG_03357	0	0	0	0	0
CNAG_01727	46	33	223	272	76
CNAG_06545	0	0	123	72	0
CNAG_01117	1	17	41	48	15
CNAG_00099	0	0	149	68	0
CNAG_02974	15	32	51	39	27
CNAG_06182	0	0	137	52	0
CNAG_05825	0	0	130	44	0
CNAG_01340	0	0	119	64	0
CNAG_03891	25	39	43	40	20
CNAG_06443	12	10	60	80	17
CNAG_01148	0	0	128	52	0
CNAG_06599	0	0	0	0	0
CNAG_02129	3	18	26	25	0
CNAG_06746	0	4	65	49	7
CNAG_03944	0	0	48	38	10
CNAG_06101	13	38	48	42	22
CNAG_03962	0	0	83	36	0
CNAG_03341	0	0	110	37	0
CNAG_05199	16	8	39	53	12
CNAG_01144	0	0	73	56	0
CNAG_01000	13	14	20	12	39
CNAG_07373	0	0	6	2	90
CNAG_07552	0	0	119	3	0
CNAG_04052	0	0	97	27	0
CNAG_06087	0	0	41	27	38
CNAG_06400	1	5	21	28	2
CNAG_06474	13	19	8	19	15
CNAG_00640	0	3	20	29	5
CNAG_03554	0	0	29	9	2
CNAG_02257	0	2	58	27	1
CNAG_00785	1	10	20	20	11
CNAG_00116	4	8	25	34	4
CNAG_06377	4	5	27	34	6
CNAG_03482	8	15	9	11	13
RPS0	7	5	19	25	7
CNAG_05555	0	2	26	32	4
CNAG_02943	0	0	5	80	0
CNAG_06150	2	1	25	26	1
CNAG_00034	1	3	18	25	5
CNAG_06208	0	3	32	45	1
CNAG_03577	0	5	24	26	4
CNAG_00483	6	3	15	18	2
CNAG_04609	0	0	20	23	0
CNAG_01325	0	0	0	0	0
CNAG_01224	0	5	25	28	5
CNAG_06840	2	6	20	21	0
CNAG_00656	0	6	18	20	6
CNAG_04762	1	3	22	35	1
RPS1	1	7	19	23	2
CNAG_07361	14	18	10	7	5
CNAG_04445	4	8	20	26	3
CNAG_01480	5	6	19	14	6
CNAG_01430	0	0	0	0	0
CNAG_02234	0	2	16	14	4
CNAG_03959	2	4	20	20	2
CNAG_02331	0	2	16	24	0
CNAG_06683	0	0	54	10	0
CNAG_04640	0	1	26	18	3
CNAG_03706	0	0	32	43	12
CNAG_01152	0	4	22	27	2
CNAG_07347	0	0	19	13	1
CNAG_01167	0	0	45	16	0
CNAG_04726	1	4	16	19	4
CNAG_03299	0	3	15	13	0
CNAG_03771	0	0	32	32	0
CNAG_06095	0	6	17	26	2
CNAG_01990	3	3	22	18	2
CNAG_06447	3	5	19	18	4
CNAG_05235	4	6	14	17	5
CNAG_05918	0	5	22	17	0
CNAG_04904	1	3	10	2	6
CNAG_03484	0	0	24	22	10
CNAG_01170	0	5	21	20	2
CNAG_01840	1	4	15	17	8
CNAG_04883	0	6	13	18	3
CNAG_06747	2	2	24	26	2
CNAG_02928	2	0	17	28	0
CNAG_05884	0	1	12	16	0
CNAG_05232	0	1	17	16	4
CNAG_03053	3	3	15	17	2
CNAG_04021	0	3	11	12	5
CNAG_03767	0	0	40	12	0
CNAG_03787	1	5	11	15	2
CNAG_04441	0	0	22	37	0
CNAG_01884	0	0	17	23	0
CNAG_04028	0	0	25	36	0
CNAG_03637	0	0	39	17	0
CNAG_01153	1	6	15	17	3
CNAG_02193	0	0	17	28	7
CNAG_01655	0	0	10	11	1
CNAG_04220	0	0	33	14	0
CNAG_00809	1	0	14	13	1
CNAG_05465	1	7	11	11	1
CNAG_06231	0	3	11	12	0
CNAG_07941	4	11	4	4	5
CNAG_02144	0	3	16	12	1
CNAG_03780	3	3	8	11	3
CNAG_05762	4	4	18	16	1
CNAG_00988	1	4	16	4	0
CNAG_05759	0	0	19	6	0
CNAG_00680	0	0	18	16	17
CNAG_03198	0	6	11	15	3
CNAG_00741	0	5	10	11	3
TIF32	0	0	5	12	2
CNAG_04157	0	0	13	24	5
CNAG_01726	0	0	47	0	0
CNAG_05525	0	2	12	12	1
CNAG_05131	0	0	22	12	1
CNAG_00812	0	0	30	18	0
CNAG_02134	0	0	26	8	0
CNAG_00672	0	0	10	14	4
CNAG_03747	0	5	9	13	1
CNAG_04068	1	1	13	14	0
CNAG_03000	2	3	12	11	2
CNAG_00423	0	0	11	22	5
CNAG_03283	0	5	7	15	4
CNAG_05753	2	2	13	7	2
CNAG_07839	2	2	8	8	3
CNAG_01991	0	1	4	1	1
CNAG_07676	0	3	9	12	6
CNAG_04799	2	2	7	9	3
CNAG_02437	0	0	28	3	0

CNAG_02166	0	0	12	1	0	CNAG_01091	0	1	11	11	1
CNAG_01638	6	6	6	1	7	CNAG_00055	0	0	13	8	0
CNAG_01976	2	3	5	14	3	CNAG_01235	0	0	10	1	0
CNAG_02100	0	0	6	2	0	CNAG_03251	0	0	6	5	2
CNAG_05070	0	0	12	2	0	CNAG_01951	0	1	4	10	1
CNAG_04479	0	0	14	17	5	CNAG_00377	2	0	13	0	0
CNAG_02115	0	0	36	2	1	CNAG_03824	0	3	6	11	1
CNAG_03853	3	5	8	10	6	CNAG_04934	0	1	6	7	2
CNAG_03739	0	1	8	11	2	CNAG_02359	0	1	4	7	1
CNAG_04584	0	0	14	10	1	CNAG_00626	1	1	8	9	0
CNAG_05750	0	3	13	9	1	TIF34	0	0	9	7	0
CNAG_00779	0	3	7	12	0	CNAG_05689	0	0	6	13	0
CNAG_05976	0	0	15	19	0	CNAG_07979	0	0	10	7	0
CNAG_06605	0	0	11	14	0	CNAG_02710	0	0	9	8	0
CNAG_05814	1	3	4	10	3	CNAG_02754	0	2	8	7	1
CNAG_05552	0	0	31	1	0	CNAG_05353	0	0	14	0	0
CNAG_01316	0	0	21	18	0	CNAG_00705	0	0	17	3	1
CNAG_02330	0	2	8	12	2	CNAG_06273	0	0	9	9	0
CNAG_04448	0	1	11	17	0	CNAG_02426	0	0	9	10	0
CNAG_01733	0	0	14	18	0	CNAG_07914	0	0	3	12	0
CNAG_04851	0	0	14	4	0	CNAG_02671	0	0	4	12	0
CNAG_02376	0	0	25	4	0	CNAG_01750	32	24	165	201	61
CNAG_03715	0	0	14	19	1	CNAG_05343	1	1	1	2	0
CNAG_07635	0	0	15	10	7	CNAG_07660	6	1	3	2	1
CNAG_01486	0	0	11	12	0	NAT10	0	0	6	4	0
NIP1	0	0	1	3	0	CNAG_02936	0	0	3	0	0
CNAG_01332	0	0	7	10	0	CNAG_01414	0	0	8	6	1
CNAG_04168	0	0	26	4	0	CNAG_00260	0	0	10	3	3
CNAG_06811	1	2	7	9	3	CNAG_00770	0	0	16	1	0
CNAG_06745	0	3	31	28	0	CNAG_01182	0	0	5	6	0
CNAG_07362	0	0	27	2	0	CNAG_01053	0	0	20	0	0
CNAG_00232	0	1	5	9	1	CNAG_03602	0	0	11	9	0
CNAG_00280	0	0	12	13	0	CNAG_01628	2	2	2	2	2
CNAG_00655	1	3	11	11	0	CNAG_00771	0	1	5	7	1
CNAG_01274	0	0	4	5	0	CNAG_04698	0	0	8	2	3
CNAG_04513	0	0	19	0	0	CNAG_03835	0	0	0	0	0
CNAG_06585	0	0	19	2	0	CNAG_00703	0	2	3	4	1
CNAG_01641	0	0	19	1	0	CNAG_03658	0	0	4	0	13
CNAG_07004	1	6	8	6	3	CNAG_04074	0	0	7	2	0
CNAG_06096	0	3	4	4	1	CNAG_07032	2	5	3	5	4
CNAG_01413	0	2	8	6	3	CNAG_07925	0	0	4	0	0
CNAG_04969	0	4	4	8	5	CNAG_01870	0	0	5	2	0
CNAG_02982	0	0	16	3	0	CNAG_04990	0	0	7	10	1
CNAG_03347	0	0	10	5	0	CNAG_01025	0	0	16	7	0
CNAG_03510	0	2	6	6	0	CNAG_01189	0	0	4	0	0
CNAG_06475	6	9	3	9	5	CNAG_01187	0	0	9	10	0
CNAG_06118	1	1	8	4	0	CNAG_05172	0	0	14	0	0
CNAG_02981	0	0	25	0	0	CNAG_02237	0	7	4	1	4
CNAG_06633	2	3	8	7	1	CNAG_00147	0	0	6	2	0
CNAG_00417	0	0	12	8	0	CNAG_04864	0	0	18	0	0
CNAG_02948	0	0	6	7	0	INT6	0	0	6	6	0
CNAG_00108	0	0	19	5	0	CNAG_03418	0	0	4	5	0
CNAG_00774	0	6	8	6	4	CNAG_07494	0	0	9	5	0
CNAG_06600	0	0	12	4	0	CNAG_04776	0	0	7	7	0
CNAG_07756	1	0	5	0	5	CNAG_02091	0	0	8	5	0
CNAG_06919	0	1	8	13	0	CNAG_01819	0	0	9	13	0
CNAG_04304	0	0	7	4	0	CNAG_06646	1	3	3	4	2
CNAG_05102	0	0	26	0	0	CNAG_02701	0	0	0	2	0
CNAG_06699	1	2	4	4	2	CNAG_03814	0	0	9	8	1
CNAG_00104	0	0	2	5	0	CNAG_06222	0	0	1	6	0
CNAG_05904	1	1	4	11	2	CNAG_06611	0	0	3	2	0
CNAG_05899	0	0	8	5	0	CNAG_00088	0	1	7	8	0
CNAG_00305	1	0	5	5	3	CNAG_07346	0	0	7	9	0
CNAG_05309	0	0	1	24	0	CNAG_00327	0	0	0	0	0
CNAG_05556	0	3	5	7	0	CNAG_03876	0	0	8	6	0
CNAG_03459	0	0	6	7	0	CNAG_04300	0	0	3	7	2
CNAG_05936	0	0	16	0	0	CNAG_05179	0	0	4	10	0
CNAG_00441	3	6	2	2	6	CNAG_02382	0	0	10	9	0
CNAG_03168	0	0	8	3	1	CNAG_00482	1	0	6	5	3
TIF35	0	0	8	10	0	CNAG_01881	3	2	3	6	2
CNAG_00083	0	0	18	0	0	CNAG_02458	0	0	1	1	0

CNAG_04948	0	1	8	8	2	CNAG_00121	0	0	2	9	0
CNAG_06535	0	0	6	6	2	CNAG_00775	0	0	1	3	0
CNAG_03603	0	0	5	9	0	CNAG_02890	0	0	0	5	0
CNAG_06769	0	0	15	0	0	CNAG_04071	0	0	5	6	1
CNAG_05661	0	0	13	0	0	CNAG_01365	0	0	6	0	0
CNAG_03458	0	0	12	4	0	CNAG_02263	0	0	3	2	0
CNAG_07573	0	0	12	0	0	CNAG_00666	0	0	10	0	0
COII	0	0	5	8	0	CNAG_00111	0	0	5	2	0
CNAG_05800	0	2	3	6	1	CNAG_00058	0	0	6	4	0
CNAG_02457	0	0	3	4	0	CNAG_01780	0	0	2	5	0
CNAG_02545	0	2	5	6	1	CNAG_07487	0	0	8	3	0
CNAG_00565	0	0	5	3	0	CNAG_04149	0	0	12	0	0
CNAG_07863	0	0	5	3	1	CNAG_07630	0	0	7	2	0
CNAG_01650	0	0	4	13	0	CNAG_02378	0	0	8	5	0
CNAG_01361	0	0	9	7	0	CNAG_03106	0	0	4	9	0
CNAG_04131	0	0	0	0	0	CNAG_04828	0	3	26	18	0
CNAG_00641	0	0	17	0	0	CNAG_02585	0	1	3	3	1
CNAG_01790	0	0	7	11	0	CNAG_00681	1	1	3	1	0
CNAG_00821	0	1	3	6	1	CNAG_06847	2	1	3	0	2
CNAG_03645	0	0	6	4	0	CNAG_02788	0	0	7	6	0
CNAG_07427	0	2	3	2	2	CNAG_00788	0	0	1	7	0
CNAG_05221	2	2	12	13	2	CNAG_02033	0	0	5	4	0
CNAG_03766	0	0	4	4	0	CNAG_01211	0	0	4	2	0
CNAG_04050	0	1	3	7	1	CNAG_04840	0	0	5	7	0
CNAG_04954	0	0	7	2	0	CNAG_07409	0	0	7	0	0
CNAG_02917	0	4	1	5	0	CNAG_02842	0	0	4	7	0
CNAG_01300	1	1	9	0	2	CNAG_05101	0	0	8	0	0
CNAG_01291	0	1	9	3	0	CNAG_03271	0	0	2	7	0
CNAG_04676	0	0	3	1	0	CNAG_04770	0	0	7	5	0
CNAG_01018	0	0	7	5	0	CNAG_01736	0	0	0	0	0
CNAG_00447	0	0	8	5	0	CNAG_00747	0	1	1	3	0
CNAG_05475	0	0	4	5	0	CNAG_07558	0	0	2	2	0
CNAG_01168	0	0	4	6	0	CNAG_05592	0	0	1	1	0
CNAG_06113	0	0	10	9	0	CNAG_03722	0	0	6	3	0
CNAG_02695	0	0	15	0	0	CNAG_01837	0	0	0	0	0
CNAG_03303	1	1	4	0	2	CNAG_01360	1	0	0	0	1
CLF1	0	0	2	6	0	ADK1	0	0	4	2	1
CNAG_07511	0	0	5	5	0	CNAG_00661	0	0	7	0	0
CNAG_06199	0	0	8	2	0	CNAG_01863	0	0	9	0	0
CNAG_03285	0	0	7	4	0	CNAG_02400	0	0	5	4	1
CNAG_03813	0	0	8	4	0	CNAG_04365	0	0	7	0	0
CNAG_04434	0	0	0	0	0	CNAG_06696	0	0	1	6	0
CNAG_06716	0	0	7	9	0	CNAG_03226	0	1	0	0	0
CNAG_03655	0	0	6	0	0	CNAG_02110	0	0	0	1	0
CNAG_02421	0	1	5	6	0	CNAG_04398	0	0	10	0	0
CNAG_03839	0	1	1	0	4	CNAG_05980	0	0	5	5	0
CNAG_07318	0	0	2	0	0	CNAG_00372	0	0	9	0	0
CNAG_04460	0	0	6	3	0	CNAG_01437	0	0	6	6	0
CNAG_03355	0	0	2	0	0	CNAG_06412	0	0	7	3	0
CNAG_01586	0	0	5	4	0	CNAG_00819	0	1	4	2	3
CNAG_01988	0	0	0	0	0	CNAG_01428	1	1	2	7	0
CNAG_02686	0	0	0	3	0	CNAG_01761	0	1	3	6	0
CNAG_05258	0	0	2	5	0	CNAG_04605	0	1	4	1	0
CNAG_01173	0	3	0	0	6	CNAG_06453	0	0	6	3	1
CNAG_06315	0	0	3	11	0	CNAG_06384	0	1	1	0	4
CNAG_04709	0	0	5	6	0	CNAG_05105	0	0	2	2	0
CNAG_01916	0	0	13	0	0	CNAG_06112	0	0	3	4	0
CNAG_02736	1	0	3	4	0	CNAG_04985	0	0	2	5	2
CNAG_00509	0	0	5	5	0	CNAG_06153	0	0	2	2	0
CNAG_04011	0	1	1	6	0	CNAG_05590	0	0	1	0	0
CNAG_03249	0	0	7	3	0	CNAG_03886	0	0	5	1	0
CNAG_02301	0	0	9	5	0	ERB1	0	0	6	4	0
CNAG_04180	0	0	6	9	0	CNAG_01564	0	0	4	1	0
TIF6	0	0	6	6	0	HOG1	0	0	2	4	0
CNAG_06908	3	6	3	2	0	CNAG_00960	0	0	3	0	0
FKS1	0	0	0	0	0	CNAG_04170	0	0	9	0	0
CNAG_05059	1	3	2	2	1	CNAG_07439	0	0	4	3	0
CNAG_03435	0	2	4	3	2	CNAG_02316	0	0	0	8	0
CNAG_00992	0	2	1	4	0	CNAG_03513	0	0	7	0	0
CNAG_02816	0	0	0	0	0	CNAG_03183	0	0	11	0	0
CNAG_05650	0	0	2	2	1	CNAG_04765	0	0	3	3	0

CNAG_01568	0	0	4	1	0	CNAG_03861	0	0	4	4	0
CNAG_00793	1	0	2	0	0	CNAG_02367	0	0	3	2	0
CNAG_04002	0	0	6	3	0	CNAG_01035	0	0	5	3	1
CNAG_03345	0	0	4	1	0	CNAG_04048	0	0	4	1	0
CNAG_05696	0	0	3	2	0	TPS2	0	0	2	2	0
CNAG_01664	0	0	6	3	0	CNAG_01636	0	0	1	3	0
CNAG_04678	0	0	1	3	0	CNAG_06779	0	0	4	5	0
CNAG_01402	0	0	3	3	0	CNAG_00006	0	0	3	3	0
CNAG_02761	0	0	5	2	0	CNAG_04683	0	0	1	4	0
CNAG_01023	0	0	11	1	0	CNAG_04221	0	0	0	0	0
CNAG_04973	0	0	1	1	0	CNAG_00063	0	0	5	4	0
CNAG_00560	0	0	2	2	0	CNAG_01744	0	0	5	4	0
CNAG_01709	0	0	7	2	0	CNAG_01789	0	0	5	5	0
CNAG_04976	0	0	5	1	0	CNAG_00708	0	0	2	8	0
CNAG_03507	0	0	0	0	0	CNAG_02082	0	0	0	0	0
CNAG_07522	0	3	0	0	1	CNAG_01271	0	0	1	6	0
CNAG_03246	0	0	3	3	0	CNAG_02520	0	0	5	0	0
CNAG_07720	0	0	2	1	0	CNAG_06687	0	0	0	0	0
CNAG_00072	0	0	5	3	0	CNAG_03675	0	0	4	0	0
CNAG_00018	0	0	6	2	0	CNAG_06949	0	0	4	0	0
CNAG_01264	0	0	2	3	0	CNAG_04728	0	0	7	0	0
CNAG_04958	0	0	3	5	0	CNAG_02022	0	0	3	1	1
CNAG_03724	0	0	7	1	0	CNAG_03416	0	1	1	2	0
CNAG_07864	0	0	6	5	0	CNAG_04194	0	0	4	2	1
CNAG_04694	0	0	2	4	0	CNAG_01236	0	0	1	3	0
CNAG_03064	0	0	5	2	0	CNAG_01557	0	0	2	5	0
CNAG_05690	0	0	7	0	0	CNAG_02923	0	0	0	4	0
CNAG_07735	0	0	8	0	0	PTP2	0	0	1	0	0
CNAG_06220	0	0	0	9	0	CNAG_06279	0	0	0	2	0
CNAG_06723	1	1	1	4	1	CNAG_02507	0	0	1	1	0
CNAG_05068	1	3	1	2	0	CNAG_04402	0	0	3	2	0
CNAG_07851	0	0	1	2	0	CNAG_05256	0	0	3	2	0
CNAG_02051	0	0	3	1	0	CNAG_03789	0	0	3	3	0
CNAG_02880	0	0	3	3	0	CNAG_03124	0	0	4	3	0
CNAG_01984	0	0	1	2	0	CNAG_01961	0	0	4	3	0
CNAG_04803	0	0	1	0	0	CNAG_03563	0	0	0	0	0
CNAG_03931	0	0	4	2	0	CNAG_00829	0	0	1	0	0
CNAG_04327	0	0	3	1	0	CNAG_00062	0	0	0	5	0
CNAG_04370	0	0	3	0	0	CNAG_01549	0	0	4	2	0
CNAG_07363	0	0	2	2	0	CNAG_01270	0	0	4	4	0
CNAG_06689	0	0	3	1	0	CNAG_05091	0	0	1	4	0
CNAG_06630	0	0	4	1	0	CNAG_04484	0	0	0	0	0
CNAG_00046	0	0	3	2	0	CNAG_05926	0	0	1	6	0
CNAG_01136	0	0	2	4	1	CNAG_04528	0	0	0	0	0
CNAG_01132	0	0	5	2	0	CNAG_01875	0	0	0	0	0
CNAG_06370	0	0	4	2	0	CNAG_01897	0	0	7	0	0
CNAG_00534	0	0	4	4	0	CNAG_02403	0	2	1	2	1
CNAG_03127	0	0	5	5	0	CNAG_08022	0	0	4	1	1
CNAG_01179	0	0	5	0	0	CNAG_05222	1	0	2	3	0
CNAG_06563	0	0	6	4	0	CNAG_05422	0	0	3	0	0
CNAG_02002	0	0	2	4	0	CNAG_01833	0	0	3	1	0
CNAG_00603	0	0	6	2	0	CNAG_03805	0	0	2	3	0
CNAG_00722	0	0	4	4	0	CNAG_04957	0	0	3	2	2
NOP7	0	0	2	2	0	CLU1	0	0	0	0	0
CNAG_01850	0	0	0	0	0	CNAG_03584	0	0	3	4	0
CNAG_02340	0	0	4	3	0	CNAG_04444	0	0	2	1	0
CNAG_04286	0	0	7	3	0	CNAG_04977	0	0	3	2	0
CNAG_00808	0	0	5	2	0	CNAG_01137	0	0	0	0	0
CNAG_05655	0	0	7	0	0	YTM1	0	0	2	2	0
CNAG_02922	0	0	2	0	0	CNAG_07719	0	0	3	2	0
CNAG_07464	0	0	7	0	0	CNAG_06335	0	0	0	1	0
CNAG_03862	0	1	2	2	1	CNAG_03409	0	0	3	0	0
CNAG_02817	0	3	1	4	0	CNAG_04334	0	0	1	2	0
CNAG_04668	0	0	1	1	0	CNAG_05518	0	0	0	0	0
CNAG_05218	0	0	3	2	0	CNAG_05455	0	0	3	1	0
CNAG_07590	0	0	4	0	0	CNAG_05694	0	0	2	3	0
CNAG_03753	0	0	2	3	0	CNAG_02209	0	0	2	3	0
CNAG_04321	0	0	1	0	0	CNAG_03665	0	0	0	1	0
CNAG_06175	0	0	2	1	0	CNAG_06333	0	0	2	0	0
CNAG_02785	0	0	1	0	0	CNAG_04802	0	0	4	1	0
CNAG_00464	0	0	3	2	0	CNAG_03048	0	0	1	2	0

CNAG_05635	0	0	1	2	0	CNAG_03961	0	0	2	4	0
CNAG_01146	0	0	3	0	0	CNAG_02485	0	0	3	1	0
CNAG_04292	0	0	0	4	0	CNAG_03730	0	0	2	1	0
CNAG_02725	0	0	3	3	0	CNAG_03917	0	0	4	0	0
CNAG_06351	0	0	3	4	0	CNAG_05905	0	0	2	0	0
CNAG_04072	0	0	4	1	0	CNAG_01438	0	0	3	0	0
CNAG_07469	0	0	6	0	0	CNAG_06283	0	0	2	0	0
CNAG_05757	0	0	2	0	0	CNAG_03666	0	0	3	0	0
CNAG_07967	0	0	6	0	0	CNAG_03325	0	0	0	0	0
CNAG_03297	0	0	6	0	0	CNAG_03375	0	0	0	0	0
URE1	0	0	0	0	0	CNAG_02034	0	0	5	0	0
CNAG_01198	0	0	5	0	0	CNAG_04279	0	0	4	0	0
CNAG_01563	0	0	8	0	0	CNAG_07509	0	0	4	0	0
CNAG_05876	0	0	0	0	0	CNAG_04062	0	0	3	0	0
CNAG_03627	1	1	2	2	0	CNAG_02714	0	0	0	3	0
CNAG_02113	0	0	2	2	0	CNAG_03904	0	0	2	3	1
CNAG_01470	0	2	0	1	0	CNAG_00713	0	0	2	0	0
CNAG_01010	0	0	1	2	0	CNAG_05069	0	2	1	0	0
CNAG_00292	0	0	2	2	0	CNAG_04716	0	0	3	1	0
CNAG_00678	0	0	2	3	0	CNAG_04823	0	0	2	2	0
CNAG_05391	0	0	5	0	0	CNAG_01307	0	0	2	1	0
CNAG_01190	0	0	2	1	0	CNAG_02916	0	0	2	1	0
CNAG_04383	0	0	1	2	0	CNAG_03225	0	0	1	2	0
CNAG_02291	0	0	0	0	0	CNAG_00512	0	0	0	2	0
CNAG_01355	0	0	3	2	0	CNAG_03186	0	0	3	1	0
CNAG_01813	0	0	1	3	0	CNAG_05613	0	0	0	0	3
CNAG_08025	0	0	0	3	0	CCP1	0	0	1	2	0
CNAG_00337	0	0	1	1	0	CNAG_03260	0	0	0	3	0
CNAG_06456	0	0	2	1	0	CNAG_02239	0	0	2	1	0
CNAG_01204	0	0	4	2	0	CNAG_04687	0	0	2	0	0
CNAG_06626	0	0	2	3	0	CNAG_04259	0	0	3	2	0
CNAG_01679	0	0	1	2	0	CNAG_02726	0	0	2	2	0
CNAG_02145	0	0	2	2	0	CNAG_03721	0	0	1	2	0
CNAG_00271	0	0	5	1	0	CNAG_06078	0	1	0	0	2
CNAG_04165	0	0	4	0	0	CNAG_01696	0	0	4	1	0
CNAG_02208	0	0	0	0	0	CNAG_01345	0	0	2	3	0
CNAG_07561	0	0	1	4	0	CNAG_04510	0	0	6	0	0
CNAG_03315	0	0	3	3	0	CNAG_07669	0	0	3	0	0
CNAG_03439	0	0	3	3	0	CNAG_03636	0	0	3	1	0
CNAG_07778	0	0	3	1	0	CNAG_03487	0	0	2	0	0
CNAG_06613	0	0	4	1	0	CNAG_05622	0	0	2	0	0
CNAG_01745	0	0	2	4	0	CNAG_01715	0	0	2	0	0
CNAG_03790	0	0	3	2	0	CNAG_06451	0	0	3	0	0
CNAG_05198	0	0	4	0	0	CNAG_05805	0	0	2	0	0
CNAG_07637	0	0	0	5	0	CNAG_03003	0	0	2	0	0
CNAG_07322	0	0	4	0	0	CNAG_06077	0	0	2	0	0
CNAG_06157	0	0	0	0	4	CNAG_02418	0	0	0	0	0
CNAG_04235	0	0	0	2	0	CNAG_01103	0	0	4	0	0
CNAG_02486	0	0	3	0	0	CNAG_05111	0	0	0	2	0
CNAG_02720	0	0	4	0	0	CNAG_06744	0	0	4	0	0
CNAG_05907	0	0	0	0	0	CNAG_07374	0	0	4	0	0
CNAG_04051	0	0	0	0	0	CNAG_05363	0	0	0	4	0
CNAG_01372	0	0	6	0	0	CNAG_03557	0	0	3	0	0
CNAG_04790	0	0	6	0	0	CNAG_03217	0	0	2	0	0
CNAG_04906	0	0	3	3	0	CNAG_06102	4	9	12	12	6
CNAG_02315	0	1	2	3	0	CNAG_04981	0	0	2	2	0
CNAG_05269	0	0	2	3	0	CNAG_05875	0	0	1	2	0
CNAG_02811	0	0	3	0	0	CNAG_04666	0	0	2	3	0
CNAG_06472	0	0	2	1	0	CNAG_02094	0	0	2	1	0
CNAG_02753	0	0	2	1	0	CNAG_02310	0	0	1	2	0
CNAG_03620	0	0	2	0	0	CNAG_02036	0	0	2	1	0
CNAG_02435	0	0	2	0	0	CNAG_04267	0	0	3	0	0
CNAG_05782	0	0	3	0	0	CNAG_01644	0	0	3	1	0
CNAG_06005	0	0	2	1	0	CNAG_04090	0	0	3	0	0
CNAG_01388	0	0	0	0	0	CNAG_04192	0	0	0	0	0
CNAG_00690	0	0	2	0	0	CNAG_04395	0	0	2	0	0
CNAG_01812	0	0	3	1	0	CNAG_00535	0	0	0	3	0
CNAG_01120	0	2	0	1	0	CNAG_02801	0	0	2	0	0
CNAG_05789	0	0	3	1	0	CNAG_01577	0	0	2	0	0
CNAG_01807	0	0	0	2	0	CNAG_05437	0	0	0	3	0
CNAG_04257	0	0	3	2	0	CNAG_00845	0	0	2	0	0

CNAG_04073	0	0	0	2	0
CNAG_03779	0	0	0	3	0
CNAG_01039	0	0	0	0	0
CNAG_07681	0	0	2	0	0
CNAG_00761	0	0	0	2	0
CNAG_02154	0	0	4	0	0
CNAG_02589	0	0	2	0	0
CNAG_04356	0	0	0	0	0
CNAG_01797	0	0	0	2	0
CNAG_00252	0	0	3	0	0
CNAG_01111	0	0	0	2	0
CNAG_05132	0	0	1	2	0
CNAG_06144	0	0	1	2	0
CNAG_02546	0	0	2	1	0
CNAG_02313	0	0	2	1	0
CNAG_06390	0	0	0	2	0
CNAG_00635	0	0	0	0	0
CNAG_05339	0	0	0	0	0
CNAG_07942	0	0	0	0	0
CNAG_03319	0	0	0	0	0
CNAG_03583	0	0	2	0	0
CNAG_00585	0	0	2	0	0
CNAG_05409	0	0	3	0	0
CNAG_06826	0	0	2	0	0

CNAG_03322	0	0	0	2	0
CNAG_05246	0	0	2	0	0
CNAG_00764	0	0	2	0	0
CNAG_04231	0	0	2	0	0
CNAG_02854	0	0	2	0	0
CNAG_00067	0	0	2	0	0
CNAG_05462	0	0	0	0	0
CNAG_06839	0	0	2	0	0
CNAG_01201	0	0	2	0	0
CNAG_03760	0	0	0	0	0
CNAG_03049	0	0	2	0	0
CNAG_02232	0	0	0	2	0
CNAG_03329	0	0	2	0	0
CNAG_03286	0	0	0	0	0
CNAG_06772	0	0	2	0	0
CNAG_00615	0	0	2	0	0
CNAG_00514	0	0	2	0	0
CNAG_05751	0	0	0	2	0
CNAG_04514	0	0	1	0	0
CNAG_02511	0	0	0	0	0
CNAG_03621	0	0	0	0	0
CNAG_04282	0	0	0	0	0

Appendix VI-Bridgin homologs

Species	**Accession no**
Mixia osmundae	G7DWY8
Puccinia graminis f. sp. tritici	E3KCL8
Melampsora larici-populina	F4S8M4
Leucosporidium creatinivorum	
Microbotryum intermedium	A0A238FJH5
Microbotryum saponariae	A0A2X0LQG2
Rhodosporidium toruloides	
Ustilago maydis	A0A0D1DPH3
Pseudozyma hubeiensis	R9NZN5
Malassezia globosa	A8PWL9
Malassezia sympodialis	A0A1M8A1N1
Tilletiopsis washingtonensis	A0A316ZAX2
Meira miltonrushii	A0A316VA03
Acaromyces ingoldii	A0A316YSV5
Tilletiaria anomala	A0A066VSV2
pseudomicrostroma glucosiphilum	A0A316UEN0
Jaminaea rosea	A0A316UYL4
Tilletia indica	A0A177TID9
Ceraceosorus guamensis	
Wallemia mellicola	
Wallemia ichthyophaga	
Phaffia rhodozyma	A0A0F7SRP3
Cryptococcus neoformans	J9VZK6
Tremella mesenterica	A0A4Q1BJ24
Trichosporon asahii var. asahi	K1VV34
Cutaneotrichosporon oleaginosum	A0A0J0XHU1
Dacryopinax primogenitus	M5GBU5
Calocera cornea	A0A165CTL7
Exidia glandulosa	A0A166AXE1
Serendipita vermifera	A0A0C3AKB0
Serendipita indica	G4TNP7
Rhizoctonia solani	A0A074RVZ3
Thanatephorus cucumeris	A0A0B7F5K0
Sistotremastrum niveocremeum	A0A164YF35
Sistotremastrum suecicum	A0A166I0S5
Sphaerobolus stellatus	A0A0C9ULP1
Pyrrhoderma noxium	A0A286UFB8
Schizopora paradoxa	A0A0H2S3Y6
Neolentinus lepideus	A0A165T1S9
Gloeophyllum trabeum	S7RDK8
Ganoderma sinense	A0A2G8S5W6
Dichomitus squalens	R7T019
Heterobasidion irregulare	W4JVH8
Bondarzewia mesenterica	A0A4S4LR08
Coprinopsis cinerea	A8P147
Galerina marginata	A0A067TAH3
Piloderma croceum	A0A0C3FVY5
Fibularhizoctonia sp.	A0A167WGE2
Pisolithus microcarpus	A0A0C9Z0K2
Rhizopogon vesiculosus	A0A1J8Q4V7
Jaapia argillacea	A0A067PMZ1
Saccharomyces cerevisiae	
Schizosaccharomyces pombe	
Pneumocystis jirovecii	L0PBB4
Saitoella complicata	A0A0E9NBI7
Allomyces macrogynus	
Encephalitozoon intestinalis	
Basidiobolus meristosporus	
Smittium culicis	A0A1R1XCN4
Spizellomyces punctatus	
Batrachochytrium dendrobatidis	A0A177WFM7
Mucor circinelloides f. lusitanicus	
Jimgerdemannia flammicorona	A0A433Q7W7
Rozella allomycis	A0A075B1N2
Paramicrosporidium saccamoebae	A0A2H9TFY5

Tieghemostelium lacteum	A0A152A412
Dictyostelium discoideum	Q54WT0
Homo sapiens	P46013
Gallus gallus	R4GLV4
Xenopus tropicalis	F6VGN1
Drosophila melanogaster	
Acyrthosiphon pisum	J9JW72
Caenorhabditis elegans	
Micromonas pusilla	
Arabidopsis thaliana	
Plasmodium falciparum	
Trypanosoma brucii	
Naegleria gruberi	

Bibliography

Abad, M.A., Zou, J., Medina-Pritchard, B., Nigg, E.A., Rappsilber, J., Santamaria, A., and Jeyaprakash, A.A. (2016). Ska3 Ensures Timely Mitotic Progression by Interacting Directly With Microtubules and Ska1 Microtubule Binding Domain. Sci. Rep. *6*, 34042.

Abràmoff, M.D., Magalhães, P.J., and Ram, S.J. (2005). Image processing with ImageJ Part II. Biophotonics Int. *11*, 36–43.

Akiyoshi, B., and Gull, K. (2014). Discovery of unconventional kinetochores in kinetoplastids. Cell *156*, 1247–1258.

Akiyoshi, B., Nelson, C.R., Ranish, J.A., and Biggins, S. (2009). Quantitative proteomic analysis of purified yeast kinetochores identifies a PP1 regulatory subunit. Genes Dev. *23*, 2887–2899.

Akiyoshi, B., Sarangapani, K.K., Powers, A.F., Nelson, C.R., Reichow, S.L., Arellano-Santoyo, H., Gonen, T., Ranish, J.A., Asbury, C.L., and Biggins, S. (2010). Tension directly stabilizes reconstituted kinetochore-microtubule attachments. Nature *468*, 576–579.

Alushin, G.M., Lander, G.C., Kellogg, E.H., Zhang, R., Baker, D., and Nogales, E. (2014). High-Resolution Microtubule Structures Reveal the Structural Transitions in αβ-Tubulin upon GTP Hydrolysis. Cell *157*, 1117–1129.

Amaro, A.C., Samora, C.P., Holtackers, R., Wang, E., Kingston, I.J., Alonso, M., Lampson, M., McAinsh, A.D., and Meraldi, P. (2010). Molecular control of kinetochore-microtubule dynamics and chromosome oscillations. Nat. Cell Biol. *12*, 319–329.

De Antoni, A., Pearson, C.G., Cimini, D., Canman, J.C., Sala, V., Nezi, L., Mapelli, M., Sironi, L., Faretta, M., Salmon, E.D., et al. (2005). The Mad1/Mad2 Complex as a Template for Mad2 Activation in the Spindle Assembly Checkpoint. Curr. Biol. *15*, 214–225.

Aravamudhan, P., Goldfarb, A.A., and Joglekar, A.P. (2015). The kinetochore encodes a mechanical switch to disrupt spindle assembly checkpoint signalling. Nat. Cell Biol. *17*, 868–879.

Baker, R.E., Fitzgerald-Hayes, M., and O'Brien, T.C. (1989). Purification of the yeast centromere binding protein CP1 and a mutational analysis of its binding site. J. Biol. Chem. *264*, 10843–10850.

Bancroft, J., Auckland, P., Samora, C.P., and McAinsh, A.D. (2015). Chromosome congression is promoted by CENP-Q- and CENP-E-dependent pathways. J. Cell Sci. *128*, 171–184.

Barth, T.K., Schade, G.O.M., Schmidt, A., Vetter, I., Wirth, M., Heun, P., Thomae, A.W., and Imhof, A. (2014). Identification of novel Drosophila centromere-associated proteins. Proteomics *14*, 2167–2178.

Basilico, F., Maffini, S., Weir, J.R., Prumbaum, D., Rojas, A.M., Zimniak, T., De Antoni, A., Jeganathan, S., Voss, B., van Gerwen, S., et al. (2014). The pseudo GTPase CENP-M drives human kinetochore assembly. Elife *3*, e02978.

Black, B.E., and Cleveland, D.W. (2011). Epigenetic centromere propagation and the nature of CENP-A nucleosomes. Cell *144*, 471–479.

Black, B.E., Foltz, D.R., Chakravarthy, S., Luger, K., Woods, V.L., and Cleveland, D.W. (2004). Structural determinants for generating centromeric chromatin. Nature *430*, 578–582.

Black, B.E., Jansen, L.E.T., Maddox, P.S., Foltz, D.R., Desai, A.B., Shah, J. V., and Cleveland, D.W. (2007). Centromere Identity Maintained by Nucleosomes Assembled with Histone H3 Containing the CENP-A Targeting Domain. Mol. Cell *25*, 309–322.

Blackwell, M. (2011). The Fungi: 1, 2, 3 … 5.1 million species? Am. J. Bot. *98*, 426–438.

Blumenthal, T. (2004). Operons in eukaryotes. Brief. Funct. Genomic. Proteomic. *3*, 199–211.

Bock, L.J., Pagliuca, C., Kobayashi, N., Grove, R.A., Oku, Y., Shrestha, K., Alfieri, C., Golfieri, C., Oldani, A., Dal Maschio, M., et al. (2012). Cnn1 inhibits the interactions between the KMN complexes of the yeast kinetochore. Nat. Cell Biol. *14*, 614–624.

Boettcher, B., and Barral, Y. (2013). The cell biology of open and closed mitosis. Nucl. (United States) *4*, 160–165.

Boveri, T. (1904). Ergebnisse über die Konstitution der chromatischen Substanz des Zellkerns. Von Theodor Boveri. (Jena,: G. Fischer,).

Brinkley, B.R., and Stubblefield, E. (1966). The fine structure of the kinetochore of a mammalian cell in vitro. Chromosoma *19*, 28–43.

Bruce, D. (2001). The Nobel Prize for Physiology or Medicine 2001. Genome Biol. *2*, spotlight-20011008-02.

Buscaino, A., Allshire, R., and Pidoux, A. (2010). Building centromeres: Home sweet home or a nomadic existence? Curr. Opin. Genet. Dev. *20*, 118–126.

Cai, M.J., and Davis, R.W. (1989). Purification of a yeast centromere-binding protein that is able to distinguish single base-pair mutations in its recognition site. Mol. Cell. Biol. *9*, 2544–2550.

Callejas, A., Ordoñez, N., Rodriguez, M.C., and Castañeda, E. (1998). First isolation of Cryptococcus neoformans var. gattii, serotype C, from the environment in Colombia. Med. Mycol. *36*, 341–344.

Carroll, C.W., and Straight, A.F. (2006). Centromere formation: From epigenetics to self-assembly. Trends Cell Biol. *16*, 70–78.

Carroll, C.W., Silva, M.C.C., Godek, K.M., Jansen, L.E.T., and Straight, A.F. (2009). Centromere assembly requires the direct recognition of CENP-A nucleosomes by CENP-N. Nat. Cell Biol. *11*, 896–902.

Carroll, C.W., Milks, K.J., and Straight, A.F. (2010). Dual recognition of CENP-A nucleosomes is required for centromere assembly. J. Cell Biol. *189*, 1143–1155.

Casadevall, A., and Perfect, J.R. (1998). Cryptococcus neoformans (American Society of Microbiology).

Chang, L., and Barford, D. (2014). Insights into the anaphase-promoting complex: a molecular machine that regulates mitosis. Curr. Opin. Struct. Biol. *29*, 1–9.

Chao, W.C.H., Kulkarni, K., Zhang, Z., Kong, E.H., and Barford, D. (2012). Structure of the mitotic checkpoint complex. Nature *484*, 208–213.

Cheerambathur, D.K., Prevo, B., Hattersley, N., Lewellyn, L., Corbett, K.D., Oegema, K., and Desai, A. (2017). Dephosphorylation of the Ndc80 Tail Stabilizes Kinetochore-Microtubule Attachments via the Ska Complex. Dev. Cell *41*, 424-437.e4.

Cheeseman, I.M. (2014). The Kinetochore. Cold Spring Harb. Perspect. Biol. *6*, a015826–a015826.

Cheeseman, I.M., Niessen, S., Anderson, S., Hyndman, F., Yates, J.R., Oegema, K., and Desai, A. (2004). A conserved protein network controls assembly of the outer kinetochore and its ability to sustain tension. Genes Dev. *18*, 2255–2268.

Cheeseman, I.M., Chappie, J.S., Wilson-Kubalek, E.M., and Desai, A. (2006). The Conserved KMN Network Constitutes the Core Microtubule-Binding Site of the Kinetochore. Cell *127*, 983–997.

Chikashige, Y., Kinoshita, N., Nakaseko, Y., Matsumoto, T., Murakami, S., Niwa, O., and Yanagida, M. (1989). Composite motifs and repeat symmetry in S. pombe centromeres: direct analysis by integration of NotI restriction sites. Cell *57*, 739–751.

Ciferri, C., De Luca, J., Monzani, S., Ferrari, K.J., Ristic, D., Wyman, C., Stark, H., Kilmartin, J., Salmon, E.D., and Musacchio, A. (2005). Architecture of the Human Ndc80-Hec1 Complex, a Critical Constituent of the Outer Kinetochore. J. Biol. Chem. *280*, 29088–29095.

Ciferri, C., Pasqualato, S., Screpanti, E., Varetti, G., Santaguida, S., Dos Reis, G., Maiolica, A., Polka, J., De Luca, J.G., De Wulf, P., et al. (2008). Implications for Kinetochore-Microtubule Attachment from the Structure of an Engineered Ndc80 Complex. Cell *133*, 427–439.

Clarke, L., and Baum, M.P. (1990). Functional analysis of a centromere from fission yeast: a role for centromere-specific repeated DNA sequences. Mol. Cell. Biol. *10*, 1863–1872.

Clarke, L., and Carbon, J. (1980). Isolation of a yeast centromere and construction of functional small circular chromosomes. Nature *287*, 504–509.

Collin, P., Nashchekina, O., Walker, R., and Pines, J. (2013). The spindle assembly checkpoint works like a

rheostat rather than a toggle switch. Nat. Cell Biol. *15*, 1378–1385.

Coue, M. (1991). Microtubule depolymerization promotes particle and chromosome movement in vitro. J. Cell Biol. *112*, 1165–1175.

Cuylen, S., Blaukopf, C., Politi, A.Z., Muller-Reichert, T., Neumann, B., Poser, I., Ellenberg, J., Hyman, A.A., and Gerlich, D.W. (2016). Ki-67 acts as a biological surfactant to disperse mitotic chromosomes. Nature *535*, 308–312.

D'Archivio, S., and Wickstead, B. (2017). Trypanosome outer kinetochore proteins suggest conservation of chromosome segregation machinery across eukaryotes. J. Cell Biol. *216*, 379–391.

Davidson, R.C., Cruz, M.C., Sia, R.A.L., Allen, B., Alspaugh, J.A., and Heitman, J. (2000). Gene disruption by biolistic transformation in serotype D strains of Cryptococcus neoformans. Fungal Genet. Biol. *29*, 38–48.

DeLuca, K.F., Meppelink, A., Broad, A.J., Mick, J.E., Peersen, O.B., Pektas, S., Lens, S.M.A., and DeLuca, J.G. (2018). Aurora A kinase phosphorylates Hec1 to regulate metaphase kinetochore–microtubule dynamics. J. Cell Biol. *217*, 163–177.

Dhatchinamoorthy, K., Shivaraju, M., Lange, J.J., Rubinstein, B., Unruh, J.R., Slaughter, B.D., and Gerton, J.L. (2017). Structural plasticity of the living kinetochore. J. Cell Biol. *216*, 3551–3570.

Dimitrova, Y.N., Jenni, S., Valverde, R., Khin, Y., and Harrison, S.C. (2016). Structure of the MIND Complex Defines a Regulatory Focus for Yeast Kinetochore Assembly. Cell *167*, 1014-1027.e12.

Dong, Y., Vanden Beldt, K.J., Meng, X., Khodjakov, A., and McEwen, B.F. (2007). The outer plate in vertebrate kinetochores is a flexible network with multiple microtubule interactions. Nat. Cell Biol. *9*, 516–522.

Drinnenberg, I.A., deYoung, D., Henikoff, S., and Malik, H.S. ingh (2014). Recurrent loss of CenH3 is associated with independent transitions to holocentricity in insects. Elife *3*, 1–19.

Drinnenberg, I.A., Henikoff, S., and Malik, H.S. (2016). Evolutionary Turnover of Kinetochore Proteins: A Ship of Theseus? Trends Cell Biol. *26*, 498–510.

Dromer, F., Ronin, O., and Dupont, B. (1992). Isolation of Cryptococcus neoformans var. gattii from an Asian patient in France: evidence for dormant infection in healthy subjects. J. Med. Vet. Mycol. *30*, 395–397.

Dubin, M., Fuchs, J., Gräf, R., Schubert, I., and Nellen, W. (2010). Dynamics of a novel centromeric histone variant CenH3 reveals the evolutionary ancestral timing of centromere biogenesis. Nucleic Acids Res. *38*, 7526–7537.

Dumesic, P.A., Homer, C.M., Moresco, J.J., Pack, L.R., Shanle, E.K., Coyle, S.M., Strahl, B.D., Fujimori, D.G., Yates, J.R., and Madhani, H.D. (2015). Product binding enforces the genomic specificity of a yeast Polycomb repressive complex. Cell *160*, 204–218.

Dumont, S., and Mitchison, T.J. (2009). Force and Length in the Mitotic Spindle. Curr. Biol. *19*, R749–R761.

Dunleavy, E.M., Almouzni, G., and Karpen, G.H. (2011). H3.3 is deposited at centromeres in S phase as a placeholder for newly assembled CENP-A in G 1 phase. Nucleus *2*, 146–157.

Earnshaw, W.C. (2015). Discovering centromere proteins: from cold white hands to the A, B, C of CENPs. Nat. Rev. Mol. Cell Biol. *16*, 443–449.

Earnshaw, W.C., and Rothfield, N. (1985). Identification of a family of human centromere proteins using autoimmune sera from patients with scleroderma. Chromosoma *91*, 313–321.

Emanuele, M.J., Lan, W., Jwa, M., Miller, S.A., Chan, C.S.M., and Stukenberg, P.T. (2008). Aurora B kinase and protein phosphatase 1 have opposing roles in modulating kinetochore assembly. J. Cell Biol. *181*, 241–254.

Endl, E., and Gerdes, J. (2000). Posttranslational modifications of the KI-67 protein coincide with two major checkpoints during mitosis. J. Cell. Physiol. *182*, 371–380.

Erhardt, S., Mellone, B.G., Betts, C.M., Zhang, W., Karpen, G.H., and Straight, A.F. (2008). Genome-wide analysis reveals a cell cycle–dependent mechanism controlling centromere propagation. J. Cell Biol. *183*, 805–818.

Falk, S.J., Lee, J., Sekulic, N., Sennett, M.A., Lee, T.-H., and Black, B.E. (2016). CENP-C directs a structural transition of CENP-A nucleosomes mainly through sliding of DNA gyres. Nat. Struct. Mol. Biol. *23*, 204–208.

Foley, E.A., and Kapoor, T.M. (2013). Microtubule attachment and spindle assembly checkpoint signalling at the kinetochore. Nat. Rev. Mol. Cell Biol. *14*, 25–37.

Foltz, D.R., Jansen, L.E.T., Black, B.E., Bailey, A.O., Yates, J.R., and Cleveland, D.W. (2006). The human CENP-A centromeric nucleosome-associated complex. Nat. Cell Biol. *8*, 458–469.

Fries, B.C., and Casadevall, A. (1998). Serial Isolates of Cryptococcus neoformans from Patients with AIDS Differ in Virulence for Mice . J. Infect. Dis. *178*, 1761–1766.

Fukagawa, T., and De Wulf, P. (2009). Kinetochore Composition, Formation, and Organization. In The Kinetochore:, (New York, NY: Springer New York), pp. 1–59.

Gaitanos, T.N., Santamaria, A., Jeyaprakash, A.A., Wang, B., Conti, E., and Nigg, E.A. (2009). Stable kinetochore–microtubule interactions depend on the Ska complex and its new component Ska3/C13Orf3. EMBO J. *28*, 1442–1452.

Garcia-Hermoso, D., Janbon, G., and Dromer, F. (1999). Epidemiological evidence for dormant Cryptococcus neoformans infection. J. Clin. Microbiol. *37*, 3204–3209.

Gascoigne, K.E., and Cheeseman, I.M. (2013). CDK-dependent phosphorylation and nuclear exclusion coordinately control kinetochore assembly state. J. Cell Biol. *201*, 23–32.

Gascoigne, K.E., Takeuchi, K., Suzuki, A., Hori, T., Fukagawa, T., and Cheeseman, I.M. (2011). Induced ectopic kinetochore assembly bypasses the requirement for CENP-A nucleosomes. Cell *145*, 410–422.

Gasteiger, E., Hoogland, C., Gattiker, A., Duvaud, S., Wilkins, M.R., Appel, R.D., and Bairoch, A. (2005). The Proteomics Protocols Handbook (Totowa, NJ: Humana Press).

Goldman, D.L., Khine, H., Abadi, J., Lindenberg, D.J., Pirofski La, Niang, R., and Casadevall, A. (2001). Serologic evidence for Cryptococcus neoformans infection in early childhood. Pediatrics *107*, E66.

Granados, D.P., and Castañeda, E. (2005). Isolation and characterization of Cryptococcus neoformans varieties recovered from natural sources in Bogotá, Colombia, and study of ecological conditions in the area. Microb. Ecol. *49*, 282–290.

Grigoriev, I. V., Nikitin, R., Haridas, S., Kuo, A., Ohm, R., Otillar, R., Riley, R., Salamov, A., Zhao, X., Korzeniewski, F., et al. (2014). MycoCosm portal: Gearing up for 1000 fungal genomes. Nucleic Acids Res. *42*, 699–704.

Grishchuk, E.L., Molodtsov, M.I., Ataullakhanov, F.I., and McIntosh, J.R. (2005). Force production by disassembling microtubules. Nature *438*, 384–388.

Grishchuk, E.L., Efremov, A.K., Volkov, V.A., Spiridonov, I.S., Gudimchuk, N., Westermann, S., Drubin, D., Barnes, G., McIntosh, J.R., and Ataullakhanov, F.I. (2008). The Dam1 ring binds microtubules strongly enough to be a processive as well as energy-efficient coupler for chromosome motion. Proc. Natl. Acad. Sci. *105*, 15423–15428.

Guimaraes, G.J., Dong, Y., McEwen, B.F., and DeLuca, J.G. (2008). Kinetochore-Microtubule Attachment Relies on the Disordered N-Terminal Tail Domain of Hec1. Curr. Biol. *18*, 1778–1784.

Guse, A., Carroll, C.W., Moree, B., Fuller, C.J., and Straight, A.F. (2011). In vitro centromere and kinetochore assembly on defined chromatin templates. Nature *477*, 354–358.

Hansemann, D. (1890). Ueber asymmetrische Zelltheilung in Epithelkrebsen und deren biologische Bedeutung. Arch. Für Pathol. Anat. Und Physiol. Und Für Klin. Med. *119*, 299–326.

Hara, M., and Fukagawa, T. (2017). Critical Foundation of the Kinetochore: The Constitutive Centromere-Associated Network (CCAN) (Progress in Molecular and Subcellular Biology).

Hara, M., and Fukagawa, T. (2018). ScienceDirect Kinetochore assembly and disassembly during mitotic entry and exit. Curr. Opin. Cell Biol. *52*, 73–81.

Hara, M., and Fukagawa, T. (2019). Where is the right path heading from the centromere to spindle microtubules ? Cell Cycle *0*, 1–13.

Hara, M., Ariyoshi, M., Okumura, E., Hori, T., and Fukagawa, T. (2018). Multiple phosphorylations control recruitment of the KMN network onto kinetochores. Nat. Cell Biol. *20*, 1378–1388.

Hasson, D., Panchenko, T., Salimian, K.J., Salman, M.U., Sekulic, N., Alonso, A., Warburton, P.E., and Black, B.E. (2013). The octamer is the major form of CENP-A nucleosomes at human centromeres. Nat. Struct. Mol. Biol. *20*, 687–695.

Hawksworth, D.L. (2001). The magnitude of fungal diversity: the 1.5 million species estimate revisited. Mycol. Res. *105*, 1422–1432.

Hayashi-Takanaka, Y., Maehara, K., Harada, A., Umehara, T., Yokoyama, S., Obuse, C., Ohkawa, Y., Nozaki, N., and Kimura, H. (2015). Distribution of histone H4 modifications as revealed by a panel of specific monoclonal antibodies. Chromosom. Res. *23*, 753–766.

Hayashi, T., Fujita, Y., Iwasaki, O., Adachi, Y., Takahashi, K., and Yanagida, M. (2004). Mis16 and Mis18 are required for CENP-A loading and histone deacetylation at centromeres. Cell *118*, 715–729.

Heitman, J., Howlett, B.J., Crous, P.W., Stukenbrock, E.H., James, T.Y., and Gow, N.A.R. (2017). The Fungal Kingdom (American Society of Microbiology).

Helgeson, L.A., Zelter, A., Riffle, M., MacCoss, M.J., Asbury, C.L., and Davis, T.N. (2018). Human Ska complex and Ndc80 complex interact to form a load-bearing assembly that strengthens kinetochore–microtubule attachments. Proc. Natl. Acad. Sci. *115*, 2740–2745.

Henikoff, S. (2001). The Centromere Paradox: Stable Inheritance with Rapidly Evolving DNA. Science (80-.). *293*, 1098–1102.

Hinshaw, S.M., and Harrison, S.C. (2019). The structure of the Ctf19c/CCAN from budding yeast. Elife *8*, 1–21.

Hiruma, Y., Sacristan, C., Pachis, S.T., Adamopoulos, A., Kuijt, T., Ubbink, M., von Castelmur, E., Perrakis, A., and Kops, G.J.P.L. (2015). Competition between MPS1 and microtubules at kinetochores regulates spindle checkpoint signaling. Science (80-.). *348*, 1264–1267.

Hooff, J.J., Tromer, E., Wijk, L.M., Snel, B., and Kops, G.J. (2017). Evolutionary dynamics of the kinetochore network in eukaryotes as revealed by comparative genomics. EMBO Rep. *18*, 1559–1571.

van Hooff, J.J.E., Snel, B., and Kops, G.J.P.L. (2017). Unique Phylogenetic Distributions of the Ska and Dam1 Complexes Support Functional Analogy and Suggest Multiple Parallel Displacements of Ska by Dam1. Genome Biol. Evol. *9*, 1295–1303.

Hori, T., Amano, M., Suzuki, A., Backer, C.B., Welburn, J.P., Dong, Y., McEwen, B.F., Shang, W.H., Suzuki, E., Okawa, K., et al. (2008). CCAN Makes Multiple Contacts with Centromeric DNA to Provide Distinct Pathways to the Outer Kinetochore. Cell *135*, 1039–1052.

Hori, T., Shang, W.H., Takeuchi, K., and Fukagawa, T. (2013). The CCAN recruits CENP-A to the centromere and forms the structural core for kinetochore assembly. J. Cell Biol. *200*, 45–60.

Hori, T., Shang, W.-H., Toyoda, A., Misu, S., Monma, N., Ikeo, K., Molina, O., Vargiu, G., Fujiyama, A., Kimura, H., et al. (2014). Histone H4 Lys 20 Monomethylation of the CENP-A Nucleosome Is Essential for Kinetochore Assembly. Dev. Cell *29*, 740–749.

Hornung, P., Troc, P., Malvezzi, F., Maier, M., Demianova, Z., Zimniak, T., Litos, G., Lampert, F., Schleiffer, A., Brunner, M., et al. (2014). A cooperative mechanism drives budding yeast kinetochore assembly downstream of CENP-A. J. Cell Biol. *206*, 509–524.

Howell, B.J., McEwen, B.F., Canman, J.C., Hoffman, D.B., Farrar, E.M., Rieder, C.L., and Salmon, E.D. (2001). Cytoplasmic dynein/dynactin drives kinetochore protein transport to the spindle poles and has a role in mitotic spindle checkpoint inactivation. J. Cell Biol. *155*, 1159–1172.

Howell, B.J., Moree, B., Farrar, E.M., Stewart, S., Fang, G., and Salmon, E.. (2004). Spindle Checkpoint Protein Dynamics at Kinetochores in Living Cells. Curr. Biol. *14*, 953–964.

Hua, S., Wang, Z., Jiang, K., Huang, Y., Ward, T., Zhao, L., Dou, Z., and Yao, X. (2011). CENP-U Cooperates with Hec1 to Orchestrate Kinetochore-Microtubule Attachment. J. Biol. Chem. *286*, 1627–1638.

Huff, J.T., and Zilberman, D. (2014). Dnmt1-Independent CG Methylation Contributes to Nucleosome Positioning in Diverse Eukaryotes. Cell *156*, 1286–1297.

Huisin'T Veld, P.J., Jeganathan, S., Petrovic, A., Singh, P., John, J., Krenn, V., Weissmann, F., Bange, T., and Musacchio, A. (2016). Molecular basis of outer kinetochore assembly on CENP-T. Elife *5*, 1–24.

Idnurm, A., Bahn, Y.S., Nielsen, K., Lin, X., Fraser, J.A., and Heitman, J. (2005). Deciphering the model pathogenic fungus Cryptococcus neoformans. Nat. Rev. Microbiol. *3*, 753–764.

Ishihama, Y., Oda, Y., Tabata, T., Sato, T., Nagasu, T., Rappsilber, J., and Mann, M. (2005). Exponentially Modified Protein Abundance Index (emPAI) for Estimation of Absolute Protein Amount in Proteomics by the Number of Sequenced Peptides per Protein. Mol. Cell. Proteomics *4*, 1265–1272.

Jakopec, V., Topolski, B., and Fleig, U. (2012). Sos7, an Essential Component of the Conserved Schizosaccharomyces pombe Ndc80-MIND-Spc7 Complex, Identifies a New Family of Fungal Kinetochore Proteins. Mol. Cell. Biol. *32*, 3308–3320.

Janbon, G., Ormerod, K.L., Paulet, D., Byrnes, E.J., Yadav, V., Chatterjee, G., Mullapudi, N., Hon, C.C., Billmyre, R.B., Brunel, F., et al. (2014). Analysis of the Genome and Transcriptome of Cryptococcus neoformans var. grubii Reveals Complex RNA Expression and Microevolution Leading to Virulence Attenuation. PLoS Genet. *10*.

Janczyk, P.Ł., Skorupka, K.A., Tooley, J.G., Matson, D.R., Kestner, C.A., West, T., Pornillos, O., and Stukenberg, P.T. (2017). Mechanism of Ska Recruitment by Ndc80 Complexes to Kinetochores. Dev. Cell *41*, 438-449.e4.

Jansen, L.E.T., Black, B.E., Foltz, D.R., and Cleveland, D.W. (2007). Propagation of centromeric chromatin requires exit from mitosis. J. Cell Biol. *176*, 795–805.

Jenni, S., and Harrison, S.C. (2018). Structure of the DASH/Dam1 complex shows its role at the yeast kinetochore-microtubule interface. Science (80-.). *360*, 552–558.

Jeyaprakash, A.A., Santamaria, A., Jayachandran, U., Chan, Y.W., Benda, C., Nigg, E.A., and Conti, E. (2012). Structural and Functional Organization of the Ska Complex, a Key Component of the Kinetochore-Microtubule Interface. Mol. Cell *46*, 274–286.

Joglekar, A. (2016). A Cell Biological Perspective on Past, Present and Future Investigations of the Spindle Assembly Checkpoint. Biology (Basel). *5*, 44.

Joglekar, A.P., Bouck, D., Finley, K., Liu, X., Wan, Y., Berman, J., He, X., Salmon, E.D., and Bloom, K.S. (2008). Molecular architecture of the kinetochore-microtubule attachment site is conserved between point and regional centromeres. J. Cell Biol. *181*, 587–594.

Joglekar, A.P., Bloom, K., and Salmon, E.D. (2009). In Vivo Protein Architecture of the Eukaryotic Kinetochore with Nanometer Scale Accuracy. Curr. Biol. *19*, 694–699.

Kang, Y.H., Park, C.H., Kim, T.-S., Soung, N.-K., Bang, J.K., Kim, B.Y., Park, J.-E., and Lee, K.S. (2011). Mammalian Polo-like Kinase 1-dependent Regulation of the PBIP1-CENP-Q Complex at Kinetochores. J. Biol. Chem. *286*, 19744–19757.

Karsenti, E., and Vernos, I. (2001). The Mitotic Spindle : A Self-Made Machine. *294*, 543–548.

Kato, H., Jiang, J., Zhou, B.-R., Rozendaal, M., Feng, H., Ghirlando, R., Xiao, T.S., Straight, A.F., and Bai, Y. (2013). A Conserved Mechanism for Centromeric Nucleosome Recognition by Centromere Protein CENP-C. Science (80-.). *340*, 1110–1113.

Kelley, L.A., Mezulis, S., Yates, C.M., Wass, M.N., and Sternberg, M.J.E. (2015). The Phyre2 web portal for protein modeling, prediction and analysis. Nat. Protoc. *10*, 845–858.

Kemmler, S., Stach, M., Knapp, M., Ortiz, J., Pfannstiel, J., Ruppert, T., and Lechner, J. (2009). Mimicking Ndc80 phosphorylation triggers spindle assembly checkpoint signalling. EMBO J. *28*, 1099–1110.

Khodjakov, A., and Pines, J. (2010). Centromere tension: A divisive issue. Nat. Cell Biol. *12*, 919–923.

Kiermaier, E., Woehrer, S., Peng, Y., Mechtler, K., and Westermann, S. (2009). A Dam1-based artificial kinetochore is sufficient to promote chromosome segregation in budding yeast. Nat. Cell Biol. *11*, 1109–1115.

Kim, S., and Yu, H. (2015). Multiple assembly mechanisms anchor the KMN spindle checkpoint platform at human mitotic kinetochores. J. Cell Biol. *208*, 181–196.

Kim, J.O., Zelter, A., Umbreit, N.T., Bollozos, A., Riffle, M., Johnson, R., MacCoss, M.J., Asbury, C.L., and Davis, T.N. (2017). The Ndc80 complex bridges two Dam1 complex rings. Elife *6*, 1–22.

Kimura, H., Hayashi-Takanaka, Y., Goto, Y., Takizawa, N., and Nozaki, N. (2008). The Organization of Histone H3 Modifications as Revealed by a Panel of Specific Monoclonal Antibodies. Cell Struct. Funct. *33*, 61–73.

Kitamura, E., Tanaka, K., Kitamura, Y., and Tanaka, T.U. (2007). Kinetochore microtubule interaction during S phase in Saccharomyces cerevisiae. Genes Dev. *21*, 3319–3330.

KJ, K.-C., and JE., B. (1978). Distribution of alpha and alpha mating types of Cryptococcus neoformans among natural and clinical isolates. Am. J. Epidemiol. *108*, 337–340.

Kline, S.L., Cheeseman, I.M., Hori, T., Fukagawa, T., and Desai, A. (2006). The human Mis12 complex is required for kinetochore assembly and proper chromosome segregation. J. Cell Biol. *173*, 9–17.

Kouprina, N., Tsouladze, A., Koryabin, M., Hieter, P., Spencer, F., and Larionov, V. (1993). Identification and genetic mapping ofCHL genes controlling mitotic chromosome transmission in yeast. Yeast *9*, 11–19.

Kozubowski, L., and Heitman, J. (2012). Profiling a killer, the development of Cryptococcus neoformans. FEMS Microbiol. Rev. *36*, 78–94.

Kozubowski, L., Yadav, V., Chatterjee, G., Sridhar, S., Yamaguchi, M., Kawamoto, S., Bose, I., Heitman, J., and Sanyal, K. (2013). Ordered kinetochore assembly in the human-pathogenic basidiomycetous yeast Cryptococcus neoformans. MBio *4*.

Kwon-Chung, K.J. (1975). A New Genus, Filobasidiella, the Perfect State of Cryptococcus neoformans. Mycologia *67*, 1197.

Kwon-Chung, K.J. (1976). A new species of Filobasidiella, the sexual state of Cryptococcus neoformans B and C serotypes. Mycologia *68*, 943–946.

Kwon-Chung, K.J., Edman, J.C., and Wickes, B.L. (1992). Genetic association of mating types and virulence in Cryptococcus neoformans. Infect. Immun. *60*, 602–605.

Lacefield, S., Lau, D.T.C., and Murray, A.W. (2009). Recruiting a microtubule-binding complex to DNA directs chromosome segregation in budding yeast. Nat. Cell Biol. *11*, 1116–1120.

Lampert, F., Hornung, P., and Westermann, S. (2010). The Dam1 complex confers microtubule plus end–tracking activity to the Ndc80 kinetochore complex. J. Cell Biol. *189*, 641–649.

Landberg, G., and Roos, G. (1991). Antibodies to Proliferating Cell Nuclear Antigen as S-Phase Probes in Flow Cytometric Cell Cycle Analysis. Cancer Res. *51*, 4570–4574.

Lang, J., Barber, A., and Biggins, S. (2018). An assay for de novo kinetochore assembly reveals a key role for the CENP-T pathway in budding yeast. Elife *7*.

Lara-Gonzalez, P., Westhorpe, F.G., and Taylor, S.S. (2012). The Spindle Assembly Checkpoint. Curr. Biol. *22*, R966–R980.

Lechner, J., and Carbon, J. (1991). A 240 kd multisubunit protein complex, CBF3, is a major component of the budding yeast centromere. Cell *64*, 717–725.

Legal, T., Zou, J., Sochaj, A., Rappsilber, J., and Welburn, J.P.I. (2016). Molecular architecture of the Dam1 complex–microtubule interaction. Open Biol. *6*, 150237.

Lengeler, K.B., Cox, G.M., and Heitman, J. (2001). Serotype AD Strains of Cryptococcus neoformans Are Diploid or Aneuploid and Are Heterozygous at the Mating-Type Locus. Infect. Immun. *69*, 115–122.

Letunic, I., and Bork, P. (2019). Interactive Tree Of Life (iTOL) v4: recent updates and new developments. Nucleic Acids Res. *47*, W256–W259.

Lin, X. (2009). Cryptococcus neoformans: Morphogenesis, infection, and evolution. Infect. Genet. Evol. *9*, 401–416.

Lin, X., and Heitman, J. (2006). The Biology of the *Cryptococcus neoformans* Species Complex. Annu. Rev. Microbiol. *60*, 69–105.

Lin, X., Hull, C.M., and Heitman, J. (2005). Sexual reproduction between partners of the same mating type in Cryptococcus neoformans. Nature *434*, 1017–1021.

Liu, S.-T., and Zhang, H. (2016). The mitotic checkpoint complex (MCC): looking back and forth after 15 years. AIMS Mol. Sci. *3*, 597–634.

Liu, D., Vleugel, M., Backer, C.B., Hori, T., Fukagawa, T., Cheeseman, I.M., and Lampson, M.A. (2010). Regulated targeting of protein phosphatase 1 to the outer kinetochore by KNL1 opposes Aurora B kinase. J. Cell Biol. *188*, 809–820.

Liu, S.T., Rattner, J.B., Jablonski, S.A., and Yen, T.J. (2006). Mapping the assembly pathways that specify formation of the trilaminar kinetochore plates in human cells. J. Cell Biol. *175*, 41–53.

Liu, X., McLeod, I., Anderson, S., Yates, J.R., and He, X. (2005). Molecular analysis of kinetochore architecture in fission yeast. EMBO J. *24*, 2919–2930.

Liu, Y., Petrovic, A., Rombaut, P., Mosalaganti, S., Keller, J., Raunser, S., Herzog, F., Musacchio, A., and Musacchio, A. (2016). Insights from the reconstitution of the divergent outer kinetochore of Drosophila melanogaster. Open Biol. *6*, 150236.

Long, A.F., Udy, D.B., and Dumont, S. (2017). Hec1 Tail Phosphorylation Differentially Regulates Mammalian Kinetochore Coupling to Polymerizing and Depolymerizing Microtubules. Curr. Biol. *27*, 1692-1699.e3.

Lücking, R., Huhndorf, S., Pfister, D.H., Plata, E.R., and Lumbsch, H.T. (2009). Fungi evolved right on track. Mycologia *101*, 810–822.

MacCallum, D.E., and Hall, P. a (2000). The biochemical characterization of the DNA binding activity of pKi67. J. Pathol. *191*, 286–298.

MacCallum, D.E., and Hall, P.A. (1999). Biochemical Characterization of pKi67 with the Identification of a Mitotic-Specific Form Associated with Hyperphosphorylation and Altered DNA Binding. Exp. Cell Res. *252*, 186–198.

Maddox, P.S., Oegema, K., Desai, A., and Cheeseman, I.M. (2004). "Holo"er than thou: Chromosome segregation and kinetochore function in C. elegans. Chromosom. Res. *12*, 641–653.

Maiato, H. (2004). The dynamic kinetochore-microtubule interface. J. Cell Sci. *117*, 5461–5477.

Malvezzi, F., Litos, G., Schleiffer, A., Heuck, A., Mechtler, K., Clausen, T., and Westermann, S. (2013). A structural basis for kinetochore recruitment of the Ndc80 complex via two distinct centromere receptors. EMBO J. *32*, 409–423.

Maresca, T.J., and Salmon, E.D. (2010). Welcome to a new kind of tension: Translating kinetochore mechanics into a wait-anaphase signal. J. Cell Sci. *123*, 825–835.

Martinez, L.R., and Casadevall, A. (2007). Cryptococcus neoformans biofilm formation depends on surface support and carbon source and reduces fungal cell susceptibility to heat, cold, and UV light. Appl. Environ. Microbiol. *73*, 4592–4601.

McEwen, B.F., Heagle, A.B., Cassels, G.O., Buttle, K.F., and Rieder, C.L. (1997). Kinetochore Fiber Maturation in PtK 1 Cells and Its Implications for the Mechanisms of Chromosome Congression and Anaphase Onset. J. Cell Biol. *137*, 1567–1580.

McEwen, B.F., Hsieh, C.-E., Mattheyses, A.L., and Rieder, C.L. (1998). A new look at kinetochore structure in vertebrate somatic cells using high-pressure freezing and freeze substitution. Chromosoma *107*, 366–375.

McIntosh, J.R., Grishchuk, E.L., Morphew, M.K., Efremov, A.K., Zhudenkov, K., Volkov, V.A., Cheeseman, I.M., Desai, A., Mastronarde, D.N., and Ataullakhanov, F.I. (2008). Fibrils Connect Microtubule Tips with Kinetochores: A Mechanism to Couple Tubulin Dynamics to Chromosome Motion. Cell *135*, 322–333.

McKinley, K.L., and Cheeseman, I.M. (2014). Polo-like Kinase 1 Licenses CENP-A Deposition at Centromeres. Cell *158*, 397–411.

McKinley, K.L., and Cheeseman, I.M. (2015). The molecular basis for centromere identity and function. Nat. Rev. Mol. Cell Biol. *17*, 16–29.

Mendiburo, M.J., Padeken, J., Fülöp, S., Schepers, A., and Heun, P. (2011). Drosophila CENH3 is sufficient for centromere formation. Science (80-.). *334*, 686–690.

Meraldi, P., McAinsh, A.D., Rheinbay, E., and Sorger, P.K. (2006). Phylogenetic and structural analysis of centromeric DNA and kinetochore proteins. Genome Biol. *7*.

Mészáros, B., Erdös, G., and Dosztányi, Z. (2018). IUPred2A: Context-dependent prediction of protein disorder as a function of redox state and protein binding. Nucleic Acids Res. *46*, W329–W337.

Miescher, F. (1871). Ueber die chemische Zusammensetzung der Eiterzellen. Med. Untersuchungen *4*, 441–460.

Milks, K.J., Moree, B., and Straight, A.F. (2009). Dissection of CENP-C-directed Centromere and Kinetochore Assembly. Mol. Biol. Cell *20*, 4246–4255.

Miller, S.A., Johnson, M.L., and Stukenberg, P.T. (2008). Kinetochore Attachments Require an Interaction between Unstructured Tails on Microtubules and Ndc80Hec1. Curr. Biol. *18*, 1785–1791.

Miranda, J.L., Wulf, P. De, Sorger, P.K., and Harrison, S.C. (2005). The yeast DASH complex forms closed rings on microtubules. Nat. Struct. Mol. Biol. *12*, 138–143.

Mitchell, T.G., and Perfect, J.R. (1995). Cryptococcosis in the era of AIDS--100 years after the discovery of Cryptococcus neoformans. Clin. Microbiol. Rev. *8*, 515–548.

Mitchison, T., and Kirschner, M. (1984). Dynamic instability of microtubule growth. Nature *312*, 237–242.

Mizuguchi, G., Xiao, H., Wisniewski, J., Smith, M.M., and Wu, C. (2007). Nonhistone Scm3 and Histones CenH3-H4 Assemble the Core of Centromere-Specific Nucleosomes. Cell *129*, 1153–1164.

Monda, J.K., and Cheeseman, I.M. (2018). The kinetochore-microtubule interface at a glance. J. Cell Sci. *131*.

Monen, J., Maddox, P.S., Hyndman, F., Oegema, K., and Desai, A. (2005). Differential role of CENP-A in the segregation of holocentric C. elegans chromosomes during meiosis and mitosis. Nat. Cell Biol. *7*, 1248–1255.

Morgan, T.H. (1915). The mechanism of Mendelian heredity (The Malpe Press).

Moroi, Y., Peebles, C., Fritzler, M.J., Steigerwald, J., and Tan, E.M. (1980). Autoantibody to centromere (kinetochore) in scleroderma sera. Proc. Natl. Acad. Sci. U. S. A. *77*, 1627–1631.

Morris, G.F., and Mathews, M.B. (1989). Regulation of proliferating cell nuclear antigen during the cell cycle. J. Biol. Chem. *264*, 13856–13864.

Musacchio, A. (2015). The Molecular Biology of Spindle Assembly Checkpoint Signaling Dynamics. Curr. Biol. *25*, R1002–R1018.

Musacchio, A., and Desai, A. (2017). A Molecular View of Kinetochore Assembly and Function. Biology (Basel). *6*, 5.

Musacchio, A., and Salmon, E.D. (2007). The spindle-assembly checkpoint in space and time. Nat. Rev. Mol. Cell Biol. *8*, 379–393.

Navarro-Mendoza, M.I., Pérez-Arques, C., Panchal, S., Nicolás, F.E., Mondo, S.J., Ganguly, P., Pangilinan, J., Grigoriev, I. V., Heitman, J., Sanyal, K., et al. (2019). Early Diverging Fungus Mucor circinelloides Lacks Centromeric Histone CENP-A and Displays a Mosaic of Point and Regional Centromeres. Curr. Biol. 1–12.

Nechemia-arbely, Y., Miga, K.H., Shoshani, O., Aslanian, A., Mcmahon, M.A., Lee, A.Y., Fachinetti, D., Iii, J.R.Y., Ren, B., and Cleveland, D.W. (2019). mechanism to maintain centromere identity by restricting CENP-A to centromeres. Nat. Cell Biol. *21*.

Ng, C.T., Deng, L., Chen, C., Lim, H.H., Shi, J., Surana, U., and Gan, L. (2019). Electron cryotomography analysis of Dam1C/DASH at the kinetochore–spindle interface in situ. J. Cell Biol. *218*, 455–473.

Nielsen, K., Cox, G.M., Wang, P., Toffaletti, D.L., Perfect, J.R., and Heitman, J. (2003). Sexual cycle of Cryptococcus neoformans var. grubii and Virulence of congenic a and α isolates. Infect. Immun. *71*, 4831–4841.

Nielsen, K., Cox, G.M., Litvintseva, A.P., Mylonakis, E., Malliaris, S.D., Benjamin, D.K., Giles, S.S., Mitchell, T.G., Casadevall, A., Perfect, J.R., et al. (2005). Cryptococcus neoformans Strains Preferentially Disseminate to the Central Nervous System during Coinfection. Infect. Immun. *73*, 4922–4933.

Nishino, T., Takeuchi, K., Gascoigne, K.E., Suzuki, A., Hori, T., Oyama, T., Morikawa, K., Cheeseman, I.M., and Fukagawa, T. (2012). CENP-T-W-S-X forms a unique centromeric chromatin structure with a histone-like fold. Cell *148*, 487–501.

Nishino, T., Rago, F., Hori, T., Tomii, K., Cheeseman, I.M., and Fukagawa, T. (2013). CENP-T provides a structural platform for outer kinetochore assembly. EMBO J. *32*, 424–436.

Nuria Cortes-Silva, J.U., Kiuchi, T., Hsieh, E., Cornilleau, G., Ladid, I., Dingli, F., Loew, D., Katsuma, S., and Drinnenberg, I.A. (2019). CenH3-independent kinetochore assembly in Lepidoptera requires CENP-T. BioRxiv.

O'Donnell, K.L., and McLaughlin, D.J. (1984). Postmeiotic Mitosis, Basidiospore Development, and Septation in Ustilago Maydis. Mycologia *76*, 486–502.

Obuse, C., Yang, H., Nozaki, N., Goto, S., Okazaki, T., and Yoda, K. (2004). Proteomics analysis of the centromere complex from HeLa interphase cells: UV-damaged DNA binding protein 1 (DDB-1) is a component of the CEN-complex, while BMI-1 is transiently co-localized with the centromeric region in interphase. Genes to Cells *9*, 105–120.

Okada, M., Cheeseman, I.M., Hori, T., Okawa, K., McLeod, I.X., Yates, J.R., Desai, A., and Fukagawa, T. (2006). The CENP-H–I complex is required for the efficient incorporation of newly synthesized CENP-A into centromeres. Nat. Cell Biol. *8*, 446–457.

Oliferenko, S. (2018). Understanding eukaryotic chromosome segregation from a comparative biology perspective. J. Cell Sci. *131*.

Ortiz, J., Stemmann, O., Rank, S., and Lechner, J. (1999). A putative protein complex consisting of Ctf19, Mcm21, and Okp1 represents a missing link in the budding yeast kinetochore. Genes Dev. *13*, 1140–1155.

Oya, E., Nakagawa, R., Yoshimura, Y., Tanaka, M., Nishibuchi, G., Machida, S., Shirai, A., Ekwall, K., Kurumizaka, H., Tagami, H., et al. (2019). H3K14 ubiquitylation promotes H3K9 methylation for heterochromatin assembly. EMBO Rep. *e48111*.

Paddy, M.R., Saumweber, H., Agard, D.A., and Sedat, J.W. (1996). Time-resolved, in vivo studies of mitotic spindle formation and nuclear lamina breakdown in Drosophila early embryos. J. Cell Sci. *109 (Pt 3*, 591–607.

Padeganeh, A., De Rop, V., and Maddox, P.S. (2013). Nucleosomal composition at the centromere: a numbers game. Chromosom. Res. *21*, 27–36.

Padmanabhan, S., Thakur, J., Siddharthan, R., and Sanyal, K. (2008). Rapid evolution of Cse4p-rich centromeric DNA sequences in closely related pathogenic yeasts, Candida albicans and Candida dubliniensis. Proc. Natl. Acad. Sci. U. S. A. *105*, 19797–19802.

Park, B.J., Wannemuehler, K.A., Marston, B.J., Govender, N., Pappas, P.G., and Chiller, T.M. (2009).

Estimation of the current global burden of cryptococcal meningitis among persons living with HIV/AIDS. AIDS *23*, 525–530.

Paweletz, N. (2001). Walther Flemming: pioneer of mitosis research. Nat. Rev. Mol. Cell Biol. *2*, 72–75.

Pearson, C.G., Yeh, E., Gardner, M., Odde, D., Salmon, E.D., and Bloom, K. (2004). Stable Kinetochore-Microtubule Attachment Constrains Centromere Positioning in Metaphase. Curr. Biol. *14*, 1962–1967.

Pekgöz Altunkaya, G., Malvezzi, F., Demianova, Z., Zimniak, T., Litos, G., Weissmann, F., Mechtler, K., Herzog, F., and Westermann, S. (2016). CCAN Assembly Configures Composite Binding Interfaces to Promote Cross-Linking of Ndc80 Complexes at the Kinetochore. Curr. Biol. *26*, 2370–2378.

Pellman, D. (2001). A CINtillating New Job for the APC Tumor Suppressor. Science (80-.). *291*, 2555–2556.

Perpelescu, M., and Fukagawa, T. (2011). The ABCs of CENPs. Chromosoma *120*, 425–446.

Petrovic, A., Pasqualato, S., Dube, P., Krenn, V., Santaguida, S., Cittaro, D., Monzani, S., Massimiliano, L., Keller, J., Tarricone, A., et al. (2010). The MIS12 complex is a protein interaction hub for outer kinetochore assembly. J. Cell Biol. *190*, 835–852.

Petrovic, A., Mosalaganti, S., Keller, J., Mattiuzzo, M., Overlack, K., Krenn, V., De Antoni, A., Wohlgemuth, S., Cecatiello, V., Pasqualato, S., et al. (2014). Modular Assembly of RWD Domains on the Mis12 Complex Underlies Outer Kinetochore Organization. Mol. Cell *53*, 591–605.

Petrovic, A., Keller, J., Liu, Y., Overlack, K., John, J., Dimitrova, Y.N., Jenni, S., van Gerwen, S., Stege, P., Wohlgemuth, S., et al. (2016). Structure of the MIS12 Complex and Molecular Basis of Its Interaction with CENP-C at Human Kinetochores. Cell *167*, 1028-1040.e15.

Pidoux, A.L., Choi, E.S., Abbott, J.K.R., Liu, X., Kagansky, A., Castillo, A.G., Hamilton, G.L., Richardson, W., Rappsilber, J., He, X., et al. (2009). Fission Yeast Scm3: A CENP-A Receptor Required for Integrity of Subkinetochore Chromatin. Mol. Cell *33*, 299–311.

Pinsky, B.A., Kung, C., Shokat, K.M., and Biggins, S. (2006). The Ipl1-Aurora protein kinase activates the spindle checkpoint by creating unattached kinetochores. Nat. Cell Biol. *8*, 78–83.

Pohler, J.R.G., Otterlei, M., and Warbrick, E. (2005). An in vivo analysis of the localisation and interactions of human p66 DNA polymerase delta subunit. BMC Mol. Biol. *6*, 17.

Posch, M., Khoudoli, G.A., Swift, S., King, E.M., DeLuca, J.G., and Swedlow, J.R. (2010). Sds22 regulates aurora B activity and microtubule–kinetochore interactions at mitosis. J. Cell Biol. *191*, 61–74.

Potter, S.C., Luciani, A., Eddy, S.R., Park, Y., Lopez, R., and Finn, R.D. (2018). HMMER web server: 2018 update. Nucleic Acids Res. *46*, W200–W204.

Powers, A.F., Franck, A.D., Gestaut, D.R., Cooper, J., Gracyzk, B., Wei, R.R., Wordeman, L., Davis, T.N., and Asbury, C.L. (2009). The Ndc80 Kinetochore Complex Forms Load-Bearing Attachments to Dynamic Microtubule Tips via Biased Diffusion. Cell *136*, 865–875.

Primorac, I., and Musacchio, A. (2013). Panta rhei: The APC/C at steady state. J. Cell Biol. *201*, 177–189.

Primorac, I., Weir, J.R., Chiroli, E., Gross, F., Hoffmann, I., van Gerwen, S., Ciliberto, A., and Musacchio, A. (2013). Bub3 reads phosphorylated MELT repeats to promote spindle assembly checkpoint signaling. Elife *2013*, 1–20.

Przewloka, M.R., Zhang, W., Costa, P., Archambault, V., D'Avino, P.P., Lilley, K.S., Laue, E.D., McAinsh, A.D., and Glover, D.M. (2007). Molecular analysis of core kinetochore composition and assembly in Drosophila melanogaster. PLoS One *2*.

Rago, F., Gascoigne, K.E., and Cheeseman, I.M. (2015). Distinct organization and regulation of the outer kinetochore KMN network downstream of CENP-C and CENP-T. Curr. Biol. *25*, 671–677.

Richter, M.M., Poznanski, J., Zdziarska, A., Czarnocki-cieciura, M., Lipinszki, Z., Dadlez, M., Glover, D.M., Przewloka, M.R., Dadlez, M., and Dm, G. (2016). Network of protein interactions within the Drosophila inner kinetochore. Open Biol. *6*, 150238.

Rieder, C.L. (1982). The Formation, Structure, and Composition of the Mammalian Kinetochore and Kinetochore Fiber.

del Rio, A., Perez-jimenez, R., Liu, R., Roca-cusachs, P., Fernandez, J.M., and Sheetz, M.P. (2009). Stretching Single Talin Rod. Science (80-.). *323*, 638–641.

Roos, U.-P. (1973). Light and electron microscopy of rat kangaroo cells in mitosis. Chromosoma *41*, 195–220.

Rosin, L.F., and Mellone, B.G. (2017). Centromeres Drive a Hard Bargain. Trends Genet. *33*, 101–117.

Roy, B., and Sanyal, K. (2011). Diversity in requirement of genetic and epigenetic factors for centromere function in fungi. Eukaryot. Cell *10*, 1384–1395.

Roy, B., Burrack, L.S., Lone, M.A., Berman, J., and Sanyal, K. (2011). CaMtw1, a member of the evolutionarily conserved Mis12 kinetochore protein family, is required for efficient inner kinetochore assembly in the pathogenic yeast Candida albicans. Mol. Microbiol. *80*, 14–32.

Ruff, J.A., Lodge, J.K., and Baker, L.G. (2009). Three galactose inducible promoters for use in C. neoformans var. grubii. Fungal Genet. Biol. *46*, 9–16.

Sacristan, C., and Kops, G.J.P.L. (2015). Joined at the hip: Kinetochores, microtubules, and spindle assembly checkpoint signaling. Trends Cell Biol. *25*, 21–28.

Samejima, I., Spanos, C., De Lima Alves, F., Hori, T., Perpelescu, M., Zou, J., Rappsilber, J., Fukagawa, T., and Earnshaw, W.C. (2015). Whole-proteome genetic analysis of dependencies in assembly of a vertebrate kinetochore. J. Cell Biol. *211*, 1141–1156.

Sanchez-Perez, I., Renwick, S.J., Crawley, K., Karig, I., Buck, V., Meadows, J.C., Franco-Sanchez, A., Fleig, U., Toda, T., and Millar, J.B.A.A. (2005). The DASH complex and Klp5/Klp6 kinesin coordinate bipolar chromosome attachment in fission yeast. EMBO J. *24*, 2931–2943.

Sanchez-Pulido, L., Pidoux, A.L., Ponting, C.P., and Allshire, R.C. (2009). Common Ancestry of the CENP-A Chaperones Scm3 and HJURP. Cell *137*, 1173–1174.

Sanyal, K., Baum, M., and Carbon, J. (2004). Centromeric DNA sequences in the pathogenic yeast Candida albicans are all different and unique. Proc. Natl. Acad. Sci. U. S. A. *101*, 11374–11379.

Sarangapani, K.K., and Asbury, C.L. (2014). Catch and release: How do kinetochores hook the right microtubules during mitosis? Trends Genet. *30*, 150–159.

Schleiffer, A., Maier, M., Litos, G., Lampert, F., Hornung, P., Mechtler, K., and Westermann, S. (2012). CENP-T proteins are conserved centromere receptors of the Ndc80 complex. Nat. Cell Biol. *14*, 604–613.

Schmidt, J.C., Arthanari, H., Boeszoermenyi, A., Dashkevich, N.M., Wilson-Kubalek, E.M., Monnier, N., Markus, M., Oberer, M., Milligan, R.A., Bathe, M., et al. (2012). The Kinetochore-Bound Ska1 Complex Tracks Depolymerizing Microtubules and Binds to Curved Protofilaments. Dev. Cell *23*, 968–980.

Schönenberger, F., Deutzmann, A., Ferrando-May, E., and Merhof, D. (2015). Discrimination of cell cycle phases in PCNA-immunolabeled cells. BMC Bioinformatics *16*, 180.

Schueler, M.G., and Sullivan, B.A. (2006). Structural and Functional Dynamics of Human Centromeric Chromatin. Annu. Rev. Genomics Hum. Genet. *7*, 301–313.

Selmecki, A., Gerami-Nejad, M., Paulson, C., Forche, A., and Berman, J. (2008). An isochromosome confers drug resistance in vivo by amplification of two genes, ERG11 and TAC1. Mol. Microbiol. *68*, 624–641.

Selmecki, A.M., Dulmage, K., Cowen, L.E., Anderson, J.B., and Berman, J. (2009). Acquisition of aneuploidy provides increased fitness during the evolution of antifungal drug resistance. PLoS Genet. *5*, 1–16.

Shepperd, L.A., Meadows, J.C., Sochaj, A.M., Lancaster, T.C., Zou, J., Buttrick, G.J., Rappsilber, J., Hardwick, K.G., and Millar, J.B.A. (2012). Phosphodependent recruitment of Bub1 and Bub3 to Spc7/KNL1 by Mph1 kinase maintains the spindle checkpoint. Curr. Biol. *22*, 891–899.

Sikorski, R.S., and Hieter, P. (1989). A system of shuttle vectors and yeast host strains designed for efficient manipulation of DNA in Saccharomyces cerevisiae. Genetics *122*, 19–27.

Silió, V., McAinsh, A.D., and Millar, J.B. (2015). KNL1-Bubs and RZZ Provide Two Separable Pathways for Checkpoint Activation at Human Kinetochores. Dev. Cell *35*, 600–613.

Singh, T.R., Saro, D., Ali, A.M., Zheng, X.-F., Du, C., Killen, M.W., Sachpatzidis, A., Wahengbam, K., Pierce, A.J., Xiong, Y., et al. (2010). MHF1-MHF2, a Histone-Fold-Containing Protein Complex, Participates in the Fanconi Anemia Pathway via FANCM. Mol. Cell *37*, 879–886.

De Souza, C.P.C., and Osmani, S.A. (2007). Mitosis, not just open or closed. Eukaryot. Cell *6*, 1521–1527.

De Souza, C.P.C., Osmani, A.H., Hashmi, S.B., and Osmani, S.A. (2004). Partial nuclear pore complex disassembly during closed mitosis in Aspergillus nidulans. Curr. Biol. *14*, 1973–1984.

Spencer, F., Gerring, S.L., Connelly, C., and Hieter, P. (1990). Mitotic chromosome transmission fidelity mutants in Saccharomyces cerevisiae. Genetics *124*, 237–249.

Sridhar, S., Dumbrepatil, A., Sreekumar, L., Sankaranarayanan, S.R., Guin, K., and Sanyal, K. (2017). Centromere and Kinetochore: Essential Components for Chromosome Segregation. Gene Regul. Epigenetics Horm. Signal. 259–288.

Steiner, F.A., and Henikoff, S. (2014). Holocentromeres are dispersed point centromeres localized at transcription factor hotspots. Elife *2014*, 1–22.

Stewart, R.J., Farrell, K.W., and Wilson, L. (1990). Role of GTP hydrolysis in microtubule polymerization: evidence for a coupled hydrolysis mechanism. Biochemistry *29*, 6489–6498.

Straube, A., Weber, I., and Steinberg, G. (2005). A novel mechanism of nuclear envelope break-down in a fungus: nuclear migration strips off the envelope. EMBO J. *24*, 1674–1685.

Strzalka, W., and Ziemienowicz, A. (2011). Proliferating cell nuclear antigen (PCNA): A key factor in DNA replication and cell cycle regulation. Ann. Bot. *107*, 1127–1140.

Sukroongreung, S., Kitiniyom, K., Nilakul, C., and Tantimavanich, S. (1998). Pathogenicity of basidiospores of Filobasidiella neoformans var. neoformans. Med. Mycol. *36*, 419–424.

Sutradhar, S., Yadav, V., Sridhar, S., Sreekumar, L., Bhattacharyya, D., Ghosh, S.K., Paul, R., and Sanyal, K. (2015). A comprehensive model to predict mitotic division in budding yeasts. Mol. Biol. Cell *26*, 3954–3965.

Sutton, W.S. (1902). On the morphology of the chromosome group in Brachystola magna. Biol. Bull. *14*, 24–39.

Sutton, W.S. (1903). The Chromosomes in Heredity Author (s): Walter S . Sutton Published by : The University of Chicago Press in association with the Marine Biological Stable URL : http://www.jstor.org/stable/1535741. *4*, 231–251.

Suzuki, A., Hori, T., Nishino, T., Usukura, J., Miyagi, A., Morikawa, K., and Fukagawa, T. (2011). Spindle microtubules generate tension-dependent changes in the distribution of inner kinetochore proteins. J. Cell Biol. *193*, 125–140.

Suzuki, A., Badger, B.L., and Salmon, E.D. (2015). A quantitative description of Ndc80 complex linkage to human kinetochores. Nat. Commun. *6*, 8161.

Suzuki, A., Badger, B.L., Haase, J., Ohashi, T., Erickson, H.P., Salmon, E.D., and Bloom, K. (2016). How the kinetochore couples microtubule force and centromere stretch to move chromosomes. Nat. Cell Biol. *18*, 382–392.

Suzuki, A., Gupta, A., Long, S.K., Evans, R., Badger, B.L., Salmon, E.D., Biggins, S., and Bloom, K. (2018). A Kinesin-5, Cin8, Recruits Protein Phosphatase 1 to Kinetochores and Regulates Chromosome Segregation. Curr. Biol. *28*, 2697-2704.e3.

Sykes, J., and Greene, C. (2011). Infectious Diseases of the Dog and Cat 4th Edition.

Tachiwana, H., Kagawa, W., Shiga, T., Osakabe, A., Miya, Y., Saito, K., Hayashi-Takanaka, Y., Oda, T.,

Sato, M., Park, S.Y., et al. (2011). Crystal structure of the human centromeric nucleosome containing CENP-A. Nature *476*, 232–235.

Takeo, K., Ogura, Y., Virtudazo, E., Raclavsky, V., and Kawamoto, S. (2004). Isolation of a CDC28 homologue from Cryptococcus neoformans that is able to complement cdc28 temperature-sensitive mutants of Saccharomyces cerevisiae. FEMS Yeast Res. *4*, 737–744.

Takeuchi, K., Nishino, T., Mayanagi, K., Horikoshi, N., Osakabe, A., Tachiwana, H., Hori, T., Kurumizaka, H., and Fukagawa, T. (2014). The centromeric nucleosome-like CENP–T–W–S–X complex induces positive supercoils into DNA. Nucleic Acids Res. *42*, 1644–1655.

Tanaka, K. (2012). Dynamic regulation of kinetochore-microtubule interaction during mitosis. J. Biochem. *152*, 415–424.

Tanaka, K., Li Chang, H., Kagami, A., and Watanabe, Y. (2009). CENP-C Functions as a Scaffold for Effectors with Essential Kinetochore Functions in Mitosis and Meiosis. Dev. Cell *17*, 334–343.

Taylor TN, Krings M, T. EL (2015). Fossil Fungi (Elsevier).

Thakur, J., and Henikoff, S. (2016). CENPT bridges adjacent CENPA nucleosomes on young human α-satellite dimmers. Genome Res. *26*, 1178–1187.

Thakur, J., and Sanyal, K. (2012). A coordinated interdependent protein circuitry stabilizes the kinetochore ensemble to protect CENP-A in the human pathogenic yeast Candida albicans. PLoS Genet. *8*.

Tien, J.F., Umbreit, N.T., Gestaut, D.R., Franck, A.D., Cooper, J., Wordeman, L., Gonen, T., Asbury, C.L., and Davis, T.N. (2010). Cooperation of the Dam1 and Ndc80 kinetochore complexes enhances microtubule coupling and is regulated by aurora B. J. Cell Biol. *189*, 713–723.

Toffaletti, D.L., Rude, T.H., Johnston, S.A., Durack, D.T., and Perfect, J.R. (1993). Gene transfer in Cryptococcus neoformans by use of biolistic delivery of DNA. J. Bacteriol. *175*, 1405–1411.

Tromer, E.C., van Hooff, J.J.E., Kops, G.J.P.L., and Snel, B. (2019). Mosaic origin of the eukaryotic kinetochore. Proc. Natl. Acad. Sci. *116*, 12873–12882.

Umbreit, N.T., Gestaut, D.R., Tien, J.F., Vollmar, B.S., Gonen, T., Asbury, C.L., and Davis, T.N. (2012). The Ndc80 kinetochore complex directly modulates microtubule dynamics. Proc. Natl. Acad. Sci. *109*, 16113–16118.

Vagnarelli, P., Ribeiro, S.A., and Earnshaw, W.C. (2008). Centromeres: Old tales and new tools. FEBS Lett. *582*, 1950–1959.

Vallardi, G., Cordeiro, M.H., and Saurin, A.T. (2017). A Kinase-Phosphatase Network that Regulates Kinetochore-Microtubule Attachments and the SAC. pp. 457–484.

del Valle, J., de la Oliva, N., Muller, M., Stieglitz, T., and Navarro, X. (2015). Biocompatibility evaluation of parylene C and polyimide as substrates for peripheral nerve interfaces. In 2015 7th International IEEE/EMBS Conference on Neural Engineering (NER), (IEEE), pp. 442–445.

Varma, D., and Salmon, E.D. (2012). The KMN protein network - chief conductors of the kinetochore orchestra. J. Cell Sci. *125*, 5927–5936.

Varshney, N., Som, S., Chatterjee, S., Sridhar, S., Bhattacharyya, D., Paul, R., and Sanyal, K. (2019). Spatio-temporal regulation of nuclear division by Aurora B kinase Ipl1 in Cryptococcus neoformans. PLoS Genet. *15*, e1007959.

Venkei, Z., Przewloka, M.R., Ladak, Y., Albadri, S., Sossick, A., Juhasz, G., Novak, B., and Glover, D.M. (2012). Spatiotemporal dynamics of Spc105 regulates the assembly of the Drosophila kinetochore. Open Biol. *2*, 110032–110032.

Vleugel, M., Hoogendoorn, E., Snel, B., and Kops, G.J.P.L. (2012). Perspective Evolution and Function of the Mitotic Checkpoint.

Wan, X., O'Quinn, R.P., Pierce, H.L., Joglekar, A.P., Gall, W.E., DeLuca, J.G., Carroll, C.W., Liu, S.T., Yen, T.J., McEwen, B.F., et al. (2009). Protein Architecture of the Human Kinetochore Microtubule Attachment Site. Cell *137*, 672–684.

Wang, X., Hsueh, Y.P., Li, W., Floyd, A., Skalsky, R., and Heitman, J. (2010). Sex-induced silencing defends the genome of Cryptococcus neoformans via RNAi. Genes Dev. *24*, 2566–2582.

Wei, R.R., Sorger, P.K., and Harrison, S.C. (2005). Molecular organization of the Ndc80 complex, an essential kinetochore component. Proc. Natl. Acad. Sci. U. S. A. *102*, 5363–5367.

Wei, R.R., Schnell, J.R., Larsen, N.A., Sorger, P.K., Chou, J.J., and Harrison, S.C. (2006). Structure of a Central Component of the Yeast Kinetochore: The Spc24p/Spc25p Globular Domain. Structure *14*, 1003–1009.

Wei, R.R., Al-Bassam, J., and Harrison, S.C. (2007). The Ndc80/HEC1 complex is a contact point for kinetochore-microtubule attachment. Nat. Struct. Mol. Biol. *14*, 54–59.

Weir, J.R., Faesen, A.C., Klare, K., Petrovic, A., Basilico, F., Fischböck, J., Pentakota, S., Keller, J., Pesenti, M.E., Pan, D., et al. (2016). Insights from biochemical reconstitution into the architecture of human kinetochores. Nature *537*, 249–253.

Welburn, J.P.I., Grishchuk, E.L., Backer, C.B., Wilson-Kubalek, E.M., Yates, J.R., and Cheeseman, I.M. (2009). The Human Kinetochore Ska1 Complex Facilitates Microtubule Depolymerization-Coupled Motility. Dev. Cell *16*, 374–385.

Welburn, J.P.I., Vleugel, M., Liu, D., Yates, J.R., Lampson, M.A., Fukagawa, T., and Cheeseman, I.M. (2010). Aurora B Phosphorylates Spatially Distinct Targets to Differentially Regulate the Kinetochore-Microtubule Interface. Mol. Cell *38*, 383–392.

Wendell, K.L., Wilson, L., and Jordan, M.A. (1993). Mitotic block in HeLa cells by vinblastine: ultrastructural changes in kinetochore-microtubule attachment and in centrosomes. J. Cell Sci. *104 (Pt 2*, 261–274.

Westermann, S., and Schleiffer, A. (2013). Family matters: Structural and functional conservation of centromere-associated proteins from yeast to humans. Trends Cell Biol. *23*, 260–269.

Westermann, S., Avila-Sakar, A., Wang, H.W., Niederstrasser, H., Wong, J., Drubin, D.G., Nogales, E., and Barnes, G. (2005). Formation of a dynamic kinetochore-microtubule interface through assembly of the Dam1 ring complex. Mol. Cell *17*, 277–290.

Westhorpe, F.G., Fuller, C.J., and Straight, A.F. (2015). A cell-free CENP-A assembly system defines the chromatin requirements for centromere maintenance. J. Cell Biol. *209*, 789–801.

Wickes, B.L., Mayorga, M.E., Edman, U., and Edman, J.C. (1996). Dimorphism and haploid fruiting in Cryptococcus neoformans: association with the alpha-mating type. Proc. Natl. Acad. Sci. *93*, 7327–7331.

Williams, J.S., Hayashi, T., Yanagida, M., and Russell, P. (2009). Fission Yeast Scm3 Mediates Stable Assembly of Cnp1/CENP-A into Centromeric Chromatin. Mol. Cell *33*, 287–298.

Winey, M. (1995). Three-dimensional ultrastructural analysis of the Saccharomyces cerevisiae mitotic spindle. J. Cell Biol. *129*, 1601–1615.

Wisniewski, J., Hajj, B., Chen, J., Mizuguchi, G., Xiao, H., Wei, D., Dahan, M., and Wu, C. (2014). Imaging the fate of histone Cse4 reveals de novo replacement in S phase and subsequent stable residence at centromeres. Elife *3*, e02203.

De Wulf, P., McAinsh, A.D., and Sorger, P.K. (2003). Hierarchical assembly of the budding yeast kinetochore from multiple subcomplexes. Genes Dev. *17*, 2902–2921.

Wynne, D.J., and Funabiki, H. (2015). Kinetochore function is controlled by a phosphodependent coexpansion of inner and outer components. J. Cell Biol. *210*, 899–916.

Yadav, V., and Sanyal, K. (2018). Sad1 Spatiotemporally Regulates Kinetochore Clustering To Ensure High-Fidelity Chromosome Segregation in the Human Fungal Pathogen Cryptococcus neoformans. MSphere *3*, 1–12.

Yadav, V., Sreekumar, L., Guin, K., and Sanyal, K. (2018a). Five pillars of centromeric chromatin in fungal pathogens. PLoS Pathog. *14*, 1–7.

Yadav, V., Sun, S., Billmyre, R.B., Thimmappa, B.C., Shea, T., Lintner, R., Bakkeren, G., Cuomo, C.A.,

Heitman, J., and Sanyal, K. (2018b). RNAi is a critical determinant of centromere evolution in closely related fungi. Proc. Natl. Acad. Sci. *115*, 3108–3113.

Yamagishi, Y., Sakuno, T., Goto, Y., and Watanabe, Y. (2014). Kinetochore composition and its function: Lessons from yeasts. FEMS Microbiol. Rev. *38*, 185–200.

Yan, K., Yang, J., Zhang, Z., McLaughlin, S.H., Chang, L., Fasci, D., Ehrenhofer-Murray, A.E., Heck, A.J.R., and Barford, D. (2019). Structure of the inner kinetochore CCAN complex assembled onto a centromeric nucleosome. Nature.

Yan, Z., Delannoy, M., Ling, C., Daee, D., Osman, F., Muniandy, P.A., Shen, X., Oostra, A.B., Du, H., Steltenpool, J., et al. (2010). A Histone-Fold Complex and FANCM Form a Conserved DNA-Remodeling Complex to Maintain Genome Stability. Mol. Cell *37*, 865–878.

Yang, M., Li, B., Liu, C.-J., Tomchick, D.R., Machius, M., Rizo, J., Yu, H., and Luo, X. (2008). Insights into Mad2 Regulation in the Spindle Checkpoint Revealed by the Crystal Structure of the Symmetric Mad2 Dimer. PLoS Biol. *6*, e50.

Ye, A.A., Cane, S., and Maresca, T.J. (2016). Chromosome biorientation produces hundreds of piconewtons at a metazoan kinetochore. Nat. Commun. *7*, 1–9.

Zelter, A., Bonomi, M., Kim, J. ook, Umbreit, N.T., Hoopmann, M.R., Johnson, R., Riffle, M., Jaschob, D., MacCoss, M.J., Moritz, R.L., et al. (2015). The molecular architecture of the Dam1 kinetochore complex is defined by cross-linking based structural modelling. Nat. Commun. *6*, 8673.

Zimmermann, L., Stephens, A., Nam, S.Z., Rau, D., Kübler, J., Lozajic, M., Gabler, F., Söding, J., Lupas, A.N., and Alva, V. (2018). A Completely Reimplemented MPI Bioinformatics Toolkit with a New HHpred Server at its Core. J. Mol. Biol. *430*, 2237–2243.

My publications

List of publications

1. Kozubowski, L. *****, Yadav, V. *****, Chatterjee, G., **Sridhar, S**., Yamaguchi, M., Kawamoto, S., Bose, I., Heitman, J., and Sanyal, K. (2013). Ordered kinetochore assembly in the human-pathogenic basidiomycetous yeast Cryptococcus neoformans. MBio *4*. *(Cover page article).*

2. Sutradhar, S. *****, Yadav, V. *****, **Sridhar, S**. *****, Sreekumar, L., Bhattacharyya, D., Ghosh, S.K., Paul, R., and Sanyal, K. (2015). A comprehensive model to predict mitotic division in budding yeasts. Mol. Biol. Cell *26*, 3954–3965. *(Cover page article).*

3. Altamirano, S., Fang, D., Simmons, C., **Sridhar, S.**, Wu, P., Sanyal, K., and Kozubowski, L. (2017). Fluconazole-Induced Ploidy Change in Cryptococcus neoformans Results from the Uncoupling of Cell Growth and Nuclear Division. MSphere *2*, 1–18.

4. **Sridhar, S**., Dumbrepatil, A., Sreekumar, L., Sankaranarayanan, S.R., Guin, K., and Sanyal, K. (2017). Centromere and Kinetochore: Essential Components for Chromosome Segregation. Gene Regul. Epigenetics Horm. Signal. 259–288.

5. Suneet, K. *****, **Sridhar, S**. *****, Agiwal, P., Sridhar, M.S., Sanyal, K., and Jain, S. (2019). Magnetic hyperthermia adjunctive therapy for fungi: in vitro studies against Candida albicans. Int. J. Hyperth. *36*, 545–553.

6. Varshney, N., Som, S., Chatterjee, S., **Sridhar, S**., Bhattacharyya, D., Paul, R., and Sanyal, K. (2019). Spatio-temporal regulation of nuclear division by Aurora B kinase Ipl1 in Cryptococcus neoformans. PLoS Genet. *15*, e1007959.

7. **Sridhar, S**., Hori, T., Nakagawa, R., Fukagawa, T., and Sanyal, K. (2019). Identification of bridgin , an unconventional linker , connects the outer kinetochore to centromeric chromatin. BioArxiv.

***, Equal contribution**